University Of Cyprus
Faculty of Pure and Applied Sciences
Department of Biological Sciences

Laboratory of Cell Biology and
Molecular Embryology
(Assistant Professor Paris A. Skourides)

A study of 40LoVe's role in Xenopus development and the development of a novel intein based method for the in vivo conjugation of Quantum Dots to target proteins

Maria Andreou

A dissertation submitted to the University of Cyprus in partial fulfillment of the requirements for the degree of Doctor of Philosophy

June 2014

VALIDATION PAGE

Doctoral Candidate: Maria Andreou

Doctoral Thesis Title: A study of 40LoVe's role in *Xenopus* development and the development of a novel intein based method for the *in vivo* conjugation of Quantum Dots to target proteins

The present Doctoral Dissertation was completed in partial fulfillment of the requirements for the degree of Doctor of Philosophy at the Department of Biological Sciences and was approved on the 28/2/2014 by the members of the Examination Committee.

Examination Committee:

Research Supervisor: Dr Paris A. Skourides, Assistant Professor

_____

Committee Member: Dr Pantelis Georgiades, Associate Professor

_____

Committee Member: Dr Katerina Strati, Lecturer

Committee Member: Dr Christos Zervas, Assistant Professor

Committee Member: Dr Maria D. Koffa, Associate Professor

DECLARATION OF DOCTORAL CANDIDATE

The present doctoral dissertation was submitted in partial fulfillment of the requirements for the degree of Doctor of Philosophy of the University of Cyprus. It is a product of original work of my own, unless otherwise mentioned through references, notes or any other statements.

Maria Andreou

Περίληψη

Η πρωτεΐνη Samba ανήκει στην οικογένεια των ετερογενών πυρηνικών ριβονουκλεοπρωτεϊνών (hnRNPs). Προηγούμενες μελέτες έχουν δείξει ότι καταστέλλει την εξάπλωση των κυττάρων του ζωικού πόλου σε υπόστρωμα φιμπρονεκτίνης και επηρεάζει την μετανάστευση των κυττάρων της νευρικής ακρολοφίας. Η πρωτεΐνη αυτή εκφράζεται σε όλα τα αναπτυξιακά στάδια με αύξησή της κατά τη νευριδίωση, ενώ όσο προχωρά η ανάπτυξη περιορίζεται στους νευρικούς ιστούς. Στην παρούσα μελέτη, εξετάσαμε την παρουσία της πρωτεΐνης αυτής σε κυτταρικό και εμβρυικό επίπεδο και γενικότερα τον ρόλο της κατά την ανάπτυξη. Η πρωτεΐνη αυτή εντοπίζεται σε ολόκληρο το κύτταρο, στον πυρήνα, το κυτταρόπλασμα και την κυτταρική μεμβράνη. Φαίνεται να προσδένεται άμεσα ή έμμεσα στους μικροσωληνίσκους κατά την μίτωση και μεταφέρεται κατά μήκος των νευραξόνων, σε ώριμα έμβρυα. Επιπρόσθετα, χρησιμοποιώντας μεθόδους *FRAP* και *FLIP* δείξαμε ότι η πρωτεΐνη Samba μεταφέρεται από τον πυρήνα στο κυτταρόπλασμα και αντίστροφα, γεγονός που επιβεβαιώνει το ρόλο της ως hnRNP. Η καταστολή της μεταγραφής με τη χρήση Morpholino, προκαλεί προβλήματα στην ανάπτυξη του νευρικού συστήματος, γεγονός που ενισχύεται και από πειράματα υπερέκφρασης. Το ίδιο Morpholino, καταστέλλει την μετάφραση του εναλλακτικού μεταγράφου 40LoVe, καθώς και του παράλογου γονιδίου hnRNP AB, που είναι 93% πανομοιότυπο με την 40LoVe. Παρά τη μεγάλη ομολογία μεταξύ των 40LoVe/Samba και hnRNP AB, εντοπίζονται διαφορετικά στο κύτταρο, πιθανόν λόγω διαφορετικής λειτουργίας. Συγκρίνοντας τις πρωτεΐνες, καταλήξαμε στο συμπέρασμα ότι ο φαινότυπος που παρουσιάζεται στο νευρικό σύστημα, οφείλεται στην καταστολή της έκφρασης των 40LoVe/Samba. Επιπρόσθετα, είδαμε ότι η hnRNP AB έχει διαφορετική λειτουργία. Το σύνολο των πειραμάτων που διενεργήθηκαν απαιτούσαν προηγμένες τεχνικές απεικόνισης, με σκοπό την ζωντανή απεικόνιση χιμαιρικών πρωτεϊνών με φθορίζουσες πρωτεΐνες. Καταφύγαμε έτσι σε εναλλακτικούς τρόπους απεικόνισης για να μειώσουμε τα προβλήματα που παρουσιάζουν οι φθορίζουσες πρωτεΐνες, όσον αφορά τη φωτοσταθερότητα και τη φωτεινότητα. Οι νανοκρύσταλλοι (Quantum Dots-QDs) είναι ημιαγωγοί, με ιδανικές οπτικές ιδιότητες για την χρήση τους σε εφαρμογές βιοαπεικόνισης. Μέχρι στιγμής δεν υπήρχαν μεθοδολογίες που να επιτρέπουν την πρόσδεση των QDs σε πρωτεΐνες *in vivo*. Έτσι, το δεύτερο μέρος της διατριβής

επικεντρώθηκε στην ανάπτυξη πειραματικής μεθοδολογίας, για την ομοιοπολική πρόσδεση πρωτεϊνών με QDs *in* vivo και για το σκοπό αυτό χρησιμοποιήθηκαν οι inteins. Το καρβοξυτελικό άκρο της intein (I_C) προσδέθηκε ομοιοπολικά *in vitro* στα QDs, ενώ το αμινοτελικό άκρο της intein (I_N) προσδέθηκε μοριακά στην υπό εξέταση πρωτεΐνη. Το RNA που δημιουργήθηκε *in vitro* και τα I_C-QD's εισάχθηκαν με μικροένεση στο έμβρυο. Αφού το RNA μεταφράζεται μέσα στον οργανισμό, το αμινοτελικό άκρο της πρωτεΐνης συνδέθηκε με το καρβοξυτελικό της άκρο και προκαλείται *in vivo* πρωτεϊνικό μάτισμα. Η πρωτεΐνη συνδεδεμένη πλέον με το QD, μπορεί να παρατηρηθεί σε πραγματικό χρόνο σε ζωντανό οργανισμό. Αυτή η μέθοδος μπορεί να χρησιμοποιηθεί για την πρόσδεση οποιασδήποτε νανοσυσκευής, σε οποιαδήποτε πρωτεΐνη, για την παρατήρηση σε όλα τα κυτταρικά διαμερίσματα ή σύμπλοκα σήμανσης σε κύτταρα του αναπτυσσόμενου εμβρύου. Με τη χρήση QDs που εκπέμπουν στο υπέρυθρο, καταφέραμε να απεικονίσουμε δομές, που με τη χρήση της πράσινης φθορίζουσας πρωτεΐνης (EGFP), ήταν μη ανιχνεύσιμες λόγω βάθους, αναδεικνύοντας έτσι και τα πλεονεκτήματα της χρήσης QDs σε τέτοιου τύπου πειράματα.

Abstract

Samba is a *Xenopus* hnRNP that was recently identified and has been shown to inhibit animal cap spreading and affect neural crest migration. It is expressed in all developmental stages and the expression appears elevated during neurula stages. At early neurula stages Samba is concentrated at the neural plate and later in the neural and neural crest tissues. At tailbud stages it is restricted in neural and neural crest derivatives including the brain, the spinal cord, the eyes and the brachial arches. Here we examined the protein localization at the cellular and embryonic level and also explored the role of the protein during development. We show that the protein is localized in the nucleus, the cytoplasm and the plasma membrane. It becomes associated with microtubules during mitosis and it is transported in axons. We also show using *FRAP* and *FLIP* that Samba shuttles between the cytosol and the nucleus consistent with a role as an hnRNP. Loss of function experiments using antisense Morpholinos leads to defective neural development in agreement with the elevated expression of Samba in neural tissues. However, we also show that the Morpholino downregulates the splice variant 40LoVe and *a paralog,* hnRNP AB, which shares 93% identity with 40Love. Despite the high homology between 40LoVe/Samba and hnRNP AB, the proteins localize in distinct manners suggesting distinct functions in the embryo. We map the differences between the two proteins to the c-terminus and show that the neural phenotype is a consequence of 40LoVe/Samba downregulation arriving at the surprising conclusion that 40LoVe/Samba and hnRNP AB despite their extremely high homology are in fact functionally distinct. The aforementioned project required the application of advanced imaging modalities including the use of fluorescent protein fusions for live imaging, FRAP and FLIP and highlighted the limitations of protein fluorophores with respect to photostability and brightness. Quantum Dots (QDs) are nanometer semiconductor nanocrystals with ideal optical properties for use in biological imaging. However no methodologies exist that will allow the covalent and site specific conjugation of QDs to target proteins in vivo. The second part of this thesis focused on developing a methodology that would resolve these issues. We describe an intein based method to site-specifically conjugate QDs to target proteins *in vivo*. This approach allows the covalent conjugation of any nanostructure

and/or nanodevice to any protein and thus the targeting of such material to any intracellular compartment or signaling complex within the cells of the developing embryo. The C-terminus half (I_C) of the intein was conjugated to QDs *in vitro*. I_C-QD's and RNA encoding PH-I_N were microinjected into Xenopus embryos. *In vivo* intein-splicing resulted in fully functional QD-PH conjugates that could be monitored in real time within live embryos. Use of Near Infra Red (NIR)-emitting QDs allowed monitoring of QD-conjugates within the embryo at depths where EGFP is undetectable demonstrating the advantages of QD's for this type of experiment.

Acknowledgements

My Ph.D. was one of the best experiences in my life. I matured as a person and learned to overcome the various obstacles in my life. I was introduced to people who had a significant effect in my life and developed me into an improved, stronger person, eager to pursue my search for knowledge and I will keep them in my heart for the rest of my life.

Firstly, I would like to thank my supervisor, Dr Paris Skourides, for providing me with the opportunity to work in his lab and receiving his guidance during my work. I would like to thank all the friends I made during this journey. I wish to thank Dr Panayiota Stylianou for her consistent encouragement during all these years. I would also like to thank her for being patient enough to teach me how to hold a frog and maintain a Xenopus facility. Furthermore, I am inclined to thank Iro Eleftheriou for her help both in and out of the lab. I would also like to express my gratitude towards Dr Andrea Ioannou for everything that we endured together and which have made us stronger characters. What is more, I would like to state my appreciation to Dr Annita Charalambous for her guidance and for her continues presence any time I asked. Last but not least, I would like to thank all former and current members of my lab, Georgia Hatzilampi, Nicoletta Petridou, Ioanna Antoniades and Neophytos Christodoulou. They were not just perfect co-workers, but they were most of all cherished friends and companions.

To conclude, I wish to address an immense thank you to all of my friends who supported me during my PhD and encouraged me whenever I was frustrated or tired. A special thanks to my family, and especially my parents, who always induced and supported my decisions. Finally, vast thanks to my husband Miltos for his consistent patience and support, especially this last year. Without him this could never have been completed.

This is dedicated to my parents, Stavros and Elli and my husband, Miltos, who supported me in every step of the way.

Thank you!!!

Table of Contents

I. List of Figures

II. List of Tables

III. List of Movies

Movie 1: GFP-Samba transported along neuronal axons.

Movie 2: GFP-Samba is localized at axon growth cones.

1. Introduction

1.1 Xenopus laevis as an experimental model

Amphibians have a long history in laboratory research. They are an excellent system for studying vertebrate development for several reasons. Amphibians are not only vertebrates, but are also tetrapods, so they have all of the fundamental features of land-dwelling vertebrates. They undergo external development, so they can be observed and relatively easily manipulated. In the present thesis *Xenopus laevis*, the African clawed frog has been used as an experimental model (Figure 1).

Figure 1 : *Xenopus laevis*

Xenopus laevis belongs to the order *Anuran*, the family of *Pipidae* and subfamily of the *Xenopodinae*. More than 20 subspecies of *Xenopodinae* have been identified. *Xenopus laevis* is allotetraploid which means it has four copies of many genes that may or may not be functional and this complicates the study of inheritance (Figure 2). Thus, *Xenopus laevis* genes frequently have pseudoalleles thought to have originated from hybridization between two different *Xenopus* species in the course of evolution (Kobel and Pasquier 1986). For these reasons, *Xenopus laevis* is not a good model for genetic studies but it is an excellent model for studying early development.

	Number of species		Chromosomes (No./cell)	DNA (pg/cell)
Hymenochirus	5	1	24	4.2
Pipa	7	1	20	
		1	22	4.8
		1	30	
Xenopus	16	1	20	3.6
		1	40	(7.2)
		8	36	5.9–8.5
		5(3)	72	11.4–12.8
		1	108	16.3

Figure 2 : Composition of the anuran family *Pipidae.* Adopted from (Kobel and Pasquier 1986).

Xenopus laevis is aquatic and can easily lay eggs repeatedly with a simple hormone injection (details in section: materials and methods) (Sive, Grainger et al. 2000). The eggs can be fertilized *in vitro* in a dish by adding sperm in a simple media or by natural mating (Figure 3). A good female frog can lay hundreds of eggs in a single day. The actual number of eggs laid and the efficiency of fertilization are unpredictable so ovulation should be induced in more than one female every day of the experiments.

The embryos are large in size; they are approximately 1 to 1.4 mm in diameter, which is an order of magnitude larger than a mouse oocyte (10 folds larger). The large size allows the developmental biologist for micromanipulation, microinjections and microdissections and labeling of the *Xenopus* embryo and makes them a good animal model for examination of early vertebrate development. They have the ability to heal well after surgery, making grafting and tissue explants experiments possible.

Figure 3 : *Xenopus laevis* natural mating

In addition to these, another important advantage of using *Xenopus* embryos as a model, is that gain-of-function experiments can be carried out by overexpression of injected mRNA encoding a protein of interest. Also, loss of function experiments using dominant negative forms of a protein, antisense RNA (Harland and Weintraub 1985), oligonucleotides (Baker, Holland et al. 1990), and morpholino oligos (MO's) (Heasman, Kofron et al. 2000; Nutt, Bronchain et al. 2001; Heasman 2002; Kenwrick, Amaya et al. 2004), which have become one of the most widely used methods for gene knock-down in *Xenopus* and other model systems, are well established and standard practice in *Xenopus*. Furthermore, new techniques like Transcription activator-like effector nucleases (TALENs) (Sinnamon, Waddell et al. 2012) and CRISPR/Cas9-mediated targeted mutagenesis (Nelson and McClelland 1992) have recently started to be used in *Xenopus* research. All these features make *Xenopus* an excellent organism for the functional characterization of genes and proteins and for Molecular and Developmental biology research in general.

1.1.1 Normal development of *Xenopus laevis*

The mature *Xenopus* egg has established animal and vegetal regions. It has a dark, pigmented half that is the animal region and a pale, yolky, and heavier half that is the vegetal region. The egg is enclosed in a protective vitelline membrane and a gelatinous coat. The high percentage of yolk in the vegetal pole enables the embryo to survive and

develop in very simple buffer in the lab environment. The second axis to form is the dorsal-ventral axis. This axis is determined by the site of sperm entry that marks the future ventral side of the embryo. This axis determination occurs via a process known as cortical rotation, in which the cortical cytoplasm rotates 30° leading to the translocation of material previously located in the vegetal pole, to the prospective dorsal side of the embryo (Gilbert 2006).

Xenopus embryo development is relatively rapid, since they go from fertilization through neurulation in approximately 18 hours at 22^{o}C. The development of the embryos begins with the first cleavage that occurs along animal-vegetal axis within 90 minutes of fertilization, and this divides the embryo into equal halves. Further cleavages follow rapidly at intervals of about 20 minutes, with no G- phases. The cells that derived are called blastomeres. Their size is decreased and the blastomere number is increased during cleavage divisions, while cells at the vegetal pole are larger than those at the animal pole (Figure 4). After that, a fluid–filled cavity, called blastocoel, develops in the animal region of the embryo, and when this occurs the embryo is then referred to as a blastula. At mid-blastula stage, there is the mid-blastula transition (MBT), which is the beginning of the zygotic genome transcription (Gilbert 2006; Winklbauer 2009).

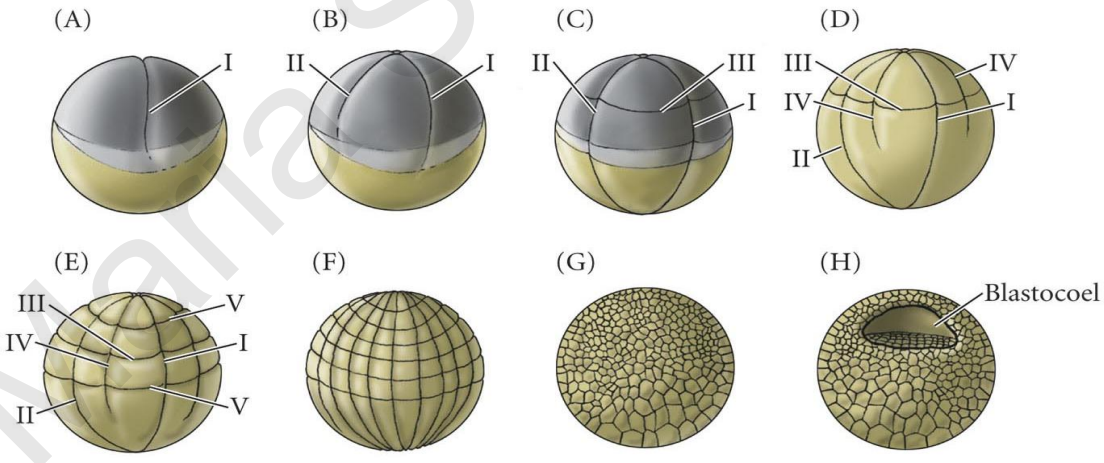

Figure 4 : Cleavage of a frog egg. (A, B) Because the vegetal pole has yolk, the second division begins in the animal region of the egg before the first division has divided the vegetal cytoplasm. (C) The third division is displaced toward the animal pole. (D-H) the vegetal hemisphere contains

larger and fewer blastomeres than the animal half. (H) Represents a cross section through a mid-gastrula stage embryo. Adopted from (Gilbert 2006).

Gastrulation is a process in early embryonic development that the three germ layers; the endoderm, mesoderm and ectoderm are shaped into a characteristic body plan and the definitive anteroposterior (AP) and dorsoventral (DV) axes are established (Suzuki, Iijima et al. 2005). The belt of tissue that plays a critical role in future development is known as the marginal zone. The process of gastrulation begins from the appearance of a condensed area of pigmentation on the dorsal side of the embryo. It involves highly integrated and regulated cell movements such as epiboly, mesoderm migration, convergent extension, and signaling events, which together result in the correct placement of tissues and the formation of the basic body plan of the embryo. The ectoderm, the most exterior germ layer, forms the skin, the nervous system, and other external tissues. Mesoderm, the middle germ layer, forms muscle, the skeletal system, and the circulatory system and the most internal germ layer, the endoderm, forms the lining of the gut and other internal organs (Gilbert 2006). Gastrulation is completed by neurulation.

Neurulation begins with the formation of the neural plate at the dorsal side of the embryo. This process creates the neural tube, neural crest and the bona fide epidermis, which covers the neural tube when it is created. While the notochord and somites are developing, the neural plate ectoderm above begins to develop into neural tube and the embryo is then called a neurula. Neurulation is completed by organogenesis. The embryo begins to look like a tadpole and we can recognize the main vertebrate features. At the anterior end the brain is already divided up into a number of regions and the eye and ear have begun to develop and posterior tail is formed last. After organogenesis is completed, the mature tadpole hatches out of its jelly covering and begins to swim and feed (Figure 5). Later, the tadpole larva will undergo metamorphosis to give rise to the adult frog (Gilbert 2006).

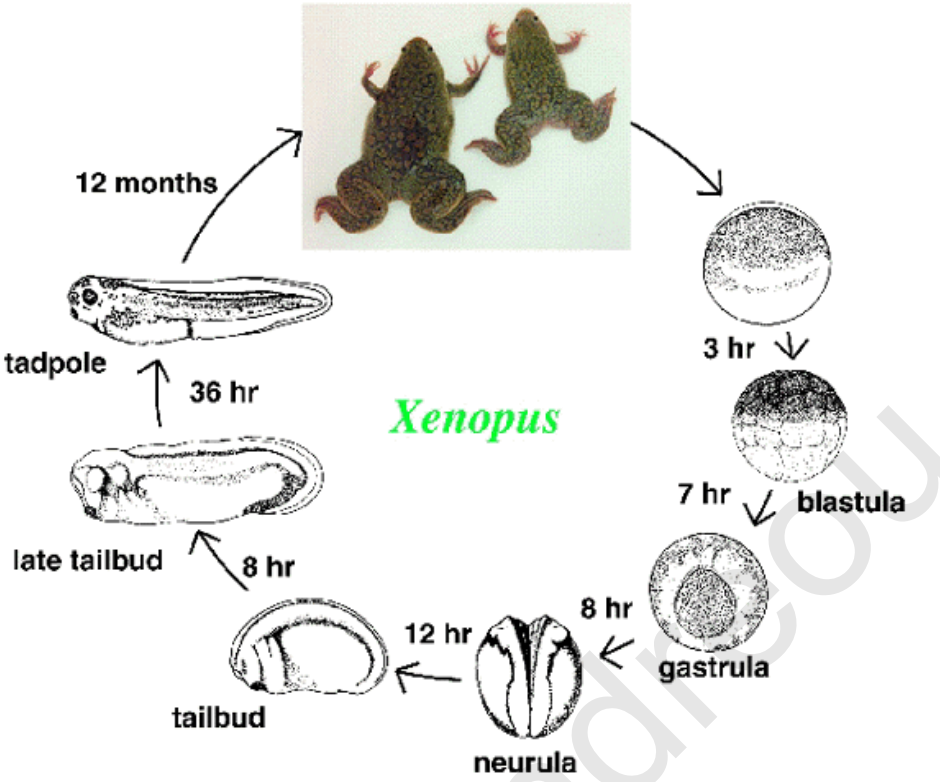

Figure 5 : *Xenopus laevis* life cycle. Adopted from Xenbase: *Xenopus* web source.

Morphogenetic movements

Morphogenetic movements in *Xenopus laevis* have been studied extensively at the cellular level and a lot of molecular information has been revealed. The morphogenetic movements are invagination, ingression, involution, epiboly, intercalation and convergent extension.

Invagination is a local bending of the epithelial cell sheet to create a pocket. It is very important of the formation of placodal tissues during the formation of the developing embryo. The initial formation of the blastoporal groove is an example of this process (Gilbert 2006; Van Dusen, Yee et al. 2010).

Ingression is the migration of individual cells into the embryo. The cells leave from an epithelial sheet by transforming from epithelial cells into freely migrating cells. These cells should possibly alter their cellular architecture as well as their program of motility, and

alter their adhesive relationships to the surrounding cells. Neural crest cells are an example of a cell type that emigrates out of the neural tube to form other cell types including pigmented cells and neurons (Gilbert 2006).

Involution is a rolling of a sheet of tissue over the basal surface of an outer layer. During this process cells become internalized by invaginating and rolling over the blastopore lip (Gilbert 2006). The first site of involution is right below the dorsal marginal zone (DMZ) and an epithelial sheet rolls inward to form an underlying layer. The first pioneering cells which become internalized will form the prechordal plate (head mesoderm) and they are immediately followed by the cells of the axial mesoderm, contributing to the notochord. Involution then expands mediolaterally and finally ventrally until the invaginating cells form a full circle called the blastopore (Gilbert 2006). Involution is preceded by the formation of bottle cells, which demarcate the site of invagination initially in the dorsal side (Keller 1981).

Epiboly is a process in which the cells of the prospective ectoderm located on top of the spherical embryo move downward toward the equator (Keller 1980). Epiboly is mediated at the cellular level by radial intercalation of the deep layers of the animal cap cells. The animal cap which is made of three cell layer during gastrulation becomes a two layered structure as the cells of the lower layer intercalate radially. This creates a larger surface area which pushes the cells to move down toward the equatorial region. While fibronectin has been suggested to be required for this process nothing is known about the molecular mechanism underlying this active intercalation behaviour (Marsden and DeSimone 2001; Longo, Peirce et al. 2004).

Intercalation is a process in which rows of cells move between one another, creating an array of cells that is longer in one or more dimensions, but thinner (Gilbert 2006). A specialized form of Intercalation is **Convergent extension.** This is a process in which cells located in the dorsal region of the equatorial region converge and extend toward the dorsal midline (Keller, Danilchik et al. 1985). Convergent extension is mediated at the cellular level by active movement of dorsal equatorial cells providing convergence and also mediolateral intercalation which ultimately gives rise to the extension of the

anterior-posterior axis (Keller, Danilchik et al. 1985). The cells adapt a clear polarity in their morphology during these movements. At the molecular level experiments performed in *Xenopus* and *Zebrafish* have demonstrated that the Wnt pathway, mediated by Disheveled plays a crucial role in the establishment of cell polarity (Smith, Conlon et al. 2000; Tada and Smith 2000; Wallingford, Rowning et al. 2000).

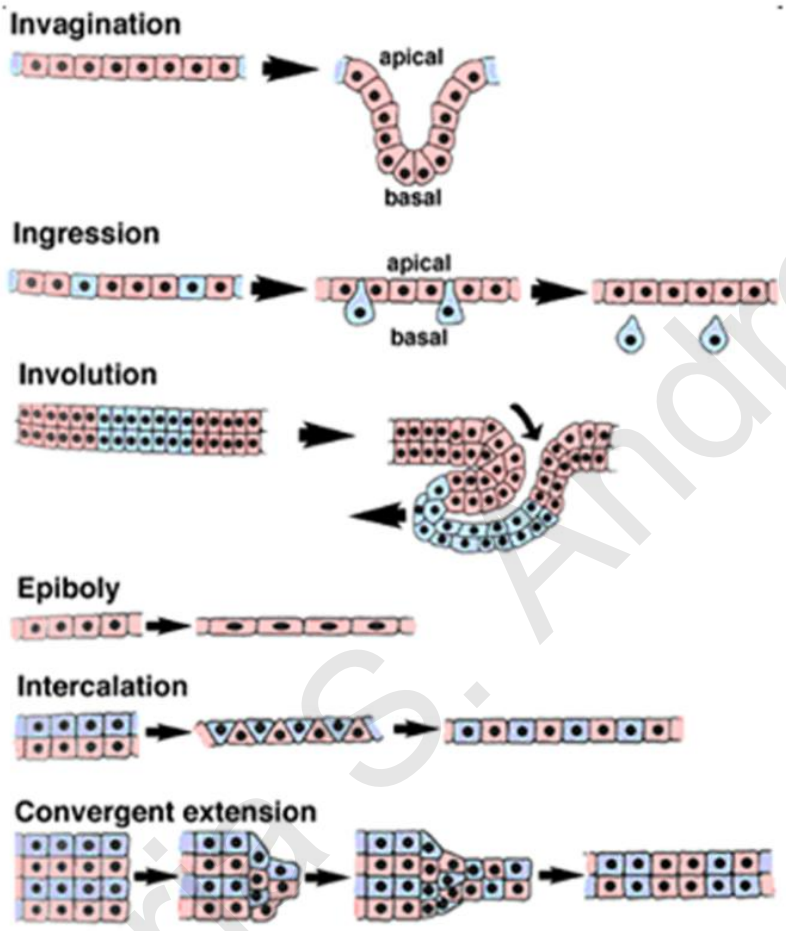

Figure 6 : Morphogenetic movements adopted from http://worms.zoology.wisc.edu.

Neurulation and neural development in Xenopus laevis

Neurulation is a major process in the developing embryo. It occurs between stages 14 and 20. During this process the neural tube is generated, which gives rise the central nervous system, the neural crest is formed, which migrates away from the dorsal surface of the neural tube and gives rise to a diverse set of cell types such as melanocytes, cartilage and peripheral neurons, are also created during neurulation (Huang and Saint-Jeannet 2004). Neurulation also creates the bona fide epidermis, which covers over the neural tube once it is created (Gilbert 2006).

After gastrulation, the neural plate is formed on the dorsal side of the embryo by rearrangements within the ectoderm resulting in convergence and extension of the dorsal ectoderm during gastrulation. Neural plate is a flat region of ectoderm that will form all of the components of the central nervous system (Eagleson and Harris 1990). Neural plate is subdivided into two regions: the prechordal neural plate, which gives rise to the forebrain and the epichordal neural plate that gives rise to the midbrain, hindbrain and the spinal cord. The neural folds, that are formed at the edges of the neural plate due to changes of the cell shape and cell adhesion, will give rise to the neural crest (Baker and Bronner-Fraser 1997). Immediately after their formation the neural folds rise, move towards to each other and finally fuse to form the neural tube. After that, the neural tube is covered by the ectoderm that creates the epidermis (Figure 7). During and after neurulation axonal elongation of the embryo occurs (Gilbert 2006).

After stage 20 all the main tissues are formed. At these stages, the tailbud stages, the placodes develop as thickenings of the deep layer of the ectoderm. The olfactory, adenohypophyseal, otic, epibrachial and dorsolateral placodes give rise to neuronal cells and the lens placode gives rise to the lens of the eye. These placodes and the cranial neural crest contribute to the formation of the cranial gaglia. During organogenesis, groups of cells splits into several independent populations, which migrate to different locations and are therefore exposed to different combinations of signaling molecules, which allow the cells to acquire different fates. After organogenesis is completed, the mature tadpole begins to swim and feed. Later, the tadpole larva will undergo metamorphosis to give rise to the adult frog (Gilbert 2006).

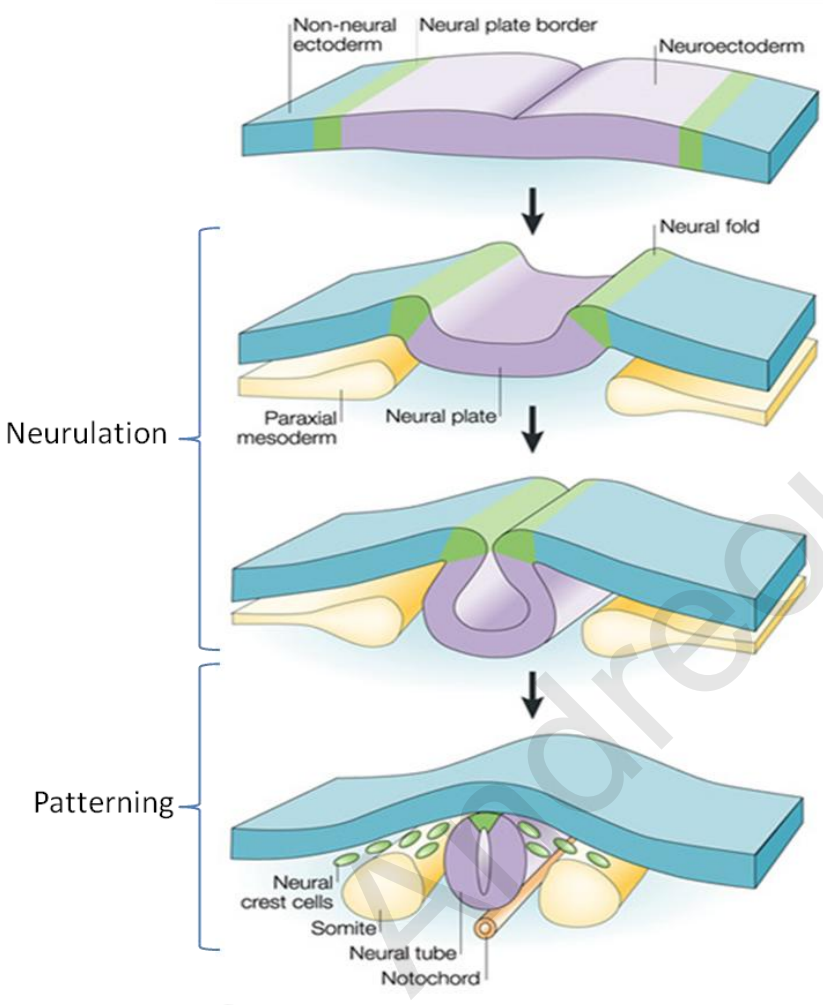

Figure 7 : Schematic representation of neural tube closure. The sides of the neural plate (purple) buckles, rolls up and fuses to form the neural tube. Neural plate border (green) is induced by signals from the neurectoderm (purple) and non-neural ectoderm (blue). Adopted from (Gammill and Bronner-Fraser 2003).

1.2 Visualization of proteins *in vivo*

Characterization of proteins in the context of a living cell is of crucial importance for a complete understanding of their function. One important advantage of using *Xenopus* embryos as a model organism is that fluorescent proteins and fluorophores can easily be microinjected in the developing embryo. Using these techniques it is easy to visualize morphogenetic movements as well as the real time dynamics of proteins into a living cell. Fluorescence microscopy is an essential tool in biology, especially molecular and cellular

biology, as it allows amongst others imaging molecules of interest, intracellular and intercellular events. Different fluorescent proteins have been widely used before untagged or tagged with the protein of interest (Kubota, Furuta et al. 1995; Siomi, Siomi et al. 1995). Biological imaging techniques depend primarily on the use of organic fluorophores and fluorescent proteins. However major drawbacks, such as low probe brightness, poor photostability, wide emission spectra and oxygen sensitivity, are limiting their use in certain applications. Issues of low brightness and photostability become more serious, when using organic or protein fluorophores, with emissions in the highly desirable Near Infra Red (NIR) region of the spectrum. The NIR region of the spectrum (700–950nm) is ideal for imaging through tissues because light scattering diminishes with increasing wavelength and hemoglobin electronic and water vibrational overtone absorptions approach their minimum over this spectral domain. Furthermore, living tissue auto fluorescence also reaches a minimum at this range and the fluorescent signal can, even in the case of organic fluorophores, be detected *in vivo* at subnanomolar quantities and at depths sufficient for experimental or clinical imaging (Rao, Dragulescu-Andrasi et al. 2007).

The introduction of Quantum Dots (QDs) as fluorescent probes led to significant improvements of *in vitro* and *in vivo* biological imaging. QDs are semiconductor nanocrystals with superior optical properties which arise from the electrons' confinement in dimensions smaller than a critical threshold (Michalet, Pinaud et al. 2005; Smith, Duan et al. 2008; Smith, Wen et al. 2010). The optical properties of Quantum Dots are a result from their chemical synthesis and their physical characteristics. QDs are nanometer-scale semiconductor crystallites (known as nanocrystals or quantum dots) which have the potential to revolutionize biological imaging. They have dimensions in the range of 2-10 nm and they constituted from 200-1000 atoms. The nanocrystals are often composed of atoms from groups II-VI (e.g. CdSe, CdTe, CdS and ZnSe) or III-V (e.g InP and InAs) elements in the periodic table and are defined as particles with physical dimensions smaller than the exciton Bohr radius (Chan, Maxwell et al. 2002; Michalet, Pinaud et al. 2005). As mentioned before, QDs are single crystals of few nanometers size and shape and this feature can be controlled by the duration and temperature used during synthesis and by the ligand molecules which are used for their synthesis. This leads QDs to have

composition and size dependent absorption and emission (Figure 8). The range of emission wavelength is 400 to 1350 nm and it depends on the size which varies from 2 to 9.5 nm (Michalet, Pinaud et al. 2005).

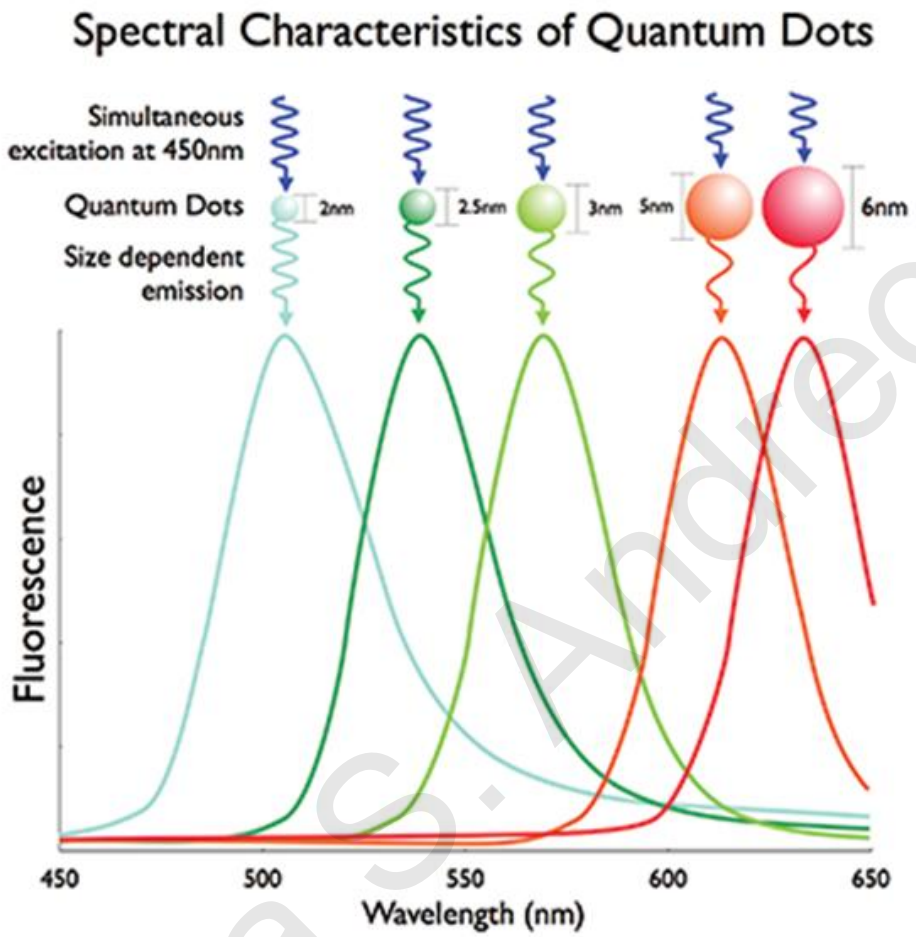

Figure 8 : A. Emission and sizes of quantum dots of different composition. The range of emission wavelength is 400 to 1350 nm, with size from 2 to 9.5 nm. Quantum-dot size relates to emission wavelength. Quantum dots absorb higher-energy/shorter-wavelength light and down-converts the light into lower-energy/longer-wavelength light. Adopted from (Chen, Hardev et al. 2013).

Quantum Dots provide distinct advantages over traditional fluorescent markers and they are 10 to 100 times brighter (Kawasaki and Player 2005; Smith, Duan et al. 2008). These colloidal particles act as robust, broadly tunable nanoemitters that can be excited by a single light source and provide distinct advantages over current *in vitro* and *in vivo*

markers (e.g., organic dyes and fluorescent proteins). In addition to extremely high fluorescence intensity, QD's offer a wide excitation spectrum, which makes the use of a single excitation filter possible. They have narrow and tunable emission spectra, which reduce spectral overlap making the simultaneous use of more colors possible. Therefore it is possible to use all the excitation wavelengths without having problems of bleed-through between each other (Arya, Kaul et al. 2005; Michalet, Pinaud et al. 2005). Also the large stokes shift increases the detection sensitivity, which provides large separation between the excitation and the emission is an important advantage. Sensitivity of QD's is higher than the conventional fluorescence dyes. The separation of the absorption and emission peaks increases the sensitivity by reducing the autofluorescence of the sample being examined.

One of the most important advantage of the QD's is the resistance to photobleaching (Medintz, Uyeda et al. 2005; Michalet, Pinaud et al. 2005). Phobleaching is a process in which the molecular structure of a dye is destroyed as a result of the excitation light and then it is non fluorescent anymore. In simple words this leads to photodegratation of the dye (Arya, Kaul et al. 2005). QD's are remarkably photostable, 100 to 1000 folds from the commercial fluorophores. This attribute is due to their transparent ZnS shells which enables their fluorescence to extinguish at a slow rate. The long fluorescence lifetime of QD's enables the use of time-gated detection and to separate their signal from that of shorter lived species (such as background autofluorescence which exists in the cells).

These features provide the capability of using this nanomaterial in multiparameter *in vivo* and *in vitro* applications. Summarizing, the characteristics of the Quantum Dots, mentioned above makes them good imaging-tool candidates in the world of bio-imaging and biological applications in basic and applied biology.

1.2.1 Biological applications

QD's have properties that provide advantages beneficial for a number of different science applications as compared to the standard fluorophores. The improved brightness and photostability exhibited by QD's are justification for their increased use in imaging and labeling experiments. The robustness of their signal strength also affords utility in targeting and detection applications. Over the years QD's have been tested in lots of applications including immunofluorescence assays, DNA and RNA targeting (fluorescence in situ hybridization in chromosomes) and *in vivo* targeting of cancer cells or bacteria. The most successful use of QD's have been the immunofluorescence assay labeling proteins, microtubules, actin, nuclear proteins of fixed cells and tissues (Michalet, Pinaud et al. 2005; Xing and Rao 2008; Walling, Novak et al. 2009).

Successful experiments *in vitro* prompted investigators to use QD's for *in vivo* applications. Experiments showed that visible spectrum emitting QD´s can be used successfully to obtain single cell resolution (superficial tissues) of the events of early *Xenopus* development including gastrulation (Dubertret, Skourides et al. 2002). They performed *in vivo* imaging by microinjecting QD's in the blastomeres of early stage *Xenopus* embryos. The fluorescence of the nanocrystals could be followed from the time of the injection to the tadpole stage thus showing that the QD's were stable *in vivo* (Figure 9).

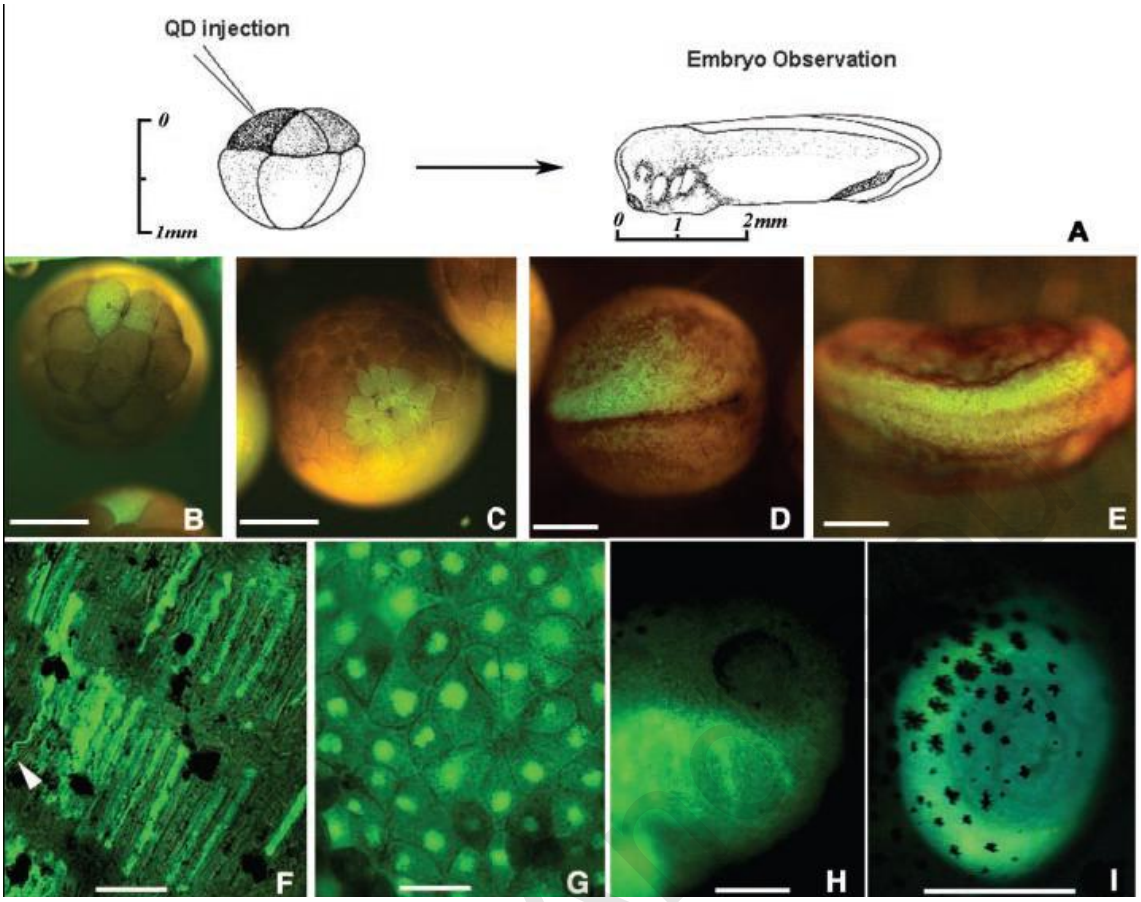

Figure 9 : QD labeling of *Xenopus* embryos at different stages and specific QD intracellular localizations. (A) Schematic showing the experimental strategy. QD-micelles were injected into an individual blastomere between 1.5 and 3 nl of QD's. (B) to (E), transmission and fluorescence images have been superposed. Injection of one cell out of an eight-cell-stage embryo resulted in labeling of individual blastomeres. (F) Intracellular labeling of an axon (arrow) and somites at tadpole stage 40. (G) QD's localized in the nucleus during mid-blastula stages. (H) Labeled neural crest cells migrating into the branchial arches. (I) QD's fluorescence observed in the gut of an injected embryo. Adopted from (Dubertret, Skourides et al. 2002).

QD's, as mentioned, are much more resistance to photobleaching than other fluorophores as proven by *in vitro* experiments (Bruchez, Moronne et al. 1998). This resistance also remains as shown by *in vivo* experiments. After 80 minutes of constant UV excitation (at 450nm) under the microscope the intensity of Quantum Dots remained the same but the membrane GFP (injected to the embryos as QD's) had photobleached

(Figure 10). This shows the great photostability of QDs during time in biological systems (Dubertret, Skourides et al. 2002).

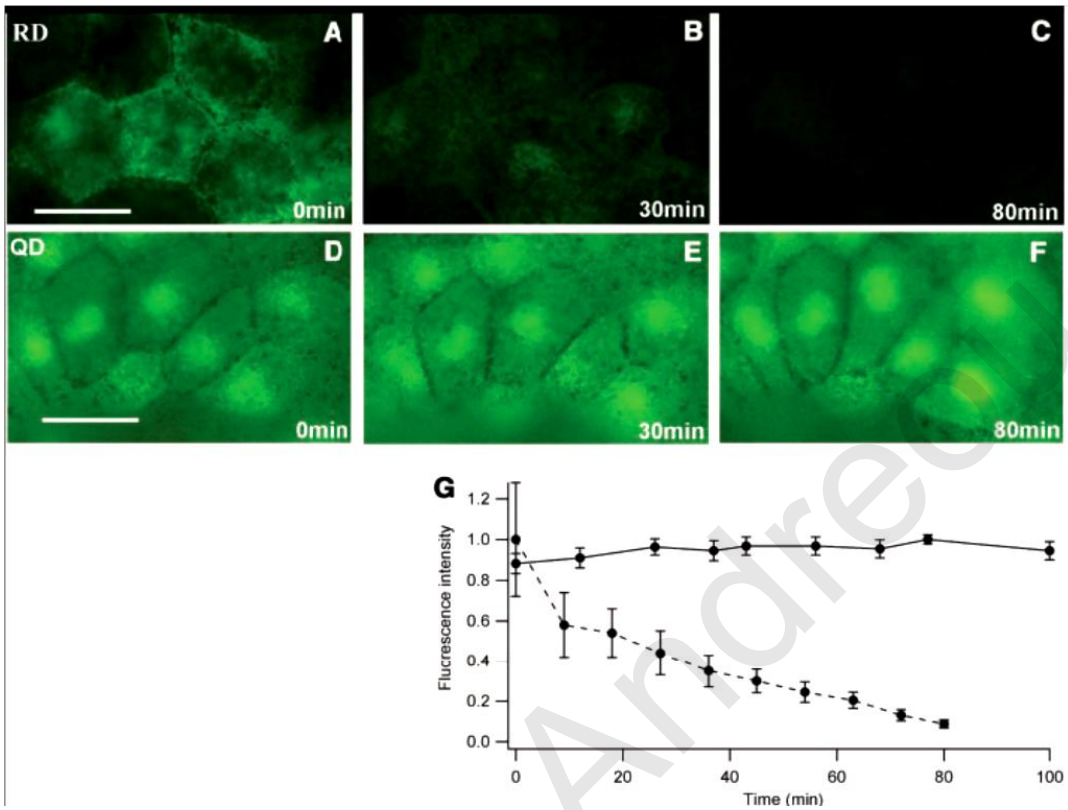

Figure 10 : Comparison of QD's and RG-D (Rhodamine Green Dextran) for resistance to photobleaching. (A to C) Consecutive images of RG-D injected *Xenopus* animal pole blastomeres. (D to F) Consecutive images of QD's injected *Xenopus* animal pole blastomeres. During each experiment, the injected embryos were excited continuously at 450 nm. (G) Graph presenting the variation of fluorescence intensity of one cell of the RG-D–injected embryo (dotted line) and of one cell of the QD-injected embryo (solid line). Adopted from (Dubertret, Skourides et al. 2002).

In addition, the Near Infra Red (NIR) region of the spectrum (700–950 nm) is ideal for imaging through tissues because light scattering diminishes with increasing wavelength, and hemoglobin electronic and water vibrational overtone absorptions approach their minimum over this spectral domain (Hawrysz and Sevick-Muraca 2000; Intes, Ripoll et al. 2003; Kalchenko, Shivtiel et al. 2006 ; Rao, Dragulescu-Andrasi et al. 2007). NIR QD´s have

been used for imaging of tumors and sentinel lymphnodes in mice and pigs respectively (Figure 11) (Kim, Lim et al. 2003; Stroh, Zimmer et al. 2005).

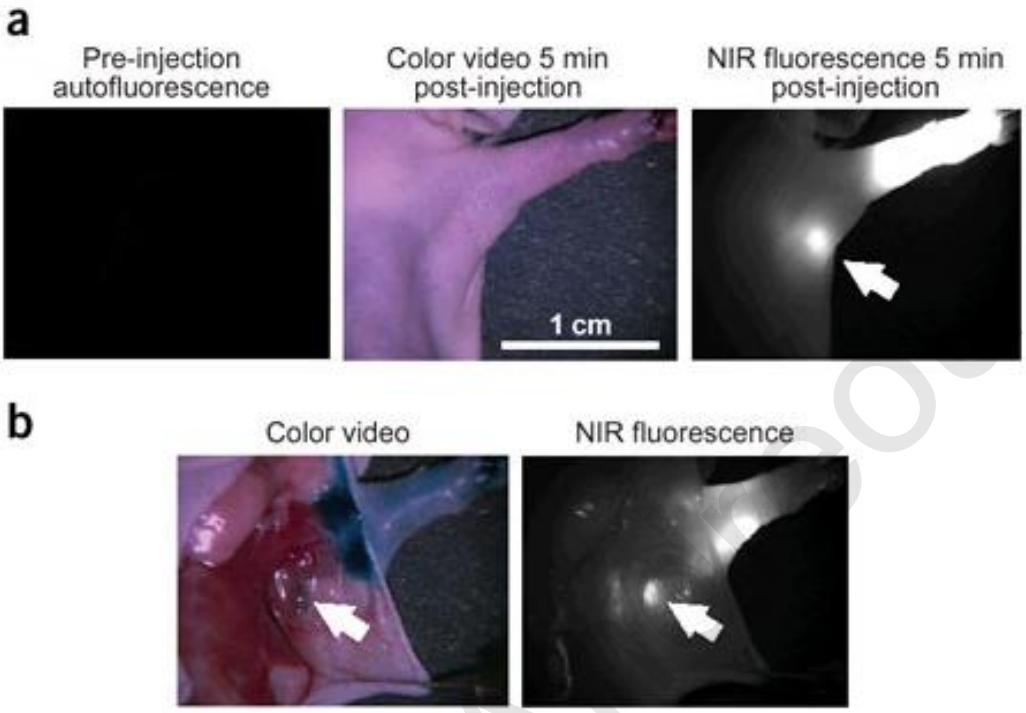

Figure 11 : NIR QD sentinel lymph node mapping in the mouse. (a) Images of mouse injected intradermally with 10 pmol of NIR QD's in the left paw. Left, pre-injection NIR autofluorescence image; middle, 5 min post-injection white light colour video image; right, 5 min post-injection NIR fluorescence image. Arrow indicates the putative axillary sentinel lymph node. (b) Images of the mouse shown in a 5 min after reinjection with 1% isosulfan blue and exposure of the actual sentinel lymph node. Isosulfan blue and NIR QD's were localized in the same lymph node (arrows). Adopted from (Kim, Lim et al. 2003).

Furthermore, living tissue auto fluorescence also reaches a minimum at this range and the fluorescent signal can, even in the case of organic fluorophores, be detected *in vivo* at subnanomolar quantities and at depths sufficient for experimental or clinical imaging (Weissleder, Tung et al. 1999; Tung, Mahmood et al. 2000). Additionally, commercially available NIR-QDs have been used successfully for *in vivo* imaging for the visualization of deep tissue movements with single cell resolution in mesoderm migration in *Xenopus* embryos (Stylianou and Skourides 2009) (Figure 12).

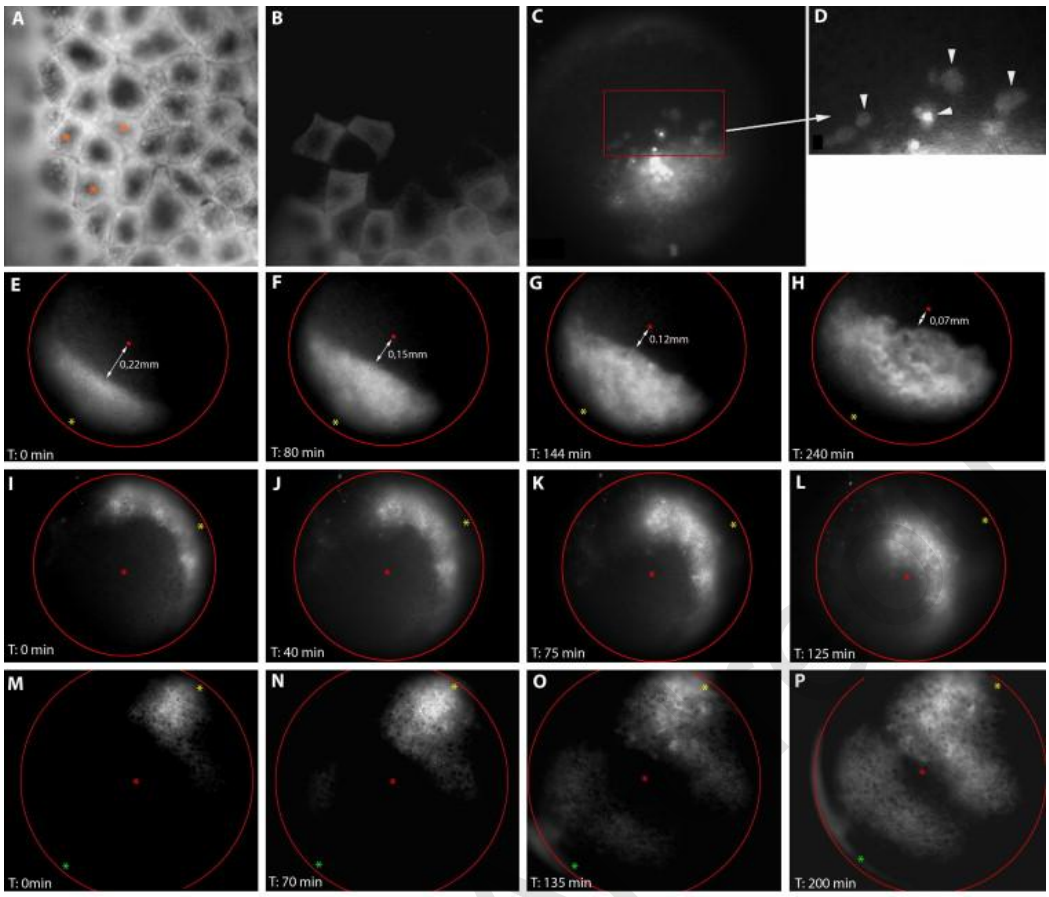

Figure 12 : NIR QD's can be used to label and image mesodermal cells during gastrulation. (A and B) NIR QD (800-nm peak emission) labeled animal pole cells in a living embryo viewed with two filter sets. (A) The embryo was imaged with 600 nm long pass emission filter allowing all wavelengths above 600 nm to reach the camera and in B the same area of the same embryo was imaged with an 800-nm long pass filter set allowing all wavelengths above 800 nm to reach the camera. Autofluorescence in the 600–750 nm range is so intense that the labelled cells (three indicated with red stars in A) cannot be differentiated from unlabelled neighboring cells. (C and D) NIR QD labeled cells break free from their neighbors and become interspersed within non labelled regions and can be visualized through the pigmented animal cap. (E–H) Four frames from a time-lapse movie of an embryo injected at the DMZ (yellow star) at the four-cell stage with NIR QD's. The mesodermal front becomes clearly visible as it moves towards the top of the blastocoel (red star). (I–L) Four frames from a time-lapse movie of an embryo injected with cell tracker QD's at early gastrula. The Qtracker QD's were injected into the blastocoel cavity. Using this approach QD's labelled vegetal pole cells (not visible) and the mesodermal belt (DMZ yellow star, top of the BCR red star, VMZ green star). (M–P) Injection of NIR QD's at both the DMZ (yellow star) and VMZ (green star) enables visualization of the mesodermal mantle closure (DMZ yellow star, top of the BCR red star, VMZ green star). Adopted from (Stylianou and Skourides 2009).

The full potential of QDs is yet to be realized however because of limitations related to their relatively large size (typically 20-30nm for biocompatible red-emitting QDs) (Michalet, Pinaud et al. 2005), multivalency and the inability to genetically encode them. The first two issues have been resolved to a large extent with the synthesis of new types of QDs with much smaller hydrodynamic radii (Liu, Choi et al. 2007) and monovalent nanocrystals (Howarth, Liu et al. 2008). The third issue remains elusive and therefore addressed in this work using a simple intein-based method that allows the site-specific conjugation of QDs to any protein target *in vivo*, effectively overcoming the requirement to genetically encode QDs for tagging target proteins. In addition, this approach can be used to conjugate other nanostructures or nanodevices to target proteins and as a result to any intracellular compartment or protein signalling complex within the cell.

1.2.2 Conjugation of QDs for specific tagging of proteins

Existing methods of QD-protein conjugation generally use either random chemical coupling with reactive amino acids (e.g. –NH2, -COOH, -SH) on the protein surface or non-covalent complexation mediated by electrostatic interactions and ligand-recognition. A survey of site-specific bioconjugation methods led us to the intein-mediated ligation system.

Inteins are polypeptide sequences that are able to self-excise, rejoining the two flanking extein sequences by a native peptide bond (Easterling, Styblo et al. 2002; Evans and Xu 2002; Giriat and Muir 2003; Muralidharan and Muir 2006). Inteins have been found in a number of homologous genes from phylogenetically diverse species. They were found in the yeasts *Saccharomyces cerevisiae (Kane, Yamashiro et al. 1990)* and *Candida tropicali (Gu, Xu et al. 1993)*, the mycobacteria *Mycobacterium tuberculosis (Davis, Jenner et al. 1992)* and *Mycobacterium feprae* (Davis, Thangaraj et al. 1994) and extreme thermophile archaebacteria *Thermococcus litoralis (Hodges, Perler et al. 1992)* and *Pyrococcus* species strain GB-D (Xu, Southworth et al. 1993). Inteins were first identified in TFP1 gene of *S. cerevisiae*, which encodes a vacuolar H^+-ATPase. The open reading frame sequence of the gene encodes 1071 amino acids, an 119 kDa protein, but when the protein was detected

in SDS-PAGE it appeared in molecular weight of 69 kDa (Figure 13) (Kane, Yamashiro et al. 1990). The VMA1 gene of *S. cerevisiae,* encoding the catalytic site for ATP hydrolysis in the vacuolar membrane H^+-translocating adenosine triphospahatase, has proven the same since the nucleotide sequence predicts to encode a 118 kDa protein, which is no longer than 67 kDa in SDS-PAGE gels. The N- and C-terminal are highly homologous to the H^+-ATPases of other organisms, but the internal region containing 454 amino acids, has no sequence similarities to them. This region was present in the final mRNA but was excised after translation and it is similar to a yeast endonuclease (Hirata, Ohsumk et al. 1990).

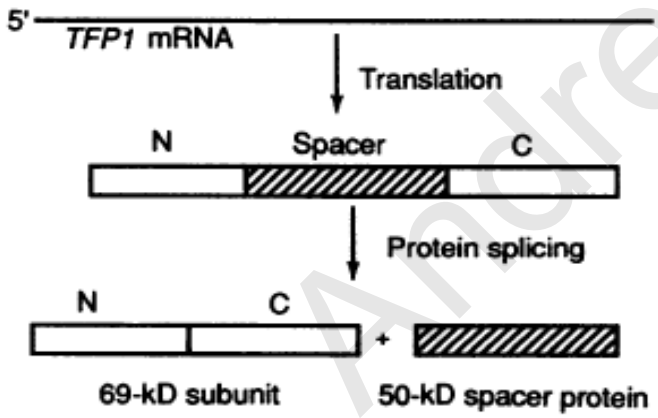

Figure 13 : Schematic representation of the TPF1 gene product to form the 69 kDa and 50 kDa products. Adopted from (Kane, Yamashiro et al. 1990).

Protein splicing is an autocatalytic process that takes place after translation. In this process an internal part, called intein is excised from the pre-mature protein. The protein regions before and after the intein are called exteins. These names have arise from INternal proTEIN and EXternal proTEIN (Perler, Davis et al. 1994). The N-extein is the N-terminus and the C-extein the C-terninus of the protein. These regions are fused after the intein excision with a peptide bond, without any enzymes or other factors. When this process finishes the mature protein and the intein are formed (Perler, Davis et al. 1994; Saleh and Perler 2006; Elleuche and Poggeler 2010).

This process is composed of four nucleophillic attacks, mediated by three of the four conserved residues in the splice junctions. The first step forms a thioester bond at the N-

extein/intein junction. The second step leads to a transesterification, which transfers the N-extein to the side-chain on the first residue of the C-extein. The third step is the cyclization of the conserved Asparagine residue at the C-terminus of the intein releases the intein and links the exteins by thioester bond. In the fourth step, a rearrangement of the thioester bond to a peptide bond occurs by a spontaneous S-N or O-N acyl shift and finally the last amino acid of Intein transforms to Asparagine through hydrolysis of the product (Figure 14) (Saleh and Perler 2006; Elleuche and Poggeler 2010; Tori, Dassa et al. 2010).

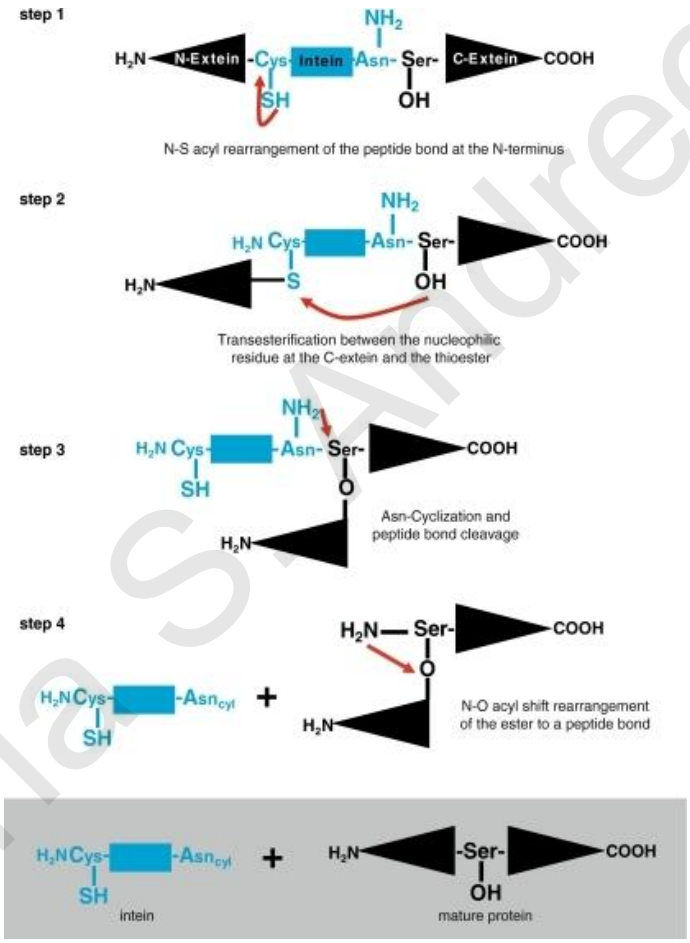

Figure 14 : The splicing mechanism of inteins takes place in four steps. Adopted form (Elleuche and Poggeler 2010).

Nearly 200 intein and intein-like sequences have been found in a wide variety of host proteins and in microorganisms belonging to bacteria, archaea and eukaryotes (Perler 2002). Inteins share only low levels of sequence similarity but they share striking

similarities in structure, reaction mechanism and evolution (Saleh and Perler 2006). It is thought that inteins first originated with just the splicing domain and then acquired the endonuclease domain, with the latter conferring genetic mobility to the intein (Perler 2002).

However, during intein evolution some inteins lost sequence continuity and are found in a form called split inteins, in which the intein of the precursor protein comes from two genes. The reaction of the split inteins may occur in trans with the intein and host protein split in two. After translation of the two genes, the two intein parts ligate their neighboring protein parts to each other, producing the mature protein (Caspi, Amitai et al. 2003). The DnaE protein of *Synechocystis* sp. PCC6803 is encoded by a split gene interrupted by intein sequences and the products of the split DnaE gene can undergo protein *trans*-splicing to form an intact DnaE protein (Wu, Hu et al. 1998). There are many kinds of naturally found split inteins and others that may be chemically produced and they consist a valuable tool in biotechnology (Wu, Hu et al. 1998; Saleh and Perler 2006).

In conclusion, inteins catalyze the splicing reaction through formation of an active thioester intermediate and have been widely used for *in vitro* protein semi-synthesis (Giriat and Muir 2003), segmental isotopic labelling (Zuger and Iwai 2005) and *in vivo* protein cyclization (Scott, Abel-Santos et al. 1999). In this case we will use the DnaE split intein to site-specifically conjugate QDs to the C-terminus of the PH domain of Akt and Btk, in vivo in a vertebrate embryo to label proteins with QDs.

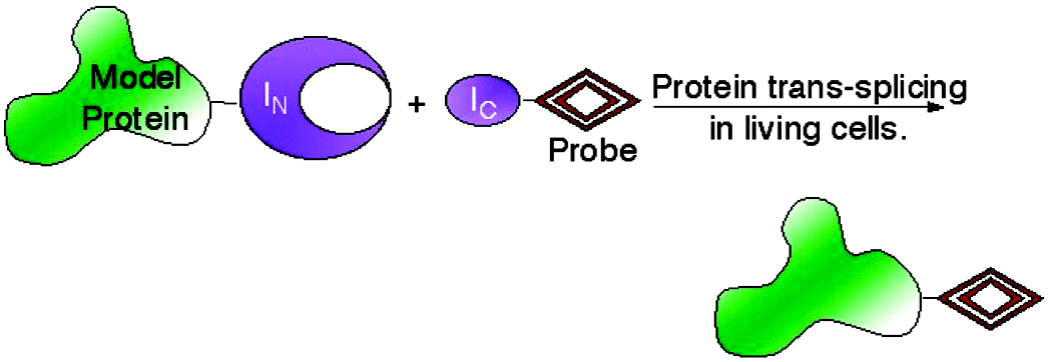

Figure 15: Intein-mediated ligation system. A protein was genetically tagged with one-half of a split intein and the other half was linked *in vitro* to the synthetic probe. This fusion had been delivered into cells using a transduction peptide. The association of the intein halves in the cytosol, triggers protein trans-splicing, resulting in the ligation of the probe to the target protein through a peptide bond. Adopted from (Giriat and Muir 2003).

We selected to illustrate the method by fusion of the Pleckstrin-homology (Musco, Stier et al.) domains of two proteins Akt and Btk with the N-terminus half of a split intein (I_N). These proteins were found to show growth-factor-stimulated and wortmannin-sensitive translocation from the cytosol to the plasma membrane in several cell types, indicating their ability to recognize PIP_3 (Figure 16) (Varnai, Bondeva et al. 2005). They were chosen due to their ability to translocate to the cell membrane upon PIP_3 production by PI_3-K (Varnai, Bondeva et al. 2005) and would thus provide a clear visual confirmation of the conjugation in the intact embryo. Previous studies have reported that UVB irradiation induces Akt activation and consequent translocation to the plasma membrane via a PI-$_3$K/PDK dependent pathway as well as via Erks and p38 kinase through their downstream kinase, mitogen and stress-activated protein kinase Msk1(Kabuyama, Hamaya et al. 1998; Nomura, Kaji et al. 2001).

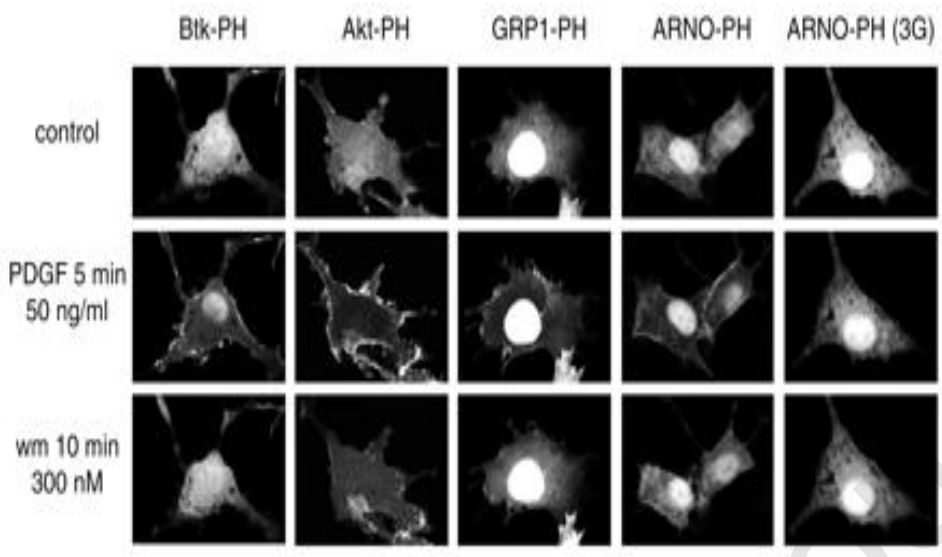

Figure 16 : Localization and wortmannin-sensitive translocation of expressed PH-GFP chimeras that recognize PIP_3 in NIH 3T3 cells. PH domains travel to the plasma membrane after PDGF stimulation and after the treatment by the PI 3-kinase inhibitor wortmannin this was reversed. Adopted from (Varnai, Bondeva et al. 2005).

The complementary C-terminus half of the intein (I_C) will be biotinylated and conjugated *in vitro* to streptavidin-coated QD's. QDs conjugated to streptavidin are able to bind with high affinity and specificity to proteins biotinylated under physiological conditions (Howarth, Takao et al. 2005). After that the Intein-QD conjugate will have to be injected to the *Xenopus laevis* blastomeres together with the GFP-PH-I_N mRNA. The mRNA will be translated into protein and *in vivo* intein-splicing should result in fully functional QD-PH (Figure 17) conjugates that could be monitored in real time within live embryos.

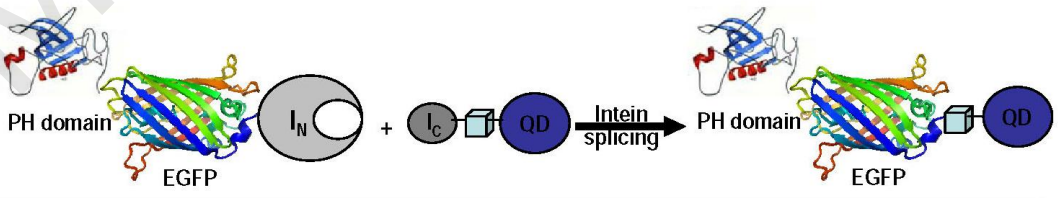

Figure 17 : Schematic representation of site-specific intein-mediated conjugation of QD's to target protein.

1.3 RNA-binding proteins

The RNA-binding proteins have very important roles during important cell procedures. They are regulating significant processes like transcription, RNA splicing, polyadenylation, mRNA stability, mRNA localization and translation (Curtis, Lehmann et al. 1995; Johnstone and Lasko 2001). RNA-binding proteins usually bind regulatory sequences that are located in the 5'UTR or the 3'UTR or on both sites of the mRNAs in order to promote them for post-transcriptional regulation (Schisa, Pitt et al. 2001).

The first RNA-binding proteins that have been described were the heterogeneous nuclear ribonucleoproteins (hnRNPs) that play important roles in different posttranscriptional processes. The first evidence for the existence of hnRNP complexes came into view in chromosome loops consisted of particles connected by thin strands, while looking at lampbrush chromosomes in amphibian oocytes, (Gall 1956). These thin strands and particles were shown to be hnRNA (pre-mRNA) and RNPs, respectively (Sommerville and Scheer 1981) . Using electron microscopy they have shown that hnRNP complexes are similar to the model for the packaging of DNA by histones (Miller and Bakken 1972).

In general, hnRNPs are proteins that bind hnRNAs and facilitate their interaction with other components that are necessary for the pre-mRNA processing. These hnRNP complexes in vertebrate cells consist of more than 20 proteins (Pinol-Roma, Choi et al. 1988). The presence of different hnRNPs in the same cell compartments shows that they are involved in the same procedures and also share the same structural features (Dreyfuss, Matunis et al. 1993).

1.3.1 hnRNPs structure

hnRNPs consist of multiple domains that have specific roles for each hnRNP. These proteins have at least one RNA binding motif and an auxiliary domain, which regulate the protein-protein interactions and subcellular localization. There are three known RNA-binding motifs, the RNP consensus sequence–RNA-binding domain (RNP-CS-RBD), also known as RNA recognition motif (Glinka, Herrmann et al.) (Ziegler, Liddington et al. 2006), the RGG (Arg-Gly-Gly) boxes (Kiledjian and Dreyfuss 1992) that may also play another role

besides RNA binding and the K-homology domain (Burd and Dreyfuss 1994). The auxiliary domains are divergent in protein sequence that mediate functional specificity and the best characterized are those of the hnRNP A/B group (Weighardt, Biamonti et al. 1996).

Some of the known hnRNPs share the same RBD that is approximately 90 amino acids and contains a central residue of 8 aromatic and positively charged amino acids (Swanson, Nakagawa et al. 1987). That domain is characterized by β_1-α_1-β_2-β_3-α_2-β_4 structure (Hoffman, Query et al. 1991) (Figure 18). The RRM contacts RNA using the RNP-1 consensus sequence which is present on the β_3 sheet and the RNP-2 sequence which is on the β_1 sheet with hydrophobic interactions and bind single stranded nucleic acids in a non sequence specific manner (Liker, Fernandez et al. 2000; Perez-Alvarado, Martinez-Yamout et al. 2003). Furthermore, the β_2 and β_4 strands, the linker regions, the C- and the N-termini of the RRM are responsible for the high affinity binding of specific sequences in many proteins. The C-terminus is also responsible of differentiating RNA from DNA by interacting with the –OH group of the sugar ring (Allers and Shamoo 2001) and can also inhibit or enhance the RNA binding affinity of the protein (Mazza, Segref et al. 2002).

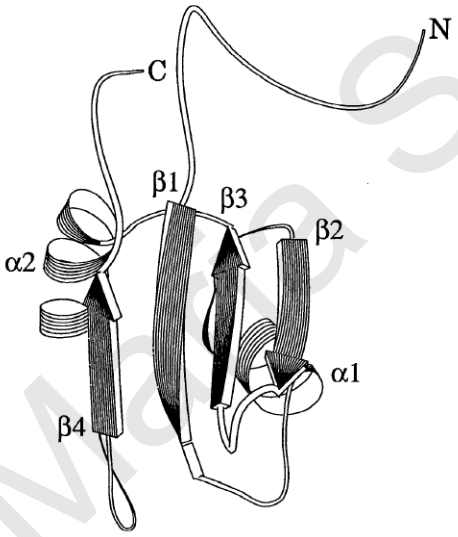

Figure 18 : Schematic drawing of the hnRNP C RRM (residues 2-94). The arrows show the β-sheet and the curled ribbons are the α-helices (Hoffman, Query et al. 1991; Wittekind, Gorlach et al. 1992).

As mentioned before, some hnRNPs do not contain RRMs but still bind RNA via other sequences like the K-homology (Mikheev, Mikheev et al.) domain, the quasi-RRMs (qRRMs) and the Glysine-rich domain (GRD or RGG). The KH domain is an approximately 70 amino acid domain that has a β_1-α_1-α_2-β_2-β'-α' structure and binds nucleic acids in the gap between the b-sheet and the a-helices and can only bind four bases in this narrow channel (Musco, Stier et al. 1996; Jensen, Musunuru et al. 2000). The qRRMs contain an extra β_3' loop compare to classic RRMs and lack the RNP motifs (Simpson, Monie et al. 2004; Dominguez and Allain 2006).

Glycine-rich domains (GRDs) have diverse functions that usually depend on the additional amino-acids that are present in these regions. The GRD or the RGG box is a 26 amino acid peptide that contains Arg-Gly-Gly (RGG) repeats and aromatic residues and has a positive charge to bind nucleic acids (Kiledjian and Dreyfuss 1992). GRD domain has been shown to be required for self-interaction of hnRNP A1 (Cartegni, Maconi et al. 1996), to be essential for the splicing activity of hnRNP A1 (Mayeda, Munroe et al. 1994) and to contain non classical nuclear localization signal and promote nucleocytoplasmic shuttling and nuclear import through an interaction with transportin 1 in the case of hnRNP H/F (Van Dusen, Yee et al. 2010). The number and the spacing between the RGG repeats vary in different proteins (Kiledjian and Dreyfuss 1992) and has also been shown that the GRD domains of different hnRNP are involved in protein-protein interactions and they are responsible for the localization of the proteins (McNally, Yee et al. 2006). Furthermore, the RGG domain of GRDs has been shown to bind proteins that are responsible for the transport into the nucleus (Burd and Dreyfuss 1994) and in some cases promotes nuclear localization in a manner that is regulated by arginine methylation like in the case of hnRNP A2 (Schaeffer, Bardoni et al. 2001). In general, GRDs may have various functions that primarily depend on the few additional amino acids in the region and are required for regulation of a specific set of RNA targets or implicated in posttranslational modifications.

Auxiliary domains are widely divergent and the amino acid sequence of these domains is not conserved, although they are often enriched in some amino acids like glycines, glutamine, glutamine, proline and RS dipeptides (Burd and Dreyfuss 1994; Ziegler,

Liddington et al. 2006). Also some certain RBP auxiliary domains have features that are found in the activating site of transcription factors (Kamada and Miwa 1992). In addition to these, auxiliary domains have been shown to mediate protein-protein interaction, contribute to RNA binding and modulate RNA conformation and also determine the intracellular localization of the protein (Pinol-Roma and Dreyfuss 1991; Portman and Dreyfuss 1994). Therefore, there are different hnRNPs and they vary in domain composition (Figure 19). Their biological functions depend on these domains, since these are responsible for each function.

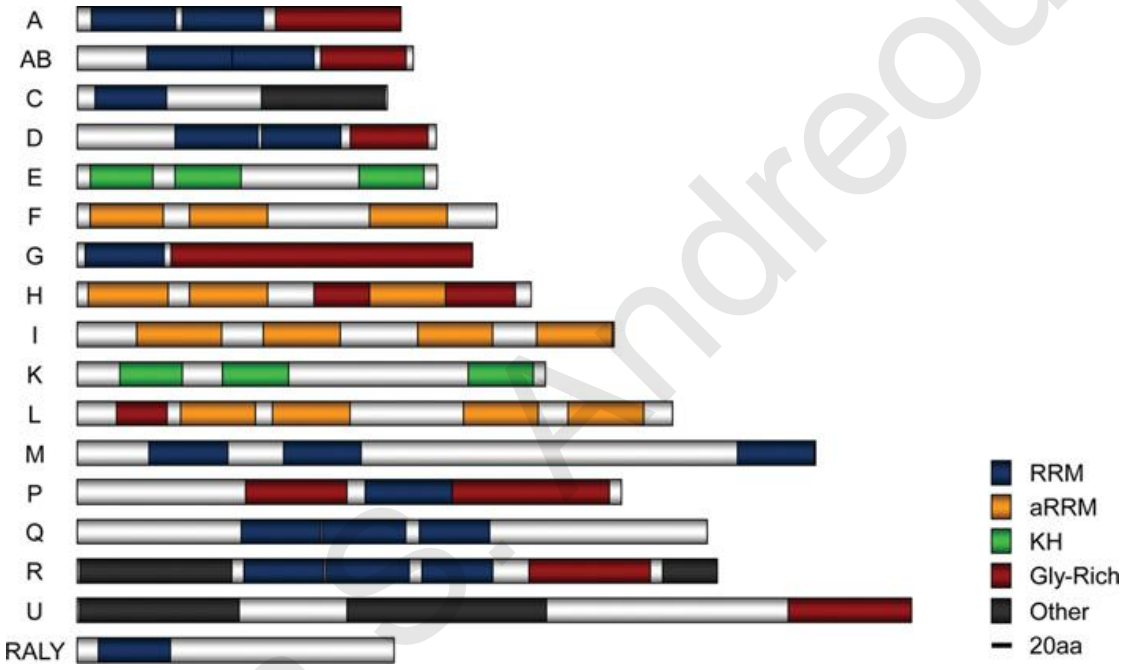

Figure 19: Known hnRNP structures. Adopted from (Han, Tang et al. 2010)

1.3.2 The role of the hnRNPs

hnRNPs were first characterized for their role in mRNA packing, but they also function in many processes that regulate gene expression. They have different functions during cell cycle (Figure 20). They participate in every step of the mRNA processing in the nucleus and the cytoplasm. They also contribute in the telomere maintenance, chromatin remodeling and DNA repair. Different hnRNPs may have overlapping roles and also they may interact or co-operate with other proteins. Therefore hnRNPs have generalized roles

like RNA packing proteins and specialized roles that depend on specific RNA-protein or protein-protein interactions (Mili, Shu et al. 2001; Venables, Koh et al. 2008).

hnRNPs are mostly localized in the nucleus but some of them shuttle between the nucleus and the cytoplasm. Some others are membrane bound receptors (Mizutani, Fukuda et al. 2000; Bajenova, Stolper et al. 2003) and some others like hnRNP Q are mainly localized in the cytoplasm (Mizutani, Fukuda et al. 2000). Some hnRNPs are found in mRNA granules and regulate mRNA trafficking (Shan, Munro et al. 2003). In that case the hnRNP-A2 is co-localized with RNA and it seems like it is forming the granules to carry RNA far to the neurites of the dendritic cell. Consequently hnRNP localization depends on function.

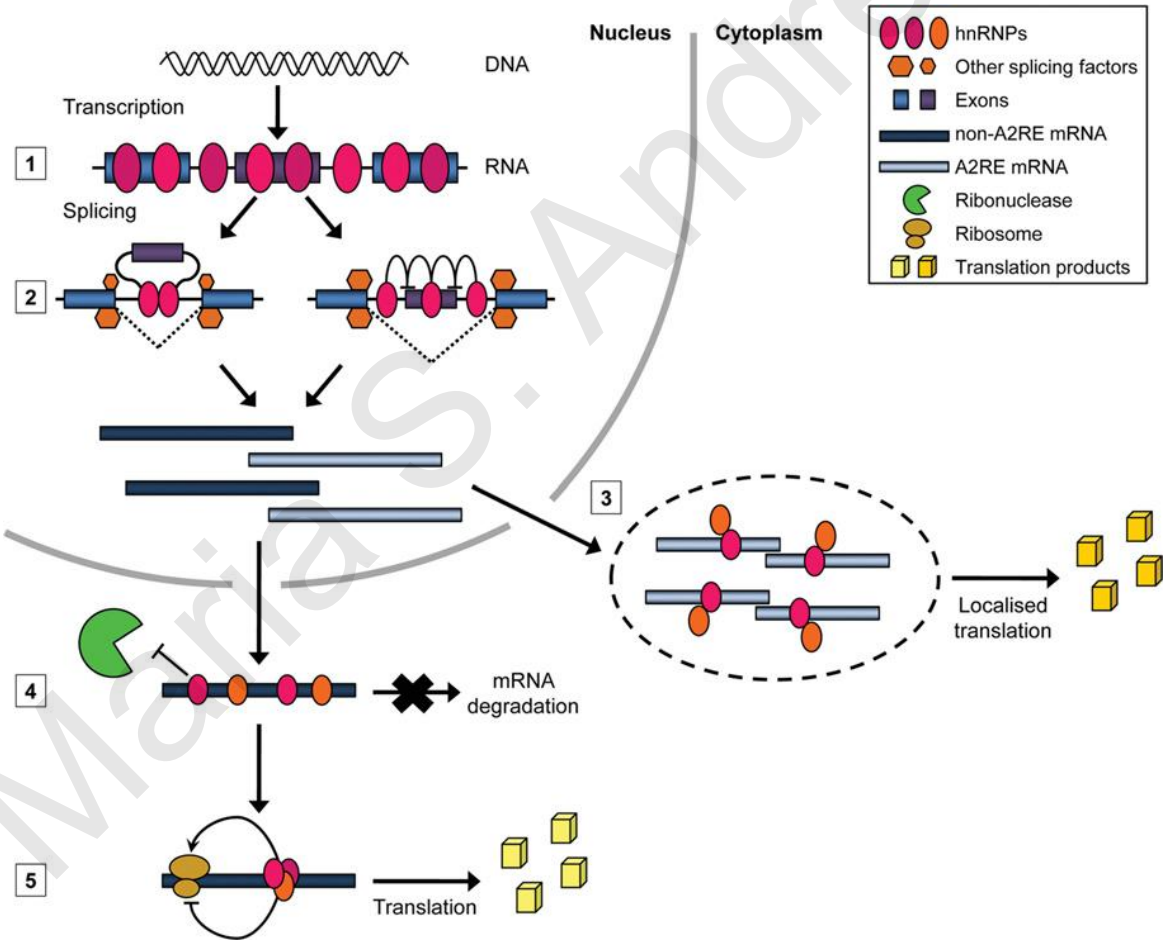

Figure 20 : Nuclear and cytoplasmic functions of hnRNPs. Adopted from (Han, Tang et al. 2010)

hnRNPs and cell cycle

During cell division the nuclear envelope breaks down and the hnRNP complexes scatter throughout the cell. hnRNP´s move to the cytosol and are excluded from the condensed chromatin until mitosis is completed and the nuclear envelope forms again (Lahiri and Thomas 1985; Leser and Martin 1987; Pinol-Roma and Dreyfuss 1991). At this stage the hnRNP complexes disassemble and hnRNP proteins return back to the nucleus independently (Pinol-Roma and Dreyfuss 1991). The independent return of the proteins back to the nucleus reveals the existence of two different models of nuclear localization, an early transcription-independent (proteins C) and a late transcription-dependent (protein A1) mode and both processes appear to be normal for nuclear assembly after mitosis. Proteins that have been previously described to show transcription-independent localization, contain classical nuclear localization signals (NLSs) and it is likely they use similar mechanisms for nuclear import like other proteins with similar types of sequences (Dingwall and Laskey 1991; Nigg, Baeuerle et al. 1991). The transcription-dependent localization is a new way of nuclear localization of proteins, and sequences within these proteins that mediate their nuclear targeting and localization are subjects of intense investigation. Studies in mitotic cells revealed a role for RNA polymerease II in hnRNP localization (Pinol-Roma and Dreyfuss 1991). In addition to this, the reassertion of hnRNPs in the nucleus during interphase is also dependent on transcription, since inhibitors of RNA pol II do not allow to hnRNPs to return back into the nucleus (Pinol-Roma and Dreyfuss 1992).

hnRNPs in neural development

It is known that RNPs play important roles in neural plasticity and development (Perrone-Bizzozero and Bolognani 2002; Si, Giustetto et al. 2003; Yao, Sasaki et al. 2006). hnRNP K is expressed in the nervous system. It binds to the 3' UTR of *middle neurofilament* (*NF-M*) mRNA, together with other RNPs including HuB, hnRNP E1 and E2 (Antic, Lu et al. 1999; Thyagarajan and Szaro 2004). It is thought to be a part of mRNP complex that provide a mechanism to control cell fate (Schnolzer, Alewood et al. 1992). It has been shown that

hnRNP K knockdown blocked axonal outgrowth and inhibited the translation of NF-M (Liu, Gervasi et al. 2008).

In neural cells, it has been shown that certain RNAs are targeted to dendrites via a specific RNA trafficking pathway called the A2 pathway. This pathway is mediated by hnRNP A2, which binds to an 11 nucleotide sequence, called A2 response element (A2RE) or RNA trafficking sequence (Gingras, Vogel et al.) (Kroll, Zhao et al. 2002). RNAs containing this sequence are recognized by hnRNP A2, in the nucleus and are exported to the cytosol where they form granules containing components of the translational machinery and molecular motors, to move along the microtubules to specific sites where the encoded protein would be translated (Kress, Yoon et al. 2004). During the transport of the mRNAs in the granules translation is suppressed and when the granules reach the targeted sites of myelin synthesis in oligodentrocytes (Kroll, Zhao et al. 2002) and to sites of synapse formation in neurons, translation is activated (Huang, Carson et al. 2003). hnRNP E1 has been shown to repress translation of A2 response element containing mRNAs in dendrites within neurons during neuronal development and when the granule reaches its destination, hnRNP E1 dissociates from the granule and translation is activated (Ostareck-Lederer and Ostareck 2004; Kosturko, Maggipinto et al. 2006). It has also been shown that hnRNP E1 functions with other proteins to induce translational stimulation (Pickering, Mitchell et al. 2003).

hnRNP R has been found at high concentrations in axons and axonal growth cones of motor neurons (Rossoll, Kroning et al. 2002). It interacts directly with the 3'UTR of β-actin mRNA and is necessary for axonal translocation of β-actin (Rossoll, Kroning et al. 2002; Glinka, Herrmann et al. 2010). Downregulation of the protein in zebrafish leads to severe disturbance of axonal elongation (Glinka, Herrmann et al. 2010).

In addition to this, previous studies have shown that hnRNP Q1 was expressed in hippocampal neurons. hnRNP Q1 formed mRNA granules containing proteins like inositol 1,4,5-trisphosphate receptor type 1 (IP_3R1) to target dendrites of central nervous system neurons in a microtubule depended manner (Gingras, Vogel et al. 2006). hnRNP Q1 is one of the three alternative splice variants (hnRNP Q2 and Q3) and is localized in the cytosol

instead of the nucleus and also has high homology with hnRNP R (Mizutani, Fukuda et al. 2000; Mourelatos, Abel et al. 2001). The expression of hnRNP Q is developmentally regulated and plays important role in neural development (Mizutani, Fukuda et al. 2000).

Moreover, there are clearly numerous studies consistent with a role for the murine hnRNP AB in regulating gene expression in the brain. Different hnRNP AB orthologs when overexpressed have lead to defects in the developing nervous system (Dichmann, Fletcher et al. 2008; Yan, Skourides et al. 2009). *In situ* hybridization screen of RNA-binding protein expression in newborn mouse heads show enrichment in the neural tissue (McKee, Minet et al. 2005) and in adult mice elevated levels of hnRNP AB mRNA are observed in the mature brain using *in situ* hybridization (Rushlow, Rajakumar et al. 1999). In addition, there have been reports that hnRNP AB plays a role in neural stem cell maintenance, differentiation and cell survival and that the subcellular distribution of the protein isoforms changes during neuronal maturation, suggesting that it has a role in regulating gene expression during neural development (Sinnamon, Waddell et al. 2012).

1.3.3 hnRNP A/B Subgroup

The hnRNPs are split into several categories depending on their domains. The hnRNP A/B group includes A1, A2/B1, A3 and A0 and its members are involved in RNA processing. hnRNPs A/B and C package transcripts in a non-sequence specific manner (Huang, Rech et al. 1994).

40LoVe has been categorized as one of the three hnRNP D family proteins in *Xenopus* (Czaplinski, Kocher et al. 2005). The family members have an N-terminal region, two central RRMs (RRM1 and RRM2), a glycine-rich domain and a conserved region responsible for the nucleoplasmic transport and binding to the nuclear import receptor Transportin (Kawamura, Tomozoe et al. 2002). The glycine-rich domain has an N-terminal area that contains multiple arginine and lysine residues (RGG box) and a C-terminal part that is rich in tyrosines and glycines (GY-rich).

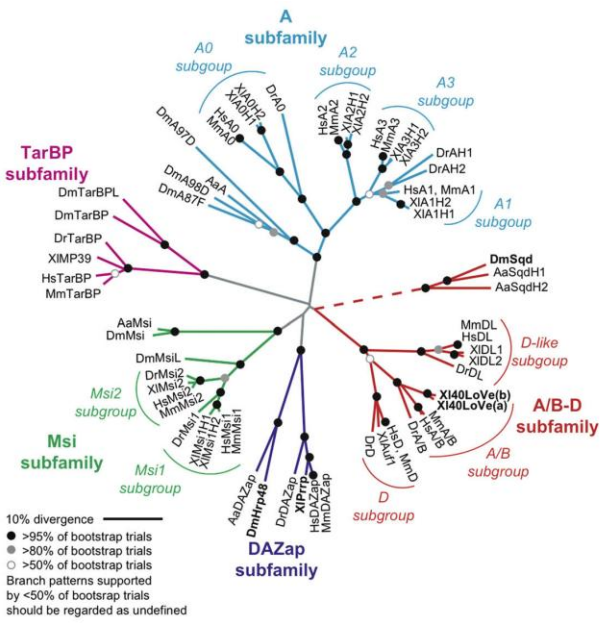

Figure 21: Phylogenetic analysis of selected 2·RBD hnRNP proteins. Adopted from (Kroll, Swenson et al. 2009)

However, 40LoVe is also closely related to the hnRNP A/B family. To determine the precise classification of 40Love a phylogenetic tree has been constructed (Figure 21). There are at least five subfamilies of 2 x RBD type hnRNPs conserved from vertebrates to invertebrates. In this phylogenetic tree is shown that 40LoVe is a member of the A/B subgroup of the A/B-D subfamily. This classification is important because the proteins in hnRNP A/B family are responsible for RNA localization and that seems to be conserved in many species and cell types (Kroll, Swenson et al. 2009). This way information may be extracted about unknown roles for new hnRNPs.

The A/B family of hnRNPs has a wide range of roles in cellular events. They are involved in RNA processing and trafficking, cell senescence, translational regulation, cell cycle regulation, stress response and miRNA processing. When they are in the nucleus they pack pre-mRNA and they are also involved in splice site selection, transcription regulation, telomere maintenance, DNA replication and splicing regulation (Han, Tang et al. 2010).

1.3.3 40LoVe

Localization of mRNAs in the cytoplasm is critical for protein localization. There are different mechanisms of mRNA transport and localization in the cytoplasm and many molecules are responsible for mRNA transport in different cell compartments. mRNA localization often requires the assembly of RNP compartments in the cytoplasm. 40LoVe is an hnRNP that is a part of these compartments and it was previously shown to be involved in mRNA localization during oogenesis (Czaplinski, Kocher et al. 2005).

A later study, revealed that the 40LoVe clone previously characterized by Czaplinski et al. is different than the one Kroll et al. identified by in vitro binding assay (Czaplinski, Kocher et al. 2005; Kroll, Swenson et al. 2009). Kroll et al. have determined that 40LoVe and their clone are encoded by distinct genes, each one represented in the EST databases, indicating that both genes are functional (Kroll, Swenson et al. 2009). Kroll et al. noted that this new clone is the one that can be crosslinked to Vg1 mRNA, confirming this result using a pull down assay (Kroll, Swenson et al. 2009).

Vg1 was the first localized RNA that was identified (Rebagliati, Weeks et al. 1985). It is encoding for transforming growth factor β (TGF-β) homolog from *Xenopus laevis* eggs and it is implicated in mesoderm and endoderm specification. During oogenesis, Vg1 is restricted to the vegetal site of the oocyte's cytoplasm and then it is inherited to the vegetal cells (Weeks and Melton 1987). There are localization elements (LE) that are located within the 3'UTR and form part of larger multifunctional RNA domains (Dalgleish, Veyrune et al. 2001). These appear to participate in the formation of RNP complexes responsible for posttranslational modifications (Hilleren and Parker 1999). The transportation and anchoring of the Vg1 mRNA requires a 3'UTR and it is called Vg1 localization element (VLE) (Mowry and Melton 1992). The *Xenopus* VLE has been shown to interact with six different RNA binding proteins. Furthermore an A:U rich sequence located downstream of the VLE, mediates translational repression and it is called Vg1 translational element (VTE) (Otero, Devaux et al. 2001). When the Vg1 mRNA has to be translated, this region has to be removed by cleavage/polyadenylation (Kolev and Huber 2003). Vg1 mRNA interacts with several proteins during its transportation. When the Vg1 mRNA is transcribed and is still in the nucleus, its VLE binds 40LoVe (Czaplinski, Kocher et al. 2005). This recruitment depends on other trans-acting factors, like VgRBP60/hnRNP I (Kress, Yoon et al. 2004), Vg1RBP/Vera (Deshler, Highett et al. 1998) and nuclear factors. When the complex moves to the cytoplasm, it binds the Proline rich RNA binding protein (Prrp) (Kroll, Swenson et al. 2009) and XStaufen (Allison, Czaplinski et al. 2004; Yoon and Mowry 2004). XStaufen binds the motor proteins kinesin-1 and kinesin-2 and that maybe is responsible for the active transport of the RNP complex (Yoon and Mowry 2004). Prrp binds directly on the VLE but also interacts with 40LoVe and VgRBP60 that may be involved in their recruitment. Higher affinity of 40LoVe to Prrp occurs only when other

ligands are bound together so that the interaction domain becomes fully exposed. It has been shown that 40LoVe binds the VLE and VTE RNAs with very low affinity like any other mRNA, but the association of the protein requires interactions with other proteins that bind the VLE with high specificity (Kroll, Swenson et al. 2009).

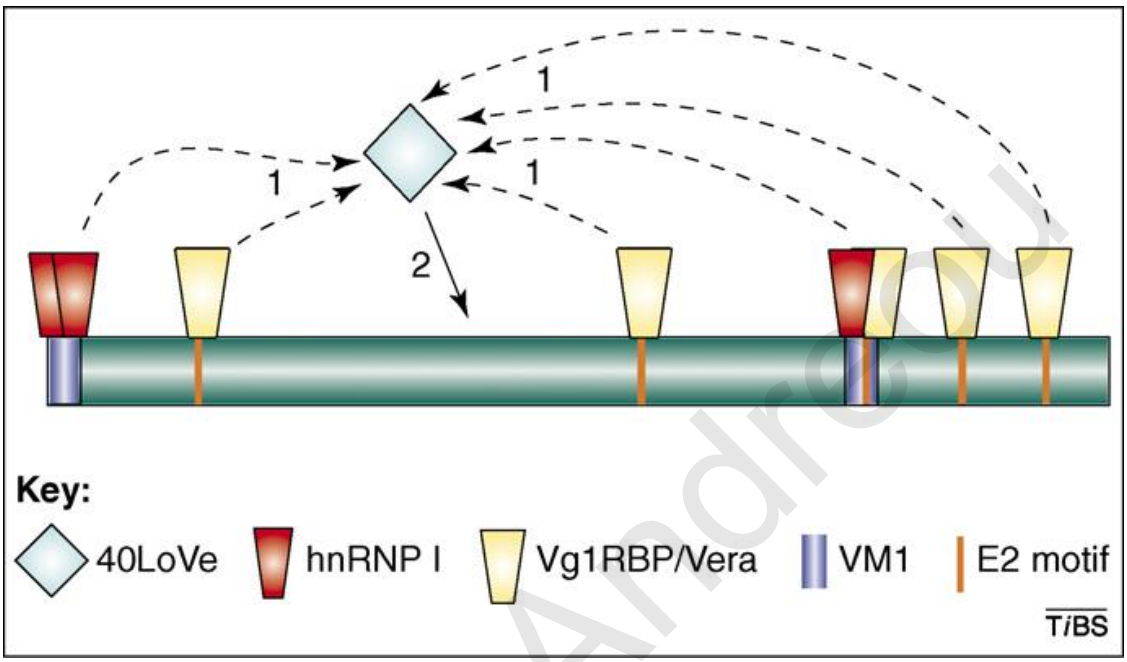

Figure 22: The VLE of Vg1 mRNA. The LE is depicted in green; the motifs that have been identified as required for localization are highlighted, as are the trans-acting factors that are known to bind these sequences. The binding of 40LoVe (pale blue diamond) to an unidentified site occurs after previous recognition of the Vg1 LE by the RNA binding proteins hnRNP I and Vg1RBP/Vera (as indicated by the numbered arrows). Adopted from (Czaplinski and Singer 2006).

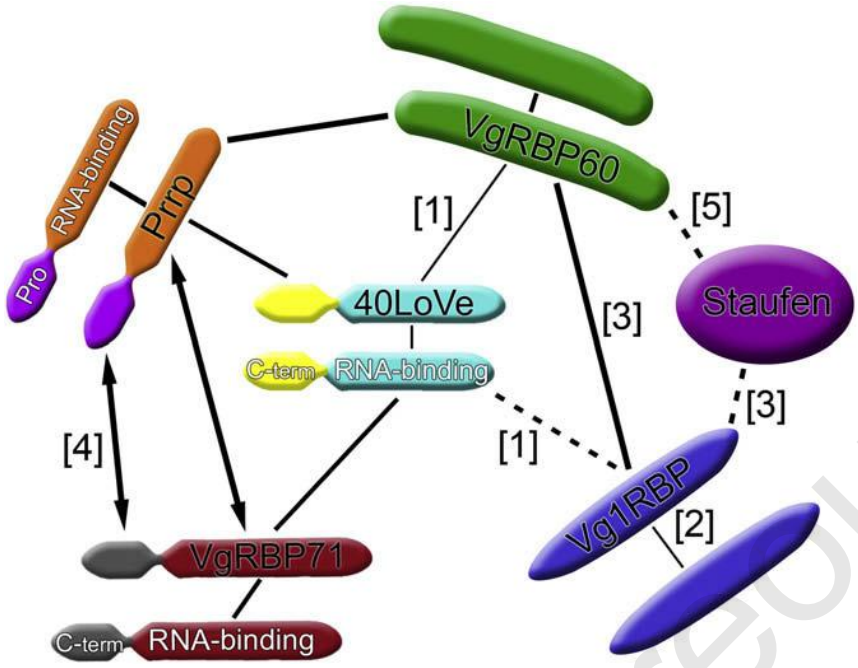

Figure 23: Summary of protein–protein interactions in the Vg1 localization RNP complex. The weight of the lines indicates the apparent strength of the protein–protein interaction (in two-hybrid assays only), with thicker lines representing stronger contacts. Single-headed arrows indicate that the protein at the tail interacts with the specific region of the protein located at the head. Double-headed arrows indicate that the specific regions of the proteins interact with each other. Dashed lines represent reported interactions that may be indirect. Numbers refer to the following citations: [1] (Czaplinski and Mattaj 2006); [2] (Git and Standart 2002); [3] (Kress, Yoon et al. 2004); [4] (Kroll, Zhao et al. 2002); [5] (Yoon and Mowry 2004). Adopted from (Kroll, Swenson et al. 2009).

A previous study showed the presence of three isoforms of 40LoVe in the oocyte and in all adult tissues (Czaplinski and Mattaj 2006). These isoforms were present in all nucleoplasmic compartments of the oocyte. They are present in the nucleus and in the cytoplasm but they are differently distributed between the compartments. The three isoforms do not derive from post-translational modifications like methylation and phosphorylation. Six splice variants of 40LoVe were found in the EST database that had small differences in size. The presence of 40LoVe splice variants has been confirmed by Reverse-Transcriptase PCR (RT-PCR) and by the presence of three proteins with small differences in size in Western Blots. They suggest that these different isoforms originate from alternative splicing as shown for other hnRNPs (Kroll, Swenson et al. 2009).

1.3.4 SAMBA

Samba is an hnRNP that was recently identified from an early gastrula (stage 10) *Xenopus laevis* library. Samba cDNA encodes a 313 amino acid protein with a calculated molecular weight of 34kDa. After sequence analysis it was shown that Samba has two RRM domains and a glycine rich carboxyl terminus. Samba is expressed maternally and its zygotic expression appears elevated at neurula stages. During gastrulation Samba is expressed in all embryonic tissues and is enriched at the dorsal and vegetal domains. At early neurula stages Samba is concentrated in the neural plate and as development proceeds it is localized in the neural and neural crest tissues. At tailbud stages it is restricted in neural and neural crest derivatives including the brain, the spinal cord, the eyes and the brachial arches (Yan, Skourides et al. 2009).

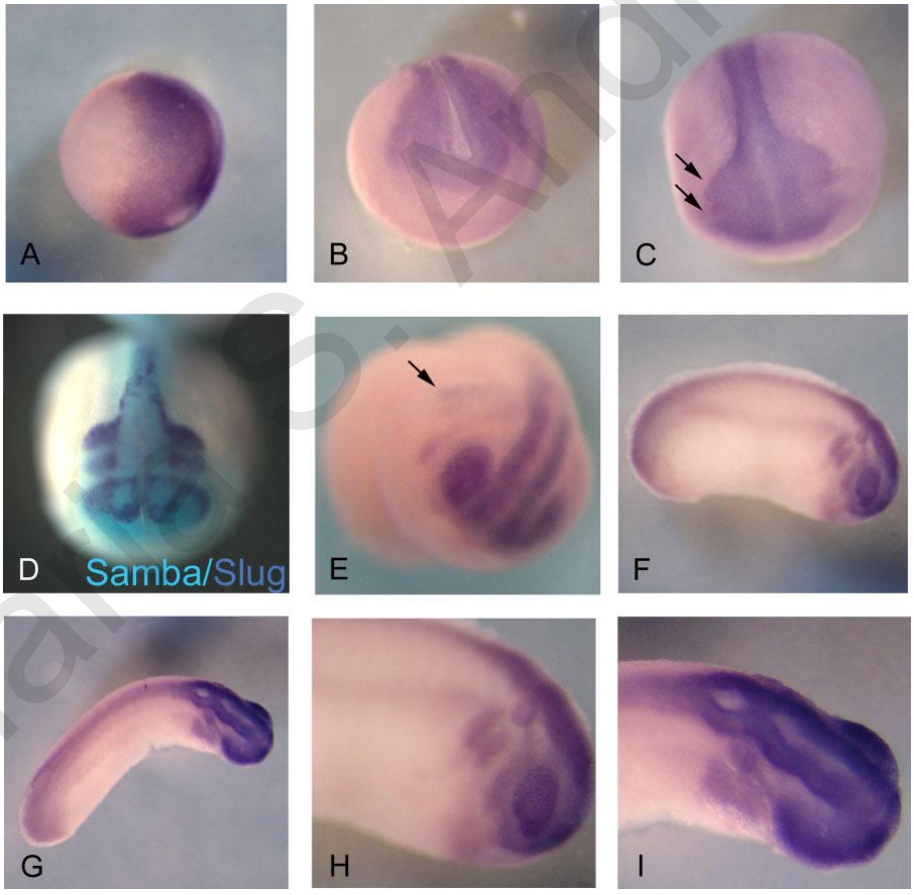

Figure 24 : Samba is expressed in the neural and neural crest derivatives as seen by in situ hybridization. A: Vegetal view of stage 10 embryos with dorsal side to the right. Samba expression is concentrated in the dorsal region. **B:** Neurula stage embryo. Samba is present in the

neural plate and crest domain. **C:** Anterior– dorsal view of late neurula stage embryo. Arrows point to the outer edge of the forming migratory crest domain, which expresses Samba. **D:** Double in situ for Slug and Samba show that Samba overlaps with Slug-expressing migrating streams but is not restricted to neural crest domain. Slug probe was developed with a violet stain and Samba with blue stain. **E:** Anterior-lateral view of tail bud stage embryo indicates that Samba is expressed in migrating lateral streams of crest cells (arrow) and optic vesicles. **F:** Lateral view of tailbud stage embryo showing that Samba remains in the crest cells, optic vesicle, and now appears in the otic vesicle as well. **G:** Dorsal view of a late tailbud stage embryo. **H,I:** Higher magnification of cranial expression in Figures F and G. Adopted from (Yan, Skourides et al. 2009).

It has been shown that overexpression of Samba affects neural and neural crest cell development. Overexpression of Samba does not appear to affect embryonic patterning but affects morphogenetic movements of a number of cell types. It has been shown that Samba inhibits activin induced animal cap spreading and affect crest cell migration (Yan, Skourides et al. 2009). Samba overexpression also blocks neural crest migration in a cell autonomous manner (Yan, Skourides et al. 2009).

1.3.5 hnRNP AB

hnRNP AB is also known as CBF-A (CArG box-binding factor A) in the mouse, since it is able to bind the CArG box DNA sequence (Kamada and Miwa 1992). hnRNP AB interacts with double-stranded DNA but with a lower efficiency than with single-stranded template. The RNP domains of CBF-A were involved in the interaction with DNA and both of them were needed for a high affinity interaction. These proteins' interaction with other proteins involves two separate interaction domains on CBF-A; the RNP domains and the carboxyl-terminal region. It is involved in transcriptional regulation and there is also evidence that this protein can influence gene expression through promoter binding (Leverrier, Cinato et al. 2000; Mikheev, Mikheev et al. 2000; Varnai, Bondeva et al. 2005). It was originally described as a repressor of transcription, while the region to which it binds in the SP6 k promoter is a positive control element (Kamada and Miwa 1992; Varnai, Bondeva et al. 2005). It can also bind to single-stranded DNA at the control elements for the transcriptional activation of the rat *spi*2 gene promoters (Leverrier, Cinato et al. 2000). The hnRNP AB protein is able to bind to double-stranded DNA at the response element

within the rat Ha-ras promoter (Mikheev, Mikheev et al. 2000). CBF-A also interacts with specific regions within the immunoglobulin *kappa* promoter. It is localized in the nucleus where it is bound on nucleophosmin by the N-terminal region of the protein and in the cytosol where is interacting with itself and to hnRNP H (Aranburu, Bennett et al. 2006). In contradiction, the association of hnRNP AB with promoter regions has also been shown to repress transcription (Gao, Guo et al. 2004; Zhao, Korzan et al. 2008). hnRNP AB forms part of a nuclear multiprotein complex that interacts with free core histones in the nucleoplasm, which may be related to post-translational modifications (Covelo, Sarandeses et al. 2006). All these findings suggest that hnRNP AB has a role in the regulation of gene expression.

hnRNP AB has been previously reported to regulate neural development and neuron cell survival (Sinnamon, Waddell et al. 2012). Sinnamon et al. demonstrate that hnRNP AB (CBF-A) plays a role in neural stem cell maintenance and differentiation. They have also noted different subcellular distribution of hnRNP AB isoforms during neuronal maturation, suggesting that hnRNP AB is regulating gene expression during neuronal development (Sinnamon, Waddell et al. 2012).

2. Project objectives

This project has two general objectives.

The first is to develop an intein based method to site-specifically conjugate Quantum Dots (QDs) to target proteins *in vivo*. We will use the *Xenopus laevis* as a model for *in vivo* conjugation of QDs to target proteins in vivo.

Objective 1: Generate the mRNA encoding the N-terminus half of the split intein fused on the protein of interest.

Objective 2: Conjugate the c-terminus half of the split intein to QDs.

Objective 3: Inject the embryos with the mRNA and QD-conjugates for *in vivo* conjugation of QDs with the protein of interest.

The second is based on the scientific hypothesis that 40LoVe/Samba has an important role during neural development and is involved in *Xenopus* neural morphogenesis.

Objective 1: Clone Samba, 40LoVe and hnRNP AB and construct various tagged versions of the proteins

Objective 2: Determine the spatial and temporal expression of *Xenopus laevis* 40LoVe/Samba and hnRNP AB

Objective 3: Examine the intracellular localization of the three proteins in vivo and in vitro and address their functional relationship

Objective 4: Map the domains important for localization of 40Love/Samba

Objective 5: Address the role of 40Love/Samba using loss of function experiments

3. Methodology

3.1 Obtaining, housing and maintenance of *Xenopus laevis* frogs

Adult frogs were obtained from several international suppliers, such as NASCO (United States) and *Xenopus* express (France/UK). Frogs were shipped in peat moss during the spring and autumn in order to avoid the extreme temperature conditions of winter and summer months. New frogs were kept separately from the older ones, and a recovery/resting period of two weeks was allowed after receiving each new shipment of frogs. This resting period was crucial and helped to increase the quality of oocytes obtained and used for the experiments (Sive, Grainger et al. 2010).

Male and female frogs were housed in separate tanks. Approximately 20 females or 30 males (males are much smaller than females) were housed in each tank of the aquarium, which was a partially self-cleaning system (12 tanks of 90 L each, Figure 25). This particular setup was very effective due to the large number of frogs we house in our lab. The system has a holding capacity of approximately 300 frogs and contains about 1700 L of water. The system drips fresh water in and out continuously and prevents accumulation of wastes. The toxic waste is therefore kept low and solid waste is drained continuously.

The quality of the ingoing water was monitored to ensure it was optimal for the frogs. Several parameters were measured once a week. These included: pH (6.5 to 7 is optimal for *Xenopus*), conductivity (hardness of the water), gH, kH, NO_3, NH_4 and NO_2. We monitored the system with the help of Aquacontroller (system observation online). In order to keep the conductivity stable at 1200µS (Godfrey and Sanders 2004), a salt solution (NaCl and Ocean salt) was gradually dispensed (in a drip wise fashion) into the incoming water sump of the aquarium system. High water quality is essential for the health of the frogs and the quality of the oocytes produced. High concentration of calcium and high gH values result in higher survival rates and normal development of *Xenopus* embryos. The hardness of the water improves the firmness of the oocytes and

the survival and normal development of embryos (Godfrey and Sanders 2004; Sive, R.M. Grainger et al. 2010). In addition, the water was pumped through biological filter to remove ammonia, nitrites and fine particles and across four high capacity UV lights to kill bacteria and other pathogens, before being pumped back to the tanks. The frogs were kept on a regular light-dark cycle of 12 hours light and 12 hours dark (controlled system of light cycle in the animal facility). The temperature of the room and the water in the aquarium was kept at 18^{o}C, which is optimal for the frogs and for all the stages of embryonic development (Sive, Grainger et al. 2000). The frogs were fed three times a week, in the morning (Monday, Wednesday, Friday), with floating food pellets (Hilken, Dimigen et al. 1995).

Figure 25: *Xenopus* facility aquarium system.

When all conditions of the aquarium are monitored properly, good female frog can lay hundreds of eggs in a single day. The actual number of eggs laid and the efficiency of fertilization are unpredictable so ovulation should be induced in more than one female every day of the experiments (3 or 4 females every time). Females can be induced to lay

repeatedly for some years, but rest periods of four months are required between ovulations. The testes from one male contains sufficient sperm to fertilize several thousand eggs (can kept in 4^{o}C for few days in a certain media) (Sive, Grainger et al. 2000).

3.1.1 Obtaining Embryos

Inducing ovulation

Ovulation was induced by administering an injection of human Chorionic Gonadotropin (hCG, Chorulon 1500 IU) into the dorsal lymph sac of the female frog. For the induction of full ovulation, 600-750 units of hCG (Intervet International B.V., Medivet Suppliers LTD, Chorulon 1500 IU), depending on frog size, was injected into the dorsal lymph sac. The injection was performed with a fine needle (26-30 gauge) attached to a 1ml syringe laterally toward the dorsal midline, across the lateral line "stitch" marks to the dorsal lymph sac (Figure 26). When the needle penetrated the sac we injected the liquid (approximately 600-750 units hCG in 1ml liquid). After the injection we waited few seconds and then slowly pulled out the needle. The frogs were kept at 16 °C and started laying eggs approximately 14 hours after injection (the hours for laying eggs depends from the temperature, (Sive, Grainger et al. 2000).

Figure 26 : Priming a female *Xenopus laevis*

Isolating the testes

One male frog was sacrificed every week. The male was euthanized by submersion into a 0.05% benzocaine solution for 30 minutes to 1 hour at room temperature. Using scissors and forceps the testes were removed from the body. The testes lie at the base of the fat bodies and were easily recognized. They are about 1cm long. The isolated testes were placed in a solution that contained 10% serum (newborn calf serum), 90% Leibovitz (L-15 Medium Leibovitz without L-glutamine from Sigma cat#L5520) with antibiotic (0.05 mg/ml gentamycin) and stored at 4ºC. Under these conditions, testes can be stored for at least 5 to 7 days, after which sperm viability drops.

Manual egg collection

After induction of ovulation, the cloaca becomes red and sensitive, so we avoid touching it when picking up the female frog. The eggs are collected in a sac near to cloaca and simultaneous lateral and vertical pressure is needed to expel them. In order to do so the frog is held with two hands and the belly is gently massaged with one thumb over a clean glass petri dish (90cm) containing 0.33X MMR (Marc's Modified Ringers solution) (Ubbels, Hara et al. 1983). The frog should begin to lay eggs within less than a minute (Figure 27). Egg collection did not continue for more than 2-3 minutes total. Egg collection was carried out every hour for the first 2-3 hours of laying and then more often as the day progresses. Females usually laid eggs for about 8 hours. A maximum of 6-8 collections are expected from a frog in 1 day. Each batch of oocytes obtained from the female frog were kept in a separate glass petri dish. Fertilization was performed as soon as possible after laying. Primed females were kept separately from the aquarium so each one could be observed independently.

A frog can be induced to lay eggs repeatedly, but it must rest between ovulations as mentioned previously. Rest periods of four months appear to be optimal. So it was useful to keep accurate records and dates of ovulations (Sive, Grainger et al. 2000).

Figure 27: Squeezing of female frogs and manual collection of eggs

In vitro fertilization

Before *in vitro fertilization* most of the 0.3xMMR buffer must be removed from the eggs in the petri dish using a plastic pipette. Forceps and scissors (cleaned with 70% ethanol before use) were used to macerate a piece of testis and mix to distribute the tissue over the eggs (Figure 28A). The eggs are tough at this point and will not break easily. The first sign of fertilization (within few minutes, approximately 20min) is a concentration of the pigmented animal hemisphere to less than one half of the egg. The eggs rotate within the vitelline membrane so that the animal hemisphere faces upward (Ubbels, Hara et al. 1983) (Figure 28B). A fertilized egg is more elastic and resistant to deformation than an unfertilized egg. This is due to the thickening of the vitelline membrane after fertilization. To assess egg quality, test fertilization is performed every day on a few eggs of the first batch. If the fertilization efficiency was poor, we tested the eggs from a second batch because the egg quality can vary from one laying to the next. Also to verify that the testes were viable we crushed a little on a microscope slide, rinsed it with 0.3XMMR (MMR activates the sperm to begin swimming), covered with coveslip and viewed under the microscope. The sperm were easy to identify by their fine helical shape and the characteristic movement. Good quality eggs and sperm produced fertilization efficiencies

of 80-100% (Sive, Grainger et al. 2000). These batches of embryos were used in all the experimental procedures.

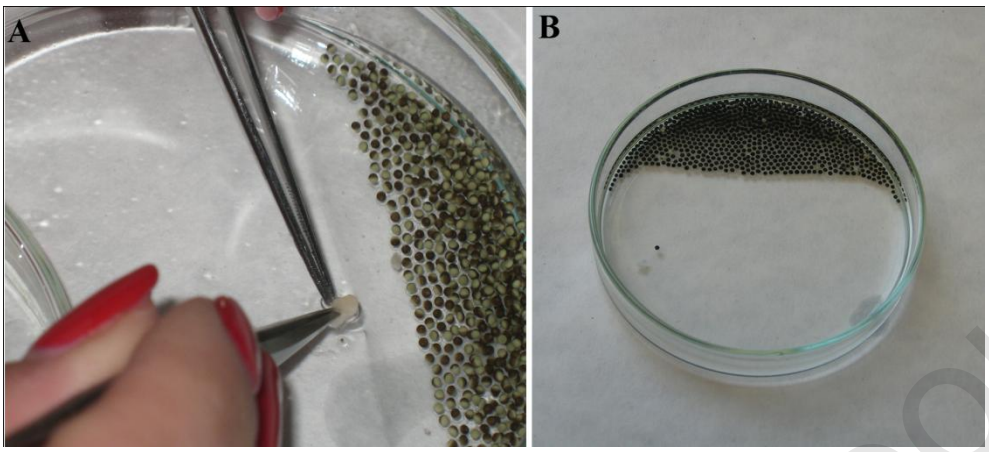

Figure 28 : Fertilization process. (A) *In vitro fertilization* and **(B)** 20 minutes after fertilization we observe the vegetal rotation and 100% fertilization.

Dejellying embryos

In order to manipulate *Xenopus* embryos, the thick jelly membranes surrounding the embryos must first be removed. In order to achieve this, embryos were gently swirled in a solution of 2% cysteine (Annex 6.2) in 0.3X MMR at pH 8 for 2-3 min (Sive, Grainger et al. 2010; Sive, R.M. Grainger et al. 2010). When the embryos began packing closely together and the jelly coats could be seen floating in the buffer, the cysteine was promptly removed and the fertilized eggs were rinsed at least 10 times in an excess of 0.33X MMR. After dejellying, the embryos were placed in a clean dish either in 0.1X MMR or 4% Ficoll in 0.33X MMR (if the embryos were going to used for microinjection procedures) and the dead embryos removed (Ubbels, Hara et al. 1983).

3.2 Microinjections

For microinjections, dejellied embryos were placed in a solution of 4% Ficoll in 0.33x MMR. Ficoll collapses the vitelline space, reduces the pressure on the embryo and therefore prevents leakage due to the microinjection procedure. The embryos were injected using a glass capillary pulled needle, forceps, a Singer Instruments MK1

micromanipulator and Harvard Apparatus pressure injector (Figure 29). Embryos were microinjected with capped mRNA which was *in vitro* transcribed using mMessage machine kits (Ambion) and antisense Morpholino oligonucleotides (MOs; see Figure 31). Sometimes mRNA or MO was co-injected with histone-GFP, membrane-GFP or membraneCherry (total 100 pg for each one). Injection volumes were kept below 10nl per blastomere (for 2 -8 cells stage embryos) (Smith and Harland 1991). For most experiments, injections were made at the 4-cell stage or 8-cell, into the ventral blastomeres (lighter) to target the epidermis, or the dorsal blastomeres (darker) to target neural tissue (Figure 30). For embryos used in Western Blot experiments the injections were done at the one-cell stage. Embryos were staged according to Neiuwkoop and Faber (Nieuwkoop 1994). After injections, embryos were reared for 2 hours or until stage 8 in 4% Ficoll in 0.33x MMR and then washed and maintained in 0.1x MMR alone. For all experiments, we injected morpholinos at 8 to 36ng per embryo and mRNAs at various amounts (Table 1)**.** Embryos were allowed to develop to the appropriate stage and then imaged live, dissected, or fixed in 1x MEMFA (Annex 6.2) (Sive, Grainger et al. 2010; Sive, R.M. Grainger et al. 2010) for 1-2 hours at room temperature (RT). Fixed embryos were either used immediately or serially dehydrated in methanol and stored at -20°C. For Live imaging, embryos were anesthetized in 0.01% benzocaine in 0.1x MMR.

Figure 29 : Pressure injector and micromanipulator setup.

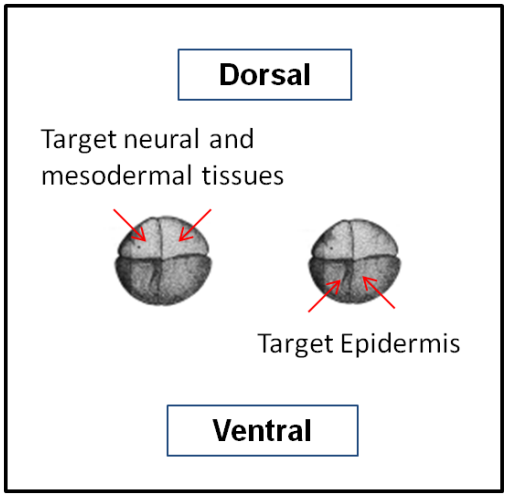

Figure 30 : Blastomeres targeted during injections. Schematic of four cell stage embryos. The lighter pigmented dorsal blastomeres give rise to mesodermal and neural tissues when targeted. The darker pigmented ventral blastomeres give rise to the epidermis when targeted.

mRNA *	Concentration** (total pg per embryo)
Samba	60-120
40LoVe	60-120
hnRNP AB	60-120
R-40LoVe	80-140
RhnRNPAB	80-140
CBFNT domain	100-140
SambaΔNLS	80-140
SambaΔGRD	80-140
SambaΔCBFNT	80-140
$hnRNPAB_N$-$40LoVe_C$	80-140
40LoVe-GRD_{AB}	80-140
$hnRNPABGRD_{40LoVe}$	80-140
***mRNA was co-injected with histoneGFP, membraneGFP or membraneCherry (total 100pg for each one).** ***Site of injection depended on the experiment. Most of the mRNA's injected in Animal pole (AP, dorsally).**	

Table 1: Concentrations of mRNA microinjections

3.3 Removing the vitelline membrane

Once the embryos reached the desired stage for micro-dissection or further processing, the vitelline membrane was manually removed with the forceps. The procedure was facilitated by coating the bottom of the dish with 1% agarose (electrophoresis grade) in 0.1x MMR. With two forceps, one to hold the embryo steady and the other (sharper pair) make a tear in the vitelline membrane. If the tear was large enough, the embryo could pop out. The naked embryos were stored in 0.1x MMR or fixed in 1x MEMFA and used for the future experiments.

3.4 Animal Cap Isolation

The first step in every microdissection procedure is dejellying removing the vitelline membrane from the embryos as described in above sections. The animal cap refers to the tissue around the animal pole of a blastula stage embryo. The fate of this tissue is to become cement gland-neuroectoderm on the dorsal side and epidermis on the ventral side. Animal caps are very useful because they are composed of pluripotent cells that can be induced to from endodermal, mesododermal, or ectodermal cell types (Ariizumi, Sawamura et al. 1991; Takashi Ariizumi, Naomi Moriya et al. 1991). With quite a bit of practice the removal of the animal cap is a relatively easy dissection process. The animal cap was removed with care in order to obtain only pure ectodermal cell populations, without contaminating with mesodermal cells. For every experiment caps from embryos of the same stage and batch were used (most of the times from the same frog) so to be sure that the tissue was as homogeneous as possible.

During the next step of the procedure, the embryos were placed in glass petri dishes coated with agarose 1% in 0.5X MMR. With the help of a sharp pair of forceps and eyebrow hair knife we cut the cap. Then, the animal cap is removed, cleaned from mesodermal cells or any adherent vegetal yolk cells and the explants cultured in different solutions depending on the experiments they will be used (cultured in 0.5X MMR or CMFM for dissociation). Animal caps were used for migration assays, convergent extension assays and immunofluorescence assays.

3.5 Dissociation of Animal Caps

Single cells derived from animal caps were used in all the experiments for migration assays, immunofluorescence assays and localization assays. Animal caps can be dissociated by exposure to a medium lacking Ca^{++} and Mg^{++} ions (CMFM, Calcium Magnesium Free Medium). Animal caps transferred to 1% agarose (agarose in CMFM) coated dishes containing Ca^{++} /Mg^{++} ion free buffer (CMFM) and activin 10μg/ml (Asashima, Nakano et al. 1990). Approximately ten animal caps were placed into a single well of a 12 well non-treated dish. The caps were incubated and swirled at room temperature for approximately 45-60 minutes. During this time the inner cap cells separate from the outer layer. The outer epithelial layer was discarded at this point and the cells were dissociated. For immunofluorescence and migration assays the cells were transferred to fibronectin (50μg/ml) coated coveslips (charged before with HCl and cleaned with distilled water, 5 minutes each) or slides (mentioned below) (Ramos and DeSimone 1996).

3.3 Chemical Synthesis

3.3.1 Chemical Synthesis of biotinylated Intein (I_C) peptide (I_C-Biotin)

A 47 amino acid peptide corresponding to C-terminal intein (I_C) is synthesized on a 0.5 mmol scale on a 4-methylbenzhydrylamine (MBHA) resin according to the in-situ neutralization/ HBTU activation protocol for Boc SPPS.

HOOC-MVKVIGRRSLGVQRIFDIGLPQDHNFLLANGAIAANCFDYKDDDDK(Ahx-Biotin)G-NH2

Modifications: Biotin conjugated to lysine via a Ahx linker (6 carbon inert linker) A 47 amino acid peptide corresponding to C-terminal intein (I_C) was synthesized on a 0.5 mmol scale on a 4-methylbenzhydrylamine (MBHA) resin according to the in-situ neutralization/HBTU activation protocol for Boc SPPS (Schnolzer, Alewood et al. 1992). In order to put a biotin at C-terminus, it was necessary to add an extra amino acid, Lys, at the C-terminus. This Lys serves as a linking point for biotin as well as a spacer between the peptide and biotin. The peptide contains a cysteine protected with the NPyS group which was added as the last amino acid in the synthesis. Following chain assembly, global

de-protection and cleavage from the support was achieved by treatment with Hydrogen fluoride (HF) containing 4% v/v pcresol, for 1 hour at 0°C. Following removal of the HF, the crude peptide product was precipitated and washed with anhydrous cold ethanol before being dissolved in aqueous acetonitrile (50% B) and lyophilized. The crude peptide was purified by preparative HPLC using a linear gradient of 25-45% B over 60 minutes. The purified peptide was characterized as the desired product by ESMS. This peptide is relatively hydrophobic and thus difficult to dissolve in water alone. It should therefore be dissolved in a small amount of organic solvent such as dimethyl suphoxide (DMSO). The lyophilized peptide was dissolved in 60% DMSO at a concentration of 1 mg/ml. This should be added drop wise, followed by vortexing after every drop until the peptide dissolves. Note if DMSO solvent is at all wet it will not freeze at -20°C, so freeze at -30°C. DMSO is hygroscopic and will absorb water if subjected to repeated freeze-thaw cycles. To minimize these issues, prepare multiple aliquots.

3.3.2 In vitro conjugation of I_C-Biotin to streptavidin-coated QDs

I_C-Biotin was diluted to 50 µM and used at 1:1 volume ratio with streptavidin-coated QDs (1 µM) (from Invitrogen or eBiosciences). The peptide is used in ~50 fold excess relative to the Streptavidin coated QDs during conjugation. This is to ensure that all biotin binding sites on the Streptavidin coated QDs are bound with peptide. According to the manufacturers, commercially available QD's from Invitrogen are multivalent, bearing 4-10 streptavidin molecules/QD, giving 16-40 biotin binding sites/QD. To allow formation of the biotin-streptavidin bond we incubate at 24°C for 1 hour. To remove any excess unbound peptide the conjugate was filtered through microcon centrifugal filter units (YM100) (Cat# 42413) by adding 400µl of 1X PBS and spinning at 8000 x g, at 4^{o}C. After that 360µl of 1X PBS were added to the I_C peptide-QD conjugation reaction and spin at 8000 x g, at 4^{o}C. This step has to be repeated 3 times until the volume of the I_C peptide-QD conjugate is concentrated down to 15µl.

This step is performed to clear I_c-peptide-QD conjugates from any unbound peptide. Given that the molecular weight (MW) cutoff of the microcentrifugal device is 100kD and given that the MW of the I_C peptide is insignificant compared to the MW of the

streptavidin coated QDs (250kD-550kD depending on the number of streptavidin molecules bound), this method ensures that the unbound peptide is removed. The probes should be placed at 4^{o}C until ready to inject.

3.3.3 Analysis of QD-peptide conjugates

Analysis of QD-peptide conjugation was performed by electrophoresis at 60 V for 4 h at 4°C using a 0.5% agarose gel. No loading buffer was added to the samples before loading. Gels were visualized under the ethidium bromide filter (515-570 nm) with a UVP Imager.

Alternatively analysis of QD peptide conjugation was performed by spotting nitrocellulose membranes (Whatman). Biotinylated I_C peptide and I_C peptide that did not contain the biotin modification at the N-terminus were spotted on nitrocellulose membrane and blocked in PBS containing 1% BSA for 30 min at room temperature. The nitrocellulose membrane was then soaked in PBS containing streptavidin-coated QDs (1:500 dilution) for 30 min at room temperature. The membrane was washed with PBS-Tween 20 (1%) twice and visualized under the ethidium bromide filter (515-570 nm) with a UVP Imager.

3.3.4 Electrophoretic analysis of protein trans-splicing

Biochemical analysis of protein-trans splicing was performed by lysis of injected Xenopus embryos at stage 10. Lysis was performed by pipetting up and down in the presence of proteinase inhibitors (Sigma) and DNAse (Roche). Lysates were then loaded onto agarose gels run at 100 V for 2 h, at 4°C. Gels were visualized with a UVP Imager.

3.4 Molecular Methods

3.4.1 RNA isolation and cDNA synthesis for RT-PCR

Embryos were placed in an autoclaved 1.5 ml capped centrifuge tube (~5 per tube). 500 µl TRIzol reagent (Invitrogen) was added, and embryos were homogenized by pipetting up and down until the sample was uniform. The sample was allowed to incubate for 10min at RT. Tubes were then centrifuged at 14000 rpm for 10min at 4°C. The supernatant (RNA) was removed and placed into a new autoclaved 1.5ml tube. An equal volume (as

supernatant) of chloroform was added, the tubes were vortexed for 15sec and allowed to incubate at RT for 3min. Tubes were then spun in a 4°C microfuge at 12000 rpm for 15min. The top phase (RNA; clear layer - not the pink layer) was placed into a new autoclaved tube. 500 µl of isopropanol was added and the tubes were allowed to stand for 10min at RT, spun at 12000 for 10min at 4°C, the supernatant was decanted and the pellet was washed with 500 µl RNAase-free 70% ethanol and RNA was recovered by centrifugation at 9000 rpm for 5min at 4°C. The supernatant was removed and the pellet was allowed to dry before being resuspended in 30 µl of sterile water. cDNA was then synthesized from RNA using the SuperScriptIII First strand synthesis kit from Invitrogen. To address the temporal expression of the protein of interest we will perform RT-PCR as described previously (Wilson and Melton 1994).

3.4.2 Plasmids and Cloning strategy

A. Inteins

All plasmids were constructed using standard molecular biology techniques and they were sequenced to verify correct coding.

pCS2++-Akt PH-EGFP-I_N

A PCR fragment amplified with Apr1 and Apr3 encoding Akt PH-EGFP, using the pAkt PH-EGFP-N1 plasmid (Varnai, Bondeva et al. 2005) as template. For the reaction we used 10ng of the pAkt PH-EGFP-N1 plasmid as template, 22.5µl of PCR mix and each of the following primers, Apr1 and Apr3 (see Table 2) at a final concentration of 0.1µM. PCR program: 95°C for 5 minutes, 35 cycles each of: 95°C for 15 seconds, 62°C for 30 seconds, 68°C for 70 seconds followed by 68°C for 10 min and 4°C until reaction termination. PCR product was inserted into the multiple cloning site of the pCS2++ plasmid between the ClaI-EcoRI restriction sites.

A PCR fragment amplified with IGpr61 and IGpr63 encoding I_N with 5 N-terminal extein residues (KFAEY). To set up the PCR reaction we used 10ng of the pJJDuet30 (from Addgene) plasmid as template, 22.5 µl of PCR mix and each of the following primers, IGpr61 and IGpr63 (see Table 2) at a final concentration of 0.1µM. We used the following PCR program: 95°C for 5 minutes, 35 cycles each of: 95°C for 15 seconds, 62°C for 30 seconds, 68°C for 40 seconds followed by 68°C for 10 min and 4°C until reaction termination. Clone the PCR product downstream of Akt PH-EGFP into the pCS2++ plasmid using EcoRI and XhoI restriction enzymes.

pCS2++-Btk PH-EGFP-I_N

A PCR fragment was amplified with IGpr62 and IGpr64 (see Table 2) encoding I_N with 5 N-terminal extein residues (KFAEY), using the pJJDuet30 plasmid (from Addgene) as template. The PCR program used was 95°C for 5 minutes, 35 cycles each of: 95°C for 15 seconds, 62°C for 30 seconds, 68°C for 40 seconds followed by 68°C for 10 min and 4°C until reaction termination. The PCR product was inserted at the C-terminus of Btk-PH-

EGFP (Varnai, Bondeva et al. 2005)on pEGFPN1 between the BsrG I and Not I restriction sites. Btk-PH-EGFP-I_N was then inserted into the multiple cloning site of the pCS2++ plasmid by restriction enzyme digest with EcoR I-Not I.

Primer Name	Primer sequence
Apr1	AAGATCGATATGAGCGACGTGGCTATTG
Apr3	AAGGAATTCCTTGTACAGCTCGTCCATGCCGAG
IGpr61	AAGGAATTCAAGTTTGCGGAATATTGCCTCAGTTTTGG
IGpr63	AAGCTCGAGTTATTTAATTGTCCCAGCG
IGpr62	TGTACAGGCGCGCGTACGGCGGCGGCGGCGGCGGCAAGTTTGCGGAA TATTGCCTCAG
IGpr64	CGCGCGGCGGCCGCTTATTTAATTGTCCCAGCG

Table 2: Primers used for Intein Cloning

B. Samba

Using cDNA prepared as described above, 40LoVe and hnRNP AB was amplified by standard PCR (list of primers found in Table 3). All constructs have been subcloned in CS108 vector provided by Harland Lab. We have used EcoRI - NotI to clone the proteins of interest (Samba, 40LoVe and hnRNP AB) and ClaI - EcoRI to clone GFP. We used Polymerase Chain Reaction (PCR) and various primers listed below to amplify each protein. 5'UTR-40LoVe and 5'UTR-hnRNP AB were obtained by Reverse trancriptase PCR. The rescue constructs were generated by modifying the 5' of the mRNAs, using synonym codons, so that the protein sequence was not affected. The GFP sequence was isolated from pEGFP-N1. The clones were then verified by sequencing. Then we used restriction digests to insert each protein in the vector and make all the constructs we will be using in the project as it is listed below. Each PCR reaction will be prepared as required using the reaction buffer, dNTPs, set of Primers and Taq. The first step is the initial denaturation at 95^{o}C for 2 minutes followed by 35 cycles at: denature 95^{o}C for 15 sec, annealing 58^{o}C for 30 sec and extension 68^{o}C for 1min.

3.4.3 RT-PCR

cDNA was synthesised using the same method mentioned above for different developmental stages and different tissues. The PCR was carried out using specific primer pairs shown in Table 3. The PCR products were run on a 1-1.5% agarose gel and images were captured using UVP iBox imaging system.

3.4.4 Mutagenesis

Using site directed mutagenesis we created a deletion mutant lacking the predicted-NLS domain found PredictProtein service (Rost, Yachdav et al. 2004).

Mutagenic primer design: Both primers were designed such that they both contained the desired mutation and annealed to the same sequence on opposite strands of the plasmid. The mutation site should be centrally located on both primers and can be up to 12 bases deletion. Both primers (forward and reverse) should be approximately 30 to 45 nucleotides in length, not including the mutation site. The primers were 30-45 bases as indicated, the melting temperatures (Portman and Dreyfuss) were ≥ 78°C, the GC content over 40% and the mutated sequence was located in the middle of the primers. SambaΔNLS primers were 45 base pairs long (Table 3), had a T_m of 81.5°C and a 42% GC content.

Procedure: In a PCR tube we added: 125ng of each primer 22.5µl Accuprime (Invitrogen) polymerase mix and 100ng GFP-Samba plasmid DNA. The cycling conditions were: 95°C for 1 min, 18 cycles of 95°C for 50 sec, 60°C for 50 sec and 68°C for 7.5min (1.5min per Kb of plasmid), 1 cycle at 68°C for 10 min. The PCR was immediately cooled to 37°C, 1µl of DpnI (10U/µl) restriction enzyme was added and the reaction incubated for 1 hour. The DpnI endonuclease (target sequence: 5´-Gm6ATC-3´) is specific for methylated DNA and it is used to digest the DNA template to be able to select for mutation-containing synthesized DNA (Nelson and McClelland 1992). 2µl of the PCR reaction was then used for transformation in TOP10 competent cells.

	Primer Name	Primer Sequence
	F/EcoRI Flag-SAMBA	AGGAATTCATGGACTACAAGGACGACGATGACAAGAAATCCGACTCCGAGCAGCAGTA
	R/ NotI SAMBA	AGGCGGCCGCTTACCATAGTTTGCACCGCCC
	F/EcoRI-5UTR-hnRNPAB	AGGAATTCAATTTGGCGATTGTTGGCGCTTGTGCTTTC
	R/FLAG-NotI-hnRNPAB	CTGCGGCCGCTTATTTGTCATCGTCATCCTTGTAGTCGTATGGCTTGTAGTTATTCTGGTGG
	F/EcoRI5UTR-Samba	AGGAATTCTCGTCGACCCACGCGTCCGCTTGGAGGAATTTGGC
	R/Flag-NotI-Samba	ctgcggccgcttaTTTGTCATCGTCATCCTTGTAGTCcctctgatgtcccccacgtc
	F/EcoRI Flag-SAMBA	AGGAATTCATGGACTACAAGGACGACGATGACAAGAAATCCGACTCCGAGCAGCAGTA
	R/SambaNoGRD	TTTTCTAGAttaaatctttatctcacacttg
	F/ClaI-GFP	AGCATCGATATGGGGATCCTGAGTAAAGGAGAA
	R/ClaI-CBFT	TTTATCGATttcaaagtagtctttcaagtccttt
	F/Resc-Samba	AGGAATTCATGGGAGGATCGGATTCGGAACAACAATACATGGAAACGAACGCCG
	R/ NotI SAMBA	AGGCGGCCGCTTACCATAGTTTGCACCGCCC
	F/Resc-hnRNPAB	AGGAATTCATGGGAGGATCGGATACGGAACAACAATGTCTAGAAACGAACGCCGAGAACG
	R/FLAG-NotI-hnRNPAB	CTGCGGCCGCTTATTTGTCATCGTCATCCTTGTAGTCGTATGGCTTGTAGTTATTCTGGTGG
	F/Resc-hnRNPAB	AGGAATTCATGGGAGGATCGGATACGGAACAACAATGTCTAGAAACGAACGCCGAGAACG
	R/hnRNP AB-N(SalI)	aaGTCGACcacctcaccaaactttgcaaagtagtctttcaagtcc
	F/40LoVe-C (SalI)	aaGTCGACtctgactgcacaatcaagatggaccccaatacggg
	R/ NotI SAMBA	AGGCGGCCGCTTACCATAGTTTGCACCGCCC
	F/Resc-hnRNPAB	AGGAATTCATGGGAGGATCGGATACGGAACAACAATGTCTAGAAACGAACGCCGAGAACG
	R/ABΔGRD	tttgcggccgctcactttatctcacacttgcttcc
	F/Resc-Samba	AGGAATTCATGGGAGGATCGGATTCGGAACAACAATACATGGAAACGAACGCCG
	R/40LoVeNoGRD	tttGTCGACctttatctcacacttgcttcc

	F/AB-GRD	aaaGTCGACattgcacaaccaaaagaagtgtatcagc
	R/FLAG-NotI-hnRNPAB	CTGCGGCCGCTTATTTGTCATCGTCATCCTTGTAGTCGTATGGCTTGTAGTTATTCTGGTGG
	F/Resc-hnRNPAB	AGGAATTCATGGGAGGATCGGATACGGAACAACAATGTCTAGAAACGAACGCCGAGAACG
	R/40LoVeNoGRD	tttGTCGACctttatctcacacttgcttcc
	F/AB-GRD	aaaGTCGACattgcacaaccaaaagaagtgtatcagc
	F/EcoRI Flag-SAMBA	AGGAATTCATGGACTACAAGGACGACGATGACAAGAAATCCGACTCCGAGCAGCAGTA
Mutagenesis	F/SambaNoNLS	ACATTTAAGGAAGAGGAACCTGTGTTCCACCATGTCAGTGGAAGC
	R/SambaNoNLS	GCTTCCACTGACATGGTGGAACACAGGTTCCTCTTCCTTAAATGT
RT-Primers	F/EcoRI-Samba	AGGAATTCATGTCCGACTCCGAGCAGCAG
	R/RT-Samba	TCCCGTATTGGGGTCCATCTTGATTG
	F-Actin	CCATTGGTAACGAGCGTTT
	R-Actin	GAGGGGCCAGACTCATCATA
	F-Sox2	GAG GAT GGA CAC TTA TGC CCA C
	R-Sox2	GGA CAT GCT GTA GGT AGG CGA
	F-Chordin	CCT CCA ATC CAA GAC TCC AGC AG
	R-Chordin	GGA GGA GGA GGA GCT TTG GGA CAA G
	F-Ntub	ATG CTG ATC TAC GCA AAC
	R-Ntub	AGA TAG CAG CTA CTG TGA G
	F-Sox10	CAGAGCAACCCTCTACATCTC
	R-Sox10	GTGTAGTATAGACTGGCTGTTCC

Table 3: Sequences of all primer sets used.

Construct Name	
Generated	**Gifted/Bought**
pCS108-Samba	**pCS2+-mGFP** (Brand lab)
pCS108-N-Flag-Samba	**pCS2+-mCherry** (Dr.Chenbei Chang)
pCS108-Samba-C-Flag	**pCS-H2B-RFP** (Dr. Reinhard Köster)
pCS108-GFP-N-Flag-Samba	**pCS-Histone-GFP** (Dr.Chenbei Chang)
pCS108-mkate-N-Flag-Samba	**pCS N-Tubulin** (Dr. Richard Harland)
pCS108-5'UTR-40LoVe-C-Flag	**pShuttle-mCherry-tubulin** (Addgene p.26768)
pCS108-5'UTR-hnRNPAB-C-Flag	**pSP72-XSlug** (Dr. Ali Brivanlou)
pCS108-R-hnRNPAB-C-Flag	**pBSK -Sox3** (Dr.Chenbei Chang)
pCS108-R-40LoVe-C-Flag	**pBSK-Sox10** (Dr.Chenbei Chang)
pCS108-GFP-R-40LoVe-C-Flag	**pBSSK - XrX1** (Dr.Chenbei Chang)
pCS108-GFP-R-hnRNPAB-C-Flag	**pEGFP-C1-Akt-PH** (Dr. Tamas Balla)
pCS108-GFP-CBFNT domain	**pEGFP-C1-Bkt-PH** (Dr. Tamas Balla)
pCS108-GFP-SambaΔNLS	**pJJDuet30** (Addgene p.11962)
pCS108-GFP-SambaΔGRD	
pCS108-C-Flag-SambaΔCBFNT	
pCS108-GFP-hnRNPAB$_N$-40LoVe$_C$-Flag$_C$	
pCS108-GFP-40LoVe-GRD$_{AB}$-Flag$_C$	
pCS108-GFP-hnRNPABGRD$_{40LoVe}$-Flag$_C$	

Table 4 : List of constructs used

3.4.5 Morpholino design

Antisense morpholino oligonucleotides (Ramos and DeSimone) were designed and ordered from Gene Tools, LLC. Morpholino (MO) antisense oligos are synthetic DNA analogs that block mRNA translation when they bind at the 5'UTR of the mRNA that codes for the protein. A control Morpholino (CoMO) that targets a human beta globin intron mutation and has no significant biological activity in *Xenopus* was also designed, to make sure that the elicited phenotype is not due to toxicity. MO1 was designed to block translation of all three proteins (40LoVe, Samba and hnRNP AB) while MO2 was designed to block translation of 40LoVe/Samba but not hnRNP AB. The Morpholino sequences and design strategy are shown on Figure 31, Table 7.

Morpholino Name	Morpholino Sequence	Target Sequence
Standard Control Oligo	CCTCTTACCTCAGTTACAATTTATA	
Samba Mo1	TATACTGCTGCTCGGAGTCGGACAT	5'- TGTTGAAGCTTGTGCTTTCAGT(ATG TCCGACTCCGAGCAGCA GTATA)TGG - 3'
Samba Mo2 3' Fluorescein	AATCGCCAAATTCCTCCAAGCGGAC	5'- CCACGC(GTCCGCTTGGAGGAATTTGGCGATT)GTTGAAGCT TGTGCTTTCAGTATGTCCGACTCCGAGCA – 3'

Figure 31: Morpholino design strategy.

3.4.6 mRNA preparation - *In vitro* transcription

Capped mRNA will be *in vitro* transcribed using mMessage Machine kits (Ambion). All the constructs that are being used have to be cloned into the pCS2++ vector that has an Sp6 promoter to be used for *in vitro* transcription. Each construct has to be linearized with AscI and transcribed using mMessage mMachine Kit (Ambion) for RNA synthesis. The procedure is as follows: the total reaction volume is 20µl and includes 2 µl reaction buffer, 10 µl NTP/CAP, 2 µl Enzyme mix, the template DNA and RNase free ddH_2O. The reaction is incubated for 2 hours at 37^oC and then 1 µl of Turbo DNAse is added for 15 min to degrade the template DNA. The mRNA is recovered with Lithium Chloride precipitation or following the transcription reaction unincorporated nucleotides were removed using a kit and resuspend in 100µl distilled RNAse/DNase free water. Subsequent to in vitro transcription the amount and quality of RNA are examined using a spectrophotometer and gel electrophoresis respectively. Aliquot and store at -80^oC until injection. The mRNA will have a Cap for the initiation of the transcription and a poly-A tail. We will use this same procedure to produce the wild type RNA, the tagged versions and the mutant forms of the gene. These mRNAs will be used for the injections as described above.

3.4.7 Probe synthesis

The antisense probes for whole mount in situ hybridization are synthesized *in vitro*. Antisense (3' to 5') Digoxigenin –labeled RNA probes are synthesized by *in vitro* transcription (Kalchenko, Shivtiel et al.) from linearized plasmid templates using bacteriophage RNA polymerases (T3, T7 or SP6) and a ribonucleotide mixture in which the UTPs are labeled with Digoxigenin (DIG-11-UTP). The methodology for the IVT reaction is as follows: the total reaction volume is 20µl and includes 14µl RNase free ddH_2O, 2 µl transcription buffer (10X), 2 µl linear DNA template (~1 µg), 1µl RNase inhibitor and 1 µl RNA polymerase. The reaction is incubated for 2 hours at 37°C. Then 2 µl DNase is added and incubated for a 15 more minutes to degrade the template DNA. The RNA probe is then precipitated using LiCl and 100% ethanol at -20°C for roughly 1-2 hours (can be left

overnight). To test the success of the IVT 1-5 µl of the probe is run on a 1% TAE agarose gel (RNase free). The probe is stored at -80°C.

3.5 Cell culture/lines

Xenopus XL-177 (epithelial) and A6 (kidney epithelial) cell lines were cultured in L-15 (leibowitz) supplemented with 10% FBS and 1% Antibiotics/antimycotics in 30cm flasks at RT. Mouse embryonic fibroblast (NIH3T3) were cultured in DMEM supplemented with 10% FBS, 1% antibiotics/antimycotics, 1% sodium pyruvate in a 37°C 5% CO_2 incubator.

Electroporation

Electroporation of *Xenopus* cell lines was carried out using the Neon Electroporation system from Invitrogen. Cells were electroporated with 1.5µg plasmid DNA and seeded in 12 well culture flasks. The parameters used for XL-177 and A6 cell lines were 1300V, 20ms pulse width, 2 pulses at roughly 2-4x10^5 cell density. When cells were ready for imaging, they were seeded onto fibronectin (50µg/ml) coated, HCl charged coverslips.

3.6 Whole-mount in situ hybridization (WISH)

Whole-mount in situ hybridization of *Xenopus* embryos was performed according to Harland (1991) (Smith and Harland 1991). The basic ISH steps are as follows:

Digoxigenin labelled probe preparation. Antisense (3' to 5') Digoxigenin –labeled RNA probes were synthesized by *in vitro* transcription (Kalchenko, Shivtiel et al.) from linearized plasmid templates using bacteriophage RNA polymerases (T3, T7 or SP6) and a ribonucleotide mixture in which the UTPs were labeled with Digoxigenin (DIG-11-UTP). To test the success of the IVT 3-5 µl of the probe was run on a1% TAE agarose gel (RNase free). The probe was then stored at -80° until use.

Day1 of ISH: The embryos were first transferred to 4ml glass vials and rehydrated through a methanol series (100% methanol, 75%methanol in PBTw (Annex 6.2), 50%methanol in

PBTw, 25%methanol in PBTw and 100%PBTw). Next, the embryos were permeabilized by incubation at room temperature for 5 min in 10µg/ml Proteinase K, washed 2X5min in 0.1 M Triethanolamine pH7-8 (TEO), 2X5 min in TEO with acetic anhydride and then post fixed in 4%PFA (paraformaldehyde) for 20 min at RT. Embryos were then incubated for 5-6 hours in Prehybridization solution (Annex 6.2) at 60-65°C and then incubated overnight at 60-65°C in hybridization solution containing the probe. Probes used: xNubp1, Sox2, Chrd, MyoD, Pax3, N-Tub, Twist, Pitx2c, Xnr1

Day2 of ISH: Post-hybridization washes in SSC, RNase step at 37°C, block (in order to prevent unspecific binding), and antibody (Ab) incubation (Anti-DIG- AP fab fragments. 1:2000) at 4°C overnight or 4hour at RT followed by a brief wash in 1xMAB (Maleic acid buffer) (Annex 7.3) and then overnight wash in 1xMAB at 4°C.

Day3-4 of ISH: Post-antibody washes with MAB solution (5x1 hour washes for overnight Ab incubation and3-4 10min washes for 4hr RT Ab incubations) and washed in Alkaline phosphatase (AP) buffer (Annex 7.3) which contained levamisole to inhibit endogenous phosphatases (2x10min washes). Visualization of the probe using BM purple. Color development varied depending on the probe used. To stop the color reaction, the embryos were washed in MAB and fixed overnight in 1xMEMFA at RT. Embryos were then bleached (Annex 7.3). Bright field images were captured on a Zeiss LumarV12 fluorescent stereomicroscope (Figure 34).

3.7 Immunofluorescence

Embryos

For **whole mount immunostaining** embryos were fixed in 3.7% formaldehyde in MEMFA (2 hours at room temperature) after the vitelline envelope was removed manually or by proteinase K treatment (1:5000 dilution in MMR) before fixation for 3min. In case we would intent to use the embryos for Acetylated tubulin staining the tadpoles were first treated with 0,01% Triton in 0,1xMMR prior to fixation to remove the first skin layer, so the ciliated cells not interfere in the embryo imaging. The embryos were permeabilized for at least 5 hours in 0.5% Triton, 5% BSA, 1% DMSO (PBDT) and blocked for 2 hours in 0.5% Triton, 5% BSA, 1% DMSO and 1% Normal Goat or Normal Donkey serum. Primary

antibody staining followed using antibodies stated in Table 5, one at a time or in combination. Embryos were incubated with primary antibodies diluted depending on the primary antibody the dilutions ranged from 1:50 to 1:5000 overnight at 4^{o}C or RT (Table 5). Embryos were then washed three times in PBDT for 10min, incubated for 2 hours RT with secondary antibodies stated in Table 5 at 1:500 dilution RT and then washed three times in PBDT. For negative control experiments the embryos incubated after block solution only with secondary antibodies and no specific staining was expected. The embryos were imaged on a Zeiss Axio Imager Z1 and on a Zeiss LSM 710 laser scanning confocal microscope (Figure 32 : Zeiss 710 Laser Scanning Confocal Microscope.). Cleared whole embryos were imaged and mounted in a similar fashion as described above. Clearing of embryos was performed by immersion the embryos in two parts benzyl benzoate and one part benzyl alcohol after dehydration (Murray's Clearing Medium). The refractive index of BB:BA closes matches the refractive index of yolk thereby rendering *Xenopus* embryos nearly transparent. Optical sectioning was achieved using a Zeiss Apotome structure illumination system (Figure 22).

Figure 32 : Zeiss 710 Laser Scanning Confocal Microscope.

Dissociated Cells

Animal caps were dissociated in CMFM (Sato and Sargent 1989) and induced in activin 10ng/ml until the sibling embryos reached stage 9 (Asashima, Nakano et al. 1990). Ectoderm was removed and the remaining cells seeded on glass coverslips. The coverslips used were first coated with 50µg/ml fibronectin incubated for 1 h at 37^{o}C in humidified chamber and washed three times with ice cold phosphate buffered saline (PBS) containing 0.5 mM MgCl2 and 0.5 mM $CaCl_2$ (PBS++). The seeded cells were then fixed for 10 min in 4% paraformaldehyde solution in PBS++. Fixation was followed by the addition of 50 mM glycine solution in PBS++ and then the cells were permeabilized using 0.2% Triton-X solution in PBS++ for 10 min. Permeabilized cells were blocked using 10% normal donkey serum (Jackson Immunoresearch) for 30 min at room temperature (RT) in humidified chamber. Primary antibodies were added to the 5% normal donkey serum solution in PBS++ and cells were incubated in the antibody solution for 45 min RT. Primary and secondary antibodies used as stated in Table 5. Cells were then imaged on a Zeiss LSM 710 laser scanning confocal microscope and on a Zeiss Axio Imager Z1 (Figure 33) using a Zeiss Axiocam MR3 and the Axiovision software 4.6.

Figure 33 : Microscope Zeiss Axio Imager Z1

Cell lines

For cell lines the IF procedure was modified slightly. Cells were seeded on charged coverslips and fixed in 4%PFA in 1xPBS or in methanol for 10min. Coverslips were then washed in 50mM Glycine for 10min and cells were permeabilized in 0.2% triton-100 in PBS for 10 min. Cells were washed several times with 1xPBS and blocked in 10% Goat serum in 1xPBS. Primary antibodies were then added (in block solution) and cells were incubated for 1 hour at RT. Primary antibodies were then washed off with 1xPBS and cells were incubated with secondary antibody solution for 1 hour at RT and then washed several times in 1xPBS. A drop of Prolong (Invitrogen) was added to a microscope slide and the coverslip was inverted onto the drop and allowed to dry before viewing under the microscope. Cells were then imaged on a Zeiss Axio Imager Z1 using a Zeiss Axiocam MR3 and the Axiovision software 4.6 and on a Zeiss LSM 710 laser scanning confocal microscope.

Antibodies	Dilutions (in block solution)
40LoVe (CvH7, C579) (provided by Dr. Iain W. Mattaj)	1:5000
GFP (Invitrogen)	1:500
Acetylated α-tubulin (sc-23950, Santa Cruz)	1:500
Flag - DYKDDDDK Epitope Tag Antibody (Novus) rat	1:500
Tubulin (E7, Hybridoma)	1:200
Histone H3[p Ser10] ()	1:500
Actin (sc-1616R , Santa cruz)	1:100
Vinculin (Hybridoma)	1:200
Alexa 488 anti-mouse (Invitrogen)	1:500
Alexa 488 anti-rabbit (Invitrogen)	1:500
Cy3 anti-mouse (Jackson Immunoresearch)	1:500
Cy3 anti-rabbit (Jackson Immunoresearch)	1:500
Cy3 anti-rat (Jackson Immunoresearch)	1:500

Table 5 : Concentrations of used Antibodies for Immunofluorescence assays.

3.8 Whole-mount TUNEL

Stored embryos were rehydrated and washed in 1xPBS. They were then incubated for 1hour at RT in TdT buffer (Invitrogen). Then, 150U/ml TdT enzyme (Invitrogen) and 0.1 µl of DdUTP (Roche) per 100 µl buffer were added to the buffer solution and the embryos were incubated overnight at RT. The next day, embryos were first washed 2x1hour at 65°C in 1 mM EDTA/PBS. Next, embryos were washed in 1xPBS 4x1hour at RT followed by 2-10min washes in 1xMAB. Embryos were then blocked in 2%BMB blocking solution for 1 hour at RT and incubated in a 1/3000 dilution of anti-digoxigenin AP antibody in BMB block for 4hours RT or overnight at 4°C. Antibody was washed away by 5x1hour washes in MAB. Endogenous phosphatases were blocked by 2x10min washes in alkaline phosphatase buffer and then NBT/BCIP (Roche) was added to the embryos (embryos were kept in the dark). Chromogenic reaction was stopped by a quick wash in 1XMAB and then the embryos were fixed overnight in 1xMEMFA at RT. The next day embryos were imaged before and after clearing in 2:1 BB: BA. Bright field images were captured on a Zeiss LumarV12 fluorescent stereomicroscope (Figure 34).

Figure 34 : Stereoscope (Discovery V12)

3.9 Immunoblotting (Western Blot Analysis)

Protein lysates were prepared by homogenizing explants or embryos (embryos in different stages) in ice cold RIPA lysis buffer (50mM TrisHCl pH7.4, 150mM NaCl, 2mM EDTA, 1% NP-40, 0.1% SDS, 1% deoxycholate 24mM) supplemented with protease inhibitors (Protease cocktail from Sigma, P8340) and 1mM PMSF (from Sigma, P7626). Homogenates were cleared by centrifugation at 15000g for 30min at 4^{o}C (Kragtorp and Miller 2006). The embryo samples were separated on SDS-polyacrylamide gels and proteins were blotted on PVDF. Membrane and blots were then blocked in 5% milk in TBSTw (TBS buffer + 0.1%Tween). Blots were incubated with primary antibodies as indicated on Table 6 in 5%milk in TBSTw overnight at 4^{o}C or 1 hour RT. Visualization was performed using HRP-conjugated antibodies (Santa Cruz Biotechnology anti-rabbit, mouse and rat) and detected using the Lumisensor chemiluminescent reagent kit (Genscript). For loading control tubulin (1:500 tubulin, Hybridoma bank) was used in every blot.

Antibody	Dilution
40LoVe (CvH7, C579) (provided by Dr. Iain W. Mattaj)	1:7000
GFP (Invitrogen)	1:500
Flag - DYKDDDDK Epitope Tag Antibody (Novus) rat	1:500
Tubulin (E7, Hybridoma)	1:200
HRP-conjugated antibody anti-rabbit	1:7000
HRP-conjugated antibody anti-mouse	1:7000
HRP-conjugated antibody anti-rat	1:7000

Table 6: Antibodies used in Western Blot.

3.10 FRAP and FLIP

FRAP and *FLIP* are techniques that are being used for observing the intracellular movement of proteins through photobleaching. For *FRAP* and *FLIP* experiments, cells expressing GFP fusion proteins were imaged using a water-immersion objective lens on the Zeiss LSM710 microscope system, before and after GFP fluorescence was photobleached by 488nm light from an argon laser in defined region of each cell. *FRAP* is used to measure the ability of a molecule to move around over time, so a fluorophore is attached to the protein of interest. For *FRAP* analysis, fluorescence intensity in the bleached area was measured as a function of time after bleaching (Axelrod, Koppel et al. 1976; Howell and Truant 2002). *FLIP* is used to study the mobility of a molecule within a compartment. In *FLIP* experiments, a region of fluorescence within the cell is photobleached and then fluorescence intensity in the unbleached area is measured as a function of time after bleaching. Over time the fluorescent signal is lost in certain compartments of the cell and this indicates that the molecule is motile and travels between the compartments (White and Stelzer 1999). *FRAP* and *FLIP* have a big advantage that do not affect the embryo viability and are very accurate techniques to observe the protein trafficking in vivo (Koster, Frahm et al. 2005).

3.11 In vivo Imaging

Embryos were observed either under a Zeiss Axio Imager Z1 microscope, using a Zeiss Axiocam MR3 and the Axiovision software 4.8 or a Zeiss LumarV12 fluorescent stereomicroscope, or under a laser scanning confocal LSM710 microscope (Zeiss) **(**Figure 32**).**

3.11.1 Data analysis

The generation of the intensity profiles and the data analysis of FRAP and FLIP experiments were performed with the ZEN2010 software. FRAP experiments were conducted using the LSM 710 confocal microscope and a Plan-Apochromat 63x/1.40 Oil DIC M27 objective lens (Zeiss). The 488nm laser line was used for GFP excitation and

emission was detected between 493-538 nm. Relative recovery rates were compared using half time for recovery of fluorescence towards the asymptote. The fluorescence recovery curve was fitted by single exponential function, given by: $F(t) = A(1-e^{-R}) + B$; - where F(t) is the intensity at time t; A and B are the amplitudes of the time-dependent and time-independent terms, respectively; τ is the lifetime of the exponential term (time constant) and the recovery rate is given by $R=1/\tau$. Immobile fractions were calculated by comparing the intensity ratio in the bleached area, just before bleaching and after recovery. For the FLIP experiments, photobleached regions consisted of a rectangle enclosing the selected region of the cell, which was repetitively photobleached during the experiment.

3.11.2 Imaging for *in vivo* conjugation of QDs to Akt-PH domain

Sylgard-coated slide preparation

Sylgard-coated slides are very useful mounting chambers for imaging embryos on an upright microscope. To make these arrange slides in a foil tray, tightly packed. Prepare the Sylgard silicone elastomer according to manufactures' instructions and pour over the slides. The volume of Sylgard poured over the slides can be adjusted to produce slides of different thickness (~1mm for gastrula stage embryos). Cure slides overnight at room temperature or for 2 hours at 60C.

Imaging

Place stage 10 *Xenopus* embryos in chambered sylgard slides in 0.1X MMR. Cut each slide with a razor blade and then cut well(s) into the cured Sylgard layer. In order to enable use of high power lenses with small working distance the depth of the chamber should be close to 1mm or less (the approximate diameter of the embryo). Remove excess buffer so that the chamber is only slightly overfilled. Using forceps turn the embryos so that the injected area faces up. Carefully place a coverslip over the embryos. The coverlsip should slightly depress the embryo creating a small flattened area.

Image on an upright epi-fluorescence microscope equipped with a cooled monochromatic CCD camera and the suitable filter sets for QDs and GFP. Filter sets for QDs may be commercially available bandpass sets optimized for the selected emission. Such sets often have wide excitation filters centred round 400nm optimized for maximum excitation. However it is preferable to use custom sets with suboptimal longer wavelength excitation to limit photodamage. Imaging NIR QDs requires that the IR blocking filter (in the case of Zeiss axiocam BG 40) is removed from the camera. Most cameras have such IR filters installed.

Image the embryos using the lowest intensity excitation that will result in acceptable signal to noise ratio in order to minimize phototoxicity and photodamage. Use of the field diaphragm to limit excitation in the area of interest is also advisable if embryos will be imaged for long periods of time. In the case of Akt, embryos can be imaged before and 5 minutes after a 10 second exposure to UV (DAPI filter works well at excitation: 360/40), to demonstrate membrane translocation of QDs after PI3K activation and PIP3 production.

If optical sectioning is required structured illumination can provide relatively good results when imaging superficial blastomeres in early embryos. In this case elevated levels of excitation will be necessary in order to bring exposure times to reasonably small values since long exposure times using this method leads to poor image quality. Using structured illumination is not advisable when imaging dynamic movement of proteins or fluorophores. This method requires acquisition of three frames per optical section. Acquisition time length is also compounded due to the presence of the grid at the position of the field diaphragm limiting the intensity of excitation. Any motion during the acquisition of the three frames will be lost and lead to poor image quality.

4. Results

4.1 Inteins

4.1.1 Cloning

Characterization of proteins in the context of a living organism is of crucial importance for a complete understanding of their function. Although organic dyes and fluorescent proteins have been used extensively for single molecule imaging, they generally emit weak signals that typically bleach in less than 10 s. QDs are an alternative probe since, in contrast to traditional fluorophores act as tunable nanoemitters that can be excited by a single light source, offer extremely high fluorescence intensity, wide excitation spectra and resistance to photobleaching (Michalet, Pinaud et al. 2005). A survey of site-specific bioconjugation methods led us to the intein-mediated ligation system. Inteins catalyze the splicing reaction through formation of an active thioester intermediate. In order to illustrate the method we selected to tag the PH domains of two proteins Akt and Btk. These were chosen due to their ability to translocate to the cell membrane upon PIP_3 production by PI3-K (Varnai, Bondeva et al. 2005) and would thus provide a clear visual confirmation of the conjugation in the intact embryo.

Briefly, we genetically tagged EGFP fusions of the PH domains of Akt and Btk with the N-terminus half of a split intein (I_N) encoding five extein residues (KFAEY). We cloned the I_N immediately downstream of the Akt-PH-EGFP into the pCS2++ vector. After cloning we *in vitro* transcribed the RNA and checked the amount and quality of the RNA using a spectrophotometer and gel electrophoresis, respectively.

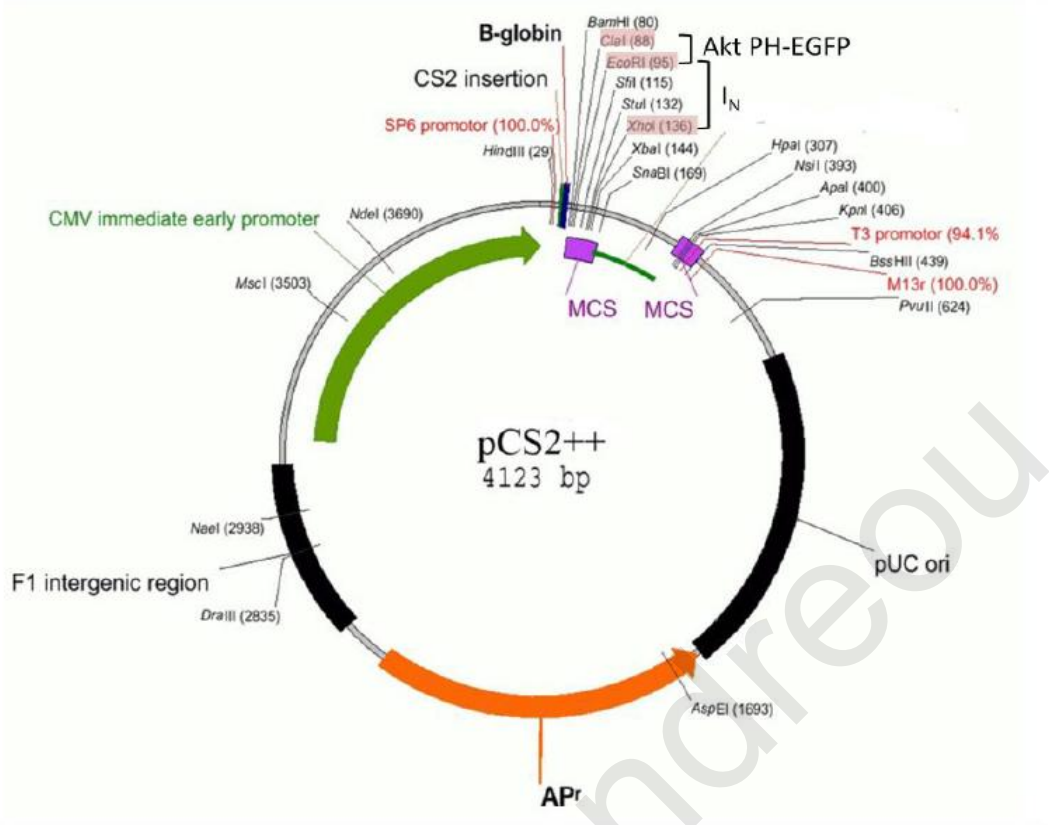

Figure 35: Plasmid Map of pCS2++ indicating restriction sites used to clone Akt PH-EGFP and I_N. DNA fragments encoding Akt PH-EGFP and I_N with 5 N-terminal extein residues (KFAEY) were cloned in frame into the pCS2++ plasmid bearing an Sp6 promoter.

4.1.2 Chemical Synthesis of biotinylated Intein (I_C) peptide (I_C-Biotin) and *In vitro* conjugation of IC-Biotin to streptavidin-coated QDs

A synthetic peptide encoding the complementary C-terminus half of the intein (I_C) was biotinylated and conjugated *in vitro* to streptavidin-coated QD´s. A 47 amino acid peptide corresponding to C-terminal intein (I_C) was synthesized on a 0.5 mmol scale on a 4-methylbenzhydrylamine (MBHA) resin according to the in-situ neutralization/HBTU activation protocol for Boc SPPS (Schnolzer, Alewood et al. 1992). In order to put a biotin at C-terminus, it was necessary to add an extra amino acid, Lys, at the C-terminus. This Lys serves as a linking point for biotin as well as a spacer between the peptide and biotin. The peptide contains a cysteine protected with the NPyS group which was added as the last

amino acid in the synthesis. The crude peptide was purified by preparative HPLC. The lyophilized peptide was dissolved in DMSO at a concentration of 1 mg/ml, since it is relatively hydrophobic and thus difficult to dissolve in water alone.

I_C-Biotin was diluted to 50 μM and used at 1:1 volume ratio with streptavidin-coated QDs (1 μM). The peptide is used around fifty fold excess relative to the streptavidin-coated QDs during conjugation, to ensure that all binding sites on the QDs are bound with peptide. According to manufacturers, commercially available QDs from Invitrogen are multivalent, bearing 4-10 streptavidin molecules per QD, giving 14-40 biotin binding sites per QD. To allow formation of the biotin-streptavidin bond we incubate at 24°C for 30 min. To remove any excess unbound peptide the conjugate was filtered through microcon centrifugal filter units (YM100).

4.1.3 Analysis of QD-peptide conjugates

In order to check if the conjugation has taken place we had to analyze the constructs. Analysis of QD-peptide conjugation was performed by electrophoresis using a 0.5% agarose gel. Gels were visualized under the filter 515-570 nm with a UVP Imager.

Alternatively analysis of QD peptide conjugation was performed by spotting nitrocellulose membrane. Biotinylated I_C peptide and I_C peptide that did not contain the biotin modification at the N-terminus were spotted on nitrocellulose membrane. After blocking the nitrocellulose membrane was then soaked in PBS containing streptavidin-coated QDs (1:500 dilution). The membrane was washed with PBS-Tween 20 (1%) and visualized under the filter 515-570 nm with a UVP Imager (Figure 36).

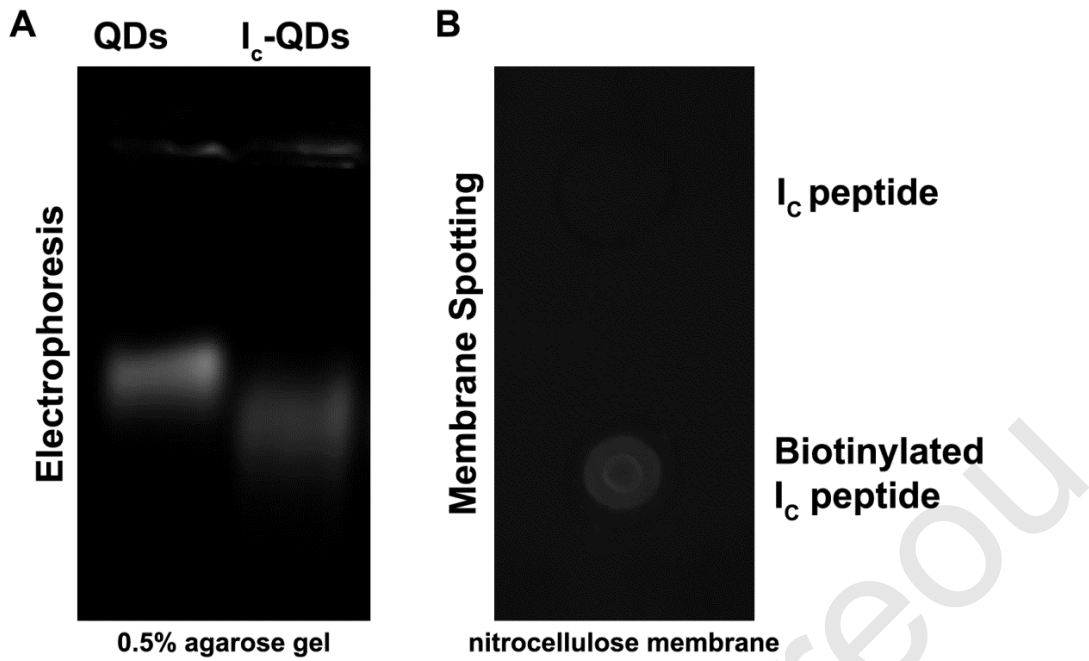

Figure 36 : Analysis of QD-peptide conjugation. (A) Analysis was performed by electrophoresis using a 0.5% agarose gel. Non-Conjugated QDs migrate slower than QDS conjugated with the Intein peptide. Gels were visualized under the filter 515-570 nm with a UVP Imager. (B) Intein peptide and Biotynylated-Intein peptide streptavidin-coated were spotted on a nitrocellulose membrane and after blocking in PBS containing 1% BSA, PBS containing streptavidin-coated QDs (1:500 dilution) was added on the membrane. In the second spot, the conjugation happened and the QDs could be visualized under the filter 515-570 nm with a UVP Imager even after washing the membrane with PBS-Tween 20 (1%).

4.1.4 In situ labeling

To demonstrate in situ labeling of the target protein with QD's we injected both blastomeres of two-cell stage *Xenopus* embryos with the probe (I_C-$QDot_{585}$), allowed the embryo to develop to the four cell stage and then injected three out of four blastomeres with RNA encoding the target protein (in this case, Akt PH-EGFP-I_N). The presence of EGFP on the PH domain allowed us to monitor and compare the distribution of the QD's vs the Akt-PH. As shown in Figure 37, QD's translocated to the membrane in cells derived from the blastomere injected with both I_C-$QDot_{585}$ and RNA, where they colocalized with Akt-PH-EGFP. On the other hand, in cells that do not express the Akt-PH-EGFP-I_N, QD's remained in the cytosol (Figure 37, third pane inset, at 20 × magnification). In addition

cells in which the Akt PH-EGFP remained cytosolic, the QD conjugates also remained in the cytosol. To further establish that QD's were successfully conjugated to Akt-PH-EGFP *in vivo* we used a biochemical approach.

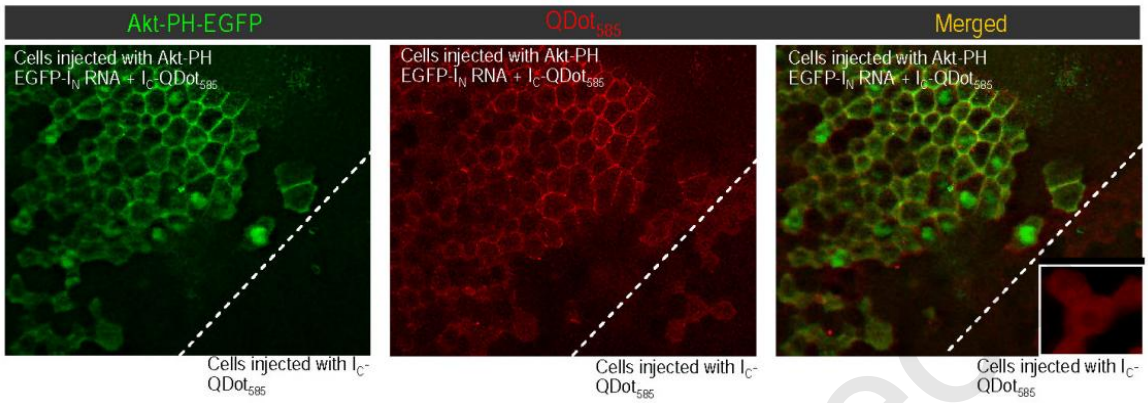

Figure 37 : Co-localization of $QDot_{585}$ with Akt-PH-EGFP on the cell membrane. Fluorescence images of stage 10 Xenopus embryos microinjected with the probe (I_C-$QDot_{585}$) shown in red, in one blastomere at the two-cell stage, and then injected with RNA encoding the target protein (Akt PH-EGFP-I_N) shown in green, in three of four blastomeres. Yellow shows the overlap between red $QDot_{585}$and green EGFP indicating successful QD-protein conjugation in a live embryo.

4.1.5 Electrophoretic analysis of protein trans-splicing

Biochemical analysis of protein-trans splicing was performed by lysis of injected *Xenopus* embryos. *Xenopus* embryos injected as described above were lysed when they reached stage 10 and loaded onto an agarose gel. $QDot_{655}$ were visualized with a band pass 650/30 emission filter under UV excitation and GFP was imaged with a band pass 500/50 filter set on a *UVP iBox* Imaging System. As shown in Figure 38 a single band of the expected molecular weight for the Btk-PH GFP appeared in lysates of *Xenopus* embryos injected with the RNA encoding the target protein (Btk PH-GFP-I_N). This band could not be detected in lysates of *Xenopus* embryos injected with the probe (I_C peptide conjugated QD_{655}) only. A higher molecular weight smeary band corresponding to the semi-synthetic product appeared only in lysates of *Xenopus* embryos injected with both the RNA encoding the target protein (Btk PH-GFP-I_N) and the probe (I_C peptide conjugated QD_{655}).

Importantly, this new band overlaps with the QD signal. The smeary appearance of the band in the agarose gel is due to the fact that the size of the protein-QD conjugates varies greatly as a result of the multivalency of commercially available streptavidin-coated QDs (4-10 streptavidin molecules with a molecular weight of 53 kD each, per QD giving 16-40 biotin binding sites implying 16-40 conjugated PH-GFP protein molecules per QD) resulting in a significant increase in size. In fact, the large size of some of the protein-QD conjugates combined with their lack of charge prevents them from migrating in the gels as they can be detected in the gel wells.

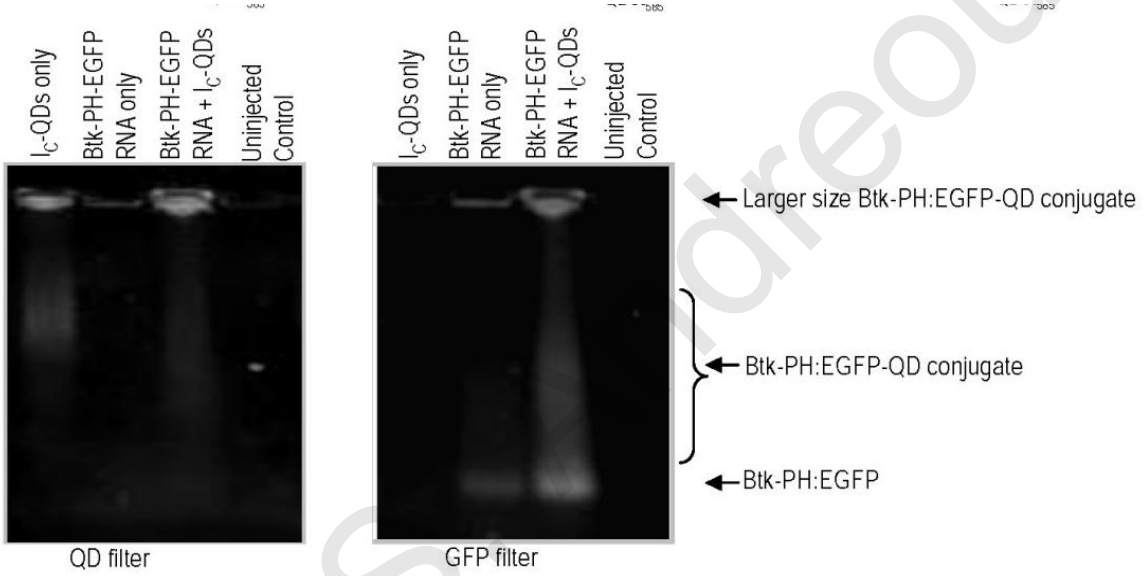

Figure 38 : Biochemical characterization of protein-QD conjugates. *Xenopus* embryos were injected with either probe (Ic-QD's) only or Btk-PH-EGFP-I_N RNA only or both, lysed at stage 10 and loaded onto a 0.5% agarose gel. $QDot_{655}$ were visualized with a band pass 650/30 emission filter under UV excitation and GFP was imaged with a band pass 500/50 filter set on *UVP iBox* Imaging System. The ligation product appears as a smeary band under both the GFP and QD filters, only in lysates of *Xenopus* embryos injected with both the RNA and the probe, and is denoted as Btk-PH-EGFP-QD conjugate. A single band corresponding to the Btk-PH-EGFP protein fusion that is not conjugated to QD's is also detectable under the GFP filter, in lysates of *Xenopus* embryos injected with RNA only or RNA and probe, but not QD's only.

4.1.6 QD-tag does not affect the primary function of the protein

Previous studies have demonstrated that UVB irradiation induces Akt activation and consequent translocation to the plasma membrane via a PI-3K/PDK dependent pathway as well as via Erks and p38 kinase through their downstream kinase, mitogen and stress-activated protein kinase Msk1 (Kabuyama, Hamaya et al. 1998; Nomura, Kaji et al. 2001). So after injecting embryos as previously described they were exposed to UV irradiation. In agreement with previous studies, upon exposure to UV light both the Akt-PH-EGFP and the QD conjugates translocated to the cell membrane within minutes, suggesting UV induced activation of PI3-K (Figure 39a). Furthermore the translocation of Akt-PH-EGFP and the QD conjugates to the plasma membrane was completely eliminated by wortmannin, a PI3-K specific inhibitor suggesting that the observed translocation is PI3-K dependent (Figure 39b). Collectively the data in Figure 38 and Figure 39 show that the QD's were successfully conjugated to Akt-PH-EGFP *in vivo* and the QD tag did not affect the primary function of the PH domain, which is to recognize PIP_3 and translocate to the cell membrane.

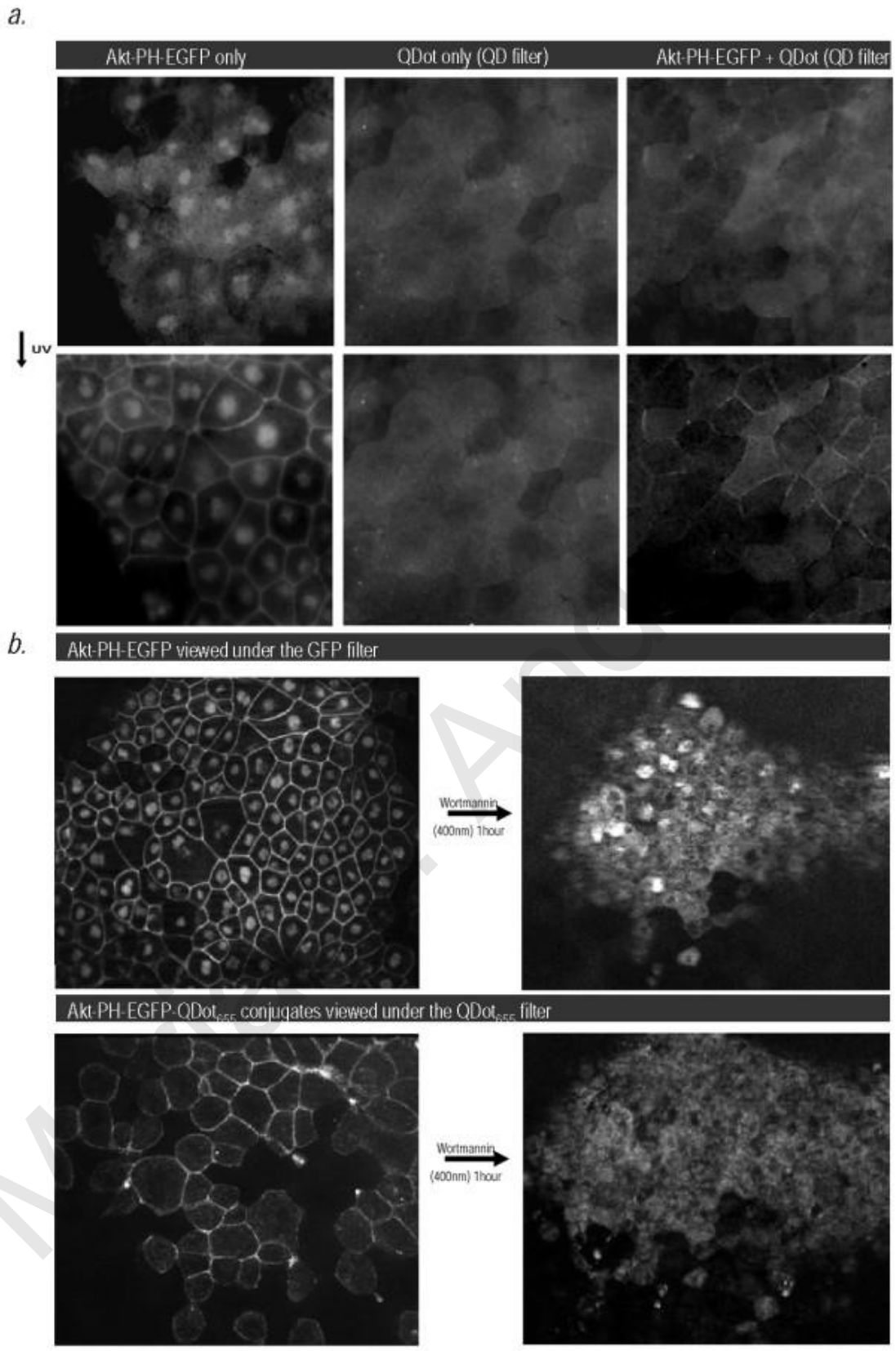

Figure 39 : UV-inducible and wortmannin-sensitive translocation of QD-Akt-PH-EGFP conjugates to the membrane. (a) Akt-PH-EGFP protein fusions and Akt-PH-$QDot_{585}$ conjugates translocate to

the cell membrane upon exposure of injected Xenopus embryos to UV radiation. Live Xenopus embryos injected as described were imaged on a Zeiss Axioimager to visualize the localization of Akt-PH-EGFP and Akt-PH-QD conjugate before and after exposure to UV radiation for 5 min. Both Akt-PH-EGFP and Akt-PH-QD conjugates translocate to the cell membrane following brief exposure to UV radiation. (b) Translocation of Akt-PH-QD conjugates ($QDot_{655}$) to the cell membrane is Wortmanin sensitive. Live Xenopus embryos were imaged on a Zeiss Axioimager to visualize the localization of Akt-PH-QD conjugate before and after treatment with Wortmannin (400 nM), a PI3-K inhibitor, for 1 hour. The Akt-PH QD conjugates become diffusely localized in the cytosol after treatment.

4.1.7 Comparison of the photostability of the QD-conjugates to that of EGFP

We went on to compare the photostability of the QD-conjugates to that of EGFP. To test this we used the $QDot_{525}$-Streptavidin from Invitrogen which have emission spectra that closely match those of EGFP and repeated the conjugation and injections as described above. It should be noted that unlike the $QDot_{585}$ Streptavidin conjugates which fail to enter the nucleus, $QDot_{525}$-Streptavidin have sufficiently small hydrodynamic radii to do so. Injected embryos were allowed to develop to stage 10 and were then imaged on an epifluorescence microscope. Figure 40 shows that continuous exposure of the embryos to excitation light (~ 480 nm) led to gradual loss of the EGFP signal, due to photobleaching, but did not affect the $QDot_{525}$-Streptavidin signal even after 20 minutes of continuous excitation. Importantly and despite the long exposure to excitation light the QD conjugates retained their membrane localization.

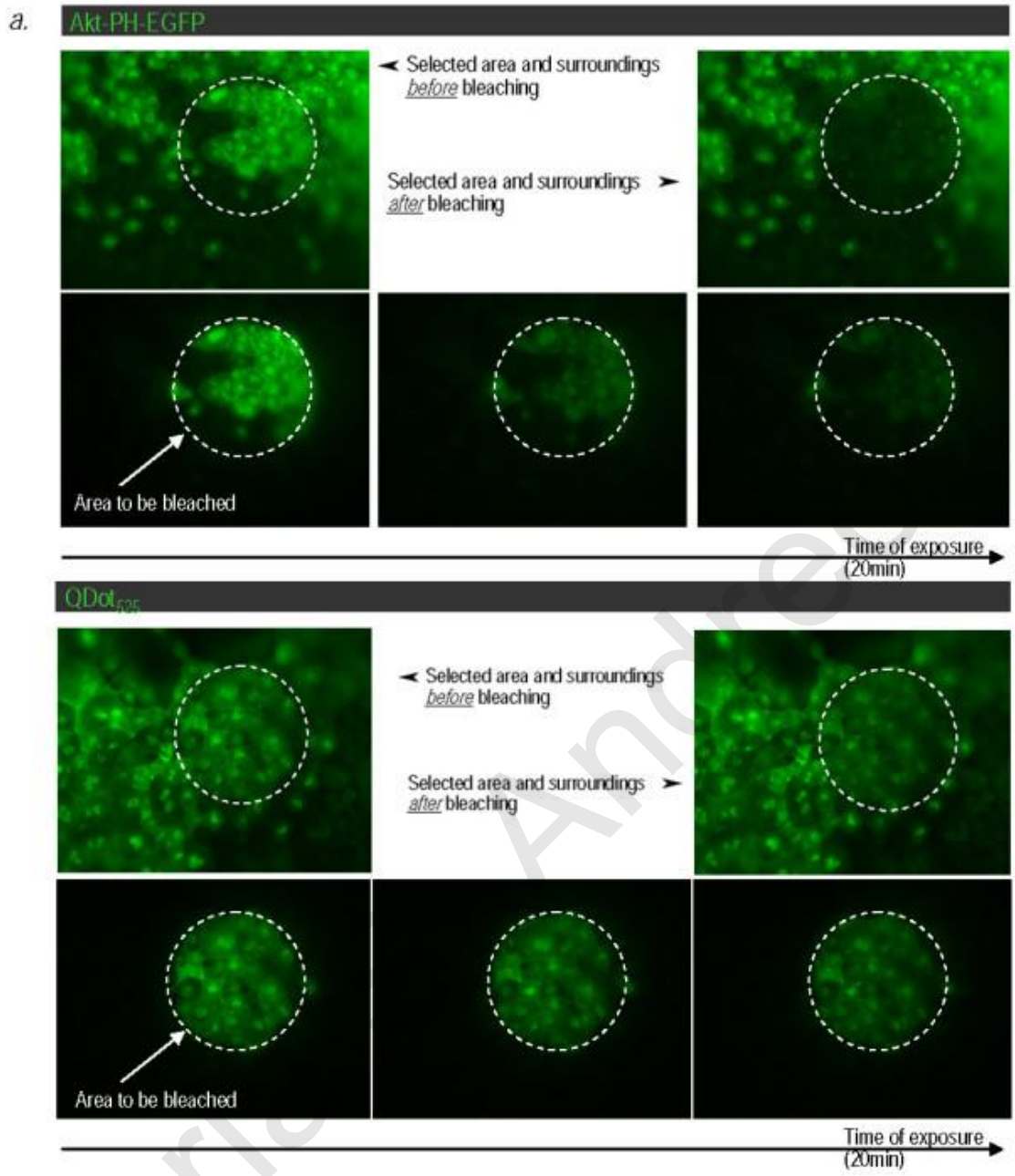

Figure 40 : QD-Akt-PH conjugates are resistant to photobleaching, unlike Akt-PH-EGFP fusions. Fluorescence images of stage 10 *Xenopus* embryos microinjected with the probe (I_C-QD_{525}) and with RNA encoding the target protein (Akt PH-EGFP-I_N), both shown in green since their emission spectra are closely matched. Embryos were exposed to continuous excitation (~ 480 nm) for > 20 min. This led to gradual loss of the EGFP signal but did not affect the $QDot_{525}$ signal.

4.1.8 Longer wavelength emitting QD's show a diminished capacity to translocate to the membrane

Despite their ideal optical properties, commercially available CdSe/ZnSe QD's especially those emitting in the NIR are large and can impair trafficking of proteins to which they are attached and limit access to crowded cellular locations such as the cell membrane or even restrict access into membrane bound intracellular compartments such as the nucleus (Groc, Lafourcade et al. 2007; Howarth, Liu et al. 2008; Stylianou and Skourides 2009). A large fraction of the QD size comes from the passivating layer, often a polyacrylic acid polymer or phospholipids micelle, required to allow conjugation of biological molecules to QD's and retention of their optical properties (Michalet, Pinaud et al. 2005). We used commercially available QD's from Invitrogen and eBiosciences (15-20 nm in diameter), that did not only have the passivating layer but were further coupled to streptavidin, as described earlier. Conjugates of Akt-PH with QD's from all the emission wavelengths tested (525, 565, 585, 605, 705, 800) could translocate to the cell membrane, However, there was a definitive size dependence in their ability to translocate to the plasma membrane, with longer wavelength emitting QD's showing a diminished capacity to do so (compare Figure 40 ($QDot_{525}$) to Figure 37 ($QDot_{585}$) and Figure 41a ($QDot_{705}$). In addition and in agreement with previously published work (Stylianou and Skourides 2009), only protein conjugates with $QDot_{525}$ (from Invitrogen) and QD_{605} (from eBiosciences), were able to translocate into the nucleus, as efficiently as an organic fluorophore conjugate (Cy3) (compare Figure 40 to Figure 37 ($QDot_{585}$), Figure 41a ($QDot_{705}$) and Figure 39b ($QDot_{655}$) and data not shown). Longer wavelength protein-QD conjugates were completely excluded from this membrane bound intracellular compartment. The fact that $QD's_{605}$ from eBiosciences but not from Invitrogen entered the nucleus could be a result of different coating of the QD's or lower number of streptavidin molecules per nanocrystal. Our present results point to the need for wider availability and commercialization of significantly smaller water soluble nanocrystals with a variety of core and shell compositions as synthesized by different groups (Fu, Gu et al. 2005; Zimmer, Kim et al. 2006; Liu, Choi et al. 2007).

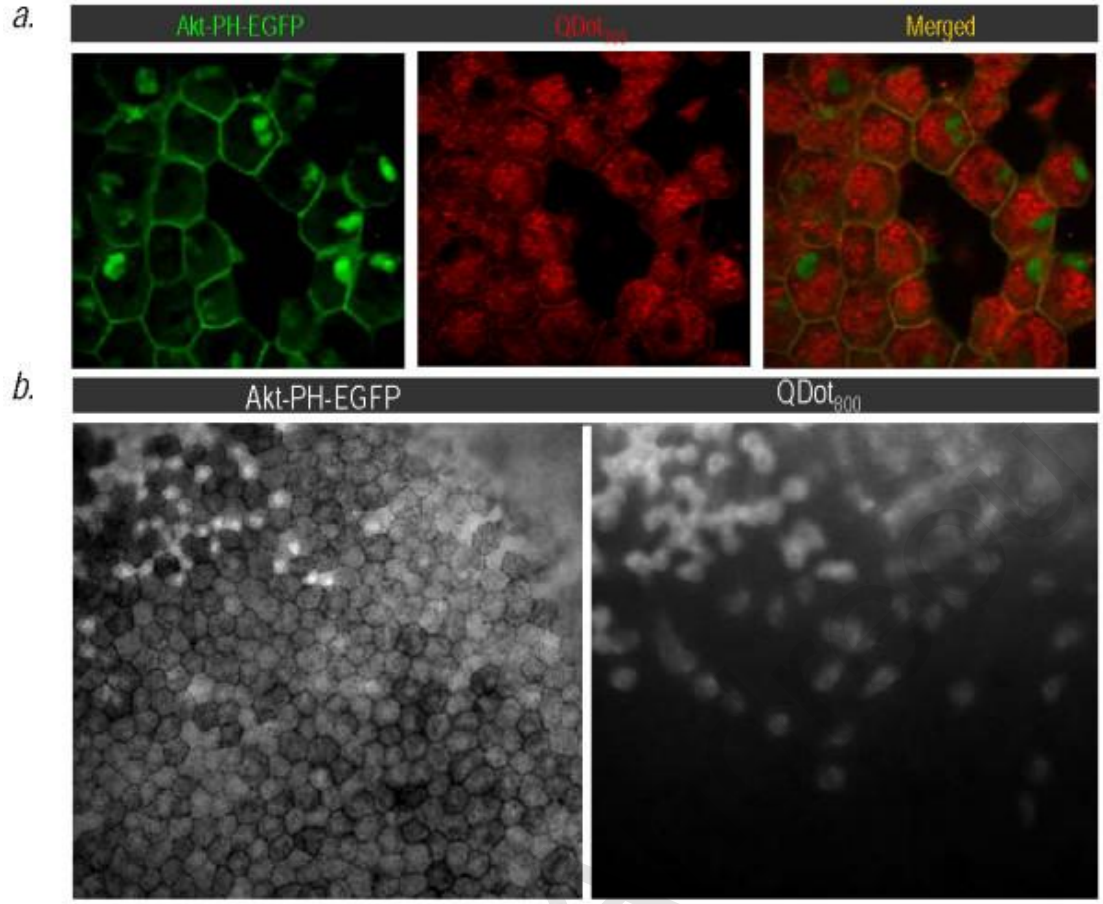

Figure 41 : Increased NIR-QDot size imposes constraints on Akt-PH-QD conjugate translocation efficiency but NIR-QD's allow visualization in deeper cell layers in a live Xenopus embryo, unlike Akt-PH-EGFP. (a) Co-localization of $QDot_{705}$ with Akt-PH-EGFP on the cell membrane**.** Note that unlike the $QDot_{585}$, the $QDot_{705}$ are not recruited as effectively to the cell membrane. (b) $QDot_{800}$ allow visualization of the Akt-PH ~ two to three layers below the superficial cell layer, where the GFP signal was either undetectable or too diffuse. The images are of the same region of the embryo imaged with a GFP (left) and a $QDot_{800}$ (Perez-Alvarado, Martinez-Yamout et al.) filter set.

4.2 Samba

4.2.1 Phylogenetic Relationship and expression pattern of 40LoVe, Samba and hnRNP AB

Samba is a previously identified hnRNP (Yan, Skourides et al. 2009) and we wanted to investigate its role in *Xenopus* development using Morpholino based loss of function approaches. To do so the precise sequence of the mRNA has to be known so that a translational blocking MO can be designed. However *Xenopus laevis* genes frequently have pseudoalleles, thought to have originated from hybridization between two different *Xenopus* species during the course of evolution and one needs to know if such paralogs exist in order to design a MO pair and effectively block translation of both transcripts (Kobel and Pasquier 1986). Previous studies have identified such cases, like the secreted protein Cerberus (Mayeda, Munroe et al.), that is required for the correct induction and patterning of the brain (Silva, Filipe et al. 2003; Kuroda, Wessely et al. 2004). Also Fibronectin (FN) a well characterized adhesive glycoprotein of the extracellular matrix is implicated in several developmental events including gastrulation, neural crest cell migration, somitogenesis, and heart formation has been reported to have a paralog requiring a pair of morpholinos for effective downregulation (DeSimone, Norton et al. 1992; DeSimone 1994). The cDNA of Samba was identified from an early gastrula *Xenopus laevis* library (Yan, Skourides et al. 2009). Using that sequence and through an EST database search, we found that there are at least three very similar transcripts; Samba, 40LoVe and hnRNP AB. These three proteins, like other hnRNPs consist of three domains with specific roles; a core RNA-binding domain (RBD or RRM-RNA recognition motif); RGG boxes that are composed of Arginine-Glycine-Glycine triplets interspersed with aromatic residues and a variable carboxy-terminal domain (Swanson, Nakagawa et al. 1987; Han, Tang et al. 2010). The c-terminus is in some cases enriched with glycine, proline or acidic residues which depending on the specific function of the protein (Swanson, Nakagawa et al. 1987; Cartegni, Maconi et al. 1996). Specifically, the glycine-rich domain (GRD) found at the c-terminus of a number of hnRNPs has been shown to be required for self-interaction and to be essential for the splicing activity of in the case of hnRNP A1 (Mayeda, Munroe et al. 1994), to contain a non classical nuclear localization signal and

promote nucleocytoplasmic shuttling and nuclear import in the case of hnRNP H/F (Kiledjian and Dreyfuss 1992; McNally, Yee et al. 2006; Van Dusen, Yee et al. 2010). Finally, several hnRNPs contain a third auxiliary domain that is variable (Han, Tang et al. 2010) and in some hnRNPs this is a CARG-binding factor A domain (CBFNT), which has been shown interact with the promoter of immunoglobulin K (Varnai, Bondeva et al. 2005).

Previous work showed that 40LoVe displays three different isoforms during oogenesis that do not result from post-translational modifications (Kroll, Swenson et al. 2009). Moreover, members of the hnRNP A/B-D subfamily frequently undergo alternative splicing to generate multiple isoforms (Norvell, Kelley et al. 1999; Kawamura, Tomozoe et al. 2002). Sequence alignment showed that 40LoVe and Samba are identical both at the nucleotide as well as the amino acid level except for a 13 amino acid deletion at the N-terminus of Samba, between the CBFNT domain (Varnai, Bondeva et al. 2005) and the RBD1 (Figure 42A). In addition, both the 3` and 5` UTR sequences of the two transcripts are identical, suggesting that these two proteins are splice variants. A comparison of hnRNP AB with 40LoVe shows that it has an overall 93% identity at the amino acid level with the differences concentrated at the amino and carboxy-termini (Figure 42A). However, although the 3´ and 5´ UTRs of hnRNP AB present significant homology to that of 40LoVe/Samba, they are not identical (Figure 42B-C). Together, these data suggest that hnRNP AB is a pseudoallele of 40LoVe/Samba. For the sake of clarity we searched the databases for the previously identified sequences. By sequence alignments we arrive at the conclusion that 40LoVe identified by Czaplinski et al (Czaplinski, Kocher et al. 2005) corresponds to what shows up in databases as Xenopus hnRNP AB and 40LoVe identified by Kroll et al. corresponds to what appears as 40LoVe in databases (Kroll, Swenson et al. 2009). Kroll et al. conclusion that 40LoVe and hnRNP AB are encoded by distinct genes is also supported by our data and we have thus used the nomenclature that appears in the databases referring to hnRNP AB and 40LoVe throughout the thesis (Kroll, Swenson et al. 2009).

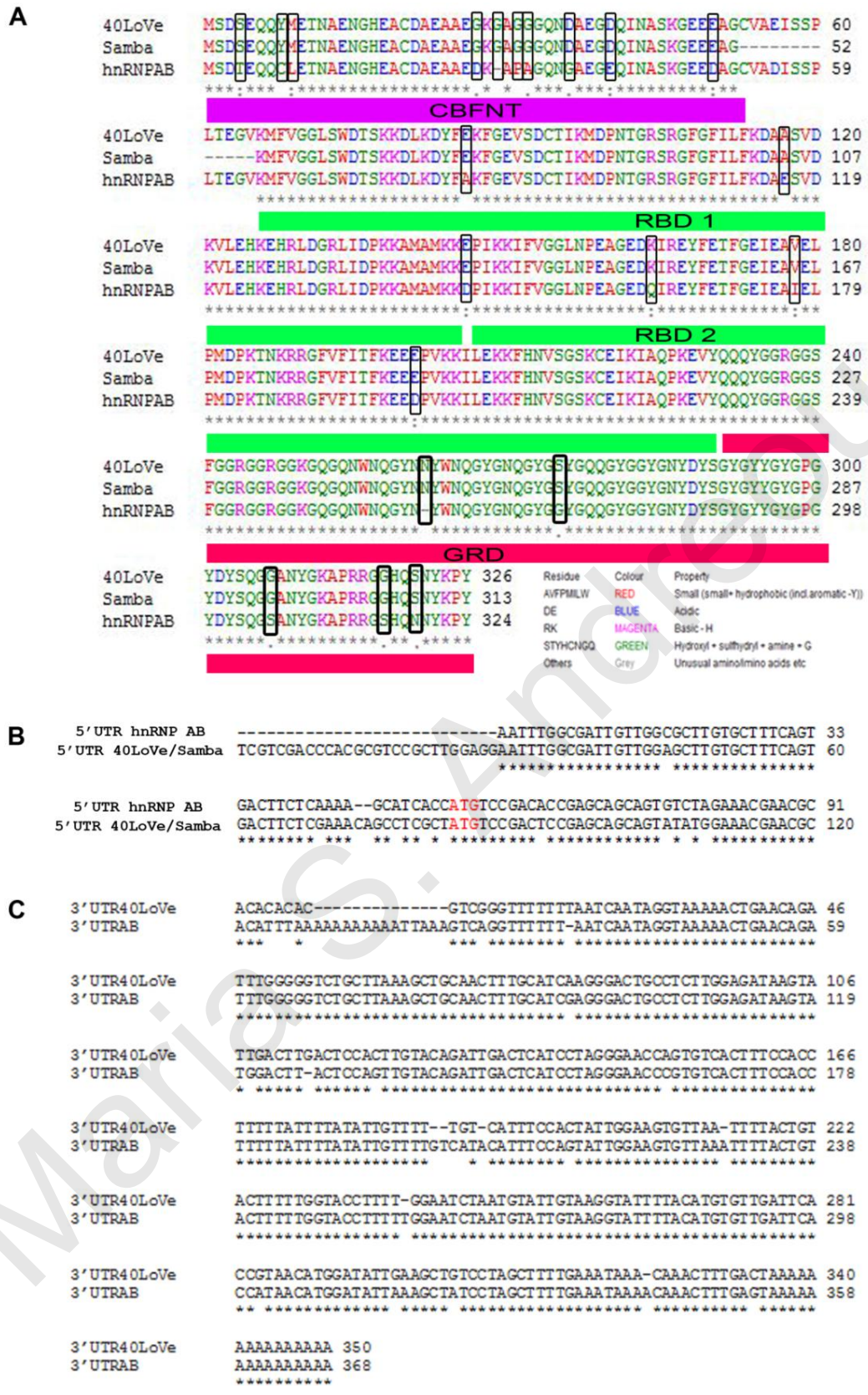

Figure 42: Samba, 40LoVe and hnRNP AB alignment. (A) The N-terminus shows high homology with the CBFNT domain identified in the GARG-binding factor A protein (Bemark et al., 1998).

There are two RNA binding domains, the RBD1 containing an RRM1 and the RBD2 containing an RRM2 (Blast). There is also a Glycine Rich domain at the C-terminus of the protein. The comparison of hnRNP AB with 40LoVe shows that they have an overall 93% identity at the amino acid level with the differences spread throughout the sequence. The black boxes indicate the differences between 40LoVe/Samba and hnRNP AB. (B) Alignment of the 5'UTR of hnRNP AB and 40LoVe/Samba. (C) Alignment of the 3'UTR of hnRNP AB and 40LoVe/Samba. The UTRs comparison shows that the two sequences share significant homology and the differences are spread throughout the sequence.

As previously described, Samba is expressed throughout development, but the primers used for reverse transcription in this study, could not differentiate between the two splice variants, as they corresponded to nucleotides 304-869 and are, as a result, showing the combined 40LoVe/Samba expression (Yan, Skourides et al. 2009). Therefore, we specifically designed a new set of primers corresponding to nucleotides 1-350 (the span which contains the 69 nucleotide deletion of Samba), to allow distinction between the two transcripts and determine whether the two are differentially expressed during development. RT-PCR amplification with this set of primers generates two bands as expected, a lower band that corresponds to Samba and a higher band that corresponds to 40LoVe (Figure 43A). As shown, 40LoVe appears to be the primary transcript of the gene since it gave a much stronger band (Figure 43A-B). These results indicate that both 40LoVe and Samba are expressed throughout development albeit at different levels (Figure 43A). We went on to use a 40LoVe polyclonal antibody in order to examine the temporal expression at the protein level. As shown in Figure 43C the antibody produces three bands the lowest of which is at the predicted size for Samba, while the other two are at the predicted size for 40LoVe and hnRNP AB. The blot shows that in agreement with the RT-PCR results these proteins are expressed throughout development with protein levels gradually increasing and that the protein levels of Samba are much lower than those of 40LoVe.

Due to the very high homology of the three transcripts it was not possible to determine potential spatial differences of expression using *in situ* hybridization. For this reasons using the same primers, we compared the expression of the two transcripts in different regions of the embryo. 40LoVe, Samba and hnRNP AB are expressed in all regions of a

stage 10,5 embryo as described before for Samba (Yan, Skourides et al. 2009) (Figure 43B). Thus, it appears that 40LoVe and Samba are under common spatiotemporal control, but with a clear bias towards generation of 40LoVe. When we examined hnRNP AB expression in the different regions of the embryo we concluded that its spatial and temporal expression dynamics are similar to those of 40LoVe and Samba (Figure 43B). As stated above due to the high degree of homology, the spatial expression of the three transcripts could not be further differentiated via *in situ*. It appears that both transcripts are expressed in neural and neural crest derivatives as described before (Yan, Skourides et al. 2009) (Figure 43D). In agreement to these, whole mount immunostained embryos using the 40LoVe polyclonal antibody, expected to react with all three proteins, showed that expression is enriched in neural tissues (Figure 43E). Since both Samba and hnRNP AB have been reported to play a role in neural development, we performed functional assays focused on neural development (Yan, Skourides et al. 2009; Sinnamon, Waddell et al. 2012).

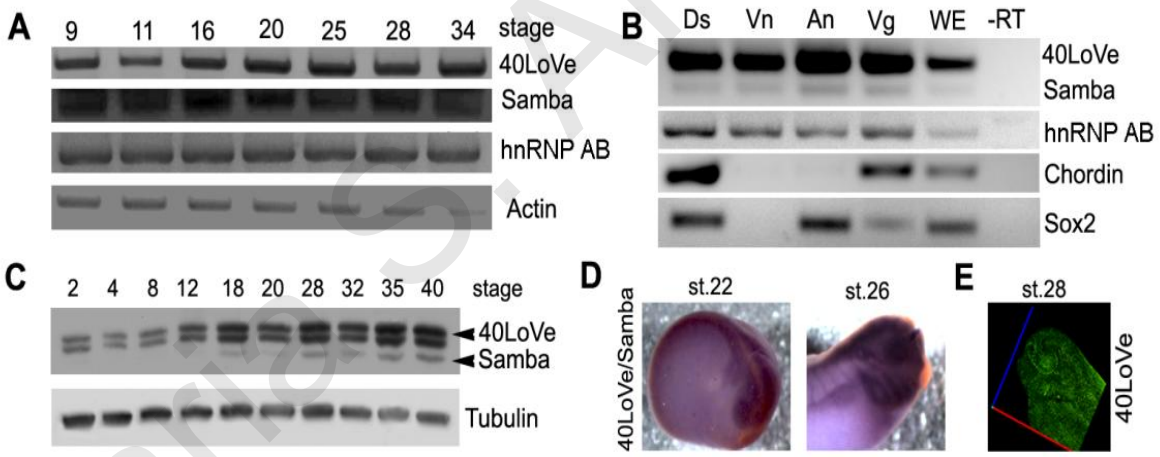

Figure 43 : Temporal and Spatial Expression of 40LoVe, Samba and hnRNP AB. (A) RT-PCR using primers corresponding to nucleotides 1-350 (containing the 69 nucleotide deletion of Samba) for 40LoVe/Samba and primers designed for hnRNP AB from the 5'UTR to the stop codon. 40LoVe, Samba and hnRNP AB are expressed throughout development. Actin was used as a normalizing control. (B) RT-PCR from different regions dissected from a stage 10.5 embryo. 40LoVe/Samba was enriched in Dorsal and Animal regions and hnRNP AB is expressed in a similar manner in all regions of the embryo. The dorsal mesodermal marker Chordin and the neural marker Sox2 were used as controls. (C) Western Blot of half embryo equivalent indicates that the three proteins are expressed throughout development and confirms that the expression levels of 40LoVe are much

higher than those of Samba and that they share similar temporal regulation. Tubulin was used as a loading control. (D) *In situ* hybridizations show that 40LoVe/Samba is expressed in neural and neural crest derivatives. (E) Whole mount immunostaining shows that 40LoVe is enriched in neural tissues.

4.2.2 Cloning

Using gastrula stage cDNAs, all three proteins (Samba, 40LoVe and hnRNP AB) untagged or with either a GFP or a Flag tag were cloned into the pCS108 vector. Primers were designed based on the provisional sequences of *Xenopus laevis* hnRNP AB from www.xenbase.org (XB-GENE-6043063) (Bowes, Snyder et al. 2010) and the NCBI database (GenBank: NM_001087020) and for 40LoVe from the NCBI database (GenBank: NM_001161893). First strand cDNA was reverse transcribed from gastrula stage *Xenopus laevis* mRNA, and the hnRNP AB specific primers were used to amplify the coding and 5' untranslated region of hnRNP AB and 4oLoVe. Sequenced clones were identical to the provisional sequences from Xenbase and NCBI.

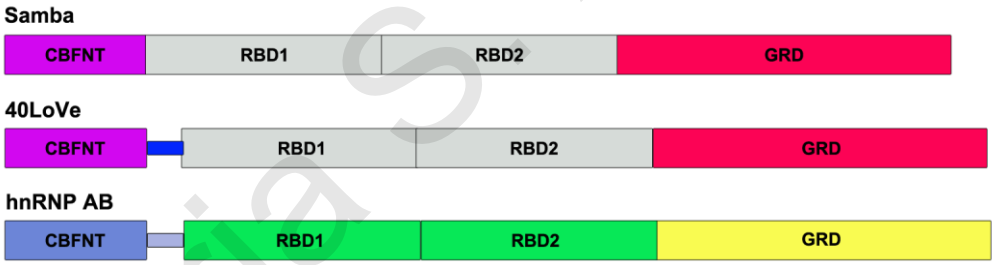

Figure 44 : Protein Structure. All three proteins consist of three domains; a CBFNT domain at the N-terminus, two RNA Recognition motifs (RRM domains) and a third Glycine rich domain (GRD).

After the cloning, *in vitro* transcription was performed and the resulting mRNAs were injected in embryos to test with western blot analysis that untagged and tagged versions of the protein were recognized by 40LoVe and tag antibodies (GFP and Flag) (Figure 45). An antibody raised against 40LoVe was obtained (Czaplinski and Mattaj 2006). Given the high sequence homology between the three proteins one would expect this polyclonal antibody to recognize all of them. As expected, the antibody did recognize all three

proteins when overexpressed. In control xenopus lysates, three distinct bands were seen. These three correspond to the molecular weights of the three tagged constructs suggesting that the three bands do in fact correspond to 40LoVe, Samba and hnRNP AB. From the western it appeared that 40LoVe and hnRNP AB are expressed at much higher levels than Samba confirming the RT PCR data.

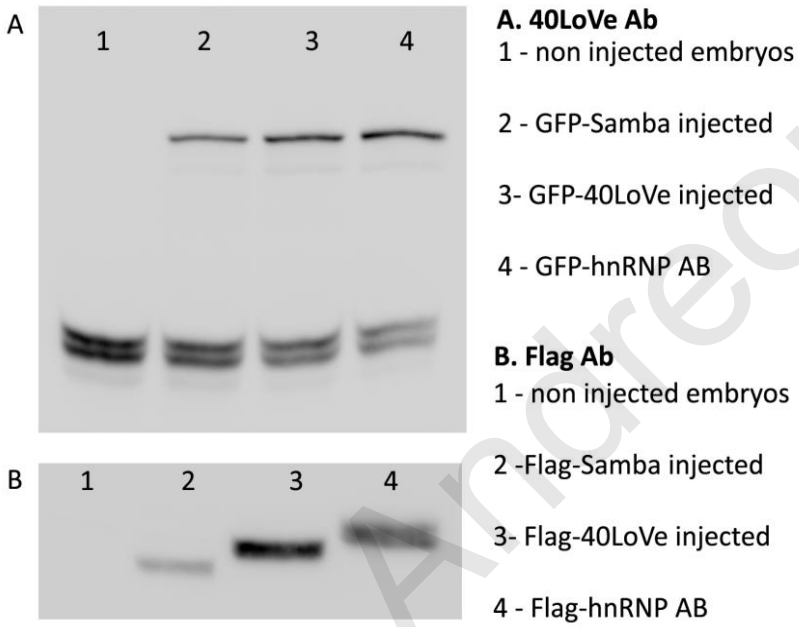

Figure 45 : Tagged versions of each protein are recognized by 40LoVe and tag antibodies. (A) WB with 40LoVe Ab shows endogenous and GFP tagged proteins. (B) WB with Flag Ab shows the three proteins. The WBs were performed on 12% SDS-PAGE gels.

Next, these constructs were used to generate modified versions of the protein (R40LoVe and RhnRNPAB) with a mutated N-terminus which could not be recognized by the Morpholino and were used to rescue the phenotype.

In addition, deletions of Samba and fusions of hnRNP AB and 40LoVe have also been generated for future experiments for the determination of regions responsible for the localization of each protein as described below (Figure 59).

4.2.3 Samba, 40LoVe and hnRNP AB localization in *Xenopus laevis* embryos

In vivo

Since it is known that protein localization is related to function, we wanted to examine the protein localization pattern of Samba, 40LoVe and hnRNP AB. Samba and 40LoVe were examined first, due to the fact that hnRNP AB appeared to be a paralog of 40LoVe. Embryos were injected with the Flag-tagged Samba and 40LoVe mRNAs. Then whole mount Immunofluorescence (IF) experiments were conducted using Flag antibody. Samba displayed variations in localization, being primarily in the nucleus and to a lesser extent in the cytoplasm and the plasma membrane during interphase in some cells and primarily cytoplasmic in other cells (Figure 46). This variation appears to be cell cycle dependent. This localization is consistent with the proposed role of the protein as an hnRNP. 40LoVe-Flag mainly localized in the nucleus and at the plasma membrane, whereas the cytoplasmic fraction was reduced compared to Samba (Figure 46).

In an effort to confirm that hnRNP AB is a paralog of 40LoVe we went on to examine its localization. Surprisingly, hnRNP AB was exclusively localized in the nucleus and no membrane or cytosolic signal was detected in interphase cells (Figure 46). Some cells displayed cytoplasmic signal, but these were a small minority and appeared to be undergoing mitosis. Given the extremely high homology between 40LoVe and hnRNP AB, and the fact that differences at the amino acid level are scattered throughout the protein, this dramatic difference in localization is surprising but also suggests that hnRNP AB may be functionally distinct from 40Love.

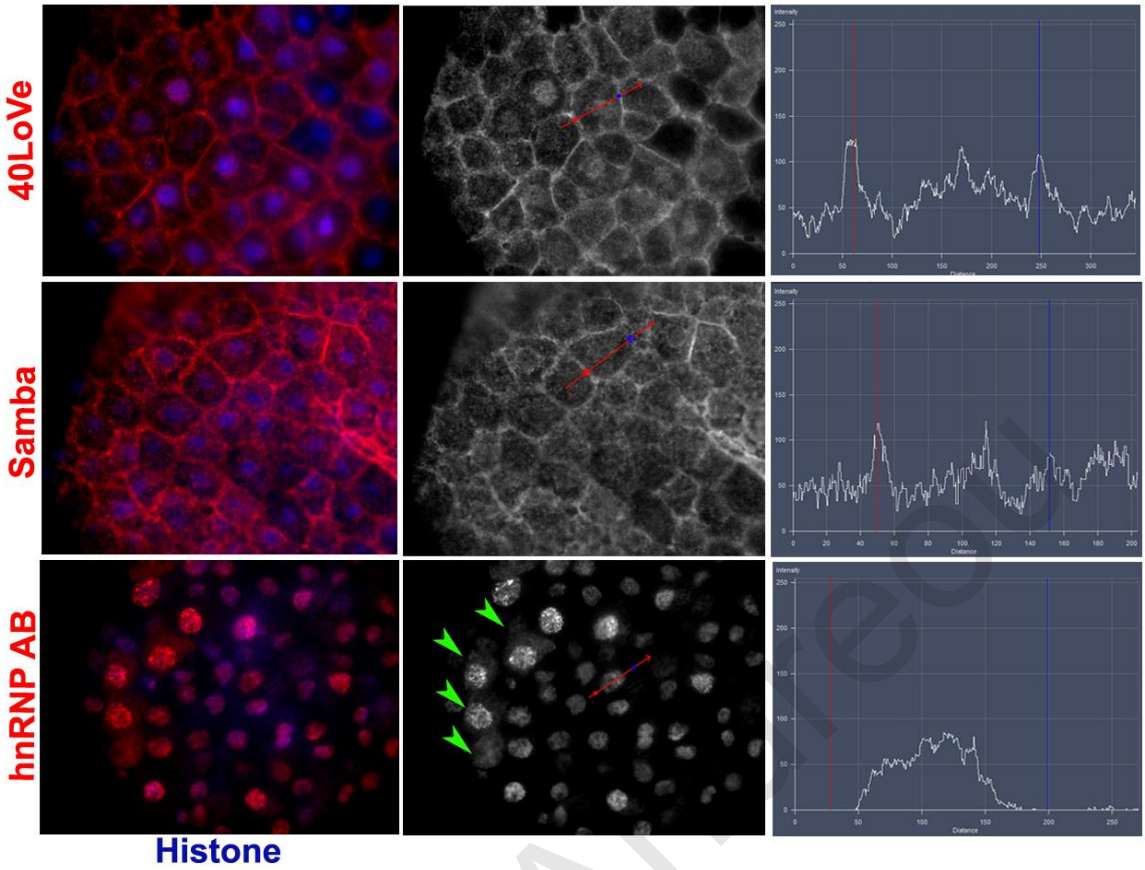

Figure 46: Localization of the proteins in fixed embryos. Flag-40LoVe, Flag-Samba and Flag-hnRNP AB were injected in embryos and IF was performed to examine their localization *in vivo*. 40LoVe and Samba predominantly localize in the nucleus and to a lesser extent in the cytoplasm during interphase. Thus, hnRNP AB is localized primarily in the nucleus, but some cells display cytosolic localization as indicated with green arrows.

In order to verify the correct localization of the tagged constructs, a 40LoVe antibody was used in whole-mount IF experiments. The antibody primarily gave a nuclear signal, in agreement with the fact that both 40LoVe and hnRNP AB are mostly found in the nucleus (Figure 47). Given the much lower expression levels of Samba, we would expect the primarily cytosolic signal of Samba to be too low to detect.

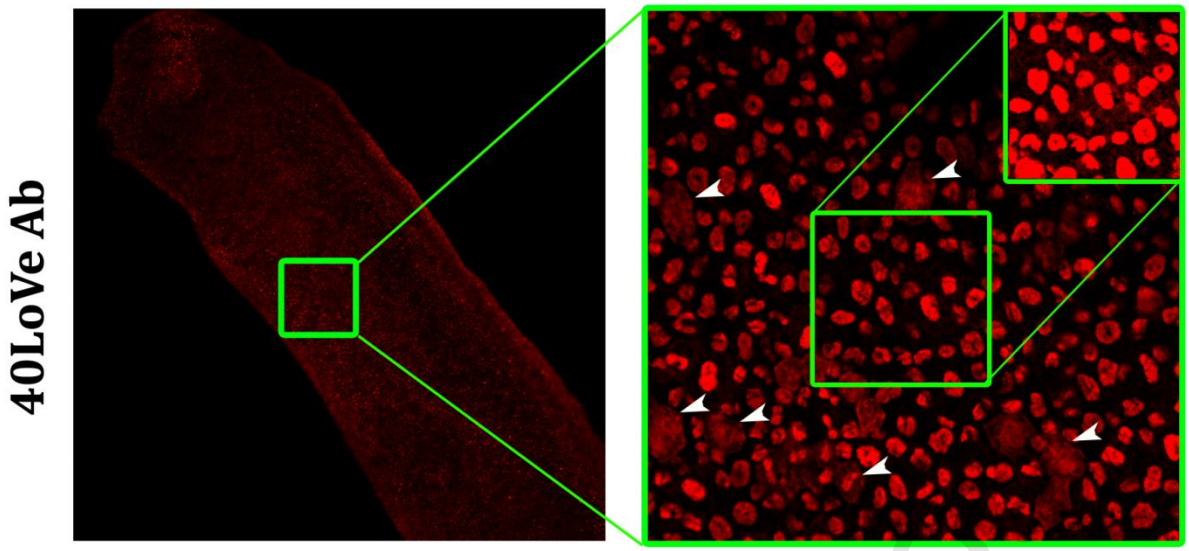

Figure 47 : 40LoVe Localization. Immunofluoresence using the anti-40LoVe antibody that recognizes all three proteins (40LoVe, Samba and hnRNP AB). The signal is mostly nuclear due to the fact that both 40LoVe and hnRNP AB are found in the nucleus. The white arrowheads show cells with cytosolic localization and if the signal is overexposed we are able to see more cytosolic signal.

Given the fact that all three proteins showed some variation in localization, which appeared to be cell cycle dependent, we decided to generate GFP fusions to observe the protein dynamics during cell division in live embryos. Both blastomeres of 2 cell stage embryos were injected at the animal pole with RNA encoding the GFP-tagged versions of each protein. We initially injected GFP-Samba RNA. Surprisingly, we observed that during mitosis, Samba localization changes dramatically and it co-localizes with the microtubules of the mitotic spindle. Once the nuclear envelope breaks down, Samba is released in the cytosol and associates with the spindle while being excluded from the chromatin. The protein remains co-localized with the spindle during all phases of cell division (Figure 48). After division and when the nuclear envelope forms again, a portion of the protein rapidly returns back into the nucleus (Figure 48). Both 40LoVe and hnRNP AB localize in a similar fashion during division, although the three proteins exhibit different localization during interphase as described above (Figure 46, Figure 49).

In an effort to confirm that the protein does in fact co-localized with the spindle during mitosis, mkate-Samba and GFP-tubulin were co-injected in two out of two blastomeres of

a two cell stage embryo and was allowed to develop to stage 14. Then the embryos were stained with Hoechst to mark the DNA and imaged on a fluorescence microscope. Our data reveal that GFP-tubulin forms the mitotic spindle and mkate-Samba remains co-localized with the spindle at all stages of cell division, while it is excluded from chromatin (Figure 50).

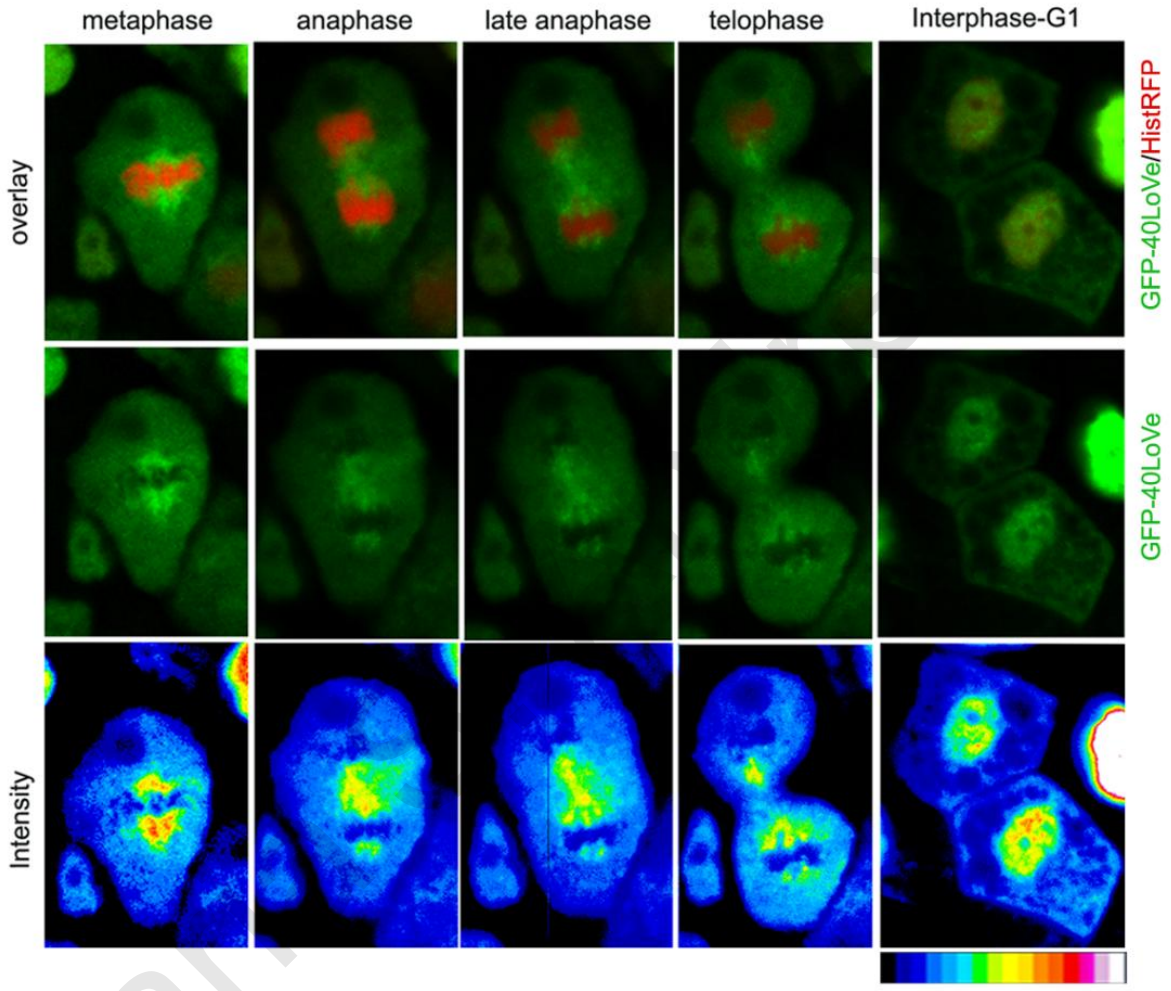

Figure 48: Samba localizes to the spindle during cell division and returns back to the nucleus immediately after division. Once the nuclear envelope breaks down Samba is released in the cytosol and associates with the spindle while being excluded from the chromatin. The protein remains co-localized with the spindle during all phases of cell division. After mitosis and when the nuclear envelope forms again, GFP-Samba gradually returns into the nucleus. The last image of each row shows the intensity of GFP-Samba.

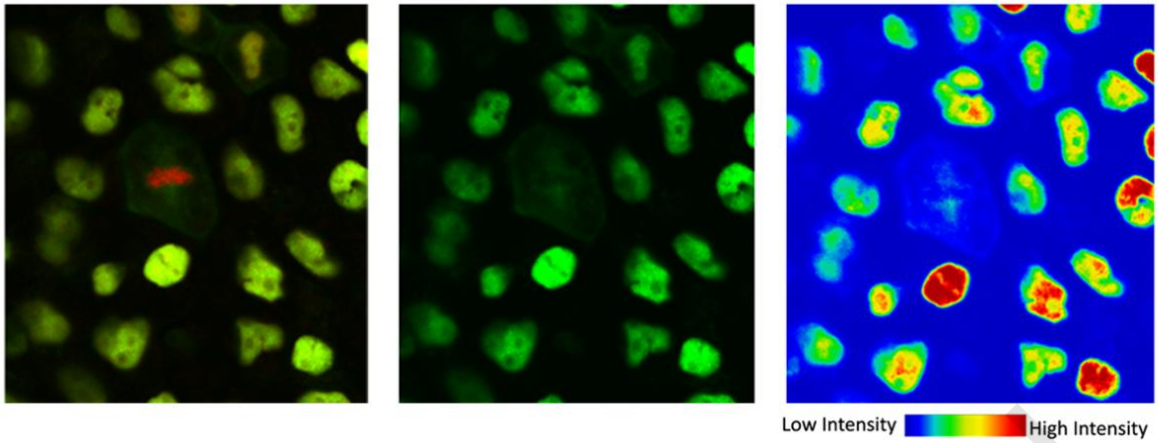

Figure 49 : hnRNP AB localization changes during division. hnRNP AB is primarily nuclear but its localization changes during division and localizes with the spindle just like Samba. Green is GFP-hnRNP AB and Red is RFP-Histone. The last image of each row shows the intensity of GFP-Samba.

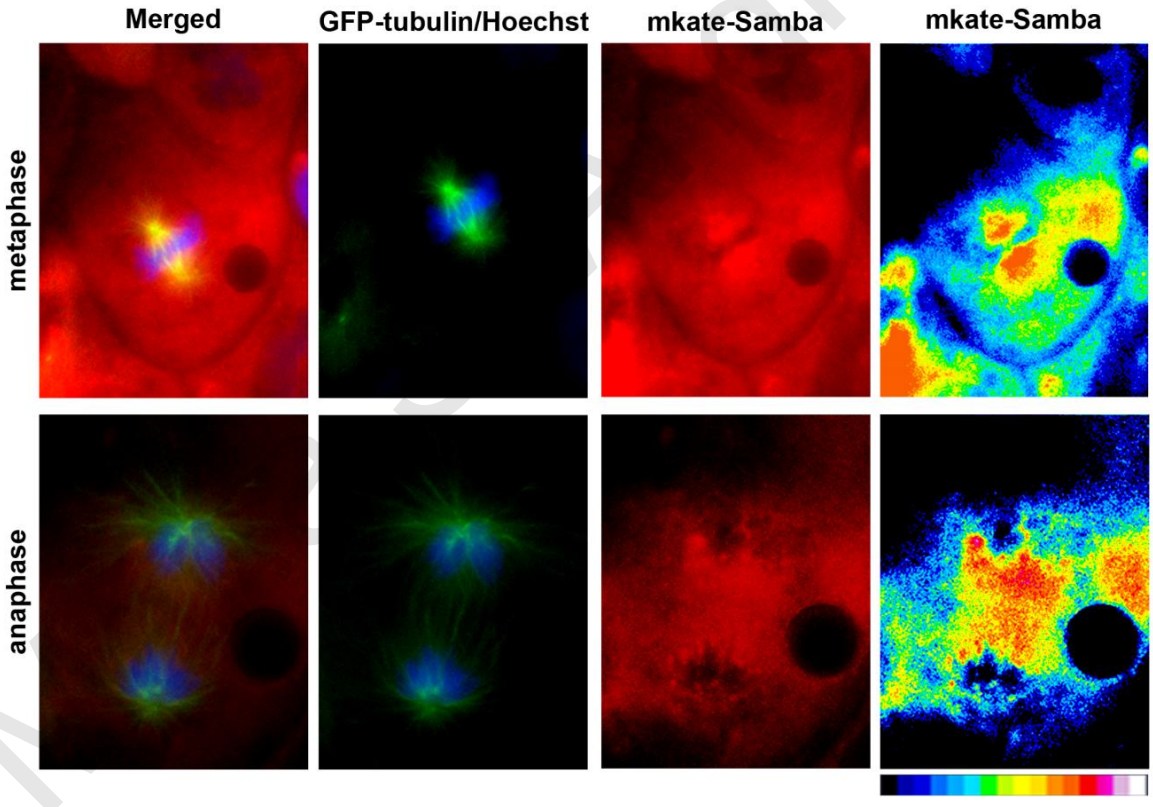

Figure 50 : Samba co-localizes with the spindle during division. Embryos were injected with mkate-Samba, GFP-tubulin and stained with Hoechst to mark the DNA. Samba is excluded from the DNA and co-localizes with the spindle. The last column shows mKate-Samba intensity coded.

In order to confirm the protein localization *in vitro,* A6 and XL177 *Xenopus* cell lines were electroporated with GFP-Samba, or GFP-hnRNP AB together with RFP-Histone (Figure 51). Samba was mainly localized in the cell nucleus and also found in the cytoplasm, while hnRNP AB was strictly found in the nucleus, confirming the *in vivo* results (Figure 46).

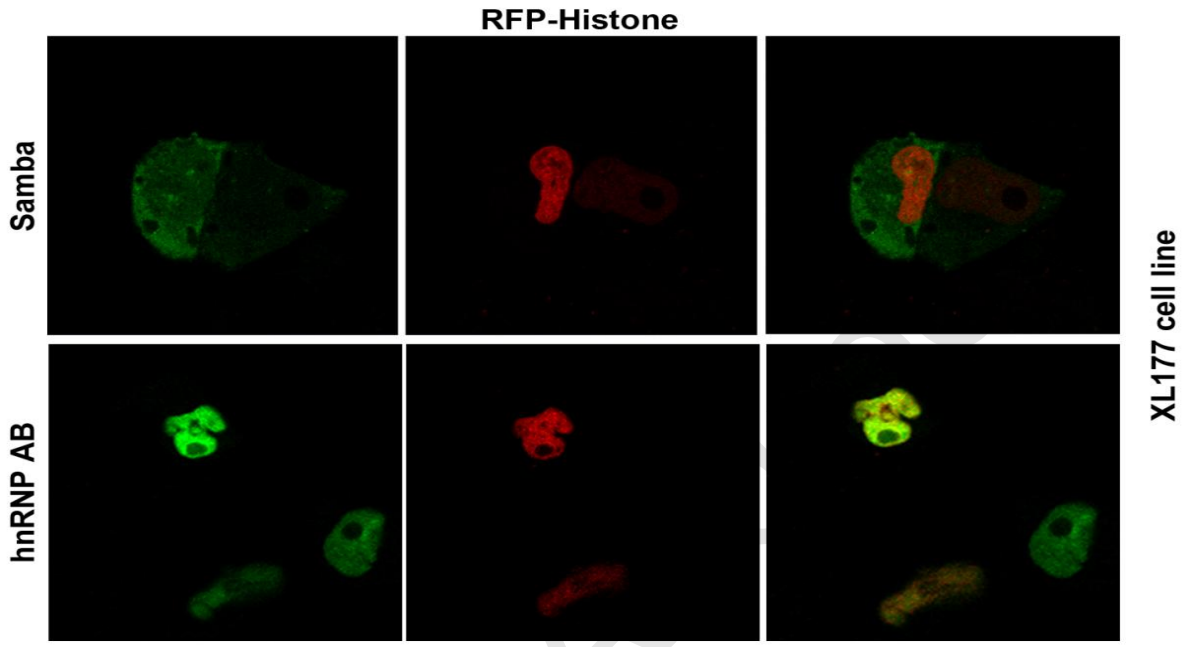

Figure 51 : *In vitro* results for Samba/40LoVe and hnRNP AB localization. Samba was localized in the nucleus and the cytosol. hnRNP AB localized in the nucleus. The proteins are GFP-tagged and Histone-RFP indicates the microtubules and the nucleus respectively.

GFP-Samba and Histone RFP were co-injected in embryos two out of two blastomeres and left to develop to stage 9. Animal Caps were dissected, dissociated and induced with activin prior to being plated on fibronectin coated coverslips. The injected cells could not migrate as controls did but they oscillated back and forth at the same spot, as previously described (Yan, Skourides et al. 2009). The localization of the protein during mitosis was then observed via time lapse microscopy. In this movie, we observed the loss of nuclear signal once the nuclear envelope broke down, followed by the return of the protein into the nucleus during telophase, when the nuclear envelope formed again (Figure 52). This experiment confirmed previous experiments showing the same results (

Figure **48**).

In an effort to explore the protein dynamics on the spindle, we used GFP-Samba electroporated cells. We selected several dividing cells and photobleached specific areas on the spindle. Our experiment revealed that the protein is moving over the spindle and the signal is recovering fast after photobleaching (Figure 53). More experiments will be required to determine if the recovery is due to cytosolic Samba coming on the spindle or the recovery is from the spindle associated pool of the protein.

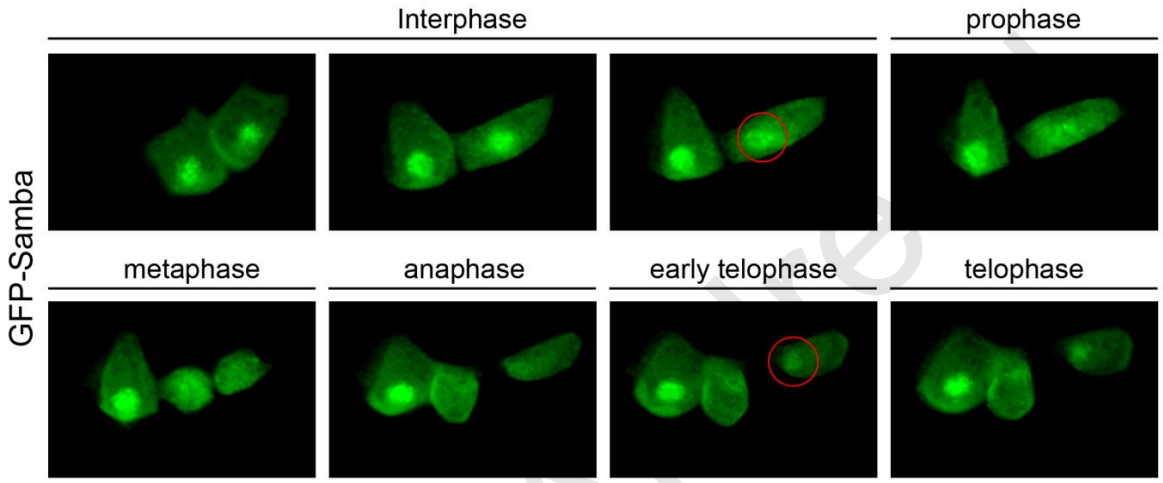

Figure 52 : GFP-Samba changes localization during cell cycle. Still images from a timelapse movie of GFP-Samba dissociated cells showing nuclear and cytosolic GFP-Samba at interphase and spindle localization during metaphase, anaphase and rearrangement back into the nucleus during telophase.

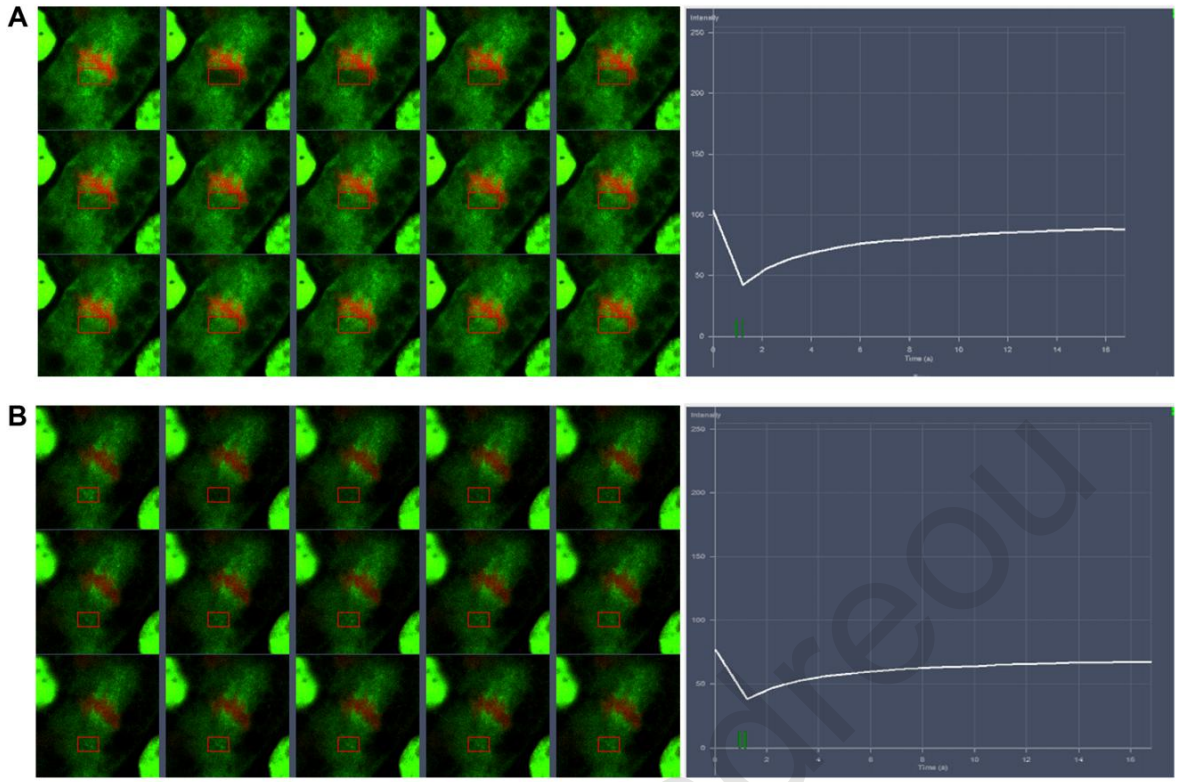

Figure 53: 40LoVe/Samba displays fast diffusion on the spindle. (A) A specific area on the spindle neighboring the DNA is photobleached (shown in red square) and the signal is recovering in less than 20 sec, as shown on the graph. (B) A specific area on the spindle neighboring the centrosome is bleached (shown in red square) and the signal is also recovering fast, as shown on the graph indicating that the protein moves on the spindle during division.

4.2.4 Localization and Shuttling of the proteins

As shown above, Samba is localized in the nucleus and the cytoplasm. The localization of 40LoVe/Samba in the cytosol and the nucleus raised the possibility that the protein shuttles between the two compartments. In addition to this, other hnRNPs have been previously reported to shuttle between the nucleus and the cytosol due to their involvement in mRNA processing and packing (Pinol-Roma and Dreyfuss 1992; Han, Tang et al. 2010). We therefore set out to investigate if the protein shuttles between these two compartments. We injected embryos with GFP-Samba mRNA and then conducted *in vivo Fluorescence Recovery After Photobleaching (FRAP*) and *Fluorescence Loss In*

Photobleaching (FLIP) experiments. *FRAP* and *FLIP* are used in order to observe the intracellular movement of proteins through photobleaching.

FRAP was used to measure the ability of Samba to move around over time. We photobleached GFP-Samba in the nucleus and measured the recovery of GFP signal in the nucleus over time. As shown in Figure 54A, the protein levels in the cytoplasm were reduced and a large amount of the GFP-tagged protein traslocated into the nucleus.

FLIP was used to study the motility of Samba from the nucleus to the cytosol. We repeatedly photobleached GFP-Samba in the cytoplasm and then fluorescence intensity in the nucleus was measured after bleaching. Over time, the fluorescence signal was reduced in the nucleus, indicating that the protein is motile and shuttles between the two compartments (Figure 54B). However, it appears that there are two nuclear fractions of Samba, an immobile and a mobile fraction, because even after repeated photobleaching and loss of nearly all of the cytosolic signal, a fraction of nuclear Samba remains while this is not true with respect to the cytosolic fraction. When the nucleus was repetitively photobleached the cytosolic signal was completely lost (Figure 55). Overall, these results suggest that Samba shuttles between the cytosol and the nucleus and this shuttling is consistent with its possible role in RNA transport as shown for other hnRNPs (Han, Tang et al. 2010).

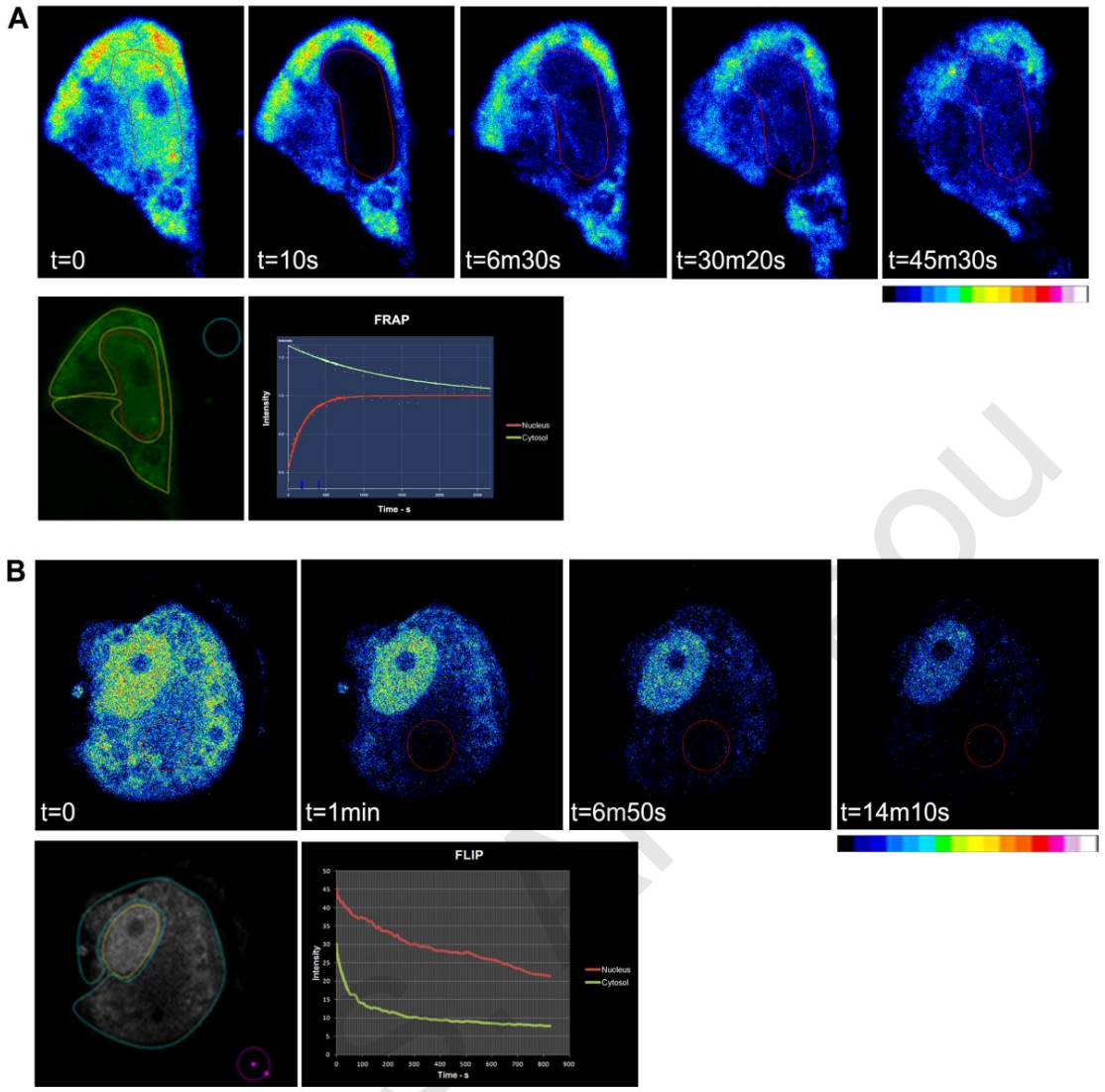

Figure 54 : Samba shuttles between the nucleus and the cytosol. (A) Snapshots from a *FRAP* experiment show the protein signal intensity when the cell nucleus was bleached. The signal intensity in the nucleus recovers fast. After 10 minutes the nuclear intensity of the protein is already increased. The bleached area is marked with a red circle. The red circle marks the bleached area and the region used to measure the intensity in the nucleus, the yellow circle is the region where the intensity in the cytosol is measured. The graph shows the fluorescence intensity in the nucleus and the cytosol. (B) Snapshots from *FLIP* experiment show the signal intensity while we repeatedly bleach the cytosol. When the cytosol is bleached repetitively, the signal intensity in the cell nucleus is reduced. The bleached area is marked with a red circle. The yellow circle marks the area in the nucleus that is measured and the blue circle marks the area measured in the cytosol. The graph shows the fluorescence intensity in the nucleus and the cytosol.

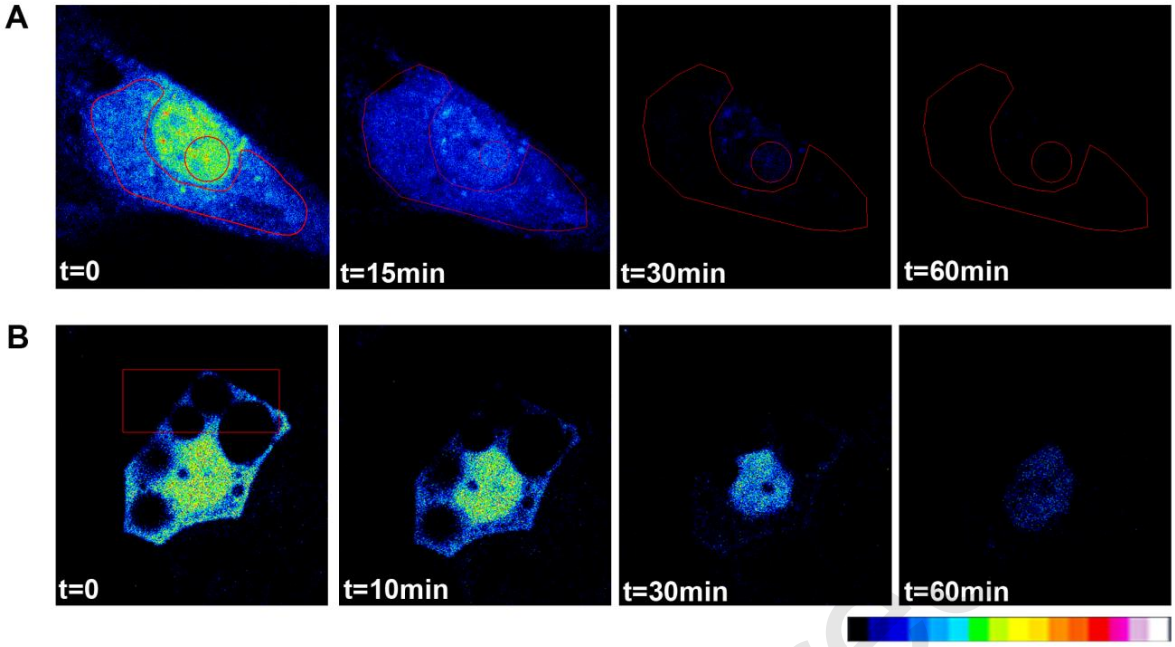

Figure 55: There are two distinct nuclear fractions of Samba, an immobile and a mobile fraction. After repeated photobleaching of the nucleus the cytosolic fraction is entirely lost. However, after repeated photobleaching and loss of nearly all of the cytosolic signal, a fraction of nuclear samba remains.

4.2.5 A possible role for Samba in axon growth

Since whole mount *in situ* hybridization data showed elevated expression of 40LoVe/Samba in neural tissues, we wanted to examine its localization in neurons. Neurons extend long axons to contact post-synaptic targets far removed from the neuronal cell body. For this reason, GFP-Samba was injected at the 2 out of 8 dorsal animal blastomeres. The embryos were left to develop until tadpole stage, where neurons were large enough to be visualized. As shown in Figure 56A, in late tadpoles, GFP-Samba appears to be transported along neuronal axons, suggesting a possible role in axonal transport of mRNAs. As previously described, signaling endosomes are transported anterogradely or retrogradely from distal axons to neuronal cell bodies by the motor protein dynein along microtubules (Cosker, Courchesne et al. 2008). It is also known that some hnRNPs are necessary for axonal translocation of mRNAs and/or proteins involved in the regulation of translation (Hoek, Kidd et al. 1998; Shan, Munro et al. 2003; Carson

and Barbarese 2005; Liu, Gervasi et al. 2008; Glinka, Herrmann et al. 2010). We also observed that GFP-Samba localizes at sites of axon growth (Figure 56B), again suggesting a possible role for Samba in this process, as previously demonstrated for hnRNP-R that mediates axonal b-actin mRNA translocation and has an essential physiological role for axon growth and presynaptic differentiation (Glinka, Herrmann et al. 2010).

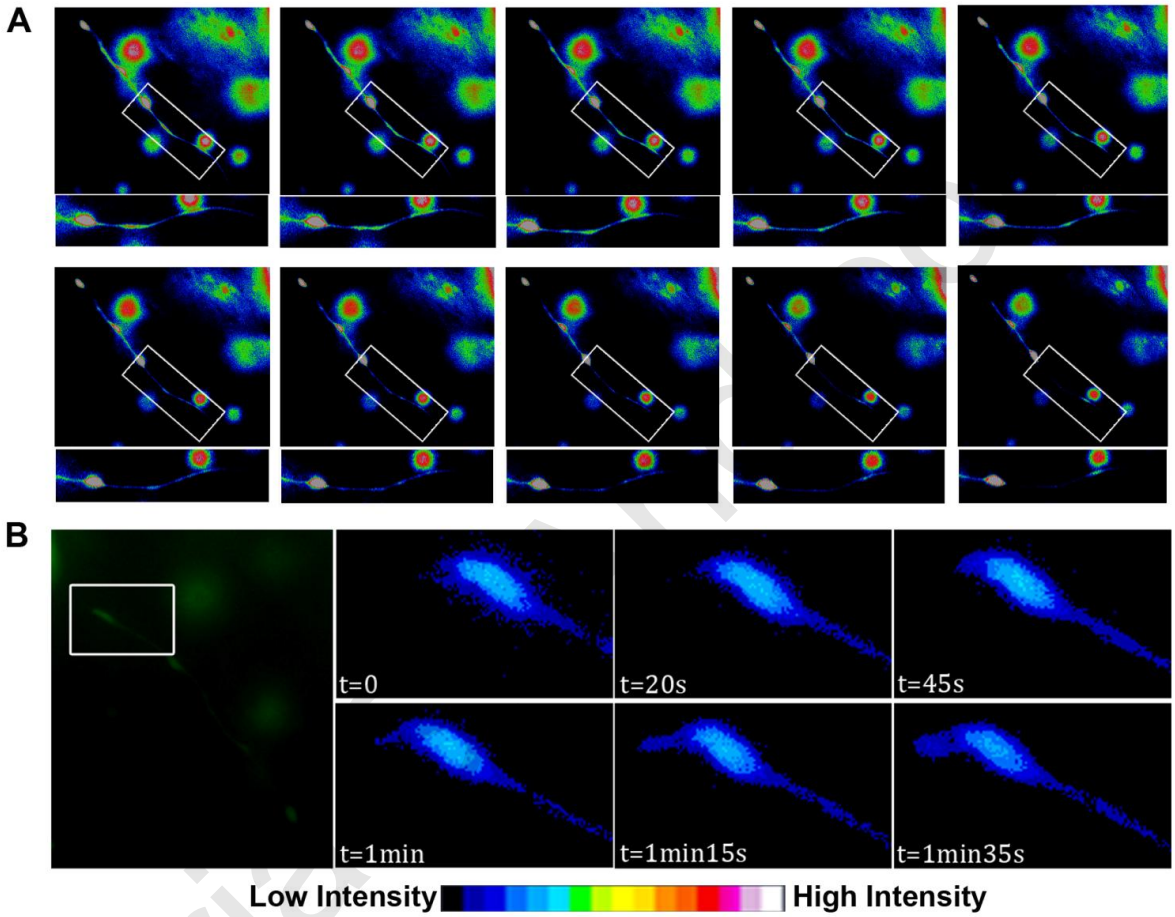

Figure 56: GFP-Samba is transported along neuronal axons and is localized at axon growth cones. (**A**) Snapshots from a timelapse movie showing GFP-Samba moving along the axon. The intensity of the signal changes suggesting that the protein is moving along the axon. The GFP signal intensity is color-coded. (**B**) Snapshots from a timelapse movie showing GFP-Samba at sites of axon growth. GFP signal is moving towards the distal peak during axon growth. Samba is concentrated at the growth cones of the axon.

4.2.6 Mapping the domains responsible for the protein localization

Generation of mutants

In an effort to investigate the structure of the proteins in respect to their localization and since 40LoVe/Samba localized in the nucleus and the cytosol, we hypothesized that the proteins should have an NLS or some other localization sequence responsible for the protein localization and shuttling between the nucleus and the cytosol. In order to investigate this possibility we used the PredictProtein service to identify an NLS in Samba (Rost, Yachdav et al. 2004). The results suggested an NLS motif in position 170 in the RRM2 domain of Samba (Figure 57). Using site directed mutagenesis we created a deletion mutant, SambaΔNLS (see methodology). The mutant constructs were then verified by sequencing. We used GFP-Samba for the generation of the mutant, since we wanted the protein to be tagged so it could be visualized in live cells. We went on to electroporate A6 cells with the mutant (SambaΔNLS) and observed that the localization of the protein remained unchanged. GFP-SambaΔNLS was localized both in the nucleus and the cytosol exactly like wild type Samba. The localization did not change in response to the predicted NLS sequence deletion and we concluded that this sequence does not function as an NLS.

Input Sequence (NLS's in Red)	MSDSEQQYMETNAENGHEACDAEAAEGKGAGGGQNDAEGDQINASKGEEEAGKMFVGGLS WDTSKKDLKDYFEKFGEVSDCTIKMDPNTGRSRGFGFILFKDAASVDKYWITKAHTIRRL IEDPKKAMAMKKEPIKKIFVGGLNPEAGEDKIREYFETFGEIEAVELPMD**PKTNKRR**GFV FITFKEEEPVKKILEKKFHNYYGYGPGYDYSQGGANYGKAYGGRGGSFGGRGGRGGKGQG QNWNQGYNNYWNQGYGNQGYGSYGQQGYGGYGNYDYSGYGVSGSKCEIKIAQPKEVYQQQ
Sequence Length	*300*
NLS's found. ***No gives position of Motif***	• *PKTNKRR 170*

Figure 57 : PredictProtein service identified an NLS in position 170. This position is located in the RRM2 domain of Samba.

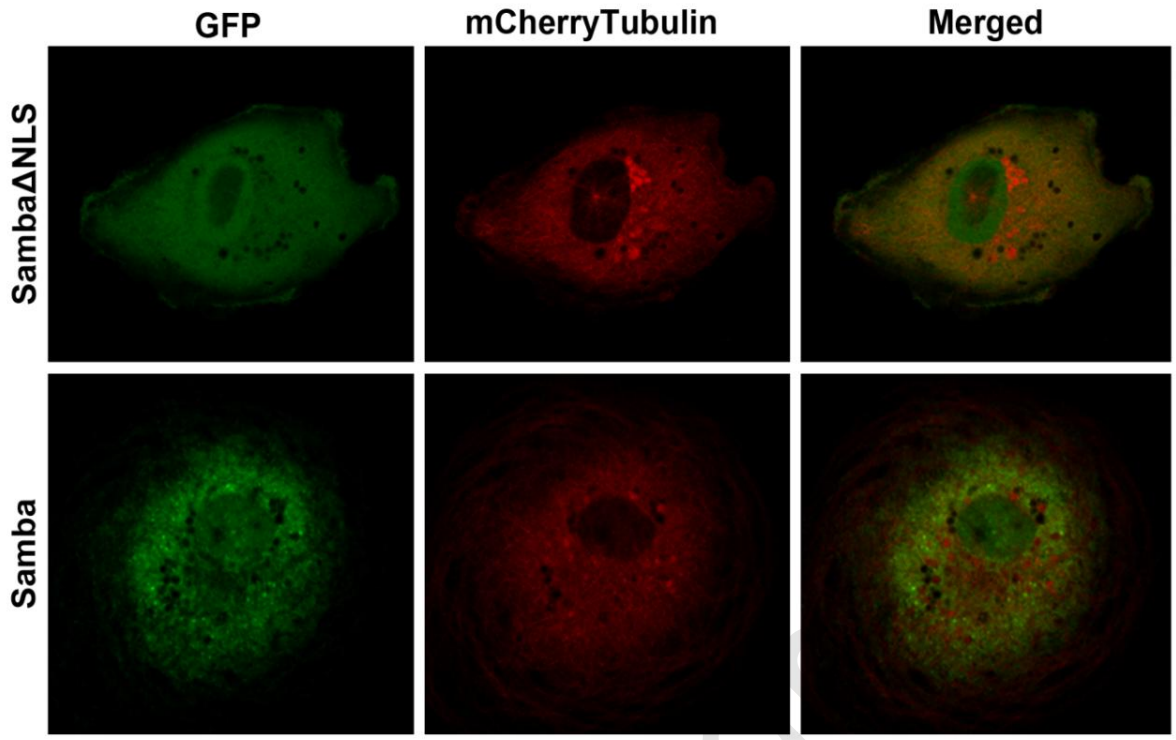

Figure 58 : SambaΔNLS was localized like Samba. SambaΔNLS was localized like Samba and no significant difference in localization was observed despite the deletion of the predicted NLS sequence.

The fact that the localization pattern of 40LoVe/Samba was strikingly different from hnRNP AB raised questions regarding the domain/domains responsible for this difference in localization. In order to address this question, mutants and fusion proteins were generated (Figure 59), to determine which protein domains are responsible for the differences in localization.

Initially, we focused on 40LoVe and hnRNP AB, which despite a 93% identity at the amino acid level display a dramatically different localization, with hnRNP AB being exclusively nuclear while 40LoVe in comparison displayed strong cytosolic and membrane localization (Figure 46). The two proteins differed in 21 amino acids, which were spread out throughout the entire protein. However most of the differences (10/21 amino acids) between the two were located at the N-terminus (CBFNT domain), so we decided to fuse the CBFNT domain of hnRNP AB with GFP and check if that domain was sufficient to

target GFP into the nucleus. As shown the CBFNT domain alone failed to target GFP into the nucleus since the fusion construct displayed the same localization as untagged GFP (Figure 60E).

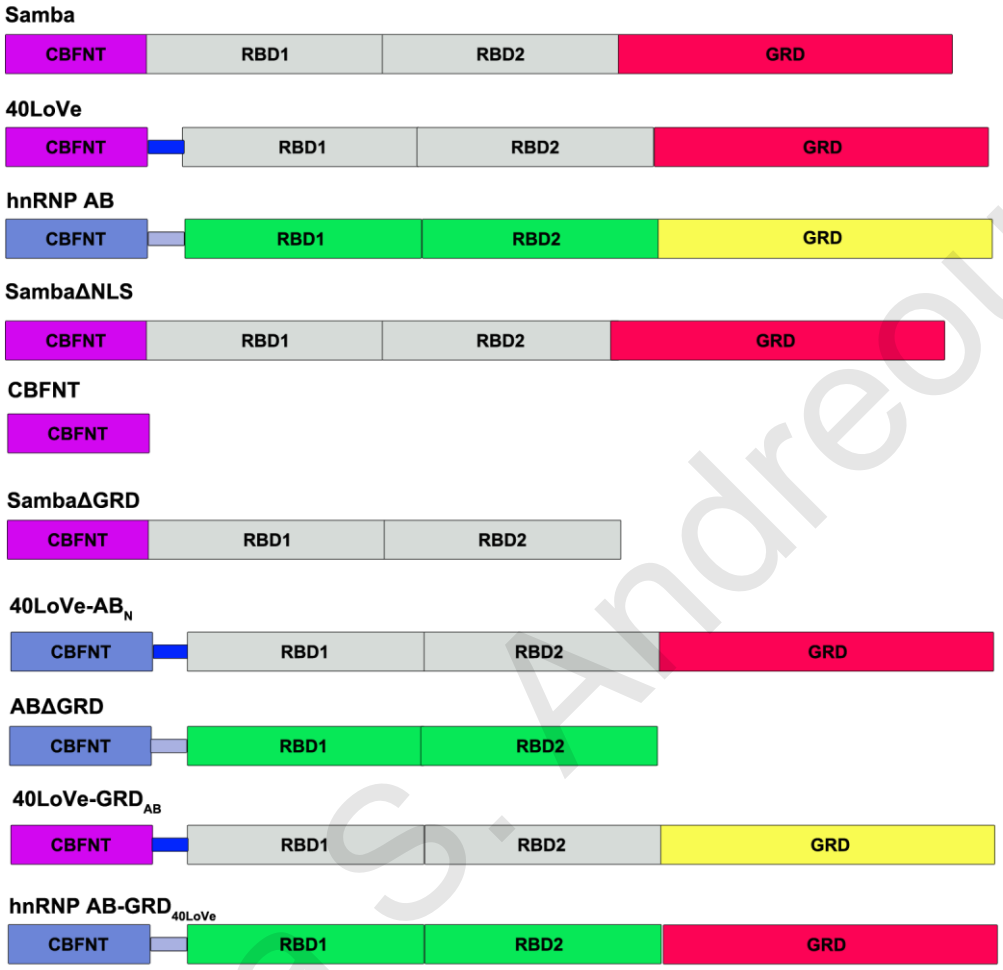

Figure 59 : Mutant proteins. Mutants were generated by deletions and fusion for the determination of the protein domains responsible for the differences in localization between the three proteins. All mutants were fused to GFP.

This result suggests that the CBFNT domain is not sufficient for nuclear localization. Since CBFNT alone was not able to target the protein to the nucleus, we hypothesized that this was due to the fact that the domain had to interact with other protein domains to be able to localize. So, we then swapped the N-terminus of 40LoVe with the N-terminus of hnRNP

AB, thus creating a fusion protein in which all other domains of 40LoVe were present. The fusion protein (40LoVeAB$_N$) localized in a similar manner as 40LoVe (Figure 60F), suggesting that the region responsible for the nuclear localization (of hnRNP AB) was not the N-terminus of the protein.

Given the fact that the GRD domains of some hnRNPs have been shown to be important for their localization (Boulikas 1993; Cartegni, Maconi et al. 1996; Schaeffer, Bardoni et al. 2001; McNally, Yee et al. 2006), we decided to delete the GRD domain of hnRNP AB and examine the localization of the mutant protein. We observed that the hnRNP AB deletion mutant (ABΔGRD) no longer localized in the nucleus (Figure 60G), suggesting that the GRD domain is responsible for the accumulation of the protein into the nucleus. The above results suggest that the few amino acid differences (5/21 amino acids shown Figure 42A) between the GRD domains of 40LoVe and hnRNP AB are responsible for the dramatic difference in localization. To examine further this possibility, we exchanged the GRD of 40LoVe with the GRD of hnRNP AB and generated 40LoVe-GRD$_{AB}$. The resulting chimeric protein behaved according to the GRD as 40LoVe-GRD$_{AB}$ was excluded from the cytoplasm and localized exclusively in the nucleus (Figure 60H). So the GRD domain is necessary for the accumulation of the protein into the nucleus. Conversely we generated an hnRNP AB in which the GRD domain was replaced with the 40LoVe/Samba GRD (hnRNP AB-GRD$_{40LoVe}$;Figure 60I). hnRNP AB-GRD$_{40LoVe}$ was localized both in the nucleus and the cytosol, just like 40LoVe. These results show that the GRD domain is necessary for the accumulation of hnRNP AB in the nucleus and that the 5 amino acid changes between the GRDs of 40LoVe and hnRNP AB are responsible for the localization differences of the two proteins.

It is known that many proteins have NLS and NES signals which control their nuclear import and export (Wen, Meinkoth et al. 1995; Cartegni, Maconi et al. 1996). It is possible that 40LoVe has an NES signal, which is not present in hnRNP AB or that hnRNP AB has an NLS signal missing from 40LoVe. In order to examine whether the GRD domain of hnRNP AB contains an NLS signal, we used the PredictProtein service (Rost, Yachdav et al. 2004), however we were not able to identify an NLS. We also tried to predict an NES sequence on the GRD of 40LoVe using the NetNES prediction method (la Cour, Kiemer et al. 2004).

Using this method we could not detect an NLS or an NES. However, non-canonical NLSs have been identified in other hnRNPs like HnRNP H/F (Van Dusen, Yee et al. 2010). Furthermore, the RGG domain of GRDs has been shown to bind proteins that are responsible for their transport into the nucleus (Burd and Dreyfuss 1994) and in some cases promotes nuclear localization in a manner that is regulated by arginine methylation, like in the case of hnRNP A2 (Schaeffer, Bardoni et al. 2001). Examination of the GRD of hnRNP AB for previously identified NLS sequences failed to reveal any classical nuclear localization signals. However, these results suggest that such a signal does in fact reside within the GRD domain of hnRNP AB and further mutational analysis will be required to determine the exact residues within the domain responsible for this activity.

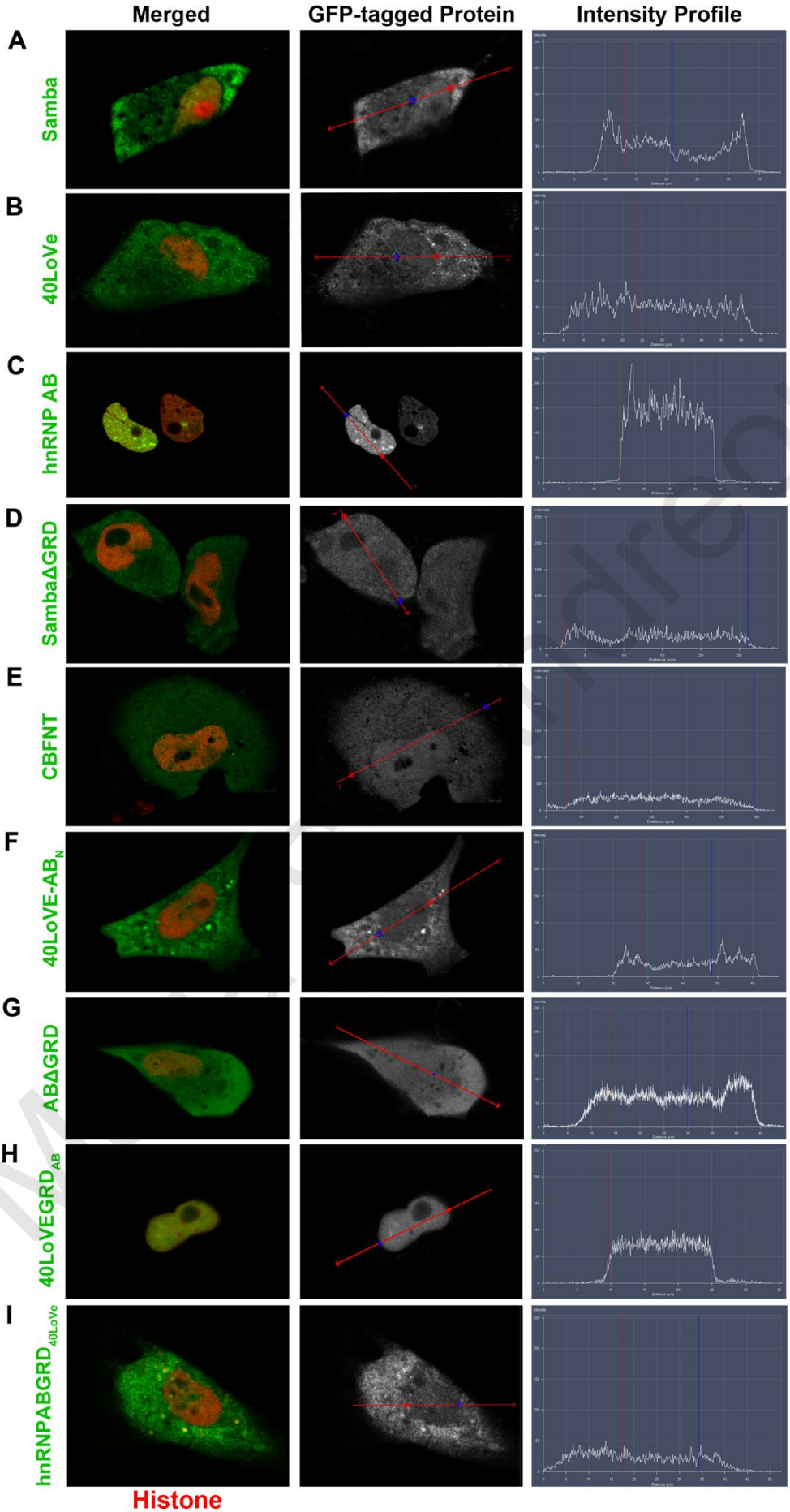
Merged
GFP-tagged Protein
Intensity Profile
A
Samba
B
40LoVe
C
hnRNP AB
D
SambaΔGRD
E
CBFNT
F
40LoVE-AB$_N$
G
ABΔGRD
H
40LoVEGRD$_{AB}$
I
hnRNPABGRD$_{40LoVe}$
Histone

Figure 60 : 40LoVe/Samba, hnRNP AB, deletion mutant and fusion construct localization in XL177 cells. In each figure cells were co-electroporated with a GFP-tagged version of the protein indicated on the left (green) and Histone-RFP to label the nucleus (Tung, Mahmood et al.). The first column shows the merged image of both the indicated construct (green) and histone (Tung, Mahmood et al.), while the second column shows the construct localization alone. The third column shows the intensity profile for each cell along the red line shown in the second column. Red and blue lines represent the boundaries of the nucleus of each cell. (A-B) Samba and 40LoVe are localized both in the nucleus and the cytosol. (C) hnRNP AB is exclusively nuclear. (D) SambaΔGRD does not display the same localization as Samba. (E) The CBFNT domain does not give any specific localization. (F) 40LoVe-AB_N localizes like 40LoVe, suggesting that the N-terminus of the protein is not responsible for nuclear retention of hnRNP AB. (G) ABΔGRD loses the strictly nuclear localization of hnRNP AB, indicating that the GRD domain is necessary for the exclusively nuclear localization of hnRNP AB. (H) 40LoVEGRD_{AB} localizes exactly like hnRNP AB, showing that the GRD domain of hnRNP AB is sufficient for nuclear retention. (I) hnRNP AB-GRD40LoVe localizes like 40LoVe, confirming that the hnRNP AB GRD is necessary for nuclear retention of hnRNP AB and that that the few amino acid differences between the GRD domains of the two proteins are responsible for their differences in localization.

4.2.7 40Love/Samba is not localized at focal adhesions

Our results showed that 40LoVe and Samba had membrane localization in embryos (Figure 46). In addition when we examined in more detail the transfected cells expressing 40LoVe and Samba, we noticed some characteristic linear structures that appeared similar to Focal Adhesions (FA) (Figure 60A, B, E). Vinculin has been previously shown to be present and has a profound role on focal adhesions (Ziegler, Liddington et al. 2006). So we went on to examine if those structures were focal adhesion, by performing IF, using an anti-vinculin antibody to visualize FAs. We saw that Samba and 40LoVe did not co-localize with vinculin at the sites of focal adhesion (Figure 61), so 40LoVe/Samba is not present on focal adhesions.

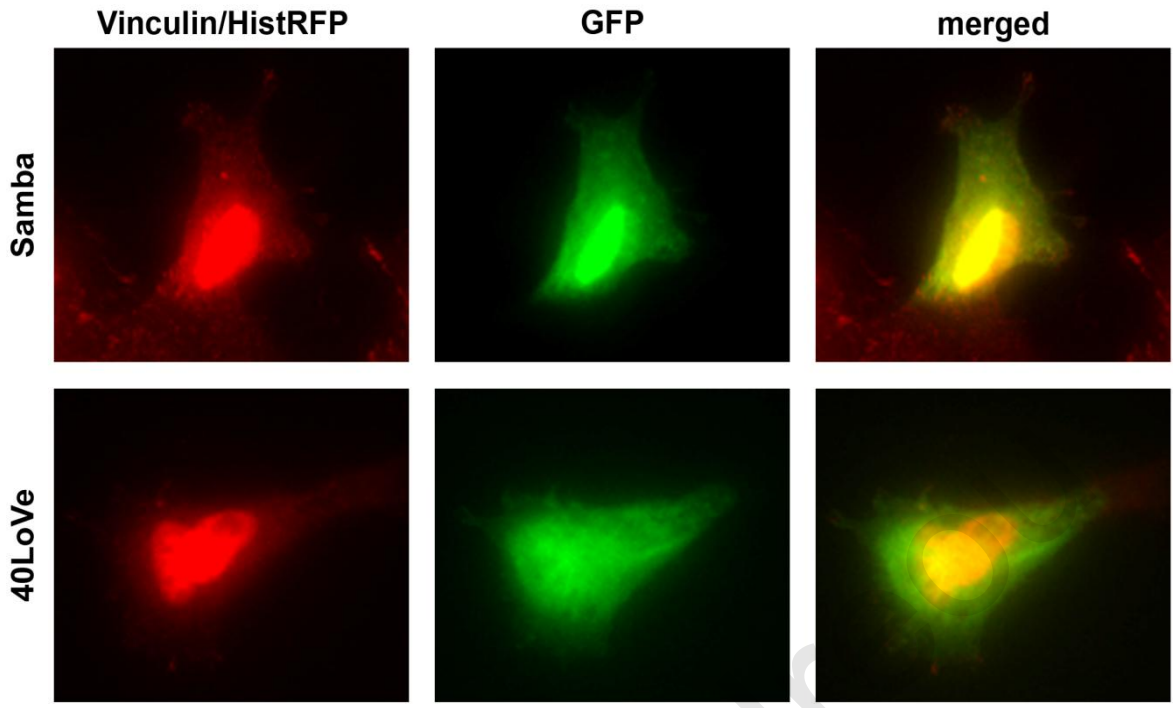

Figure 61 : 40LoVe/Samba does not localize in focal adhesions. We conducted IF in cells co-electroporated with Histone-RFP and GFP-Samba and GFP-40LoVe, respectively. We used anti-vinculin antibody that stained the focal adhesions and saw that Samba and 40LoVe did not co-localize with vinculin.

4.2.8 Samba/40LoVe localization and shuttling

As shown above, GFP-40LoVe/Samba shuttles from the cytoplasm to the nucleus (Figure 54A) and egresses from the nucleus to the cytoplasm (FLIP; Figure 54B). Given the fact that nuclear retention of hnRNP AB is dependent on its GRD domain we went on to examine if shuttling of 40LoVe/Samba required the GRD domain. Removal of 40LoVe/Samba GRD (SambaΔGRD) completely blocked nucleocytoplasmic shuttling (FRAP; Figure 62) suggesting that the GRD domain is necessary for 40LoVe/Samba shuttling. Taken together, these data show that the GRD domain is necessary for 40LoVe/Samba shuttling.

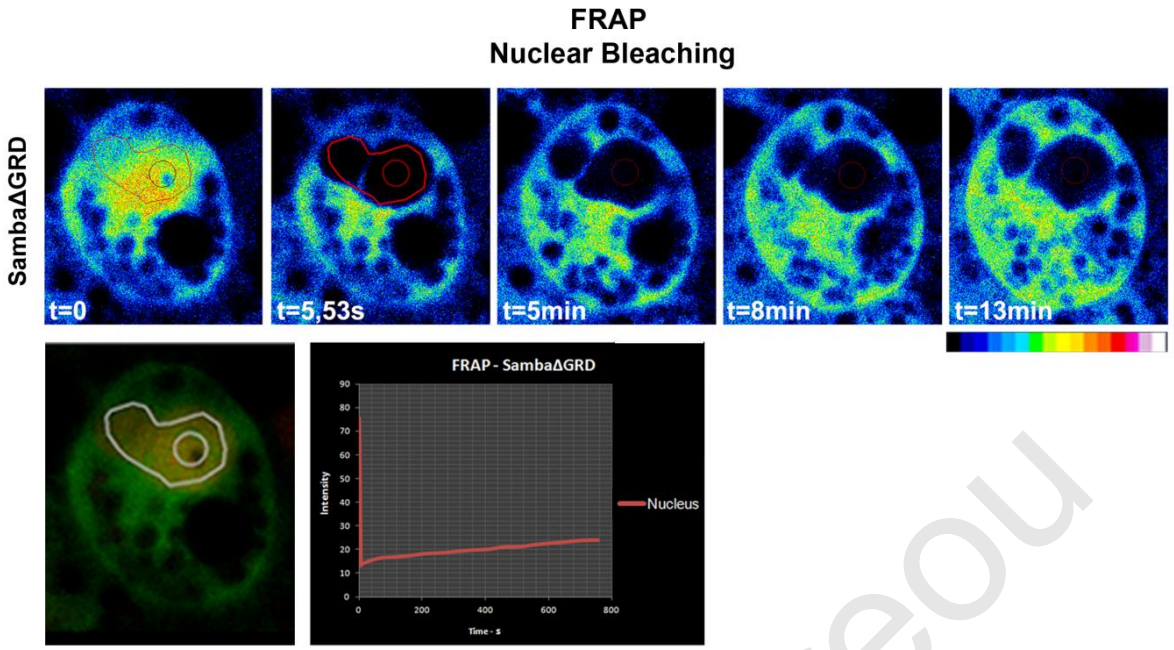

Figure 62 : SambaΔGRD is not able to shuttle between the nucleus and the cytosol. Still images from a timelapse movie of a *FRAP* experiment with GFP-SambaΔGRD. The signal intensity cannot recover after photobleaching, indicating that the GRD domain is necessary for Samba return back into the nucleus. The graph shows the fluorescence intensity in the nucleus.

To determine if the 40LoVe/Samba GRD is also sufficient for protein shuttling, we used the chimeric protein hnRNPAB-GRD$_{40LoVe}$ (Figure 60I). This chimeric protein behaved like 40LoVe/Samba in FRAP experiments showing that the 40LoVe/Samba GRD is both necessary and sufficient for nucleocytoplasmic shuttling (FRAP; Figure 63).

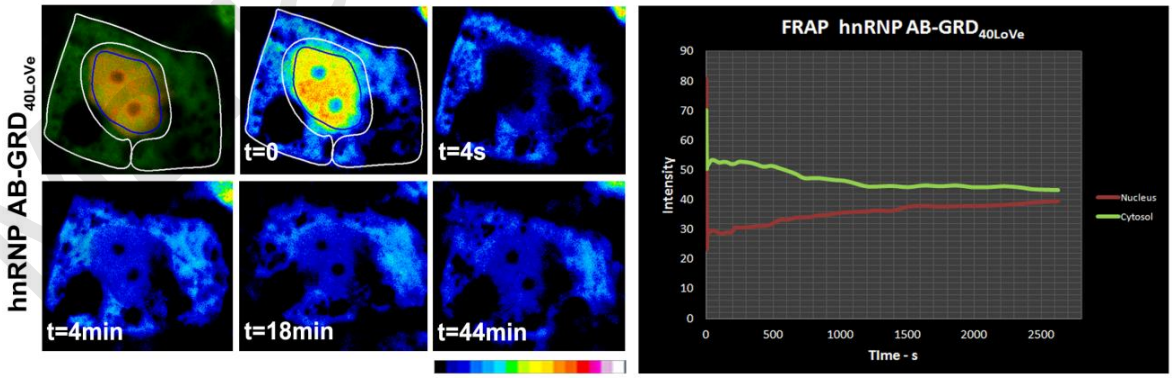

Figure 63 : The GRD domain of 40LoVe is sufficient for shuttling from the nucleus to the cytosol. Intensity-coded still images (intensity scale is shown below the set of images) from a time lapse recording of a *FRAP* experiment from an hnRNPAB-GRD$_{40LoVe}$ expressing cell. Nuclear signal

recovers while cytosolic signal decreases over time in a similar fashion to what is observed with GFP-Samba suggesting that the GRD domain of 40LoVe is sufficient to confer shuttling from the nucleus to the cytoplasm. The graph was generated from measurements in the cytosol (outlined white) and the nucleus (outlined blue). The intensity difference between the two compartments is nearly extinguished after about 40 minutes showing similar dynamics to GFP-Samba (Figure 54).

After showing that the GRD domain is necessary for Samba accumulation into the nucleus (Figure 62,Figure **63**), we carried out FLIP experiments to examine, if it is also responsible for the egression of the protein from the nucleus. We used both cells expressing 40LoVe/Samba and SambaΔGRD and conducted FLIP experiments. After repeated bleaching in the cytosol, we measured the fluorescence intensity in the nucleus and saw that the signal in the nucleus was slightly reduced in both cases. 40LoVe/Samba and SambaΔGRD are travelling from the nucleus to the cytosol in the same manner. This showed that the GRD domain is not responsible for nuclear export, since SambaΔGRD translocation out of the nucleus is not affected by the deletion of the domain (Figure 64). These results suggest that the GRD domain is necessary for nuclear import, but nuclear export of 40LoVe/Samba takes place through a different mechanism. They also suggest that the differences between 40LoVe/Samba and hnRNP AB arise from the retention of the latter through an interaction in the nucleus rather than through increased nuclear import or diminished nuclear export.

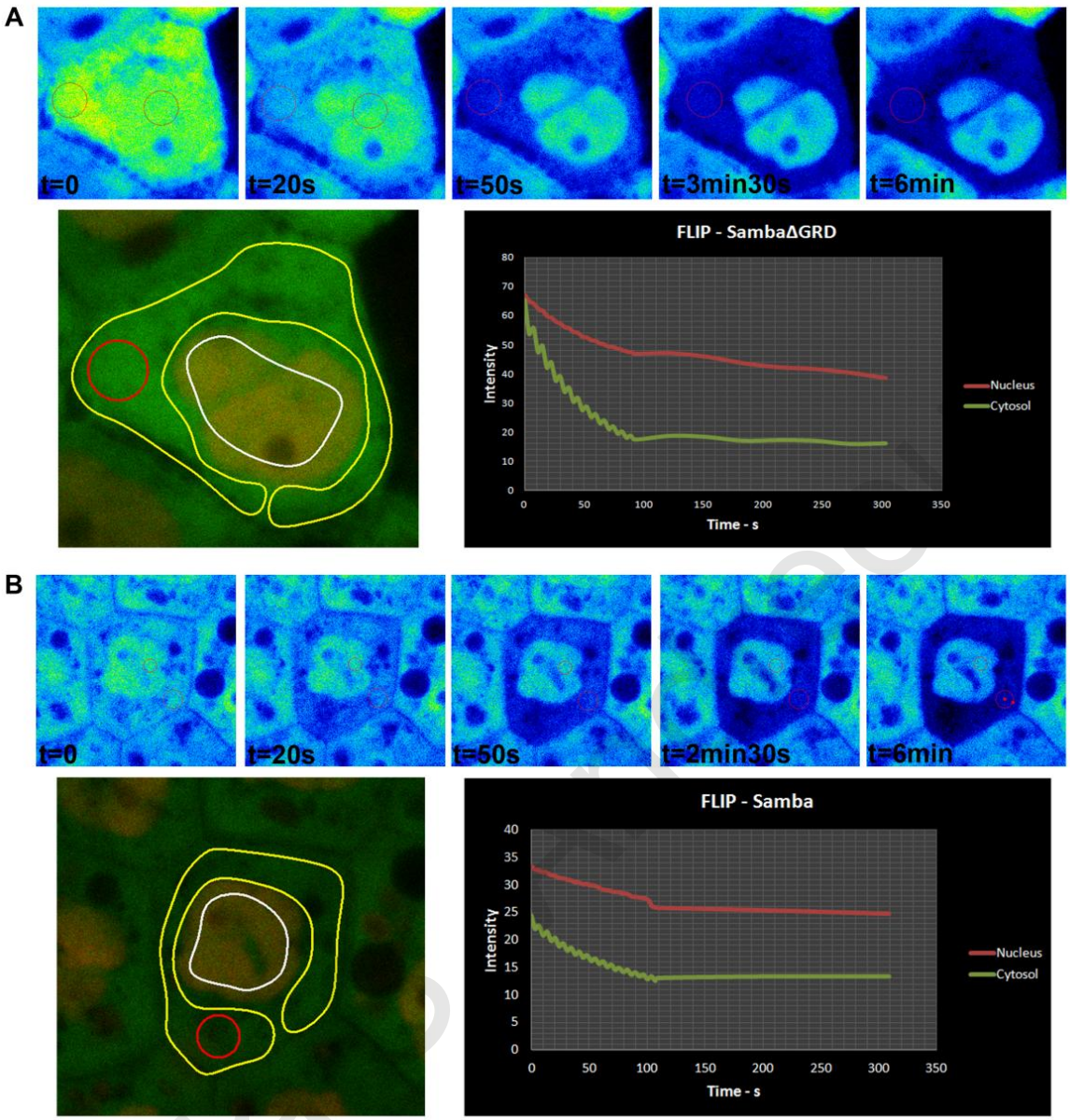

Figure 64 : GRD domain is not responsible for nuclear export of 40LoVe/Samba. The signal intensity in the nucleus is reduced in the same way in both cases after photobleaching in the cytosol. (A) FLIP in SambaΔGRD. (B) FLIP in Samba**.** Snapshots from *FLIP* experiment show the signal intensity while we repeatedly bleach the cytosol. When the cytosol is bleached repetitively, the signal intensity in the cell nucleus is reduced. The bleached area is marked with a red circle. The yellow circle marks the area in the cytosol that is measured and the white circle marks the area measured in the nucleus. The graph shows the fluorescence intensity in the nucleus and the cytosol.

The 40LoVe/Samba nucleocytoplasmic shuttling behavior and nuclear retention of hnRNP AB is conferred solely by their respective Glycine Rich Domains (GRD). In support of this, some hnRNPs have been reported to contain unconventional nuclear localization signals at the GRD (Siomi and Dreyfuss 1995; Van Dusen, Yee et al. 2010). Alternatively, the GRD domain sequence could direct hnRNPs localization indirectly, by determining the identity of their nucleic acid targets or protein partners (Han, Tang et al. 2010). Nevertheless, our results show that the five amino acid differences between 40LoVe/Samba and hnRNP AB GRD domains are sufficient to grant nuclear retention to the latter. Furthermore, it also brings to attention that slight differences in the sequences of closely related hnRNPs are sufficient to generate different subcellular localization and, as a consequence, biological functions. In other words, small differences present in highly homologous domains should not be overlooked in analysis of hnRNPs. Although the PredictProtein service failed to reveal any known NLS sequences we decided to do more alignments with several characterized canonical or non canonical NLS and NES sequences found in known hnRNPs. We searched for non classical NLS and aligned the GRD of hnRNP AB and 40LoVe/Samba with a sequence found in the GYR domain of hnRNP H/F (Van Dusen, Yee et al. 2010) and with M9, a 38 amino acid domain within hnRNP A1 that acts both as an NLS and an NES sequence (Michael, Choi et al. 1995). Our search did not reveal any canonical or non canonical NLS sequence and we decided to search for known shuttling sequences. We aligned the GRD domain with KNS, a sequence found in hnRNP K (Michael, Eder et al. 1997) and HNS, a sequence found in an mRNA-binding protein, HuR (Gallouzi and Steitz 2001). This search revealed that 40LoVe and hnRNP AB have a sequence that is very similar to the DNS signal identified in hnRNP D (Suzuki, Iijima et al. 2005). This 19 amino acid sequence in 40LoVe and hnRNP AB presents an 80% sequence identity to DNS. The DNS is rich in hydrophilic amino acids and glycine. Two interesting features arise from the alignment of the 40LoVe, hnRNP AB and hnRNP D C-terminal domains that might explain their differences in subcellular distribution (Figure 65). Firstly, all three proteins present a KPY motif that was identified as essential for nuclear import/retention of hnRNP D (Suzuki, Iijima et al. 2005). A second feature worthy of mention is the variation of the 14th residue in the hnRNP D DNS domain. This residue corresponds to Asparagine$_{350}$ in hnRNP

D and Asparagine$_{319}$ in hnRNP AB. However, in 40LoVe and Samba, the corresponding residue is switched to Serine. hnRNP D localizes like hnRNP AB (strictly nuclear) unlike 40Love and Samba suggesting that this particular Asparagine residue is likely responsible for the differences in localization between 40Love/Samba and hnRNP AB. None of the other residue differences, between the hnRNP D DNS and hnRNP AB or 40LoVE/Samba, display the same correlation. This issue however can be further clarified with point mutations in future work. An additional point of interest is that while hnRNP D is strictly nuclear like hnRNP AB, use of heterokaryons showed that hnRNP D does shuttle between the nucleus and the cytosol (Suzuki, Iijima et al. 2005). This suggests that hnRNP AB may also shuttle and that the Asparagine to Serine change between 40LoVe and hnRNP AB, generates a weaker NLS that allows a large fraction of 40LoVe to be retained in the cytosol. In addition the GRD domain sequence could also direct hnRNP localization indirectly, by determining the identity of their nucleic acid targets or protein partners (Han, Tang et al. 2010).

Figure 65 : Alignment of the proteins 40LoVe/Samba, hnRNP AB and the human hnRNP D. DNS is the 19 amino acid sequence highlighted in turquoise that has been shown to be responsible for shuttling in hnRNP D (GI:51477711). Two out of the three differences in the GRD domain between 40LoVe/Samba and hnRNP AB (shown in Figure 42) are located in this 19 amino acid sequence. The yellow highlighted amino acid is the one likely responsible for differences in localization between 40LoVe/Samba and hnRNP AB. This amino acid is an Asparagine in hnRNP D and hnRNP AB, which both are strictly nuclear, but it's a Serine in 40LoVe/Samba which show both nuclear and cytosolic localization.

4.2.9 40LoVe/ Samba knockdown

Over-expressing the various tagged and un-tagged constructs of Samba, 40LoVe and hnRNP AB in different tissues appeared to produce the same developmental phenotypes that were previously reported for Samba overexpression (Yan, Skourides et al. 2009). When the constructs were injected in a single vegetal blastomere at the 16 cell stage, they induced an abnormal growth in the ventrolateral portion of the embryos, especially pronounced at around stage 34 (Yan, Skourides et al. 2009).

In order to further explore the role of 40LoVe/Samba in *Xenopus* development, we carried out loss of function experiments using antisense morpholino oligonucleotides (Ramos and DeSimone). We designed two different morpholinos (MO's). MO1 and MO2 could target both Samba and 40LoVe, while MO1 could also target hnRNP AB (see methodology). We also ordered a standard control MO (CoMO) which has no significant biological activity. First, we tried to biochemically determine if our MOs down-regulate a Flag-tagged surrogate Samba protein which would be recognized by both MOs, using western blot analysis (Figure 66A). We also confirmed *in vitro* that MO2 could not downregulate hnRNP AB using a surrogate protein (Figure 66A). Using the 40LoVe antibody, we confirmed that both MO's downregulated the endogenous proteins, but MO2 was not as efficient as MO1 (Figure 66C). We also verified *in vivo* that our MO's knocked down the endogenous protein and that our CoMO did not, via whole-mount immunofluorescence. In MO injected cells, the characteristic nuclear and cytoplasmic staining was clearly reduced compared to adjacent control cells (Figure 66D). In contrast, CoMO injected cells showed fluorescence intensity similar to uninjected cells (Figure 66E).

Morpholino Name	Morpholino Sequence	Target Sequence
Standard Control Oligo	CCTCTTACCTCAGTTACAATTTATA	
Samba Mo1	TATACTGCTGCTCGGAGTCGGACAT	5'-TGTTGAAGCTTGTGCTTTCAGT(ATGTCCGACTCCGAGCAGCAGTATA)TGG - 3'
Samba Mo2 3' Fluorescein	AATCGCCAAATTCCTCCAAGCGGAC	5'-CCACGC(GTCCGCTTGGAGGAATTTGGCGATT)GTTGAAGCTTGTGCTTTCAGTATGTCCGACTCCGAGCA – 3'

Table 7 : MOs designed to use in the project.

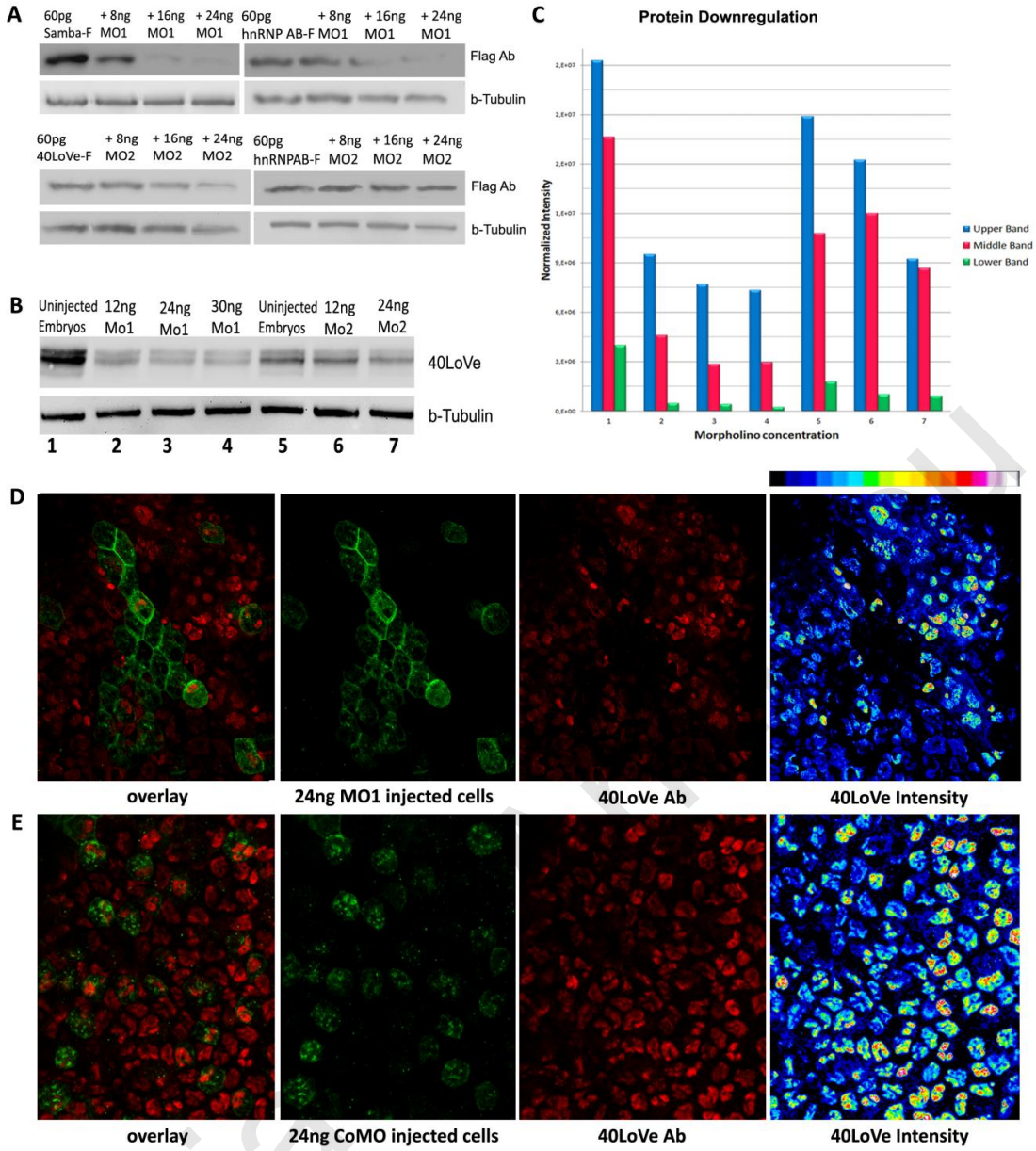

Figure 66 : Both MOs down-regulate endogenous and surrogate proteins. (A) Western Blot of half embryo equivalent injected with 60 pg of surrogate Samba-flag or hnRNP AB alone or co-injected with 8ng, 16ng and 24ng MO1 as indicated. MO1 effectively downregulates all Samba/40LoVe and hnRNP AB. Also, western Blot of half embryo equivalent injected with 60 pg of surrogate hnRNP AB or 40LoVe alone or co-injected with 8ng, 16ng and 24ng MO2 as indicated. MO2 fails to downregulate hnRNP AB, but downregulates 40LoVe/Samba. (B) Western blot indicating both MO's down-regulation of the endogenous protein with rabbit polyclonal antibody raised against 40LoVe. (C) Graph with normalized intensity of each band in the WB, indicating MO downregulation. (D-E) Immunofluorescence experiments with the 40LoVe antibody also confirmed that the MO1 down-regulates the endogenous protein, while CoMO does not.

Since we managed to determine both Morpholinos specificity, we carried on our experiments first by injecting both MO1 at one cell stage at different amounts (12ng, 24ng and 36ng) as shown in Table 8. The embryos were allowed to develop until tadpole stage, when most of the defects caused by protein downregulation, appear. All embryos were co-injected with mGFP mRNA to trace the MO expressing cells. The morpholino injected embryos had a shorter anterior-posterior axis and several head defects, the most prominent of which was reduced eye size (Figure 69). The phenotype was more severe when higher amounts of the MO were injected in the embryos (Figure 68). The numbers of embryos injected with the MO are presented in Table 8 : MO injected embryos with different amounts.

The embryos were then injected in one out of two blastomeres at the two cell stage, in order to have an internal control. We observed that the MO injected side was malformed and the uninjected side was properly formed (Figure 70B). The MO was co-injected with mGFP, in order to linage trace the side of injection when observed under a fluorescence microscope. The embryos expressing GFP on one side were used for the phenotype quantification. In order to quantify the phenotype we measured the eye diameter on both sides of the embryo. As shown in the MO-injected side the eye size was reduced by 40% compared to controls (Figure 78).

	Severe head defects	Moderate head defects	Normal head structures	Total number of embryos
12ng Mo1	23%	58%	19%	106
12ng Mo2	9%	26%	65%	65
24ng Mo1	57%	36%	7%	220
24ng Mo2	26%	44%	30%	85
36ng Mo1	74%	24%	2%	50
36ng Mo2	44%	52%	4%	27
CoMo	0	17%	83%	84
Ctls	0,5%	8%	91,5%	198

Table 8 : MO injected embryos with different amounts. Percentages of defects in embryo head structures. The total number is the mean of 3 independent experiments.

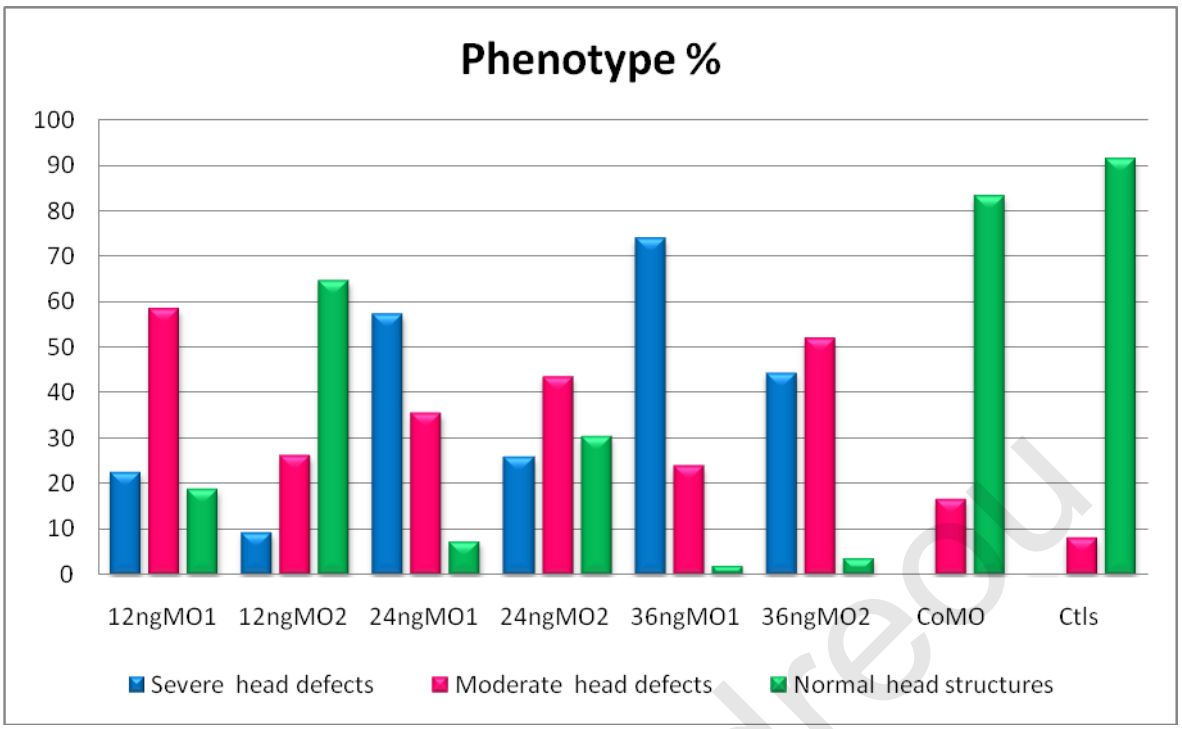

Figure 67 : Chart representing the percentages of the phenotype defects for each MO in different concentrations.

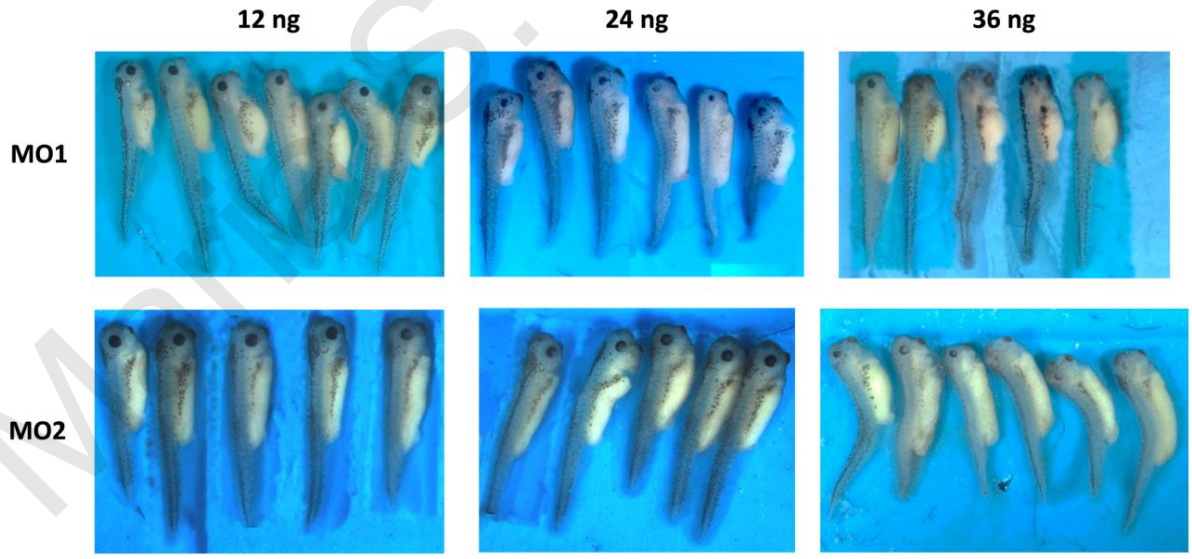

Figure 68 : MO1 and MO2 gave similar phenotypes. MO1 gave more severe phenotype at lower amounts in comparison to MO2.

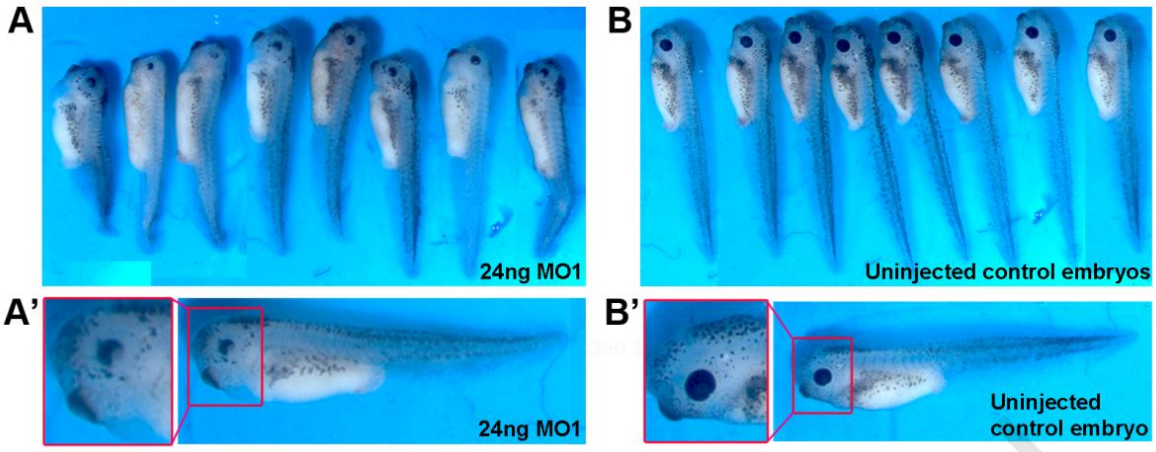

Figure 69 : 40Love/Samba morphants display generalized head defects including reduced eye size. Head structures were scored according to eye size, dorsal pigmentation, craniocephalic shape, curved tails and overall volume. A) Representative embryos injected with 24ng MO1 showing the head defects including reduced eye size and shorter axis. B) Uninjected control embryos.

Due to the fact that the head structures had several malformations and since those structures are innervated with specific neurons, we decided to examine the neurons. We performed IF using anti-Acetylated tubulin antibody to reveal the neurons and saw that the cranial neurons were not properly formed. More specifically we observed that the neurons innervating the head structures on the injected side of the embryo were not properly formed (Figure 70A). The olfactory nerve was missing and the olfactory bulb did not form (Figure 70C). The trigeminal nerve and the ophthalmic nerve were smaller and thinner (Figure 70A). Also, the maxillary and the nasociliary nerves innervating the maxillary antrum, the nasal cavity and the eye were reduced or missing (Figure 70A). In addition, the peripheral axons of the spinal cord were also reduced or even missing on the injected side of the embryo with the axonal projections being restricted with limited branching (Figure 70D-E).

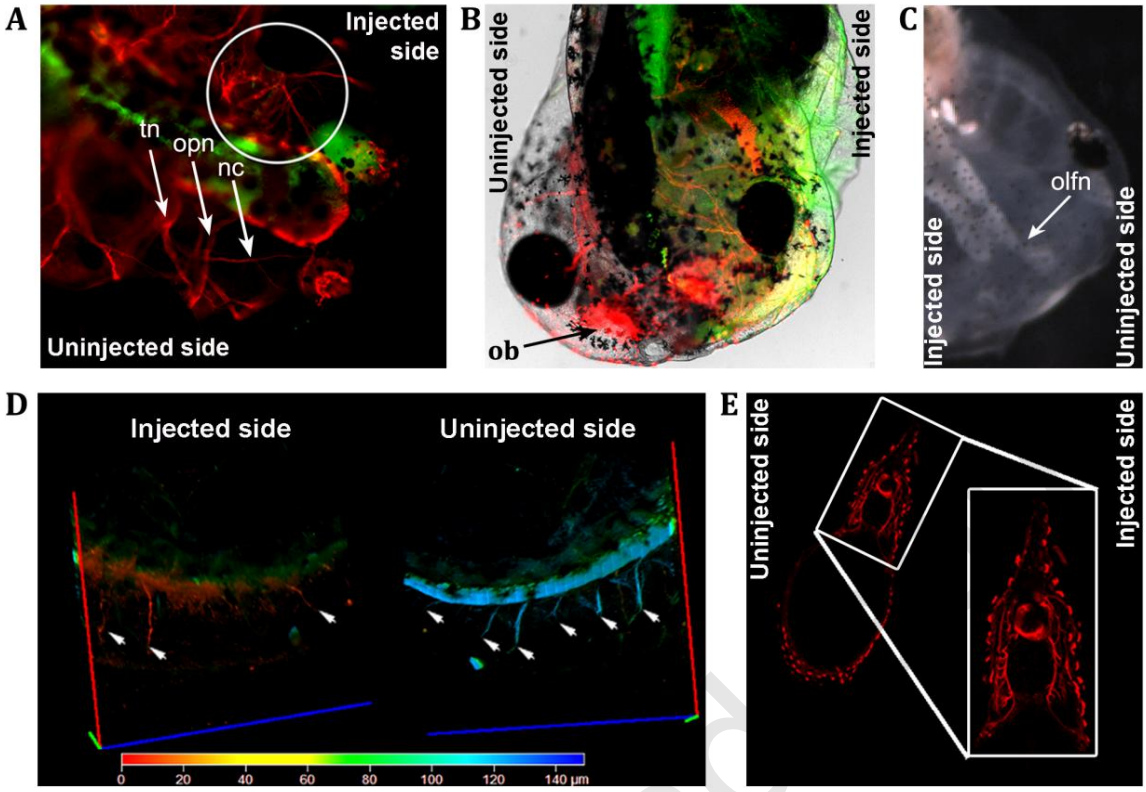

Figure 70 : 40LoVe/Samba morphants display head defects and severe axon outgrowth defects. (A) Optical sections from representative whole mount immunostained embryo for acetylated tubulin (Tung, Mahmood et al.) to reveal neurons. The presence of using GFP (green) indicates the MO-injected side of the embryo (n=20, three independent experiments). Compared to the uninjected side, the trigeminal nerve (tn), the ophthalmic nerve (on) and the nasocilliary nerves (nc) on the injected side of the embryo (marked with a white circle) are thinner and disorganized. The arrows show the properly formed neurons on the uninjected side of the tadpole. (B) Image of a representative embryo showing that the olfactory bulb (ob) is not properly formed in the injected side of the embryo (indicated with GFP) (n=20, three independent experiments). (C) Bightfield image of a representative embryo showing that the olfactory nerve (olfn) is missing and the olfactory bulb is not properly formed (n=30, three independent experiments). (D) Depth color coded (depth key at bottom of D) 3D reconstruction of optical sections of the trunk of a representative tadpole injected in the animal pole of one out two animal blastomeres with MO1 and then stained using an anti-acetylated tubulin antibody to reveal the axonal projections (n=30, three independent experiments). 3D reconstruction is shown on the injected side (left) and was then rotated 180 degrees and shown on the uninjected side (Perez-Alvarado, Martinez-Yamout et al.). Motor neuron projections rising from the spinal cord on the injected side of the embryo are absent or short in contrast to the un-injected side. (E) Maximum Intensity Projections of confocal

Z-stacks from an immunostained representative embryo showing that the axonal projections are restricted and there is limited branching of the nerves at the injected side of the embryo (n=20, three independent experiments).

4.2.10 40LoVe/Samba knockdown does not affect neural specification

To address the possibility that the observed phenotypes were due to a defect in neuronal differentiation, we carried out WISH using the neural markers Slug, Sox3, Sox10, Ntubulin and XRx1, on embryos injected in one side with MO1. Although all the markers examined were expressed and neural specification was unaffected, we observed a reduced expression of all of these markers in the MO injected side of the embryos (Figure 71, Figure 72, Figure 73). We also noticed that tissues such as the cranial sensory ganglia and the branchial arches could not properly migrate. RT-PCR experiments confirmed a reduction in neural marker expression in MO injected embryos (Figure 73). These experiments showed that neural specification was unaffected in morphant embryos, and suggested that the observed morphogenetic defects were not due to changes in neural specification. On the other hand, a specific loss of neural tissues in 40LoVe morphants despite correct neural patterning, suggests that 40LoVe is not required for neural specification but may be required for maintenance or survival of neuronal tissues in the embryo.

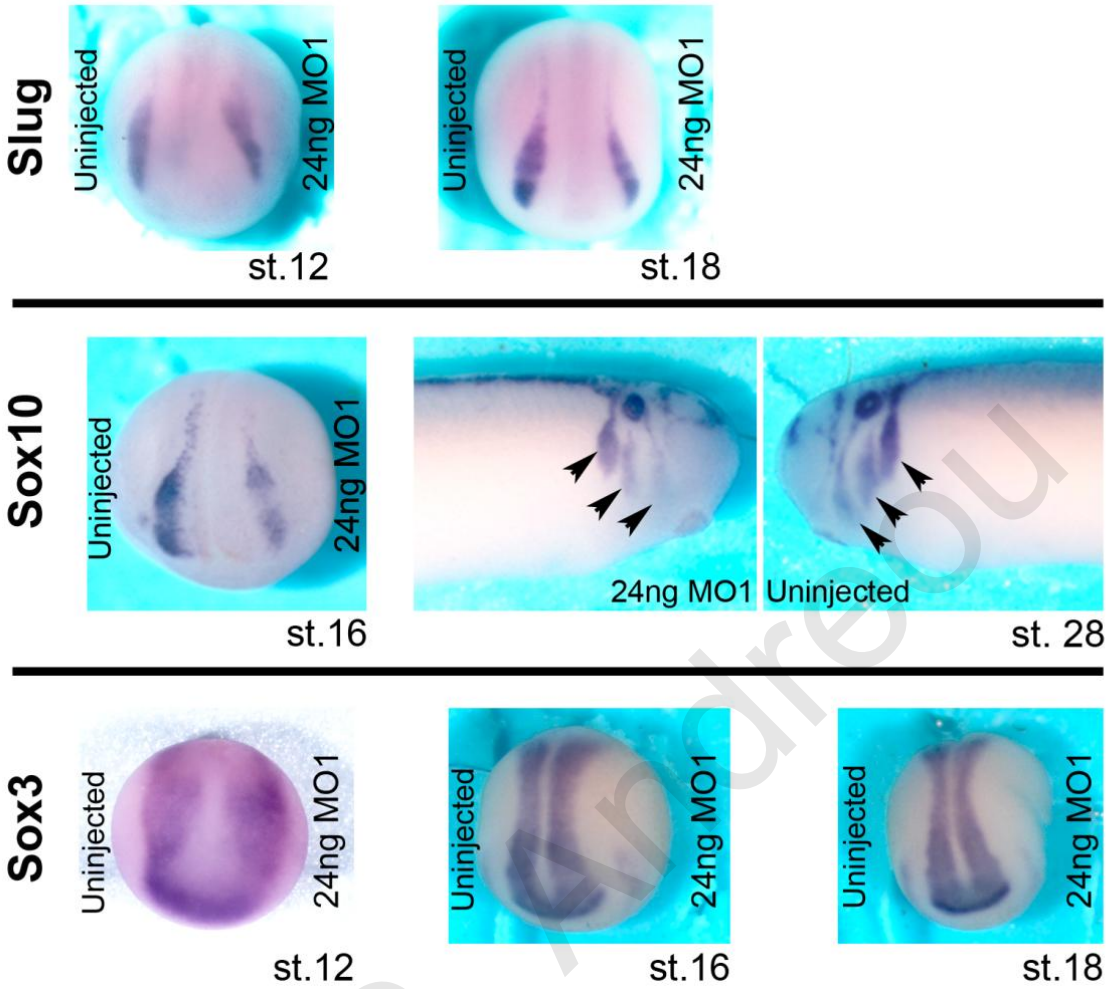

Figure 71 : Whole mount *in situ* hybridization using Slug, Sox3 and Sox10 show that the neural tissues are normally defined in MO-injected embryos. Embryos were injected in one blastomere of two cell stage so that half of the embryo was injected with 24ng of MO1. (A) Slug was expressed. (B) Sox10 showed reduced expression. (C) Sox3 was normally expressed in both sides of the embryo.

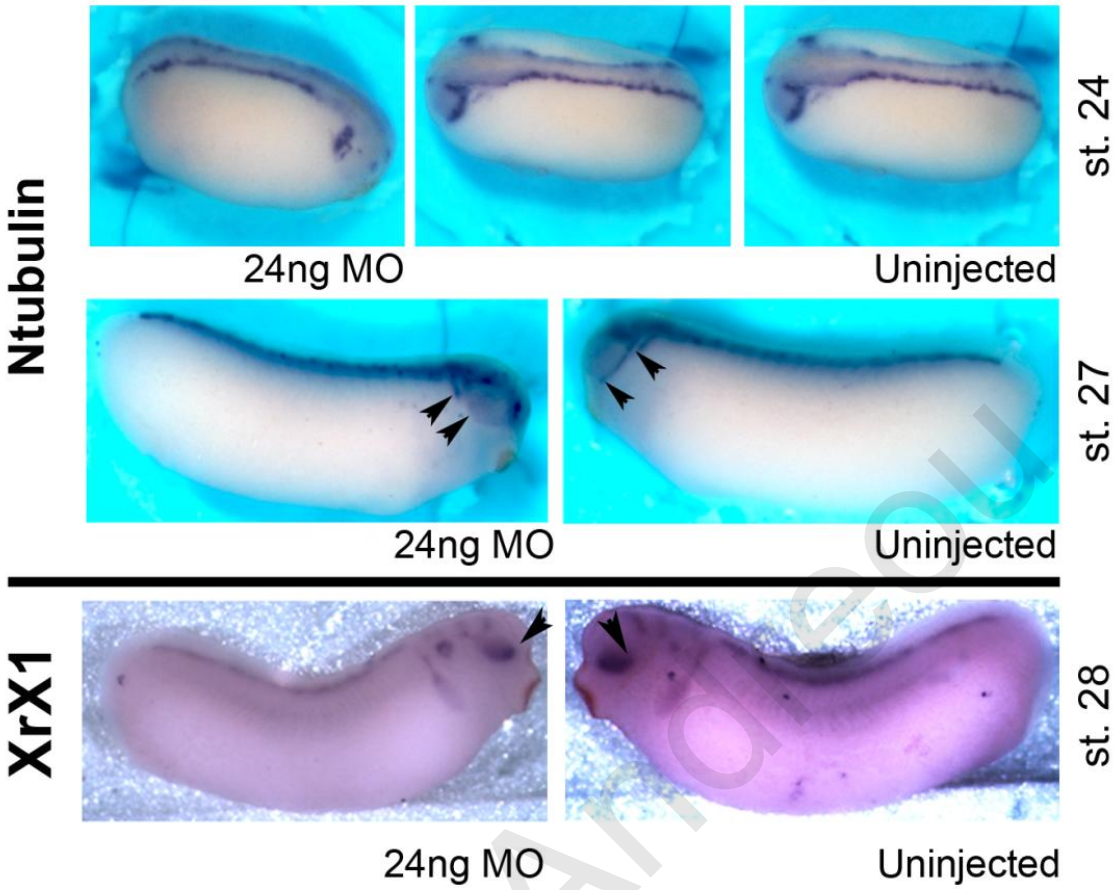

Figure 72 : Whole mount *in situ* hybridization using Ntubulin (Ntub) and XrX1 show that the neural tissues are normally defined in MO-injected embryos. Embryos were injected in one blastomere of two cell stage so that half of the embryo was injected with 24ng of MO1. (A) Ntubulin was expressed in the injected side of the embryo, although some tissues such as the cranial sensory ganglia and the branchial arches could not properly migrate (arrowheads). (B) The eye is formed but it seems reduced in size in comparison with the uninjected side of the embryo.

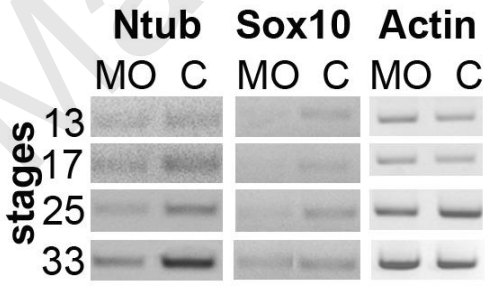

Figure 73 : RT-PCR experiments revealed a reduction in neural marker expression in MO injected embryos. Actin was used as normalized control.

4.2.11 40LoVe/Samba morphants display apoptosis in neural tissues

Since neural patterning appeared unaffected, but the expression of neural markers was reduced and neural tissues were malformed in morphants, we decided to examine if the division rate was affected in cells injected with the MO. We went on to examine the rate of cell division in injected embryos using a mitotic cell marker, Histone H3[pSer10], which detects endogenous levels of histone H3 only when phosphorylated at serine 10, which is tightly correlated with chromosome condensation during mitosis (Hendzel, Wei et al. 1997). We noted a reduction in the number of dividing cells in the eye and in the head region on the MO1 injected side of the embryos (Figure 74**Error! Reference source not found.**). These results suggest that 40LoVe/Samba is necessary for neuronal cell survival.

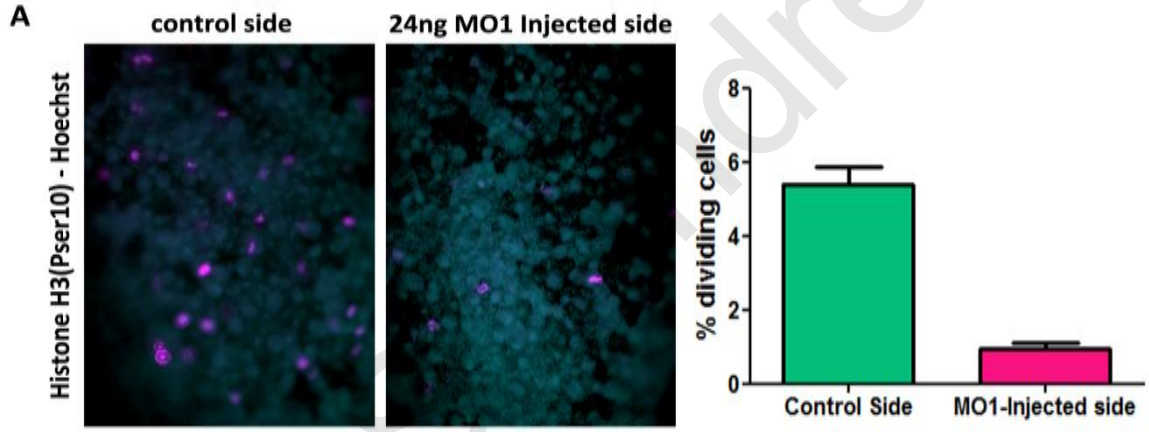

Figure 74 : 40LoVe/Samba are required for neuronal cell survival. Hoechst (cyan) and Histone H3[p Ser10] (magenta) staining reveals mitotic cells of a representative embryo injected with MO1 in one out of two animal blastomeres at the two cell stage. The images show that fewer dividing cells are present in the MO1 injected side of the embryo compared to the uninjected side of the same embryo. The graph shows quantification from 15 embryos from two independent experiments.

After that, we decided to examine cell viability in MO injected embryos via whole mount TUNEL assay. This experiment revealed increased apoptosis in the eye and other head structures in the MO-injected side of embryos (Figure 75). These results suggest that the reduced eye size and the decreased neural marker expression in morphants is due to the selective loss of neural tissues through apoptosis and suggest that 40LoVe/Samba are required for neuronal cell survival.

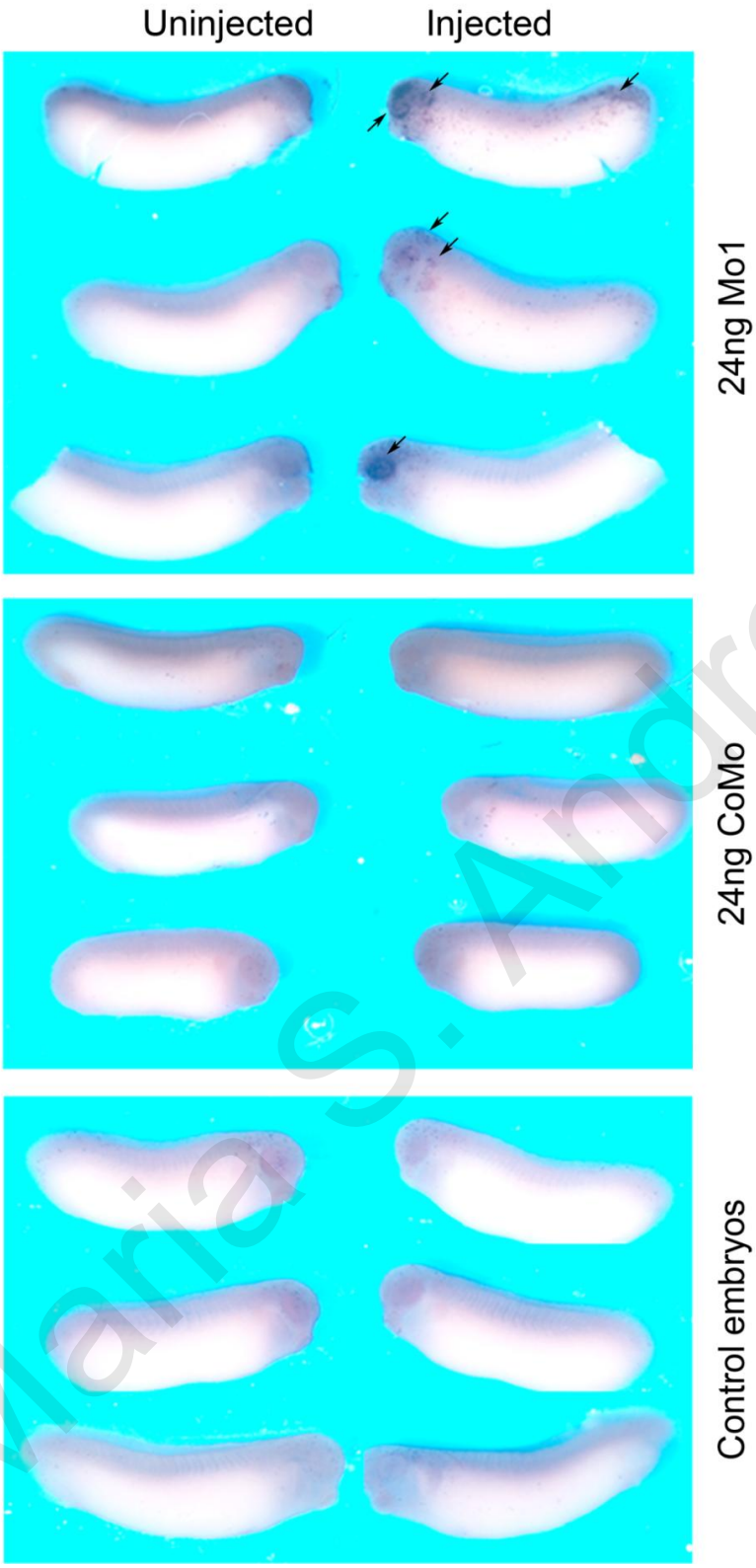

Figure 75 : Cell death was detected in MO-injected side of the embryo. TUNEL staining shows increased apoptosis in the eye and other head structures in MO-injected side of the embryo. In contrast CoMO injected embryos do not show cell death in specific tissues. Control embryos do not have any cell death.

4.2.12 Morpholino specificity

In order to determine if the MO effect was specific, we attempted to rescue the phenotype using a protein with a modified N-terminus so that the MO could not recognize it. We constructed both 40LoVe and hnRNP AB rescue constructs (R40LoVe and RhnRNP AB). As an initial experiment, we tried to rescue the phenotype by injecting 40LoVe (R40LoVe) alone. Further experiments were conducted to examine the ability of each protein or a combination of them to rescue the phenotype (Table 9). The overall phenotype was partially rescued using 80pg of R40LoVe (Figure 77C), suggesting a crucial role for this isoform. RhnRNP AB however failed to rescue the phenotype (Figure 77D). In order to quantify the phenotype we used the same approach described above. So we again measure the eye diameter of both sides in embryos injected at the one out of two blastomeres at the two cell stage. When we had the results of the eye diameter, we compared the rescued embryos with the MO-injected and the control and verified that the phenotype was successfully rescued by injection of R40LoVe mRNA. Quantification of the small eye phenotype confirmed that 40LoVe could rescue (eye size 90% of controls) while hnRNP AB failed to do so (Figure 78). This result suggests that the small eye phenotype is specific and that it is elicited by the loss of 40LoVe and not hnRNP AB confirming that the two proteins are functionally distinct in agreement with their different localization.

Since hnRNP AB fails to rescue the morphants despite its very high homology to 40LoVe, we postulated that this may happens due to its strictly nuclear localization. We then went on to examine whether the ability of 40LoVe/Samba to shuttle between the nucleus and the cytosol was functionally significant. As we showed before, swapping the 40LoVe/Samba GRD domain with that of hnRNP AB results in a purely nuclear protein 40LoVeGRD$_{AB}$. We postulated that if nucleocytoplasmic shuttling and/or cytosolic localization is necessary for 40LoVe's function the 40LoVeGRD$_{AB}$ chimera would fail to rescue the MO induced eye defects in a similar fashion as AB expression. Co-injection of the 40LoVeGRD$_{AB}$ mRNA with the MO1, indeed fails to rescue the small eye phenotype elicited by the MO (Figure 77D). These results show that the shuttling of 40LoVe/Samba is required for its function and suggests that hnRNP AB fails to rescue due to its inability to

shuttle. On the other hand, co-injection of the other chimeric protein hnRNP AB-GRD_{40LoVe}, which is able to shuttle, with MO1 does rescue the small eye phenotype, albeit with lower efficiency than expression of 40LoVe, suggesting that the cytoplasmic localization and shuttling are at least partly responsible for the differences in function (Figure 77C, Table 9).

Given the fact that Mo1 was designed to block 40LoVe, Samba and hnRNP AB translation, and since hnRNP AB was not able to rescue the phenotype, we wanted to verify that the phenotype we were observing was due to 40LoVe/Samba knockdown. So we used the second MO (MO2) that was designed to block translation of Samba and 40LoVe but not hnRNP AB (see: Figure 31). Injection of different amounts of MO2 gave the same phenotype as shown on Figure 68. The only difference was that the phenotype was milder, which is in agreement with the WB data showing that MO2 is less effective in downregulating protein levels of 40LoVe/Samba compared to MO1. Overall these results confirm that 40LoVe/Samba knockdown is responsible for the small eye phenotype.

	Severe head defects	Moderate head defects	Normal head structures	Total number of embryos
24ng MO1	60%	33%	6%	104 (n=5)
24ng MO1 + R1	17%	47%	36%	83 (n=2)
24ng MO1+ R2	10%	38%	50%	112 (n=4)
24ng MO1 +R3	59%	35%	5%	71 (n=3)
24ng MO1 +R4	54%	41%	4%	55 (n=2)
24ng MO1 +R5	5%	53%	42%	55 (n=2)
24ng CoMO	1%	16%	83%	84 (n=2)
Uninjected Controls	0	7%	93%	66 (n=4)

R1 = 60pg Samba + 60pg R40LoVe

R2 = 80pg R40LoVe

R3 = 80pg RhnRNPAB

R4 = 80pg $R40LoVeGRD_{AB}$

R5 = 80pg $RhnRNPAB\text{-}GRD_{40LoVe}$

Table 9 : Rescue Attempts. The experiments were performed n times for each case as indicated and the numbers on the table are the mean for each case.

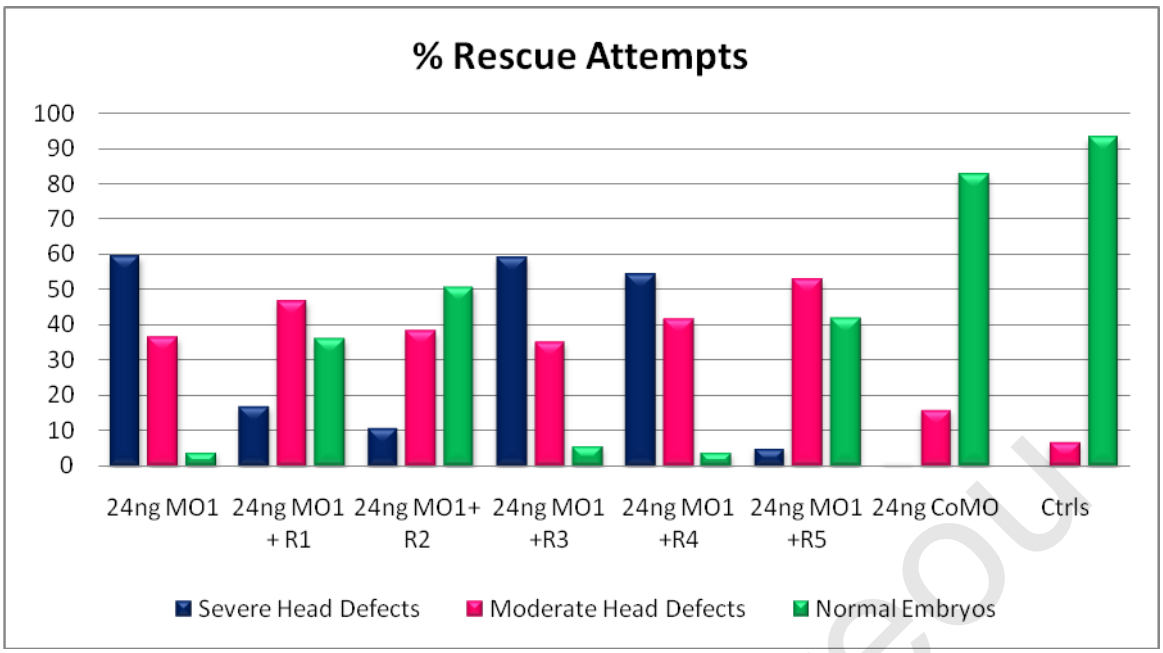

Figure 76: Chart presenting the rescue attempts. The phenotype was rescued in 50% of the embryos injected with 80pg of R40LoVe and 42% of the embryos injected with 80pg of RhnRNPAB-GRD$_{40LoVe}$. The transcripts whose products are exclusively nuclear (e.g. RhnRNP AB and R40LoVeGRD$_{AB}$) cannot rescue the phenotype.

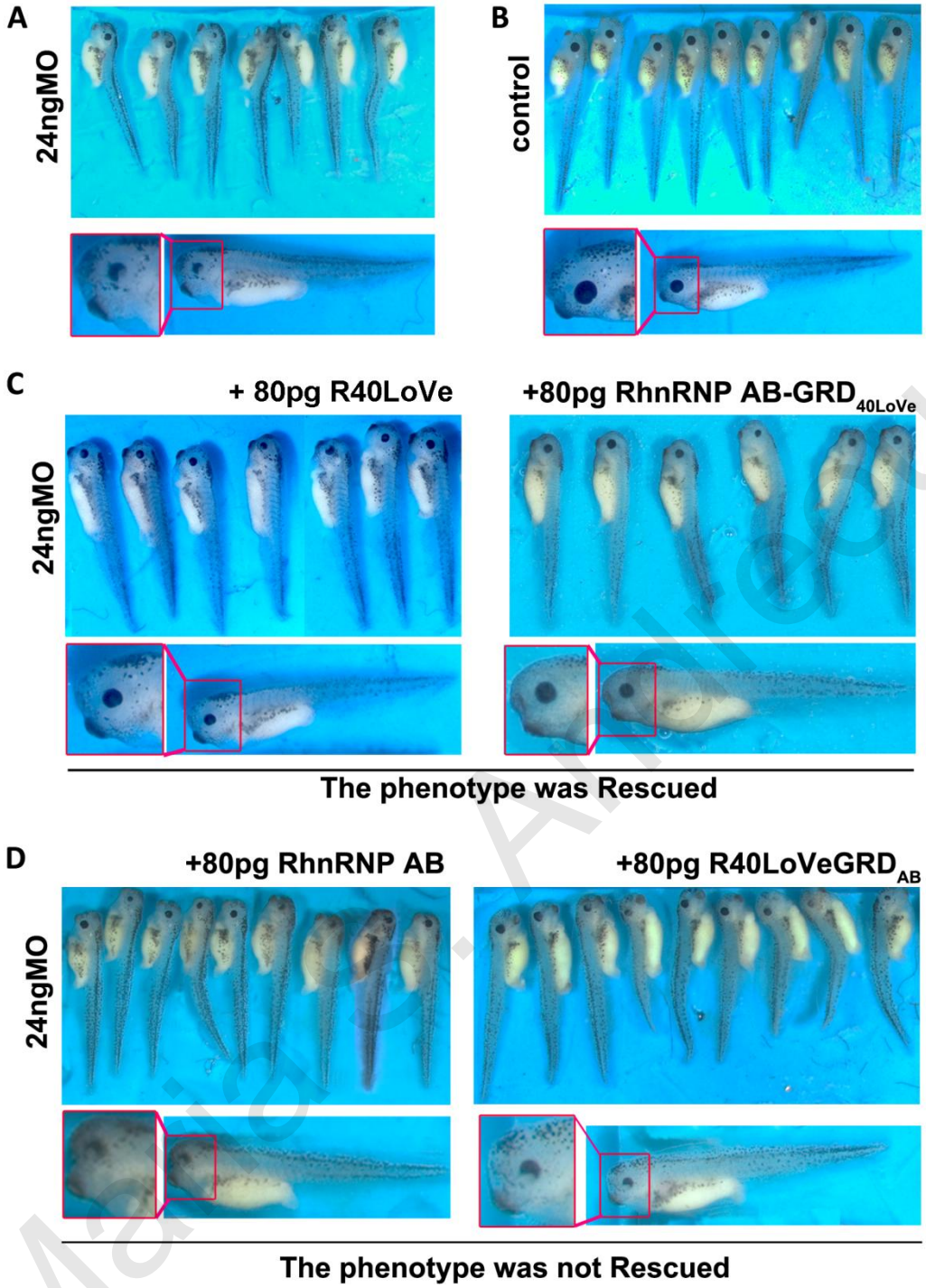

Figure 77 : R40LoVe and RhnRNP AB-GRD$_{40LoVe}$ were able to rescue the phenotype, showing that cytoplasmic localization is significant for 40LoVe function. (A) 24ng of MO1 elicited to shortened AP axis and reduced eye size. (B) Uninjected Control embryos. (C) Embryos co-injected with 24ng MO1 and 80pg of R40LoVe and hnRNP AB-GRD$_{40LoVe}$ were successfully rescued. These transcripts that have a cytosolic fraction of the protein may rescue the phenotype. (D) Embryos co-injected with 24ng MO1 and 80pg of hnRNP AB or 40LoVeGRD$_{AB}$ were not successfully rescued. These transcripts that are exclusively nuclear are not able to rescue the phenotype.

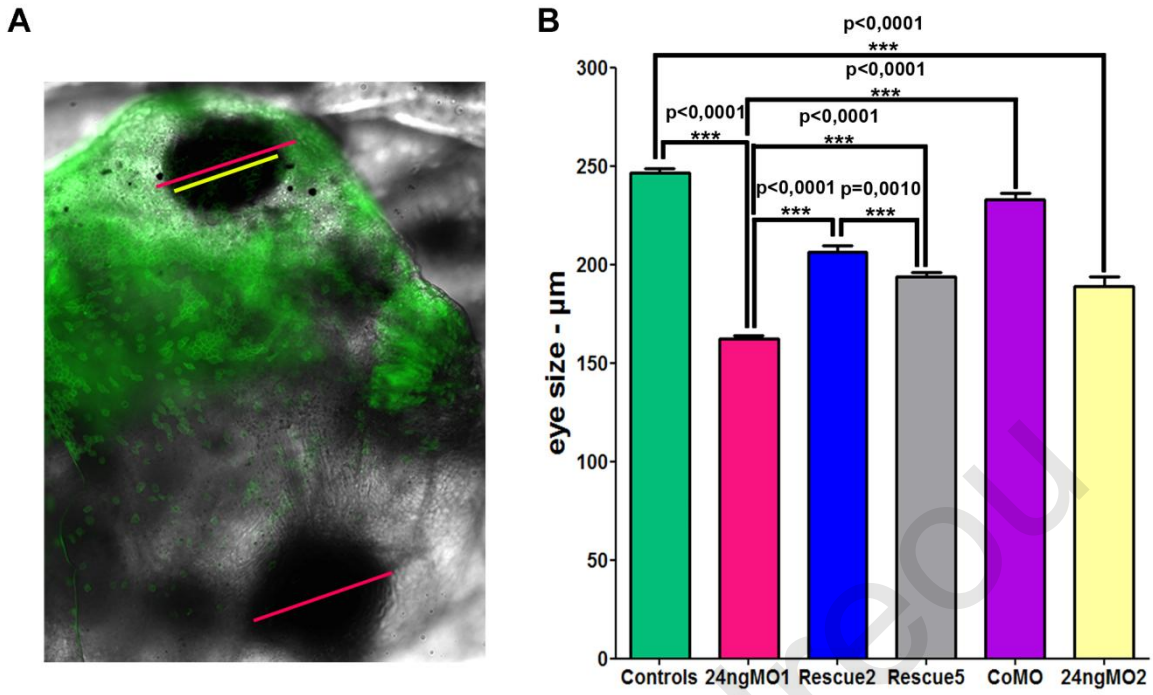

Figure 78 : Eye size was used to quantify the phenotype. (A) The eye size diameter was measured on the injected (indicated with GFP) and the un-injected side of the embryo. The figure shows a representative embryo co-injected with 24ng MO1 and mGFP in one out of two blastomeres at two cell stage. (B) Eye size was measured from embryos injected with MO1, MO2, control morpholino (CoMO), rescued (R2-R40Love co-injected with MO1 and R5-RhnRNPABGRD$_{40LoVe}$ co-injected with MO1 as shown in Table 9) and control embryos (n=80-120 for each category)). Graph shows that in MO1-injected embryos the eyes were 40% smaller than controls and it was successfully rescued by injection of R40LoVe mRNA (Rescue 2 - eye size 90% of controls). hnRNPAB-GRD$_{40LoVe}$ (Rescue 5) is also able to partially rescue the phenotype.

5. Discussion

In vivo, site-specific, covalent conjugation of Quantum Dots to proteins via split-intein splicing

Herein, we describe a simple and effective method that enables the site-specific conjugation of QD's and other artificial structures to target proteins *in vivo*. QD's were chosen as a model nanostructure due to their superior optical properties that facilitate detection and enable easy optical and biochemical evaluation of the conjugation and its effects on target protein localization and function. *S*ite-specific conjugation of QD's to proteins was afforded by intein-based protein trans-splicing. Unlike other conjugation methods, the intein method is a traceless ligation, in which the intein itself is spliced out and excluded from the final conjugation product. In addition to site-specificity, intein-based protein trans splicing has several other advantages, including high efficiency of product formation, reproducibility and versatility as it allows the targeting of any nanoparticle (QD or other) to any protein of interest.

An important feature of this conjugation method is the fact that target protein functionality is not affected upon fusion with QD's. In fact QD-PH conjugates retained full functionality of the PH domain as indicated by their ability to i) recognize PIP3, and ii) to translocate to the cell membrane in a PI3-K dependent manner (Figure 37). This should hold true for most proteins as the QD is fused post-translationally to the target protein and does not therefore influence protein folding and tertiary structure, in contrast to fluorescent protein fusions.

In addition, conjugation of QD's to the PH domain did not affect the ability of the former to resist photodegradation. Photostability is one of the main advantages of QD detection as it allows prolonged visualization of the labelled protein and thus facilitates determination of its function as well as delineation of the pathway in which it is involved. We found no loss of fluorescence intensity in PH-QD conjugate injected embryos even after 20 min of continuous illumination, whereas there was complete loss of EGFP fluorescence after 5 min of illumination (Figure 40).

Moreover, this conjugation method is easily adaptable to the needs of the individual experiment as it allows use of different streptavidin-coated QD's (emitting at different wavelengths) to observe the same target protein, without having to change any other reagent in the experiment. For instance, use of Near Infra Red (NIR)-emitting QDs allowed monitoring of QD-conjugates within the embryo at depths where EGFP is undetectable demonstrating the advantages of NIR-QD's for this type of experiment.

However, our present results point to the need for wider availability and commercialization of smaller water soluble nanocrystals and controlled nanoparticle valency. Another issue that needs to be investigated is the stability of the QD-streptavidin conjugation itself. Commercially available QDs from different vendors use different conjugation chemistries as well as different approaches to render QDs hydrophilic. How long the conjugation lasts in the cell is not known, as it is not known how long do the amphipathic polymer and micelle coats last in this environment. The combination of efficient and non-reversible fusion of QD's to target proteins with reduced QD size and monovalency could help to make the strategy we describe a standard tool for in vivo imaging of protein dynamics at the single-molecule level. In addition several inducible intein splicing systems have also been reported raising the possibility of inducible conjugation of QDs to target proteins. This would afford temporal control with respect to the conjugation reaction and open new potential applications. Finally, this methodology could be invaluable due to its potential diagnostic and therapeutic implications, as it makes the targeting of nanostructures and nanodevices to different intracellular compartments and signaling complexes a viable possibility.

40LoVe/Samba are involved in *Xenopus laevis* neural development and functionally distinct from hnRNP AB

hnRNPs are defined by common motifs and the regions of sequence divergence amongst phylogenetically close variants are concentrated in the terminal-regions of the proteins (Han, Tang et al. 2010). Here, we report functional differences between two closely related hnRNPs which correlated with their subcellular localization. In turn, the latter is determined by point variations in the GRD domain.

40LoVe has been reported to present at least four different splice variants that result in protein product differences (Kroll, Swenson et al. 2009). Amongst these, 40LoVe and its splice variant Samba differ with respect to the presence of an insert between the CBFNT and RBD domains. Our work suggests that 40LoVe and Samba are in fact splice variants since they contain identical 3' and 5' prime UTRs. RT-PCR experiments failed to detect additional variants at the RNA level. 40LoVe/Samba are also closely related to *Xenopus* hnRNP AB with differences in a total of 21 amino acids residues; 10 distributed in the amino-terminal CBFNT domain, 5 in the GRD domain and 6 in the central RBDs (RNA-binding domain). Sequence alignments between 40LoVe/Samba and *Xenopus* hnRNP AB suggested that hnRNP AB is a paralog of 40LoVe, since the UTRs are not identical but do present significant homology. This is also supported by the fact that Kroll et al. identified a 40LoVe sequence different than the one characterized by Czaplinski et al. in a previous study (Czaplinski, Kocher et al. 2005; Kroll, Swenson et al. 2009). Kroll et al. reported that the isoform they identified is the one able to bind Vg1 mRNA during oogenesis (Kroll, Swenson et al. 2009). Sequence alignment made clear that what we refer to as 40LoVe is the one identified by Kroll et. al, while what we refer to as hnRNP AB is in fact a match to the 40LoVe identified by Czalpinski et al.. Nevertheless the 4.6% sequence difference displayed between the 40LoVe/Samba and the hnRNP AB GRD domains was sufficient to produce a dramatic localization change and as a result render the two proteins functionally distinct. Together these data suggest that 40LoVe is probably the one responsible for the RNA binding and translocation in the cytosol, as mentioned for 40LoVe in oogenesis, while hnRNP AB has a distinct or an overlapping but restricted role in the nucleus. In order to determine if the three transcripts display any differences with respect to their temporal expression we carried out RT-PCR experiments. We arrive at the conclusion that all three transcripts are under the same spatiotemporal control.

Exploring the three transcripts localization at the cellular level, we saw that 40LoVe and Samba display the same localization. They are both found in the nucleus and the cytosol, while hnRNP AB is found only in the nucleus. Using GFP fusions we enabled us to monitor the protein localization live both in cultured cells as well as in the embryo. These experiments revealed that all three proteins localize in a similar fashion during cell division. Once the nuclear envelope breaks down the proteins are released in the cytosol,

and a portion co-localizes with the spindle while all three are completely excluded from the chromatin. This comes in agreement with previous studies on other hnRNPs that showed spindle localization during cell division (He, Martin et al. 1991; Pinol-Roma and Dreyfuss 1991). What role if any these proteins may play during mitosis is not understood. We were unable to detect and spindle abnormalities or mitotic defects in morphants however MO-injected embryos did display increased cell death and reduced proliferation which may be related to mitotic defects. When embryos were injected unilaterally with the MO, they displayed increased apoptosis and reduction in cell division. In future experiments it would be critical to check the spindle orientation and spindle integrity in more detail to further explore the proteins' roles in cell division. It is also possible that 40LoVe, like hnRNP A2, is part of large ribonucleoprotein complexes. These complexes are called RNA granules and contain containing RNA-binding proteins, proteins of the translational machinery and molecular motors. RNA granules have been shown to be transported along microtubules to distal dendrites where the RNA is locally translated. Although no one to our knowledge has imaged the localization of RNA granules during mitosis it is conceivable that they would bind the microtubules of the spindle given the fact that they contain microtubule based molecular motors.

Previously, hnRNP AB and hnRNP D have been phylogenetically grouped to the same hnRNP family of proteins (hnRNP AB-D subfamily) (Kroll, Swenson et al. 2009). 40LoVe phylogenetic assignment is important because many of the proteins that are implicated in RNA localization are conserved through a wide range of species and this can be helpful exploring the protein function.

Interestingly, reduction in 40LoVe/Samba, but not hnRNP AB levels, resulted in a neural phenotype. The more striking features of the morphants were reduction in eye size and limited axonal growth. Several hnRNPs and RNPs have been previously reported to play important role in neural plasticity and development (Perrone-Bizzozero and Bolognani 2002; Si, Giustetto et al. 2003; Yao, Sasaki et al. 2006). hnRNP K morphants form attenuate axons, without affecting neural cell determination. The protein has been shown to accompany RNAs from the nucleus to the cytoplasm and selectively recruits various elements and initiates translation when necessary (Bomsztyk, Denisenko et al. 2004;

Mikula, Dzwonek et al. 2006). hnRNP K, like 40LoVe has been shown to undergo nucleocytoplasmic shuttling due to the KNS sequence, that is present in the human homolog, but not in the *Xenopus* and *Drosophila* homolog (*bancal*) which also shuttle but are believed to utilize a different mechanism for shuttling (Michael, Eder et al. 1997; Charroux, Angelats et al. 1999; Habelhah, Shah et al. 2001). *Xenopus* hnRNP K, shuttling could be mediated by the ERK1/2 phosphorylation site that is implicated in the protein's cytosolic localization in HeLa cells (Habelhah, Shah et al. 2001). *Bancal* also shuttles due to its M9 motif that has been previously shown to mediate shuttling in human hnRNPs A1 and A2/B1 (Charroux, Angelats et al. 1999). hnRNP K is implicated in chromatin remodeling, transcription, splicing and translation processes and has been shown to bind transcription, splicing and translation factors. It has also been reported that the protein's interactions and functions are conserved in eukaryotes (Bomsztyk, Denisenko et al. 2004). Inhibition of hnRNP K using MO blocked axonal outgrowth and NF-M translation. It is likely that hnRNP K targets additional RNAs needed for axon development and is probably responsible for translational regulation at sites of axon growth (Liu, Gervasi et al. 2008). In addition, hnRNP R has been detected in axons and axonal growth cones in neurons (Rossoll, Kroning et al. 2002), and has been shown to affect neuronal formation. Suppression of hnRNP-R in developing zebrafish embryos using MOs, results in reduced axon growth in spinal motor neurons, without affecting motor neuron survival (Glinka, Herrmann et al. 2010). Glinka et al. also report that hnRNP R binds to the 3'-UTR region of b-actin mRNA, which is necessary for the translocation of this mRNA into neuronal processes (Tiruchinapalli, Oleynikov et al. 2003; Huttelmaier, Zenklusen et al. 2005; Glinka, Herrmann et al. 2010).

Furthermore, several studies suggested that mammalian hnRNP AB, the closest match for 40LoVe in mammals, has important roles in the development and function of the vertebrate nervous system (Rushlow, Rajakumar et al. 1999; Rushlow, Rajakumar et al. 2000; Murgatroyd, Wigger et al. 2004; Dichmann, Fletcher et al. 2008). In mice, hnRNP AB plays a role in neural stem cell maintenance and differentiation as well as cell survival. During neuronal maturation hnRNP AB changes its subcellular distribution suggesting a role in regulating gene expression (Sinnamon, Waddell et al. 2012). Interestingly, there are two murine hnRNP AB variants hnRNP AB1 (p42) and hnRNP AB2 (p37), that arise

from differential splicing of an exon of the same gene. Immunostaining of mouse brain sections revealed that the protein is expressed in the mouse brain and shows strong nuclear staining and a weaker uniform cytosolic staining. Further experiments showed that hnRNP AB1 ortholog is nuclear like *Xenopus* hnRNP AB, while hnRNP AB2 is primarily nuclear but also has a cytosolic fraction, like *Xenopus* 40LoVe. It is important to mention that hnRNP AB isoforms only appear in the cytoplasm of mature neurons. The cytosolic pool of hnRNP AB increases during neuronal maturation and the larger proportion of the cytosolic signal is attributed to hnRNP AB2 (Sinnamon, Waddell et al. 2012). Sinnamon et al. generated an hnRNP AB knockout mouse (both orthologs hnRNP AB1 and hnRNP AB2) to explore its role *in vivo*. They initially performed proteomics analysis to demonstrate that hnRNP AB regulates expression of many genes that play important roles in nervous system development. Then they used neurosphere cultures (self renewal neural stem cells that give rise to the different neural lineages) to show that it affects neural stem cell maintenance and differentiation of different neural lineages, since specific amount of hnRNP AB is necessary for the correct neural marker expression (Sinnamon, Waddell et al. 2012).

As mentioned above 40LoVe was initially phylogenetically placed in the hnRNP AB-D subfamily of proteins and is likely that it is the homolog of the mammalian hnRNP AB. Functionally, it appears that 40LoVe has similarities with the mammalian hnRNP AB and our data supports that *Xenopus* hnRNP AB is a paralog of 40LoVe. However, it is unusual for paralogs to be functionally distinct like 40LoVe and hnRNP AB are and this functional differentiation points to a gene that arose through duplication but has since evolved to be functionally distinct. In previous studies in mice, Raju et al. have reported that hnRNP AB binds to an RNA trafficking sequence (Gingras, Vogel et al.) in the 3'UTR of the myelin basic protein (MBP) mRNA. They did this using GST-pulldown and also coupled wild type RTS and scrambled RTS to streptavidin-coated Sepharose beads and incubated the beads with HeLa protein extract to show that hnRNP AB also called CBF-A specifically binds the MBP mRNA RTS. This group also showed that hnRNP AB is important for the localization of the MBP mRNA to the myelin compartment (Raju, Goritz et al. 2008). Using qRT-PCR on reverse-transcribed cDNA derived from RNA extracts of differentiating oligodendroglial precursor cell line (oli-neu cells) immunoprecipitated by CBF-A, it was shown that CBF-A is

specifically associated with the MBP mRNA. The same group also used RNA interference (RNAi,) to silence CBF-A and saw that it specifically represses MBP mRNA trafficking along oligodentrocytes (Raju, Goritz et al. 2008). A later study has also shown using RT-PCR on cDNA from RNA coprecipitated with CBF-A, that hnRNP AB binds to RTS-like sequences of certain dendritic mRNAs for their transport to the neuronal synapses (Raju, Fukuda et al. 2011). Overall the above data offer strong evidence that mammalian hnRNP AB has an important role in the transport of mRNAs to the synapse in agreement with hnRNP AB's elevated expression in neuronal tissues. Here we show that 40LoVe is transported along axons and is found at axonal growth cones consistent with the above findings in the mouse and suggests that 40LoVe is the *Xenopus* ortholog of the mammalian hnRNP AB.

Further evidence for this interpretation comes from the fact that 40LoVe downregulation also causes neural phenotype and is also localized in the nucleus and the cytosol with a primarily nuclear and a weaker cytosolic signal. 40LoVe is 63% identical to the mouse hnRNP AB (Annexes 7.2) at the amino acid level. However it is also presents a 62% identity with hnRNP D (Annexes 7.2). However, 40LoVe is not likely to be orthologus to hnRNP D, since the two proteins display different localizations and more importantly different spatial expression in the embryo and different loss of function phenotype. Murine hnRNP D is highly expressed in immune cells and shows strong staining in the skin (Lu and Schneider 2004; Sadri and Schneider 2009). hnRNP D knockout mice show sensitivity to endotoxic shock and present increased mortality as a result of an increased and prolonged TNF and IL1*β*-mediated proinflammatory response (Lu, Sadri et al. 2006). Nevertheless, human hnRNP D/AUF1 is primarily nuclear and shuttles between the nucleus and the cytosol, because of DNS localized at the c-terminus of the protein (Suzuki, Iijima et al. 2005).

Overexpression of Samba gives a similar head structure phenotype as the loss of function we report here. This phenotype was attributed to interference with neural crest migration (Yan, Skourides et al. 2009). The size of the migrating crest chains were also reduced in the morphants shown here, raising the possibility that an optimal level of 40LoVe/Samba expression is required for proper neural crest migration. Indeed, RNA binding proteins participate actively in the establishment of cell-substrate adhesion

centers (de Hoog, Foster et al. 2004; Vikesaa, Hansen et al. 2006; Yoo, Wu et al. 2006; Katz, Wells et al. 2012). Both decrease or increase in hnRNP expression levels or activity have been shown to inhibit cell spreading and migration (de Hoog, Foster et al. 2004; Vikesaa, Hansen et al. 2006; Yoo, Wu et al. 2006). Together, these data suggest that cell spreading depends on the proper balance of hnRNP levels in the cytoplasm during spreading or migration. The target mRNAs that 40LoVe associates with and are responsible for the neural crest migration phenotype are not known, but it appears that 40LoVe loss of function elicits these effects without affecting cell fate specification. Although neuronal marker expression was present in 40LoVe morphants their expression level was reduced. In addition patterning appeared unperturbed and the reduced marker expression was attributed to reduced proliferation and apoptosis of neural tissues. This is in contrast with a previous study that showed that when hnRNP AB expression levels were reduced, the expression levels of some neuronal markers was increased and of others decreased, affecting neural differentiation (Sinnamon, Waddell et al. 2012). Although WISH experiments revealed that neural specification overall is not affected in 40LoVe/Samba morphants in *Xenopus* it is possible that use of additional markers may reveal some patterning issues however given the elevated apoptosis and reduced proliferation any such variations will likely be secondary to the selective loss or reduced proliferation or specific differentiated neuronal lineages.

The participation of hnRNPs in adhesive centers in the cytoplasm could also explain the second major difference that we detected between 40LoVe/Samba and hnRNP AB. In our experimental paradigm, hnRNP AB was strictly localized in the nucleus, while 40LoVe/Samba localized both in the nucleus and the cytosol and trafficked between the compartments. The nucleocytoplasmic shuttling and/or cytosolic localization was essential for the rescue of the morphants, as the 40LoVe-GRD_{AB} mutant that is restricted to the nucleus cannot rescue the morphant phenotype. The 40LoVe/Samba nucleocytoplasmic shuttling behavior and nuclear retention of hnRNP A/B are conferred solely by their respective Glycine Rich Domains.

Nevertheless, our results show that the few amino acid differences between 40LoVe/Samba and hnRNP AB GRD domains are sufficient to grant nuclear retention to

the latter and this retention is at least in part responsible for the failure of hnRNP AB to rescue the neuronal phenotypes observed in morphants, since hnRNP AB-GRD$_{40LoVe}$ is able to partially rescue the elicited small eye phenotype. More importantly, it also brings to attention that slight differences in the sequences of closely related hnRNPs are sufficient to generate different subcellular localization and, as a consequence, influence their biological functions. Many known hnRNPs have been reported to contain unconventional nuclear localization signals and shuttling sequences in their GRD domains (Siomi and Dreyfuss 1995; Weighardt, Biamonti et al. 1995; Van Dusen, Yee et al. 2010). After an exhaustive search of different hnRNPs and their localization and shuttling sequences we found that 40LoVe and hnRNP AB have a sequence that is very similar to the DNS signal identified in hnRNP D (Suzuki, Iijima et al. 2005). This 19 amino acid sequence in 40LoVe and hnRNP AB presents an 80% sequence identity to DNS. In order to explore DNS function and the residues responsible for that, Suzuki et al. carried out deletions, alanine scanning mutagenesis and point mutations. After deleting up to seven residues from the N-terminal portion of DNS, Suzuki et al. found that the nuclear import activity was gradually reduced and similarly decreased the protein's binding to Trn-1 (Suzuki, Iijima et al. 2005). In addition to these, deletion of the last three C-terminal amino acids KPY, alanine substitution and even point mutation of either of the last two C-terminal amino acids PY completely abolished the *in vivo* and *in vitro* nuclear import activity as well as the binding to Trn-1. Consequently, these data revealed that two separate regions N-terminal seven amino acid sequence SGYGKVS (288–294) and the last two C-terminal residues PY are essential for *in vivo* and *in vitro* transport as well as for interaction with Trn-1 (Suzuki, Iijima et al. 2005). The N- and C-terminal motifs of the DNS are also conserved in other shuttling sequences like the M9 sequence of hnRNP A1 and the C-terminal tail identified in JKTBP (Michael, Choi et al. 1995; Kawamura, Tomozoe et al. 2002). The PY motif is identical in 40LoVe/Samba, hnRNP AB and hnRNP D and the seven amino acid N-terminal do not differ between 40LoVe/Samba and hnRNP AB although it is different between hnRNP D and 40LoVe/Samba/hnRNP AB. So, this seven amino acid sequence is not responsible for the protein localization differences observed between 40LoVe/Samba and hnRNP AB. This prompted us to explore the intermediate amino acids in the DNS sequence. The fact that hnRNP D localizes like hnRNP AB and

unlike 40LoVe and Samba suggests the 14th residue in the DNS domain, that is the one different between 40LoVe and hnRNP AB, but the same with hnRNP D and hnRNP AB, is probably responsible for the differences in localization. That is $Asparagine_{350}$ in hnRNP D, $Asparagine_{319}$ in hnRNP AB and $Serine_{321}$ in 40LoVe. None of the other residue differences, between the hnRNP D DNS and hnRNP AB or 40LoVE/Samba, display the same correlation. Alignments of the DNS of 40LoVe and the c-terminus of mouse hnRNP AB has revealed that they share high homology (Annexes 7.2). Only 2 out of the 19 amino acids are different and that is only 10,5% difference, compared to 31,6% difference with the human hnRNP D. Also comparing mouse hnRNP AB and *Xenopus* hnRNP AB we detect 21% differences in the DNS. This also supports the fact that 40LoVe is closely related to murine hnRNP AB. Exploring the differences in the DNS, we arrive at the conclusion that the 14th residue in the DNS is the one responsible for the differences in localization, since that amino acid is conserved in all three proteins, mouse and *Xenopus* hnRNP AB and human hnRNP D, but different in 40LoVe/Samba. This is a strong indication that this amino acid is the one responsible for cytoplasmic release of 40LoVe/Samba and future mutagenesis should verify this. It would be useful to mutate the 14th amino acid in the 40LoVe DNS to Asparagine and the reverse in hnRNP AB and explore the localization shuttling behavior as well as ability to rescue the MO1 phenotype. However, irrespective of the specific amino acid responsible for the localization differences of the two proteins, our data clearly show that the GRD domain is responsible for these differences between 40LoVe/Samba and *Xenopus* hnRNP AB. It is interesting to note that in the case of the mouse hnRNP AB, where as previously mentioned two isoforms exist, which present similar localization differences (hnRNP AB1 is almost exclusively nuclear while hnRNP AB2 is clearly also detectable in the cytosol). The two murine isoforms do not have any differences in their DNS sequence, but their difference is in the GRD domain. hnRNP AB2 which is also found in the cytosol has a deletion in its GRD domain, a deletion that is not present in either the mouse hnRNP AB1 or the Xenopus hnRNP AB. This suggests that the deletion in the hnRNP AB2 GRD in effect accomplishes the same end result as the $Asparagine_{319}$ to $Serine_{321}$ does in 40LoVe i.e. cytosolic rerelease of the protein. It is possible that both mouse hnRNP AB1 and Xenopus hnRNP AB bind a nuclear factor through their GRD and are thus immobilized in this compartment and this interaction is

disrupted by the Asparagine$_{319}$ to Serine$_{321}$ change in 40LoVe and the GRD deletion in the case of hnRNP AB2. This would allow 40LoVe/Samba and hnRNP AB2 to shuttle between the nucleus and the cytosol. Another interesting observation that warrants further study is the fact that 40LoVe/Samba clearly present two populations in the cell. One population is immobilized in the nucleus while a second one shuttles between the two compartments. How are these two subsets different and are they involved in different functions remains to be determined. It is possible that the *Xenopus* hnRNP AB is able to carry out the nuclear functions of 40LoVe and is unable to perform additional functions requiring cytosolic localization. This would suggest that hnRNP AB fails to rescue the morphants despite its very high homology to 40LoVe, due to its strictly nuclear localization. Co-injection of the MO with 40LoVeGRD$_{AB}$ mRNA, that is also nuclear, failed to rescue the small eye phenotype, but co-injection of hnRNP AB-GRD$_{40LoVe}$, that is able to shuttle, does rescue the small eye phenotype, albeit with lower efficiency than expression of 40LoVe. These results suggest that the cytoplasmic localization and shuttling are at least partly responsible for the observed differences in function. So, in future experiments we are planning to generate a point mutant of the 14th residue of 40LoVe and again attempt to rescue the phenotype as mentioned above.

How can a single amino acid lead to such dramatic changes in localization? The DNS sequence has been called a shuttling sequence and as described substation mutagenesis has been performed to uncover critical amino acids within this sequence. One important observation from our work suggests that the amino acid change between hnRNP AB and 40LoVe is not affecting the ability of 40LoVe to be imported into the nucleus, but rather it limits its ability to be retained there. More FRAP and FLIP experiments should be able to verify this once a point mutant is available of the Asparagine$_{319}$ in hnRNP AB. However we also noted that the spindle localization of hnRNP AB is stronger than that of 40LoVe and Samba. It appears that the pool of the protein that associates with the spindle is in fact the nuclear fraction in each case. Specifically, the nuclear immobilized fractions of 40LoVe and Samba. One could possibly address this possibility using FRAP to eliminate all immobile 40LoVe prior to cell division via nuclear bleaching and similarly all mobile fraction through repeated cytosolic beaching steps as described in the results section and then compare spindle localization in the two cases. If this proposition is correct then this

would strengthen the notion that Asparagine$_{319}$ in hnRNP AB is required for an interaction of the protein with a nuclear target or that more it is responsible for increased affinity of the protein for a nuclear target that "traps" hnRNP AB in the nucleus.

Overall, our work suggests that 40LoVe is likely the *Xenopus* homolog of hnRNP AB and that it is involved in neural development. We show that loss of 40LoVe leads to abnormal neural development, stemming primarily from defects in neuronal cell proliferation and survival, in agreement with work in the mouse. Furthermore, our work has brought to light that extremely small differences in an hnRNP sequence can bring about dramatic changes in localization and mobility which in turn lead to clear functional differences.

6. References

Allers, J. and Y. Shamoo (2001). "Structure-based analysis of protein-RNA interactions using the program ENTANGLE." J Mol Biol 311(1): 75-86.

Allison, R., K. Czaplinski, et al. (2004). "Two distinct Staufen isoforms in Xenopus are vegetally localized during oogenesis." RNA 10(11): 1751-1763.

Antic, D., N. Lu, et al. (1999). "ELAV tumor antigen, Hel-N1, increases translation of neurofilament M mRNA and induces formation of neurites in human teratocarcinoma cells." Genes Dev 13(4): 449-461.

Aranburu, A., M. Bennett, et al. (2006). "The kappa promoter penta-decamer binding protein CBF-A interacts specifically with nucleophosmin in the nucleus only." Mol Immunol 43(6): 690-701.

Ariizumi, T., K. Sawamura, et al. (1991). "Dose and time-dependent mesoderm induction and outgrowth formation by activin A in Xenopus laevis." Int J Dev Biol 35(4): 407-414.

Arya, H., Z. Kaul, et al. (2005). "Quantum dots in bio-imaging: Revolution by the small." Biochem Biophys Res Commun 329(4): 1173-1177.

Asashima, M., H. Nakano, et al. (1990). "Mesodermal induction in early amphibian embryos by activin A (erythroid differentiation factor)." Dev. Biol 198: 330-335.

Axelrod, D., D. E. Koppel, et al. (1976). "Mobility measurement by analysis of fluorescence photobleaching recovery kinetics." Biophys J 16(9): 1055-1069.

Bajenova, O., E. Stolper, et al. (2003). "Surface expression of heterogeneous nuclear RNA binding protein M4 on Kupffer cell relates to its function as a carcinoembryonic antigen receptor." Exp Cell Res 291(1): 228-241.

Baker, C., D. Holland, et al. (1990). "Effects of oligo sequence and chemistry on the efficiency of oligodeoxyribonucleotide-mediated mRNA cleavage." Nucleic Acids Res 18(12): 3537-3543.

Baker, C. V. and M. Bronner-Fraser (1997). "The origins of the neural crest. Part I: embryonic induction." Mech Dev 69(1-2): 3-11.

Bomsztyk, K., O. Denisenko, et al. (2004). "hnRNP K: one protein multiple processes." Bioessays 26(6): 629-638.

Boulikas, T. (1993). "Nuclear localization signals (NLS)." Crit Rev Eukaryot Gene Expr 3(3): 193-227.

Bowes, J. B., K. A. Snyder, et al. (2010). "Xenbase: gene expression and improved integration." Nucleic Acids Res 38(Database issue): D607-612.

Bruchez, M., Jr., M. Moronne, et al. (1998). "Semiconductor nanocrystals as fluorescent biological labels." Science 281(5385): 2013-2016.

Burd, C. G. and G. Dreyfuss (1994). "Conserved structures and diversity of functions of RNA-binding proteins." Science 265(5172): 615-621.

Carson, J. H. and E. Barbarese (2005). "Systems analysis of RNA trafficking in neural cells." Biol Cell 97(1): 51-62.

Cartegni, L., M. Maconi, et al. (1996). "hnRNP A1 selectively interacts through its Gly-rich domain with different RNA-binding proteins." J Mol Biol 259(3): 337-348.

Caspi, J., G. Amitai, et al. (2003). "Distribution of split DnaE inteins in cyanobacteria." Mol Microbiol 50(5): 1569-1577.

Chan, W. C., D. J. Maxwell, et al. (2002). "Luminescent quantum dots for multiplexed biological detection and imaging." Curr Opin Biotechnol 13(1): 40-46.

Charroux, B., C. Angelats, et al. (1999). "The levels of the bancal product, a Drosophila homologue of vertebrate hnRNP K protein, affect cell proliferation and apoptosis in imaginal disc cells." Mol Cell Biol 19(11): 7846-7856.

Chen, J., V. Hardev, et al. (2013). "Quantum-dot technology is bringing wide color gamut to LCDs, giving them a leg up on another advantage that once belonged to OLEDs.".

Cosker, K. E., S. L. Courchesne, et al. (2008). "Action in the axon: generation and transport of signaling endosomes." Curr Opin Neurobiol 18(3): 270-275.

Covelo, G., C. S. Sarandeses, et al. (2006). "Prothymosin alpha interacts with free core histones in the nucleus of dividing cells." J Biochem 140(5): 627-637.

Curtis, D., R. Lehmann, et al. (1995). "Translational regulation in development." Cell 81(2): 171-178.

Czaplinski, K., T. Kocher, et al. (2005). "Identification of 40LoVe, a Xenopus hnRNP D family protein involved in localizing a TGF-beta-related mRNA during oogenesis." Dev Cell 8(4): 505-515.

Czaplinski, K. and I. W. Mattaj (2006). "40LoVe interacts with Vg1RBP/Vera and hnRNP I in binding the Vg1-localization element." RNA 12(2): 213-222.

Czaplinski, K. and R. H. Singer (2006). "Pathways for mRNA localization in the cytoplasm." Trends Biochem Sci 31(12): 687-693.

Dalgleish, G., J. L. Veyrune, et al. (2001). "mRNA localization by a 145-nucleotide region of the c-fos 3'--untranslated region. Links to translation but not stability." J Biol Chem 276(17): 13593-13599.

Davis, E. O., P. J. Jenner, et al. (1992). "Protein splicing in the maturation of M. tuberculosis recA protein: a mechanism for tolerating a novel class of intervening sequence." Cell 71(2): 201-210.

Davis, E. O., H. S. Thangaraj, et al. (1994). "Evidence of selection for protein introns in the recAs of pathogenic mycobacteria." EMBO J 13(3): 699-703.

de Hoog, C. L., L. J. Foster, et al. (2004). "RNA and RNA binding proteins participate in early stages of cell spreading through spreading initiation centers." Cell 117(5): 649-662.

Deshler, J. O., M. I. Highett, et al. (1998). "A highly conserved RNA-binding protein for cytoplasmic mRNA localization in vertebrates." Curr Biol 8(9): 489-496.

DeSimone, D. W. (1994). "Adhesion and matrix in vertebrate development." Curr Opin Cell Biol 6(5): 747-751.

DeSimone, D. W., P. A. Norton, et al. (1992). "Identification and characterization of alternatively spliced fibronectin mRNAs expressed in early Xenopus embryos." Dev Biol 149(2): 357-369.

Dichmann, D. S., R. B. Fletcher, et al. (2008). "Expression cloning in Xenopus identifies RNA-binding proteins as regulators of embryogenesis and Rbmx as necessary for neural and muscle development." Dev Dyn 237(7): 1755-1766.

Dingwall, C. and R. A. Laskey (1991). "Nuclear targeting sequences--a consensus?" Trends Biochem Sci 16(12): 478-481.

Dominguez, C. and F. H. Allain (2006). "NMR structure of the three quasi RNA recognition motifs (qRRMs) of human hnRNP F and interaction studies with Bcl-x G-tract RNA: a novel mode of RNA recognition." Nucleic Acids Res 34(13): 3634-3645.

Dreyfuss, G., M. J. Matunis, et al. (1993). "hnRNP proteins and the biogenesis of mRNA." Annu Rev Biochem 62: 289-321.

Dubertret, B., P. Skourides, et al. (2002). "In vivo imaging of quantum dots encapsulated in phospholipid micelles." Science. 298: 1759-1762.

Eagleson, G. W. and W. A. Harris (1990). "Mapping of the presumptive brain regions in the neural plate of Xenopus laevis." J Neurobiol 21(3): 427-440.

Easterling, M. R., M. Styblo, et al. (2002). "Pharmacokinetic modeling of arsenite uptake and metabolism in hepatocytes--mechanistic insights and implications for further experiments." J Pharmacokinet Pharmacodyn 29(3): 207-234.

Elleuche, S. and S. Poggeler (2010). "Inteins, valuable genetic elements in molecular biology and biotechnology." Appl Microbiol Biotechnol 87(2): 479-489.

Evans, T. J. T. and M. Q. Xu (2002). "Mechanistic and kinetic considerations of protein splicing." Chem Rev 102(12): 4869-4884.

Fu, A., W. Gu, et al. (2005). "Semiconductor nanocrystals for biological imaging." Curr Opin Neurobiol 15(5): 568-575.

Gall, J. (1956). "Small granules in the amphibian oocyte nucleus and their relationship to RNA." J Biophys Biochem Cytol(2): 393–396.

Gallouzi, I. E. and J. A. Steitz (2001). "Delineation of mRNA export pathways by the use of cell-permeable peptides." Science 294(5548): 1895-1901.

Gammill, L. S. and M. Bronner-Fraser (2003). "Neural crest specification: migrating into genomics." Nat Rev Neurosci 4(10): 795-805.

Gao, C., H. Guo, et al. (2004). "S-nitrosylation of heterogeneous nuclear ribonucleoprotein A/B regulates osteopontin transcription in endotoxin-stimulated murine macrophages." J Biol Chem 279(12): 11236-11243.

Gilbert, S. (2006). Developmental Biology. Sunderland, Massachusetts USA Sinauer Associates, Inc., Puplishers.

Gingras, A. R., K. P. Vogel, et al. (2006). "Structural and dynamic characterization of a vinculin binding site in the talin rod." Biochemistry 45(6): 1805-1817.

Giriat, I. and T. W. Muir (2003). "Protein semi-synthesis in living cells." J Am Chem Soc 125(24): 7180-7181.

Git, A. and N. Standart (2002). "The KH domains of Xenopus Vg1RBP mediate RNA binding and self-association." RNA 8(10): 1319-1333.

Glinka, M., T. Herrmann, et al. (2010). "The heterogeneous nuclear ribonucleoprotein-R is necessary for axonal beta-actin mRNA translocation in spinal motor neurons." Hum Mol Genet 19(10): 1951-1966.

Godfrey, E. W. and G. E. Sanders (2004). "Effect of water hardness on oocyte quality and embryo development in the African clawed frog (Xenopus laevis)." Comp Med 54(2): 170-175.

Groc, L., M. Lafourcade, et al. (2007). "Surface trafficking of neurotransmitter receptor: comparison between single-molecule/quantum dot strategies." J Neurosci 27(46): 12433-12437.

Gu, H. H., J. Xu, et al. (1993). "Peptide splicing in the vacuolar ATPase subunit A from Candida tropicalis." J Biol Chem 268(10): 7372-7381.

Habelhah, H., K. Shah, et al. (2001). "ERK phosphorylation drives cytoplasmic accumulation of hnRNP-K and inhibition of mRNA translation." Nat Cell Biol 3(3): 325-330.

Han, S. P., Y. H. Tang, et al. (2010). "Functional diversity of the hnRNPs: past, present and perspectives." Biochem J 430(3): 379-392.

Harland, R. and H. Weintraub (1985). "Translation of mRNA injected into Xenopus oocytes is specifically inhibited by antisense RNA." J Cell Biol 101(3): 1094-1099.

Hawrysz, D. J. and E. M. Sevick-Muraca (2000). "Developments toward diagnostic breast cancer imaging using near-infrared optical measurements and fluorescent contrast agents." Neoplasia 2: 388-417.

He, D. C., T. Martin, et al. (1991). "Localization of heterogeneous nuclear ribonucleoprotein in the interphase nuclear matrix core filaments and on perichromosomal filaments at mitosis." Proc Natl Acad Sci U S A 88(17): 7469-7473.

Heasman, J. (2002). "Morpholino oligos: making sense of antisense?" Dev Biol 243(2): 209-214.

Heasman, J., M. Kofron, et al. (2000). "Beta-catenin signaling activity dissected in the early Xenopus embryo: a novel antisense approach." Dev Biol 222(1): 124-134.

Hendzel, M. J., Y. Wei, et al. (1997). "Mitosis-specific phosphorylation of histone H3 initiates primarily within pericentromeric heterochromatin during G2 and spreads in an ordered fashion coincident with mitotic chromosome condensation." Chromosoma 106(6): 348-360.

Hilken, G., J. Dimigen, et al. (1995). "Growth of Xenopus laevis under different laboratory rearing conditions." Lab Anim 29(2): 152-162.

Hilleren, P. and R. Parker (1999). "mRNA surveillance in eukaryotes: kinetic proofreading of proper translation termination as assessed by mRNP domain organization?" RNA 5(6): 711-719.

Hirata, R., Y. Ohsumk, et al. (1990). "Molecular structure of a gene, VMA1, encoding the catalytic subunit of H(+)-translocating adenosine triphosphatase from vacuolar membranes of Saccharomyces cerevisiae." J Biol Chem 265(12): 6726-6733.

Hodges, R. A., F. B. Perler, et al. (1992). "Protein splicing removes intervening sequences in an archaea DNA polymerase." Nucleic Acids Res 20(23): 6153-6157.

Hoek, K. S., G. J. Kidd, et al. (1998). "hnRNP A2 selectively binds the cytoplasmic transport sequence of myelin basic protein mRNA." Biochemistry 37(19): 7021-7029.

Hoffman, D. W., C. C. Query, et al. (1991). "RNA-binding domain of the A protein component of the U1 small nuclear ribonucleoprotein analyzed by NMR spectroscopy is structurally similar to ribosomal proteins." Proc Natl Acad Sci U S A 88(6): 2495-2499.

Howarth, M., W. Liu, et al. (2008). "Monovalent, reduced-size quantum dots for imaging receptors on living cells." Nat Methods 5(5): 397-399.

Howarth, M., K. Takao, et al. (2005). "Targeting quantum dots to surface proteins in living cells with biotin ligase." Proc Natl Acad Sci U S A 102(21): 7583-7588.

Howell, J. L. and R. Truant (2002). "Live-cell nucleocytoplasmic protein shuttle assay utilizing laser confocal microscopy and FRAP." Biotechniques 32(1): 80-82, 84, 86-87.

Huang, M., J. E. Rech, et al. (1994). "The C-protein tetramer binds 230 to 240 nucleotides of pre-mRNA and nucleates the assembly of 40S heterogeneous nuclear ribonucleoprotein particles." Mol Cell Biol 14(1): 518-533.

Huang, X. and J. P. Saint-Jeannet (2004). "Induction of the neural crest and the opportunities of life on the edge." Dev Biol 275(1): 1-11.

Huang, Y. S., J. H. Carson, et al. (2003). "Facilitation of dendritic mRNA transport by CPEB." Genes Dev 17(5): 638-653.

Huttelmaier, S., D. Zenklusen, et al. (2005). "Spatial regulation of beta-actin translation by Src-dependent phosphorylation of ZBP1." Nature 438(7067): 512-515.

Intes, X., J. Ripoll, et al. (2003). "In vivo continuous-wave optical breast imaging enhanced with Indocyanine Green." Med Phys. 30: 1039-1047.

Jensen, K., K. Musunuru, et al. (2000). "The tetranucleotide UCAY directs the specific recognition of RNA by the Nova K-homology 3 domain." Proc Natl Acad Sci U S A(97): 5740–5745.

Johnstone, O. and P. Lasko (2001). "Translational regulation and RNA localization in Drosophila oocytes and embryos." Annu Rev Genet 35: 365-406.

Kabuyama, Y., M. Hamaya, et al. (1998). "Wavelength specific activation of PI 3-kinase by UVB irradiation." FEBS Lett 441(2): 297-301.

Kalchenko, V., S. Shivtiel, et al. (2006). "Use of lipophilic near-infrared dye in whole-body optical imaging of hematopoietic cell homing." J Biomed Opt.(11): 050507.

Kamada, S. and T. Miwa (1992). "A protein binding to CArG box motifs and to single-stranded DNA functions as a transcriptional repressor." Gene 119(2): 229-236.

Kane, P. M., C. T. Yamashiro, et al. (1990). "Protein splicing converts the yeast TFP1 gene product to the 69-kD subunit of the vacuolar H(+)-adenosine triphosphatase." Science 250(4981): 651-657.

Katz, Z. B., A. L. Wells, et al. (2012). "beta-Actin mRNA compartmentalization enhances focal adhesion stability and directs cell migration." Genes Dev 26(17): 1885-1890.

Kawamura, H., Y. Tomozoe, et al. (2002). "Identification of the nucleocytoplasmic shuttling sequence of heterogeneous nuclear ribonucleoprotein D-like protein JKTBP and its interaction with mRNA." J Biol Chem 277(4): 2732-2739.

Kawasaki, E. S. and A. Player (2005). "Nanotechnology, nanomedicine, and the development of new, effective therapies for cancer." Nanomedicine 1(2): 101-109.

Keller, R. E. (1980). "The cellular basis of epiboly: an SEM study of deep-cell rearrangement during gastrulation in Xenopus laevis." J Embryol Exp Morphol 60: 201-234.

Keller, R. E. (1981). "An experimental analysis of the role of bottle cells and the deep marginal zone in gastrulation of Xenopus laevis." J Exp Zool 216(1): 81-101.

Keller, R. E., M. Danilchik, et al. (1985). "The function and mechanism of convergent extension during gastrulation of Xenopus laevis." J Embryol Exp Morphol 89 Suppl: 185-209.

Kenwrick, S., E. Amaya, et al. (2004). "Pilot morpholino screen in Xenopus tropicalis identifies a novel gene involved in head development." Dev Dyn 229(2): 289-299.

Kiledjian, M. and G. Dreyfuss (1992). "Primary structure and binding activity of the hnRNP U protein: binding RNA through RGG box." EMBO J 11(7): 2655-2664.

Kim, S., Y. T. Lim, et al. (2003). "Near-infrared fluorescent type II quantum dots for sentinel lymph node mapping." Nature Biotechnology 22: 93-97.

Kobel, H. R. and L. D. Pasquier (1986). "Genetics of polyploid Xenopus." Trends in Genetics 2: 310-315.

Kobel, H. R. and L. D. Pasquier (1986). Genetics of polyploid Xenopus, Trends Genet

Kolev, N. G. and P. W. Huber (2003). "VgRBP71 stimulates cleavage at a polyadenylation signal in Vg1 mRNA, resulting in the removal of a cis-acting element that represses translation." Mol Cell 11(3): 745-755.

Koster, M., T. Frahm, et al. (2005). "Nucleocytoplasmic shuttling revealed by FRAP and FLIP technologies." Curr Opin Biotechnol 16(1): 28-34.

Kosturko, L. D., M. J. Maggipinto, et al. (2006). "Heterogeneous nuclear ribonucleoprotein (hnRNP) E1 binds to hnRNP A2 and inhibits translation of A2 response element mRNAs." Mol Biol Cell 17(8): 3521-3533.

Kragtorp, K. A. and J. R. Miller (2006). "Regulation of somitogenesis by Ena/VASP proteins and FAK during Xenopus development." Development. 133: 685-695.

Kress, T. L., Y. J. Yoon, et al. (2004). "Nuclear RNP complex assembly initiates cytoplasmic RNA localization." J Cell Biol 165(2): 203-211.

Kroll, T. T., L. B. Swenson, et al. (2009). "Interactions of 40LoVe within the ribonucleoprotein complex that forms on the localization element of Xenopus Vg1 mRNA." Mech Dev 126(7): 523-538.

Kroll, T. T., W. M. Zhao, et al. (2002). "A homolog of FBP2/KSRP binds to localized mRNAs in Xenopus oocytes." Development 129(24): 5609-5619.

Kubota, S., R. A. Furuta, et al. (1995). "Analysis of a novel defective HTLV-I provirus and detection of a new HTLV-I-induced cellular transcript." FEBS Lett 375(1-2): 31-36.

Kuroda, H., O. Wessely, et al. (2004). "Neural induction in Xenopus: requirement for ectodermal and endomesodermal signals via Chordin, Noggin, beta-Catenin, and Cerberus." PLoS Biol 2(5): E92.

la Cour, T., L. Kiemer, et al. (2004). "Analysis and prediction of leucine-rich nuclear export signals." Protein Eng Des Sel 17(6): 527-536.

Lahiri, D. K. and J. O. Thomas (1985). "The fate of heterogeneous nuclear ribonucleoprotein complexes during mitosis." J Biol Chem 260(1): 598-603.

Leser, G. P. and T. E. Martin (1987). "Changes in heterogeneous nuclear RNP core polypeptide complements during the cell cycle." J Cell Biol 105(5): 2083-2094.

Leverrier, S., E. Cinato, et al. (2000). "Purification and cloning of type A/B hnRNP proteins involved in transcriptional activation from the Rat spi 2 gene GAGA box." Biol Chem 381(11): 1031-1040.

Liker, E., E. Fernandez, et al. (2000). "The structure of the mRNA export factor TAP reveals a cis arrangement of a non-canonical RNP domain and an LRR domain." EMBO J 19(21): 5587-5598.

Liu, W., H. S. Choi, et al. (2007). "Compact cysteine-coated CdSe(ZnCdS) quantum dots for in vivo applications." J Am Chem Soc 129(47): 14530-14531.

Liu, Y., C. Gervasi, et al. (2008). "A crucial role for hnRNP K in axon development in Xenopus laevis." Development 135(18): 3125-3135.

Longo, D., S. M. Peirce, et al. (2004). "Multicellular computer simulation of morphogenesis: blastocoel roof thinning and matrix assembly in Xenopus laevis." Dev Biol 271(1): 210-222.

Lu, J. Y., N. Sadri, et al. (2006). "Endotoxic shock in AUF1 knockout mice mediated by failure to degrade proinflammatory cytokine mRNAs." Genes Dev 20(22): 3174-3184.

Lu, J. Y. and R. J. Schneider (2004). "Tissue distribution of AU-rich mRNA-binding proteins involved in regulation of mRNA decay." J Biol Chem 279(13): 12974-12979.

Marsden, M. and D. W. DeSimone (2001). "Regulation of cell polarity, radial intercalation and epiboly in Xenopus: novel roles for integrin and fibronectin." Development 128: 3635-3647.

Mayeda, A., S. H. Munroe, et al. (1994). "Function of conserved domains of hnRNP A1 and other hnRNP A/B proteins." EMBO J 13(22): 5483-5495.

Mazza, C., A. Segref, et al. (2002). "Large-scale induced fit recognition of an m(7)GpppG cap analogue by the human nuclear cap-binding complex." EMBO J 21(20): 5548-5557.

McKee, A. E., E. Minet, et al. (2005). "A genome-wide in situ hybridization map of RNA-binding proteins reveals anatomically restricted expression in the developing mouse brain." BMC Dev Biol 5: 14.

McNally, L. M., L. Yee, et al. (2006). "Heterogeneous nuclear ribonucleoprotein H is required for optimal U11 small nuclear ribonucleoprotein binding to a retroviral RNA-processing control element: implications for U12-dependent RNA splicing." J Biol Chem 281(5): 2478-2488.

Medintz, I. L., H. T. Uyeda, et al. (2005). "Quantum dot bioconjugates for imaging, labelling and sensing." Nat Mater 4: 435-446.

Michael, W. M., M. Choi, et al. (1995). "A nuclear export signal in hnRNP A1: a signal-mediated, temperature-dependent nuclear protein export pathway." Cell 83(3): 415-422.

Michael, W. M., P. S. Eder, et al. (1997). "The K nuclear shuttling domain: a novel signal for nuclear import and nuclear export in the hnRNP K protein." EMBO J 16(12): 3587-3598.

Michalet, X., F. F. Pinaud, et al. (2005). "Quantum dots for live cells, in vivo imaging, and diagnostics." Science 307(5709): 538-544.

Michalet, X., F. F. Pinaud, et al. (2005). "Quantum dots for live cells, in vivo imaging, and diagnostics." Science. 307: 538-544.

Mikheev, A. M., S. A. Mikheev, et al. (2000). "CArG binding factor A (CBF-A) is involved in transcriptional regulation of the rat Ha-ras promoter." Nucleic Acids Res 28(19): 3762-3770.

Mikula, M., A. Dzwonek, et al. (2006). "Landscape of the hnRNP K protein-protein interactome." Proteomics 6(8): 2395-2406.

Mili, S., H. J. Shu, et al. (2001). "Distinct RNP complexes of shuttling hnRNP proteins with pre-mRNA and mRNA: candidate intermediates in formation and export of mRNA." Mol Cell Biol 21(21): 7307-7319.

Miller, O. J. and A. Bakken (1972). "Morphological studies of transcription." Acta Endocrinol Suppl (Copenh)(168): 155–177.

Mizutani, A., M. Fukuda, et al. (2000). "SYNCRIP, a cytoplasmic counterpart of heterogeneous nuclear ribonucleoprotein R, interacts with ubiquitous synaptotagmin isoforms." J Biol Chem 275(13): 9823-9831.

Mourelatos, Z., L. Abel, et al. (2001). "SMN interacts with a novel family of hnRNP and spliceosomal proteins." EMBO J 20(19): 5443-5452.

Mowry, K. L. and D. A. Melton (1992). "Vegetal messenger RNA localization directed by a 340-nt RNA sequence element in Xenopus oocytes." Science 255(5047): 991-994.

Muralidharan, V. and T. W. Muir (2006). "Protein ligation: an enabling technology for the biophysical analysis of proteins." Nat Methods 3(6): 429-438.

Murgatroyd, C., A. Wigger, et al. (2004). "Impaired repression at a vasopressin promoter polymorphism underlies overexpression of vasopressin in a rat model of trait anxiety." J Neurosci 24(35): 7762-7770.

Musco, G., G. Stier, et al. (1996). "Three-dimensional structure and stability of the KH domain: molecular insights into the fragile X syndrome." Cell 85(2): 237-245.

Nelson, M. and M. McClelland (1992). "Use of DNA methyltransferase/endonuclease enzyme combinations for megabase mapping of chromosomes." Methods Enzymol 216: 279-303.

Nieuwkoop, P. D. a. F., J. (1994). Normal Table of Xenopus laevis (Daudin). New York, Garland.

Nigg, E. A., P. A. Baeuerle, et al. (1991). "Nuclear import-export: in search of signals and mechanisms." Cell 66(1): 15-22.

Nomura, M., A. Kaji, et al. (2001). "Mitogen- and stress-activated protein kinase 1 mediates activation of Akt by ultraviolet B irradiation." J Biol Chem 276(27): 25558-25567.

Norvell, A., R. L. Kelley, et al. (1999). "Specific isoforms of squid, a Drosophila hnRNP, perform distinct roles in Gurken localization during oogenesis." Genes Dev 13(7): 864-876.

Nutt, S. L., O. J. Bronchain, et al. (2001). "Comparison of morpholino based translational inhibition during the development of Xenopus laevis and Xenopus tropicalis." Genesis 30(3): 110-113.

Ostareck-Lederer, A. and D. H. Ostareck (2004). "Control of mRNA translation and stability in haematopoietic cells: the function of hnRNPs K and E1/E2." Biol Cell 96(6): 407-411.

Otero, L. J., A. Devaux, et al. (2001). "A 250-nucleotide UA-rich element in the 3' untranslated region of Xenopus laevis Vg1 mRNA represses translation both in vivo and in vitro." RNA 7(12): 1753-1767.

Perez-Alvarado, G. C., M. Martinez-Yamout, et al. (2003). "Structure of the nuclear factor ALY: insights into post-transcriptional regulatory and mRNA nuclear export processes." Biochemistry 42(24): 7348-7357.

Perler, F. B. (2002). "InBase: the Intein Database." Nucleic Acids Res 30(1): 383-384.

Perler, F. B., E. O. Davis, et al. (1994). "Protein splicing elements: inteins and exteins--a definition of terms and recommended nomenclature." Nucleic Acids Res 22(7): 1125-1127.

Perrone-Bizzozero, N. and F. Bolognani (2002). "Role of HuD and other RNA-binding proteins in neural development and plasticity." J Neurosci Res 68(2): 121-126.

Pickering, B. M., S. A. Mitchell, et al. (2003). "Polypyrimidine tract binding protein and poly r(C) binding protein 1 interact with the BAG-1 IRES and stimulate its activity in vitro and in vivo." Nucleic Acids Res 31(2): 639-646.

Pinol-Roma, S., Y. D. Choi, et al. (1988). "Immunopurification of heterogeneous nuclear ribonucleoprotein particles reveals an assortment of RNA-binding proteins." Genes Dev 2(2): 215-227.

Pinol-Roma, S. and G. Dreyfuss (1991). "Transcription-dependent and transcription-independent nuclear transport of hnRNP proteins." Science 253(5017): 312-314.

Pinol-Roma, S. and G. Dreyfuss (1992). "Shuttling of pre-mRNA binding proteins between nucleus and cytoplasm." Nature 355(6362): 730-732.

Portman, D. S. and G. Dreyfuss (1994). "RNA annealing activities in HeLa nuclei." EMBO J 13(1): 213-221.

Raju, C. S., N. Fukuda, et al. (2011). "In neurons, activity-dependent association of dendritically transported mRNA transcripts with the transacting factor CBF-A is mediated by A2RE/RTS elements." Mol Biol Cell 22(11): 1864-1877.

Raju, C. S., C. Goritz, et al. (2008). "In cultured oligodendrocytes the A/B-type hnRNP CBF-A accompanies MBP mRNA bound to mRNA trafficking sequences." Mol Biol Cell 19(7): 3008-3019.

Ramos, J. W. and D. W. DeSimone (1996). "Xenopus embryonic cell adhesion to fibronectin: position-specific activation of RGD/synergy site-dependent migratory behavior at gastrulation." J Cell Biol 134(1): 227-240.

Rao, J., A. Dragulescu-Andrasi, et al. (2007). "Fluorescence imaging in vivo: recent advances." Curr Opin Biotechnol 18(1): 17-25.

Rao, J., A. Dragulescu-Andrasi, et al. (2007). "Fluorescence imaging in vivo: recent advances." Curr Opin Biotechnol 18(1): 17-25.

Rebagliati, M. R., D. L. Weeks, et al. (1985). "Identification and cloning of localized maternal RNAs from Xenopus eggs." Cell 42(3): 769-777.

Rossoll, W., A. K. Kroning, et al. (2002). "Specific interaction of Smn, the spinal muscular atrophy determining gene product, with hnRNP-R and gry-rbp/hnRNP-Q: a role for Smn in RNA processing in motor axons?" Hum Mol Genet 11(1): 93-105.

Rost, B., G. Yachdav, et al. (2004). "The PredictProtein server." Nucleic Acids Res 32(Web Server issue): W321-326.

Rushlow, W. J., B. Rajakumar, et al. (2000). "Changes in CArG-binding protein A expression levels following injection(s) of the D1-dopamine agonist SKF-82958 in the intact and 6-hydroxydopamine-lesioned rat." Neuroscience 98(1): 69-78.

Rushlow, W. J., N. Rajakumar, et al. (1999). "Characterization of CArG-binding protein A initially identified by differential display." Neuroscience 94(2): 637-649.

Sadri, N. and R. J. Schneider (2009). "Auf1/Hnrnpd-deficient mice develop pruritic inflammatory skin disease." J Invest Dermatol 129(3): 657-670.

Saleh, L. and F. B. Perler (2006). "Protein splicing in cis and in trans." Chem Rec 6(4): 183-193.

Sato, S. M. and T. D. Sargent (1989). "Development of neural inducing capacity in dissociated Xenopus embryos." Dev Biol. 134: 263-266.

Schaeffer, C., B. Bardoni, et al. (2001). "The fragile X mental retardation protein binds specifically to its mRNA via a purine quartet motif." EMBO J 20(17): 4803-4813.

Schisa, J. A., J. N. Pitt, et al. (2001). "Analysis of RNA associated with P granules in germ cells of C. elegans adults." Development 128(8): 1287-1298.

Schnolzer, M., P. Alewood, et al. (1992). "In situ neutralization in Boc-chemistry solid phase peptide synthesis. Rapid, high yield assembly of difficult sequences." Int J Pept Protein Res 40(3-4): 180-193.

Scott, C. P., E. Abel-Santos, et al. (1999). "Production of cyclic peptides and proteins in vivo." Proc Natl Acad Sci U S A 96(24): 13638-13643.

Shan, J., T. P. Munro, et al. (2003). "A molecular mechanism for mRNA trafficking in neuronal dendrites." J Neurosci 23(26): 8859-8866.

Si, K., M. Giustetto, et al. (2003). "A neuronal isoform of CPEB regulates local protein synthesis and stabilizes synapse-specific long-term facilitation in aplysia." Cell 115(7): 893-904.

Silva, A. C., M. Filipe, et al. (2003). "Endogenous Cerberus activity is required for anterior head specification in Xenopus." Development 130(20): 4943-4953.

Simpson, P. J., T. P. Monie, et al. (2004). "Structure and RNA interactions of the N-terminal RRM domains of PTB." Structure 12(9): 1631-1643.

Sinnamon, J. R., C. B. Waddell, et al. (2012). "Hnrpab regulates neural development and neuron cell survival after glutamate stimulation." RNA 18(4): 704-719.

Siomi, H. and G. Dreyfuss (1995). "A nuclear localization domain in the hnRNP A1 protein." J Cell Biol 129(3): 551-560.

Siomi, M. C., H. Siomi, et al. (1995). "FXR1, an autosomal homolog of the fragile X mental retardation gene." EMBO J 14(11): 2401-2408.

Sive, H. L., R. M. Grainger, et al. (2000). Early Development of *Xenopus laevis*. A Laboratory Manual. Cold Spring Harbor, New York., Cold Spring Harbor Laboratory Press, New York.

Sive, H. L., R. M. Grainger, et al. (2010). Early Development of *Xenopus laevis*: A Laboratory Manual. Cold Spring Harbor, Cold Spring Harbor Laboratory Press.

Sive, H. L., R.M. Grainger, et al., Eds. (2010). Early Development of Xenopus laevis: A Laboratory Manual.

Smith, A. M., H. Duan, et al. (2008). "Bioconjugated quantum dots for in vivo molecular and cellular imaging." Adv Drug Deliv Rev 60(11): 1226-1240.

Smith, A. M., M. M. Wen, et al. (2010). "Imaging dynamic cellular events with quantum dots The bright future." Biochem (Lond) 32(3): 12.

Smith, J. C., F. L. Conlon, et al. (2000). "Xwnt11 and the regulation of gastrulation in Xenopus." Philos Trans R Soc Lond B Biol Sci 355(1399): 923-930.

Smith, W. C. and R. M. Harland (1991). "Injected Xwnt-8 RNA acts early in Xenopus embryos to promote formation of a vegetal dorsalizing center." Cell 67(4): 753-765.

Smith, W. C. and R. M. Harland (1991). "Injected Xwnt-8 RNA acts early in Xenopus embryos to promote formation of a vegetal dorsalizing center." Cell 67(4): 753-765.

Sommerville, J. and U. Scheer (1981). "Structural organization of nascent transcripts and hnRNA molecules in amphibian oocytes." Mol Biol Rep(7): 53–56.

Stroh, M., J. P. Zimmer, et al. (2005). "Quantum dots spectrally distinguish multiple species within the tumor milieu in vivo." Nat Med. 11: 678-682.

Stylianou, P. and P. A. Skourides (2009). "Imaging morphogenesis, in Xenopus with Quantum Dot nanocrystals." Mech Dev 126(10): 828-841.

Suzuki, M., M. Iijima, et al. (2005). "Two separate regions essential for nuclear import of the hnRNP D nucleocytoplasmic shuttling sequence." FEBS J 272(15): 3975-3987.

Swanson, M. S., T. Y. Nakagawa, et al. (1987). "Primary structure of human nuclear ribonucleoprotein particle C proteins: conservation of sequence and domain structures in heterogeneous nuclear RNA, mRNA, and pre-rRNA-binding proteins." Mol Cell Biol 7(5): 1731-1739.

Tada, M. and J. C. Smith (2000). "Xwnt11 is a target of Xenopus Brachyury: regulation of gastrulation movements via Dishevelled, but not through the canonical Wnt pathway." Development 127(10): 2227-2238.

Takashi Ariizumi, Naomi Moriya, et al. (1991). "Concentration-dependent inducing activity of activin A " Development Genes and Evolution 200: 230-233.

Thyagarajan, A. and B. G. Szaro (2004). "Phylogenetically conserved binding of specific K homology domain proteins to the 3'-untranslated region of the vertebrate middle neurofilament mRNA." J Biol Chem 279(48): 49680-49688.

Tiruchinapalli, D. M., Y. Oleynikov, et al. (2003). "Activity-dependent trafficking and dynamic localization of zipcode binding protein 1 and beta-actin mRNA in dendrites and spines of hippocampal neurons." J Neurosci 23(8): 3251-3261.

Tori, K., B. Dassa, et al. (2010). "Splicing of the mycobacteriophage Bethlehem DnaB intein: identification of a new mechanistic class of inteins that contain an obligate block F nucleophile." J Biol Chem 285(4): 2515-2526.

Tung, C. H., U. Mahmood, et al. (2000). "In vivo Imaging of Proteolytic Enzyme Activity Using a Novel Molecular Reporter." Cancer Research 60: 4953-4958.

Ubbels, G. A., K. Hara, et al. (1983). "Evidence for a functional role of the cytoskeleton in determination of the dorsoventral axis in Xenopus laevis eggs." J Embryol Exp Morphol 77: 15-37.

Van Dusen, C. M., L. Yee, et al. (2010). "A glycine-rich domain of hnRNP H/F promotes nucleocytoplasmic shuttling and nuclear import through an interaction with transportin 1." Mol Cell Biol 30(10): 2552-2562.

Varnai, P., T. Bondeva, et al. (2005). "Selective cellular effects of overexpressed pleckstrin-homology domains that recognize PtdIns(3,4,5)P3 suggest their interaction with protein binding partners." J Cell Sci 118(Pt 20): 4879-4888.

Venables, J. P., C. S. Koh, et al. (2008). "Multiple and specific mRNA processing targets for the major human hnRNP proteins." Mol Cell Biol 28(19): 6033-6043.

Vikesaa, J., T. V. Hansen, et al. (2006). "RNA-binding IMPs promote cell adhesion and invadopodia formation." EMBO J 25(7): 1456-1468.

Walling, M. A., J. A. Novak, et al. (2009). "Quantum dots for live cell and in vivo imaging." Int J Mol Sci 10(2): 441-491.

Wallingford, J. B., B. A. Rowning, et al. (2000). "Dishevelled controls cell polarity during Xenopus gastrulation." Nature 405(6782): 81-85.

Weeks, D. L. and D. A. Melton (1987). "A maternal mRNA localized to the vegetal hemisphere in Xenopus eggs codes for a growth factor related to TGF-beta." Cell 51(5): 861-867.

Weighardt, F., G. Biamonti, et al. (1995). "Nucleo-cytoplasmic distribution of human hnRNP proteins: a search for the targeting domains in hnRNP A1." J Cell Sci 108 (Pt 2): 545-555.

Weighardt, F., G. Biamonti, et al. (1996). "The roles of heterogeneous nuclear ribonucleoproteins (hnRNP) in RNA metabolism." Bioessays 18(9): 747-756.

Weissleder, R., C. H. Tung, et al. (1999). "In vivo imaging of tumors with protease-activated near-infrared fluorescent probes." 17: 375-378.

Wen, W., J. L. Meinkoth, et al. (1995). "Identification of a signal for rapid export of proteins from the nucleus." Cell 82(3): 463-473.

White, J. and E. Stelzer (1999). "Photobleaching GFP reveals protein dynamics inside live cells." Trends Cell Biol 9(2): 61-65.

Wilson, P. A. and D. A. Melton (1994). "Mesodermal patterning by an inducer gradient depends on secondary cell-cell communication." Curr Biol 4(8): 676-686.

Winklbauer, R. (2009). "Cell adhesion in amphibian gastrulation." Int Rev Cell Mol Biol 278: 215-275.

Wu, H., Z. Hu, et al. (1998). "Protein trans-splicing by a split intein encoded in a split DnaE gene of Synechocystis sp. PCC6803." Proc Natl Acad Sci U S A 95(16): 9226-9231.

Xing, Y. and J. Rao (2008). "Quantum dot bioconjugates for in vitro diagnostics & in vivo imaging." Cancer Biomark 4(6): 307-319.

Xu, M. Q., M. W. Southworth, et al. (1993). "In vitro protein splicing of purified precursor and the identification of a branched intermediate." Cell 75(7): 1371-1377.

Yan, C. Y., P. Skourides, et al. (2009). "Samba, a Xenopus hnRNP expressed in neural and neural crest tissues." Dev Dyn 238(1): 204-209.

Yao, J., Y. Sasaki, et al. (2006). "An essential role for beta-actin mRNA localization and translation in Ca2+-dependent growth cone guidance." Nat Neurosci 9(10): 1265-1273.

Yoo, Y., X. Wu, et al. (2006). "Interaction of N-WASP with hnRNPK and its role in filopodia formation and cell spreading." J Biol Chem 281(22): 15352-15360.

Yoon, Y. J. and K. L. Mowry (2004). "Xenopus Staufen is a component of a ribonucleoprotein complex containing Vg1 RNA and kinesin." Development 131(13): 3035-3045.

Zhao, S., W. J. Korzan, et al. (2008). "Heterogeneous nuclear ribonucleoprotein A/B and G inhibits the transcription of gonadotropin-releasing-hormone 1." Mol Cell Neurosci 37(1): 69-84.

Ziegler, W. H., R. C. Liddington, et al. (2006). "The structure and regulation of vinculin." Trends Cell Biol 16(9): 453-460.

Zimmer, J. P., S. W. Kim, et al. (2006). "Size series of small indium arsenide-zinc selenide core-shell nanocrystals and their application to in vivo imaging." J Am Chem Soc 128(8): 2526-2527.

Zuger, S. and H. Iwai (2005). "Intein-based biosynthetic incorporation of unlabeled protein tags into isotopically labeled proteins for NMR studies." Nat Biotechnol 23(6): 736-740.

7. Annexes

7.1 Abbreviations

***40LoVe**: mRNA binding protein 40*

A2RE: A2 response element

Ab: Antibody

A-P: Anterior -Posterior

ATPase: Adenosine TriPhosphatase

A-V: Animal-Vegetal

BB:BA: Benzyl Benzoate Benzyl Alcohol

CBF-A: CArG box-binding factor A

CNS: Central Nervous System

CoMO: Control Morpholino

DMZ: Dorsal Marginal Zone

DMSO: DiMethyl SuphOxide

DNS: hnRNP D nucleocytoplasmic shuttling sequence

D-V: Dorsal-Ventral

EDC: ethyl-N'-dimethylaminopropyl-carbodiimide

Extein: EXternal protein

FA: Focal Adhesion

***FLIP:** Fluorescence Loss in Photobleaching*

FN: Fibronectin

***FRAP:** Fluorescence Recovery After Photobleaching*

***GFP**: Green Fluorescence Protein*

GRD or RGG: Glysine Rich Domain

hnRNP: heterogeneous nuclear Ribonucleoprotein

HNS : hnRNP H nucleocytoplasmic shuttling sequence

I_C: C-terminus half of a split intein

I_N: N-terminus half of a split intein

Intein: INternal protein

IF: *Immunofluoresense*

IP_3R1: inositol 1,4,5-trisphosphate receptor type 1

KH: K-homology

KNS: hnRNP K nucleocytoplasmic shuttling sequence

LE: localization elements

MAB: Maleic Acid Buffer

MBHA: 4-methylbenzhydrylamine

MBT: mid-blastula transition

MIP: Maximum Intensity Projection

MOs: Morpholino Oligos

MMR: Marc's Modified Ringers

MW: Molecular Weight

mRNA: messenger RNA

NES: Nuclear Export Signal

NF-M: medium neurofilament protein

NIR QD's: Near Infra Red Quantum Dots

NLS: Nuclear Localization Signal

NTC: Neural Tube Closure

NTDs: Neural Tube Defects

PBS: Phosphate Buffer Saline

PCR: Polymerase Chain Reaction

PFA: Paraformaldehyde

PH: pleckstrin homology

PI_3K: Phosphoinositide 3-Kinase

Prrp - Proline rich RNA binding protein

QD's: Quantum dots

qRRMs: quasi-RRMs

R40LoVe – Rescue 40LoVe

RhnRNPAB: Rescue hnRNP AB

RBD: RNA Binding Domain

RBPs: RNA-binding proteins

RFP: *Red Fluorescence Protein*

RGG: Arg-Gly-Gly

RNAi: RNA interference

RNPs: RiboNucleoProteins

RRM: RNA Recognition Motif

RT: Room Temperature

RT-PCR: Reverse Transcription Polymerase Chain Reaction

RTS: RNA trafficking sequence

TEO: Triethanolamine

TNF: Tumor Necrosis Factor

TGF-β: transforming growth factor β

UTR: Untranslated region

UV: UltraViolet

VLE: Vg1 localization element

VTE: Vg1 translational element

WB: Western Blot

WISH: Whole-Mount *In Situ* Hybridization

WT: Wild Type

7.2 Alignments

- **40LoVe with Human hnRNP D**

```
40LoVe          MSD----SEQQYMETNAENGHEACD-----------AEAAEGKGAG-----------GGQ 34
HhnRNPD         MSEEQFGGDGAAAAATAAVGGSAGEQEGAMVAATQGAAAAAGSGAGTGGGTASGGTEGGS 60
                **:    .:     :.*  * .* :           * ** *.***           **.

40LoVe          NDAEGDQINASKGEEEAG------CVAEISSPLTEGVKMFVGGLSWDTSKKDLKDYFEKF 88
HhnRNPD         AESEGAKIDASKNEEDEGHSNSSPRHSEAATAQREEWKMFIGGLSWDTTKKDLKDYFSKF 120
                 ::** :*:***.**: *        :* ::.  *  ***:*******:********.**

40LoVe          GEVSDCTIKMDPNTGRSRGFGFILFKDAASVDKVLEHKEHRLDGRLIDPKKAMAMK-KEP 147
HhnRNPD         GEVVDCTLKLDPITGRSRGFGFVLFKESESVDKVMDQKEHKLNGKVIDPKRAKAMKTKEP 180
                *** ***:*:** *********:***:: *****:::***:*:*::****:* *** ***

40LoVe          IKKIFVGGLNPEAGEDKIREYFETFGEIEAVELPMDPKTNKRRGFVFITFKEEEPVKKIL 207
HhnRNPD         VKKIFVGGLSPDTPEEKIREYFGGFGEVESIELPMDNKTNKRRGFCFITFKEEEPVKKIM 240
                :********.*:: *:******  ***:*::***** ******** ************:

40LoVe          EKKFHNVSGSKCEIKIAQPKEVY--QQQYGGRGGSFGGRGGRGGKGQGQNWNQGYNNYWN 265
HhnRNPD         EKKYHNVGLSKCEIKVAMSKEQYQQQQQQWGSRGGFAGRARGRGG-GPSQNWNQGYSNYWN 299
                ***:***. ******:* .** *  ***:*.***  *   **** * .*******.****

40LoVe          QGYGNQGYGSYGQQGYGGYGNYDYSGYG-YYGYGPGYDYSQGGANYGKAPRRGGHQSNYK 324
HhnRNPD         QGYGNYGYNS---QGYGGYGGYDYTGYNNYYGYG---DYSNQQSGYGKVSRRGGHQNSYK 353
                ***** **.*   *******.***:**. *****   ***:  :.***..******..**

40LoVe          PY 326
HhnRNPD         PY 355
                **
```

- **40LoVe, Xenopus hnRNP AB, mouse hnRNP AB, human hnRNP D**

```
40LoVe          ------------------MSDS-EQQYMETN--AENGHEACD-----AEAAEGKGAGGGQ 34
xhnRNPAB        ------------------MSDT-EQQCLETN--AENGHEACD-----AEAAEDK-APAGQ 33
mhnRNPAB        ------------------MSDAAEEQPMETTGATENGHEAAPEGEAPVEPSAAAAAPAAS 42
HhnRNPD         MSEEQFGGDGAAAAATAAVGGSAGEQEGAMVAATQGAAAAAGSGAGTGGGTASGGTEGGS 60
                                 :.:  :*       ::..  *.         :    : ...

40LoVe          NDAEGDQINASKGEEEAGCV------AEISSPLTEG--VKMFVGGLSWDTSKKDLKDYFE 86
xhnRNPAB        NGAEGEQINASKGEEDAGCV------ADISSPLTEG--VKMFVGGLSWDTSKKDLKDYFA 85
mhnRNPAB        AGSGGGTTTAPSGNQNGAEG------DQINASKNEEDAGKMFVGGLSWDTSKKDLKDYFT 96
HhnRNPD         AESEGAKIDASKNEEDEGHSNSSPRHSEAATAQREE--WKMFIGGLSWDTTKKDLKDYFS 118
                 :*   *...::: .         :  :.  *    ***:*******:********

40LoVe          KFGEVSDCTIKMDPNTGRSRGFGFILFKDAASVDKVLEHKEHRLDGRLIDPKKAMAMK-K 145
xhnRNPAB        KFGEVSDCTIKMDPNTGRSRGFGFILFKDAESVDKVLEHKEHRLDGRLIDPKKAMAMK-K 144
mhnRNPAB        KFGEVVDCTIKMDPNTGRSRGFGFILFKDSSSVEKVLDQKEHRLDGRVIDPKKAMAMK-K 155
HhnRNPD         KFGEVVDCTLKLDPITGRSRGFGFVLFKESESVDKVMDQKEHKLNGKVIDPKRAKAMKTK 178
                ***** ***:*:** *********:***:: **:**:::***:*:*::****:* *** *

40LoVe          EPIKKIFVGGLNPEAGEDKIREYFETFGEIEAVELPMDPKTNKRRGFVFITFKEEEPVKK 205
xhnRNPAB        DPIKKIFVGGLNPEAGEDQIREYFETFGEIEAIELPMDPKTNKRRGFVFITFKEEDPVKK 204
mhnRNPAB        DPVKKIFVGGLNPEATEEKIREYFGQFGEIEAIELPIDPKLNKRRGFVFITFKEEDPVKK 215
HhnRNPD         EPVKKIFVGGLSPDTPEEKIREYFGGFGEVESIELPMDNKTNKRRGFCFITFKEEEPVKK 238
                :*:*********.*:: *::*****  ***:*::***:* * ****** *******:****

40LoVe          ILEKKFHNVSGSKCEIKIAQPKEVY-QQQYGGRGGSFGGRGGRG-GKGQGQNWNQGYNNY 263
xhnRNPAB        ILEKKFHNVSGSKCEIKIAQPKEVY-QQQYGGRGGSFGGRGGRG-GKGQGQNWNQGYN-Y 261
mhnRNPAB        VLEKKFHTVSGSKCEIKVAQPKEVYQQQQYGSGGRGNRNRGNRGSGGGQSQSWNQGYGNY 275
HhnRNPD         IMEKKYHNVGLSKCEIKVAMSKEQYQQQQQWGSRGGFAGR-ARGRGGGPSQNWNQGYSNY 297
                ::***:*.*. ******:* .** * ***  .   .  .*  ** * * .*.*****. *

40LoVe          WNQGYGNQGYGSYGQQGYG-GYGNYDYSGYG-YYGYGPGYDYSQGGANYGKAPRRGGHQS 321
xhnRNPAB        WNQGYGNQGYGGYGQQGYG-GYGNYDYSGYG-YYGYGPGYDYSQGSANYGKAPRRGSHQN 319
mhnRNPAB        WNQGYG---Y----QQGYGPGYGGYDYSPYG-YYGYGPGYDYSQGSTNYGKSQRRGGHQN 327
HhnRNPD         WNQGYGNYGYN---SQGYG-GYGGYDYTGYNNYYGYG---DYSNQQSGYGKVSRRGGHQN 350
                ******   *    .**** ***.***: *. *****   ***:  :.***  ***.**.
```

```
40LoVe          NYKPY 326
xhnRNPAB        NYKPY 324
mhnRNPAB        NYKPY 332
HhnRNPD         SYKPY 355
                .****
```

SeqA	Name	Length	SeqB	Name	Length	Score
1	40LoVe	326	2	HhnRNPD	355	62.27
1	40LoVe	326	3	mhnRNPAB	332	71.78
1	40LoVe	326	4	xhnRNPAB	324	93.52
2	HhnRNPD	355	3	mhnRNPAB	332	63.55
2	HhnRNPD	355	4	xhnRNPAB	324	61.11
3	mhnRNPAB	332	4	xhnRNPAB	324	71.6

- **Mouse splice variants hnRNP AB1 and hnRNP AB2**

```
mAB1            MSDAAEEQPMETTGATENGHEAAPEGEAPVEPSAAAAAPAASAGSGGGTTTAPSGNQNGA 60
mAB2            MSDAAEEQPMETTGATENGHEAAPEGEAPVEPSAAAAAPAASAGSGGGTTTAPSGNQNGA 60
                ************************************************************

mAB1            EGDQINASKNEEDAGKMFVGGLSWDTSKKDLKDYFTKFGEVVDCTIKMDPNTGRSRGFGF 120
mAB2            EGDQINASKNEEDAGKMFVGGLSWDTSKKDLKDYFTKFGEVVDCTIKMDPNTGRSRGFGF 120
                ************************************************************

mAB1            ILFKDSSSVEKVLDQKEHRLDGRVIDPKKAMAMKKDPVKKIFVGGLNPEATEEKIREYFG 180
mAB2            ILFKDSSSVEKVLDQKEHRLDGRVIDPKKAMAMKKDPVKKIFVGGLNPEATEEKIREYFG 180
                ************************************************************

mAB1            QFGEIEAIELPIDPKLNKRRGFVFITFKEEDPVKKVLEKKFHTVSGSKCEIKVAQPKEVY 240
mAB2            QFGEIEAIELPIDPKLNKRRGFVFITFKEEDPVKKVLEKKFHTVSGSKCEIKVAQPKEVY 240
                ************************************************************

mAB1            QQQQYGSGGRGNRNRGNRGSGGGQSQSWNQGYGNYWNQGYGYQQGYGPGYGGYDYSPYGY 300
mAB2            QQQQYGSGGRGNRNRGNRGSGGGQ---------------------------------- 264
                ************************

mAB1            YGYGPGYDYSQGSTNYGKSQRRGGHQNNYKPY 332
mAB2            ----------GSTNYGKSQRRGGHQNNYKPY 285
                          **********************
```

7.3 Buffers, solutions and media

10X Marc's Modified Ringers (MMR)

0.1M NaCl

1.8mM KCl

2.0 mM $CaCl_2$

1mM $MgCl_2$

5mM HEPES

Adjust pH to 7.4 with NaOH.

Add Gentamycin gel to a final concentration of 0.05mg/mL.

Before use, dilute 1:10 (1x MMR).

1x PBDT

1x PBS

0.5% Triton-x

1% DMSO

IF Block and Ab incubation solution

1x PBDT

10% Normal goat or donkey serum

1x MEMFA (100ml)

0.1M MOPS (pH 7.4)

2mM EGTA

1mM $MgSO_4$

3.7% Formaldehyde

Prepare 10X solution of MEM and autoclave (turns yellow)

Before use add formaldehyde and dilute 1:10 (1x MEMFA)

4% Ficoll (100ml)

4g Ficoll dissolved in 0.33xMMR

2%Cysteine (100ml)

2g L-Cysteine diluted in 0.33 MMR, adjust pH to 7.8

1x PBTw

1x PBS

0.1% Tween-20

1x Alkaline Phosphatase Buffer (1L)

100ml TRIS (pH 9.5, 1M)

20ml NaCl (5M)

50ml MgCl2 (1M)

Adjust pH to 9.5, add DDW to 1L

1x Maleic Acid Buffer (MAB, 1L)

11.61g Maleic Acid (100mM)

30ml NaCl (5M)

800ml DDW

Adjust pH to 7.5, add DDW to 1l, autoclave

Hybridization solution (1L)

10g Boehringer Block

500ml Formamide

250ml SSC (20x)

Heat to 65°C for 1 hour

120ml DDW

100ml Torula RNA (10mg/ml in DDW, dissolved at 65°C; filtered)

2ml Heparin (50mg/ml in 1xSSC pH 7)

5ml Tween20 (20%)

10ml CHAPS (10%)

10ml EDTA (0.5M)

Filter (5µm)

2% WISH Antibody Blocking Buffer

10g BMB block in 1xMAB (100ml final)

Autoclave

2ml 10xBMB in 1xMAB (final 10ml)

Bleaching solution (50ml)

1.25ml 20xSSC

2.5 ml formamide

2 ml 30% peroxide

45 ml distilled water

RIPA lysis buffer

50 mM TrisHCl pH7.4

150 mM NaCl,

2 mM EDTA

1% NP-40

0.1% SDS

1% deoxycholate 24mM

7.4 Publications

Journal articles

1. 40LoVe and Samba Are Involved in *Xenopus* Neural Development and Functionally Distinct from hnRNP AB. **Andreou M**, Yan CYI, Skourides PA (2014) PLoS ONE 9(1): e85026.

2. Evaluation of total toxicity of effluents from several waste water treatment stations and major water sources of Cyprus using *Xenopus laevis* as a model organism. **Andreou Maria**, Eleftheriou Iro, Eleftheriou Anna, Christodoulou Neophytos, Antoniades Ioanna, Ioannou Andriani, Petridou Nicoletta, Stylianou Panayiota and Skourides Paris. Journal of Environmental Research and Development Vol. 6 No. 1, July-September 2011

3. Intein-mediated site-specific conjugation of Quantum Dots to proteins in vivo. Charalambous A., **Andreou M.**, Skourides PA., J Nanobiotechnology. 2009 Dec 10;7:9

4. Spatially and temporally regulated alpha6 integrin cleavage during *Xenopus laevis* development. Demetriou M.C., Stylianou P., **Andreou M.**, Yiannikouri O., Tsaprailis G., Cress A.E., Skourides P. Biochem. Biophys. Res. Commun. 2007 Dec 18

Book contributions

Nanoparticles in Biology and Medicine, Methods and Protocols, Springer Protocols, Methods in Molecular Biology Vol. 906, Humana Press, ISBN 978-1-61779-952-5, Chapter 11: *In vivo*, site-specific, covalent conjugation of Quantum Dots to proteins via split-intein splicing. Charalambous A., **Andreou M.**, Antoniades I., Christodoulou N., Skourides P.

***Copy of papers and book chapter attached**

7.5 Conferences

- **November 2012 -** University of Cyprus – Workshop for the presentation of Post-graduate research. **Poster:** The role of Samba in *Xenopus* development, Maria Andreou, Irene C.Y. Yan and Paris A. Skourides

- **September 2012 -** 14th International Xenopus Conference. **Poster:** The role of Samba in *Xenopus* development, Maria Andreou, Irene C.Y. Yan and Paris A. Skourides

- **September 2010-** *International Congress of Enviromental Research* (ICER-10), Reduit, Mauritius September 16-18, 2010. **Poster:** Evaluation of total toxicity of effluents from several waste water treatment stations and major water sources of Cyprus using *Xenopus laevis* as a model organism, Maria Andreou, Paris Skourides

- **April 2010 -** Nanotheranostics: Fabrication and Safety Concerns International. **Poster:** Intein-mediated site-specific conjugation of Quantum Dots to proteins in vivo. Andreou M., Charalambous A., Skourides PA.